A ground based gamma ray telescope of high sensitivity and low energy threshold

Dickinson, James Edwin

A Ground Based Gamma Ray Telescope of High Sensitivity and Low Energy Threshold

by James Edwin Dickinson, B.Sc.

A thesis submitted to the University of Durham in accordance with the regulations for admittance to the degree of Doctor of Philosophy

Department of Physics
University of Durham

April 1995

Abstract

The subject of this thesis is ground based gamma ray astronomy using the atmospheric Cerenkov technique. Chapter 1 defines the gamma ray region of the electromagnetic spectrum, introduces celestial gamma rays as a component of the flux of energetic particles known as cosmic rays and considers the physical mechanisms by which celestial gamma rays may be produced and absorbed. The phenomenon of Cerenkov radiation, and its production within the extensive air showers which result from the interaction of energetic cosmic rays with the atmosphere, is the subject of Chapter 2. Chapter 3 introduces the early Durham telescopes, and considers the possible improvement to instrument sensitivity afforded by invokation of more sophisticated background rejection strategies. The Mk.5 telescope, which is the subject of Chapter 4, is the vehicle by which the Durham group has sought to assess the relative merits of various signal enhancement strategies, and prove the viability of a design for a high resolution imaging detector with the additional capacity to make observations at very low energies; the Mk.6 telescope. Chapter 5 introduces a novel concept of background rejection based upon the stereoscopic imaging of extensive air showers, and describes modifications to the Mk.3 necessary to provide a complement to the Mk.5 in this capacity. Chapter 6 presents the analysis of a burst of periodic gamma ray emission from AE Aquarii, which demonstrates the efficacy of the medium resolution 'mono' imaging and stereoscopic imaging signal enhancement techniques employed by the Mk.5 and modified Mk.3 telescopes. The culmination of the evolution of the Durham telescopes is the Mk.6, described in Chapter 7. Its sensitivity is enhanced by high resolution imaging and the capacity to make observations at energies deficient in background events. Chapter 8 summarises the contemporary status of atmospheric Cerenkov astronomy.

Contents

CHAPTER 3 - THE PERFORMANCE OF GROUND BASED GAMMA RAY TELESCOPES

Preface

All of the work performed by the author has been associated with the telescopes now deployed at the Durham University gamma ray observatory at the Bohena settlement, Narrabri, New South Wales, Australia.

During the tenure of his Ph.D. the author has spent ten dark moon periods at the observatory. The majority of these have been associated with the build and commissioning of two of the Durham group's active telescopes, the Mk.5 and Mk.6 telescopes, and a substantial upgrade of the third, the Mk.3. His specific area of responsibility during telescope commissioning has been the configuration of the optics.

In Durham, the author has been responsible for the testing and alignment of the Mk.3 telescope replacement flux collector and the testing of the Mk.6 mirror sectors. In addition he has had input into several facets of the design of the Mk.6 telescope and was actively involved with its fabrication. He has been involved in several aspects of data processing pertaining to commissioning and calibration of the telescopes and has undertaken some routine data analysis.

None of the material presented in this thesis has been submitted previously for admittance to a degree in this or any other university, except where due reference is made.

Acknowledgements

I would like to express my gratitude to all whose help I have relied upon during the course of my studies.

Professors A.D. Martin and D. Bloor are thanked for the provision of the facilities of the Department of Physics, and the Particle Physics and Astronomy Research Council (formerly the Science and Engineering Research Council) for their financial support.

I would like to thank Professor Ted Turver for allowing me the opportunity to work with the Durham gamma ray astronomy group, a valuable experience I have thoroughly enjoyed, and he and Dr. Paula Chadwick for their advice and patience in their role as my supervisors.

I am in the debt of all of the staff and students of the observatory for their help throughout my course, and particularly for keeping me apprised of the rapid developments in the commissioning of the Mk.6 telescope during the composition of this thesis.

Thanks to all who I have worked with in Durham, Australia and Darlington for their help and companionship. Chris Bowden, Stella Bradbury, Paula Chadwick, Peter Cottle, Mark Dickinson, Nigel Dipper, Pete Edwards, Susan Hilton, Bill Hogg, Jamie Holder, Eric Lincoln, Lowry McComb, Chris Mullaney, Keith Orford, Ken Parkin, Steve Rayner, Ian Roberts, Mike Roberts, Malcolm Robertshaw, Ken Tindale, Steve Tummey and Ted Turver it's a pleasure to know you all.

Finally, thanks to my parents for giving me the confidence to enjoy life.

CHAPTER 1

GAMMA RAY ASTRONOMY

1.1 Introduction

Cosmic rays were first detected as a flux of ionising radiation at the Earth's surface. The existence of this ionising radiation was inferred from the results of an experiment demonstrating that charge leakage from an electroscope is greatly reduced if the instrument is shielded with metal (Rutherford and Cooke, 1903). The radiation was initially assumed to be terrestrial in origin and due entirely to decay of radioactive materials in the Earth's crust. This explanation was soon discredited with the demonstration that the rate of charge leakage did not decrease with altitude above the ground at the anticipated rate (eg. Goeckel, 1910; Hess, 1911). Indeed, above a certain altitude, ionisation increases with altitude. Subsequently the radiation responsible for this phenomenon was termed cosmic radiation, in deference to its extra terrestrial origin. The study of cosmic rays and speculation as to the nature of their progenitors has continued unabated since their discovery.

The quest to identify discrete sources of cosmic rays is daunting as the vast majority of the flux is composed of charged particles, mainly protons. Over interstellar distances all but the highest energy particles deviate from a straight path due to the influence of the galactic magnetic field (10^{-6}G), consequently losing any information about their source direction. As a result, what is seen at the Earth is a highly isotropic cosmic ray flux.

Neutral components of the cosmic radiation, which travel undeviated through the intergalactic magnetic field, comprise neutrons, neutrinos and

gamma rays. Neutrons have too short a lifetime to provide any significant flux when travelling galactic distances, whilst neutrinos have such a weak interaction with matter that their fluxes are detectable only in extreme cases. Gamma rays, however, are readily detectable and have an interaction length, at certain energies, of intergalactic distances.

The utility of gamma ray astronomy, then, is due to the fact that the gamma rays carry no charge and hence, unaffected by the galactic magnetic field, retain directionality. Also, being constrained to travel the same path from source to observer, photons can provide temporal information about their production. This information is invaluable in the study of variable and periodic sources.

1.2 Observation Techniques and the Gamma Ray Spectrum

The gamma ray region of the electromagnetic spectrum extends over almost 15 decades in energy. It is often arbitrarily defined as beginning at 0.511MeV (the rest mass of the electron) and is constrained in maximum energy only by the highest energies observed. Obviously over such a large spectrum of energies different physical processes are utilised for photon detection. Low to high energy gamma rays (0.5 MeV - 30 GeV) are absorbed early in the atmosphere and their energy dissipated through an electromagnetic cascade. Detection at these energies is therefore only possible in instruments placed above the Earth's atmosphere. At very high energies (> 30 GeV) the electromagnetic cascade contains particles of sufficient energy to radiate a detectable amount of Cerenkov light as they traverse the atmosphere (The mechanism of Cerenkov radiation is described in Chapter 2). The atmosphere is transparent to Cerenkov light facilitating detection of gamma rays of these energies from the ground. At

higher energies still (> 50 TeV) a large proportion of the electromagnetic cascade persists to ground level and is detectable in scintillation detectors. Arrays of these detectors allow reconstruction of the arrival direction of the primary and its energy.

A subdivision of the gamma ray spectrum has evolved to reflect the sensitive ranges of the various detectors employed. This subdivision is illustrated in Table 1.

Energy Range	Classification	Technique
0.5 - 5 MeV	Low Energy (LE)	Scintillation Detector (Satellite)
5 - 30 MeV	Medium Energy (ME)	Compton Telescope (Satellite)
0.03 - 30 GeV	High Energy (HE)	Spark Chamber (Satellite)
0.03 - 50 TeV	Very High Energy (VHE)	Atmospheric Cerenkov Detector (Ground Based)
0.05 - 10^5 PeV	Ultra High Energy (UHE)	Scintillation Detector Array (Ground Based)

Table 1.1: A subdivision of the Gamma Ray Spectrum in terms of the instruments used for their detection within each of the energy bands.

The subject of this thesis is the technique of atmospheric Cerenkov astronomy, also known as Very High Energy (VHE) gamma ray astronomy.

1.3 Very High Energy Cosmic Gamma Ray Production Mechanisms

1.3.1 Introduction

Many astronomical objects have been proposed as potential sources of cosmic gamma rays. These include; the galactic centre, the galactic plane, other galaxies (AGNs), supernova remnants, pulsars and primordial black holes. It is probable that different mechanisms of gamma ray production predominate in each of these predicted sources. However, in all of the models currently proposed, the production of high energy gamma rays is restricted to the same few physical processes.

Gamma ray production has been reviewed in detail by a number of authors (Fazio, 1967, ; Hillier, 1984; Ramana-Murthy and Wolfendale, 1986); the generic form of the production process is the interaction of a relativistic electron or nucleon with other matter or a magnetic field. The specific processes believed to be important at the energies pertaining to the atmospheric Cerenkov technique are considered below.

1.3.2 Gamma Ray Production Via Meson Decay

Neutral pions, the product of nucleon-antinucleon annihilation or the inelastic collision of cosmic ray protons with interstellar matter, decay into two gamma rays. Neutral pion decay is illustrated in Figure 1.1 below.

The resultant gamma ray energy spectrum is a function of the proton (cosmic ray) energy spectrum and the matter density. Individual photons are typically an order of magnitude lower in energy than the incident proton, with the source region intensity proportional to the product of the proton flux and matter density.

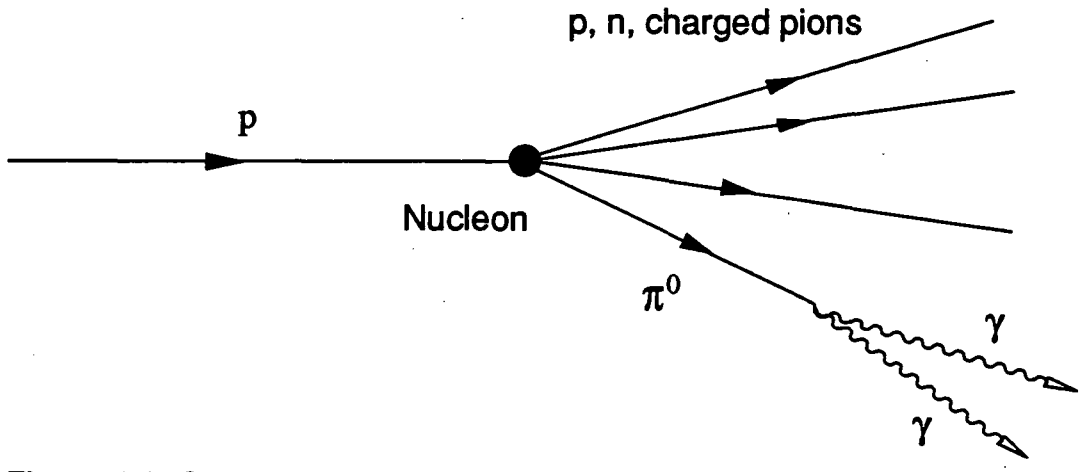

Figure 1.1: Gamma ray production via neutral pion decay.

The flux, particularly at the high energies pertinent to Cerenkov astronomy, is augmented by the decay of K mesons and hyperons which are product of a small proportion of the nucleon interactions.

1.3.3 Gamma Ray Production by Accelerated Charged Particles

1.3.3.1 *Introduction*

Within this group are three distinct mechanisms of gamma ray production, these being; Bremsstrahlung, synchrotron and curvature radiation. All are important in astrophysical processes.

1.3.3.2 Bremsstrahlung Radiation

Gamma rays are radiated via the Bremsstrahlung mechanism as a high energy electron is accelerated in the electrostatic field of a nucleus or other charged particle (see Figure 1.2 below).

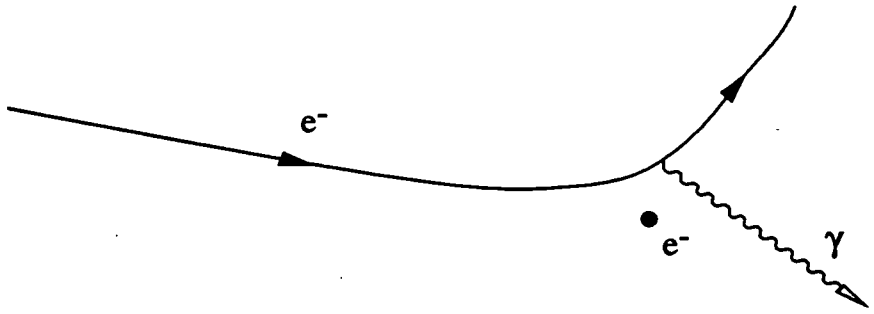

Figure 1.2: The Bremsstrahlung mechanism of gamma ray production.

The energy of the radiated gamma ray is dependent upon the extent to which the electron deviates from its path in the charge field of the nucleus, and can be comparable to that of the electron in extreme cases. This mechanism is important in regions of high matter density, with gamma ray intensity proportional to the product of the matter density and electron flux.

1.3.3.3 Synchrotron Radiation

Synchrotron radiation, illustrated in Figure 1.3, results when a relativistic electron is subject to a transverse component of a magnetic field. The electron is accelerated perpendicular to its instantaneous velocity and to the field, and emits gamma rays of energy several orders of magnitude lower than that of the electron.

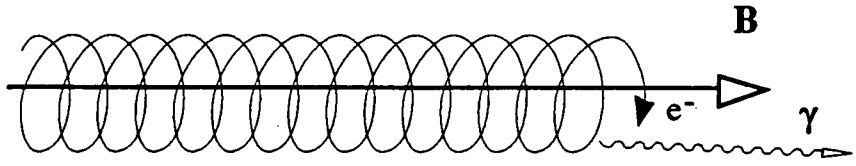

Figure 1.3: The mechanism of synchrotron radiation.

No gamma rays produced by the synchrotron process are of sufficient energy to be of direct interest to atmospheric Cerenkov astronomers.

However, their detection elsewhere in the electromagnetic spectrum betrays the presence of relativistic electrons which have the potential to produce very energetic gamma rays via other mechanisms.

1.3.3.4 Curvature Radiation

Curvature radiation is a phenomenon unique to the study of pulsars due to the requirement for an intense magnetic field. The essence of this mechanism is that relativistic electrons are constrained to move along curved magnetic field lines by the extreme fields present in the vicinity of the pulsar (10^8 T surface field).

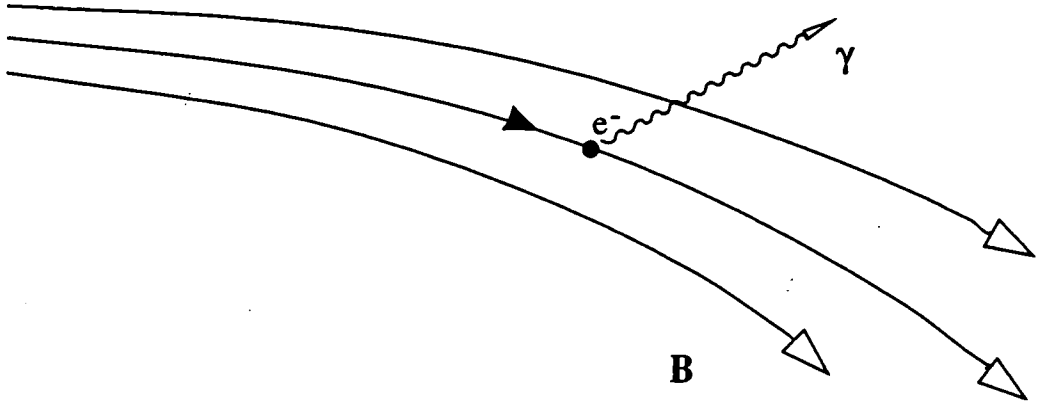

Figure 1.4: Curvature radiation of gamma rays in an intense magnetic field.

Close to the surface of the pulsar the gamma rays emitted as curvature radiation can be almost as energetic as the radiating electron.

1.3.4 Promotion of Photons to Gamma Ray Energies Via the Inverse Compton Process

A low energy photon may be accelerated to gamma ray energies through elastic collision with a relativistic electron. The electron loses the majority of

its energy in the interaction. In the interstellar medium the photon is likely to be from starlight, or the 3K background. Within a discrete source the target photon may be a product of the synchrotron process. In the case where

$$E_e >> \frac{(m_e c^2)^2}{h\nu}$$

where E_e is the energy of the electron and $h\nu$ is the energy of the ambient photon, the resultant gamma ray energy can approach that of the incident electron. Figure 1.5 illustrates this, the Compton effect.

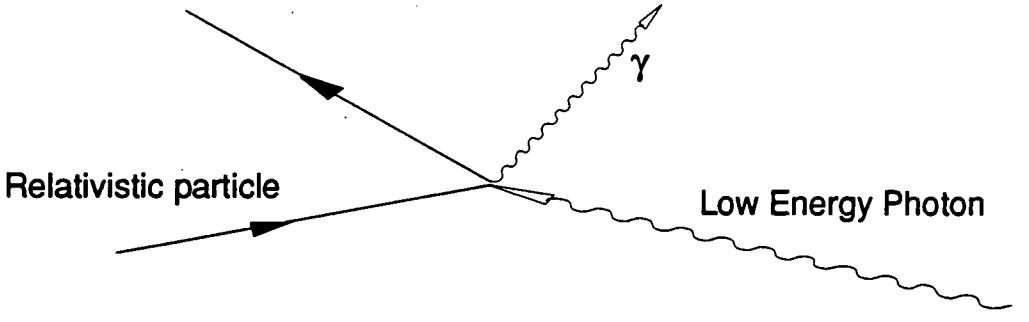

Figure 1.5: Promotion of a low energy photon to gamma ray energies via the the inverse Compton process.

1.4 Very High Energy Cosmic Gamma Ray Absorption Mechanisms

1.4.1 Introduction

One can imagine that cosmic gamma rays may be absorbed through their interaction with interstellar and intergalactic matter, photons and magnetic fields. It transpires, however, that for gamma rays of energy > 100 KeV, the collision cross section for pair production with atomic hydrogen is negligible. The radiation length of a typical photon is 25 g cm^{-2} compared with a typical intergalactic column density of $<10^{-5}$ g cm^{-2} Mpc^{-1}. This leaves the

absorption due to photons and magnetic fields.

1.4.2 Absorption by Photons

Gamma rays are absorbed via the electron-positron pair production process as a result of their interaction with the interstellar and intergalactic ambient photon flux. For the transition

$$h\nu_1 + h\nu_2 \rightarrow e^+ + e^-$$

to occur (the threshold condition) the combined photon energies must exceed $(m_e c^2)^2$. The cross section for interaction with starlight is very small and therefore only important over intergalactic distances. However, it is predicted that gamma rays with energy in excess of 10 TeV will be susceptible to pair production with the thermal microwave background which pervades the universe (Gould and Schreder, 1966; Jelley, 1966). Absorption via this mechanism becomes important for sources within the galaxy for gamma ray energies in excess of 50 TeV (see Figure 1.6). Below 50 TeV the majority of the absorption is due to pair production with photons of the IR and visible starlight background. This effect is only important for extremely distant objects but may have important implications for the study of active galactic nuclei at TeV energies (Stecker, De Jeger and Salamon, 1992).

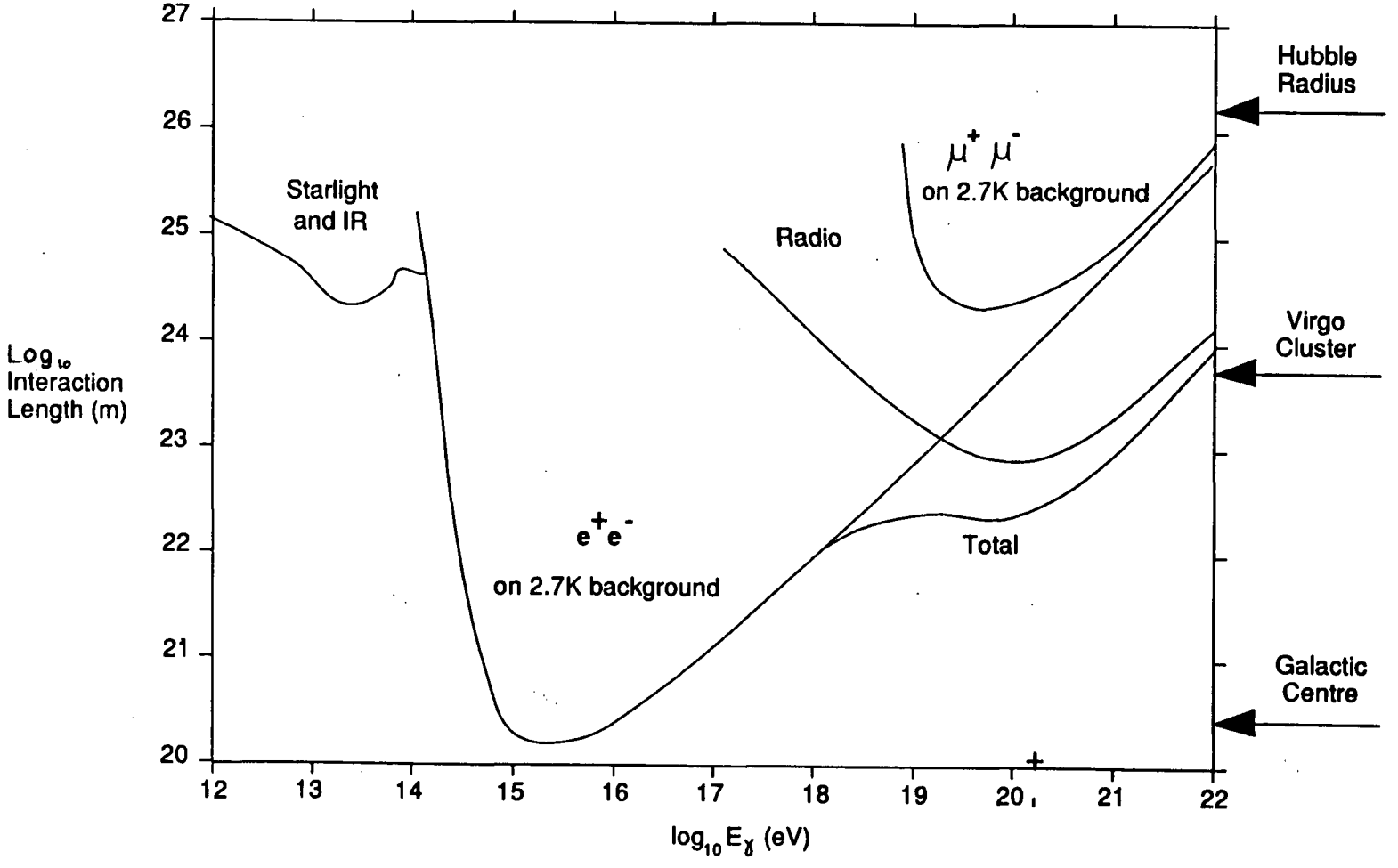

Figure 1.6: Energy dependence of the gamma ray interaction length to pair production with photons from various backgrounds (From Ramana Murthy and Wolfendale, 1986)

1.4.3 Absorption by Magnetic Fields

This is essentially the same process as that described above, with the gamma ray being scattered by a "virtual photon" from the magnetic field. Pair production by gamma rays within an intense magnetic field is discussed by Erber (1966) and Ogelman et al. (1976). For VHE gamma rays this process is only important in extreme magnetic fields (10^8 T). Magnetic fields of this magnitude only exist near the surface of neutron stars making this an unimportant mechanism of absorption over galactic distances. It is, however, an important constraint on the production sites of gamma rays emitted from neutron stars.

1.5 Summary

The gamma ray region of the electromagnetic spectrum was the last to be exploited as an astronomical window. A paper by Morrison (1958) prompted much experimental work and is generally recognised as the inception of gamma ray astronomy. All astronomical disciplines provide information on the behaviour of physical law in extremes of temperature and pressure. Gamma ray astronomy is the study of the highest energy light quanta and as such provides information about the physical processes which prevail in the most extreme environments. Of particular interest are the massive black holes which are the engines of active galactic nuclei, the emission regions in the vicinity of massive compact objects and the as yet unidentified source of cosmic rays.

The mechanism of the radiation of Cerenkov light and its production within the atmosphere is the subject of Chapter 2. The instruments used in its observation are introduced in Chapter 3.

CHAPTER 2

GROUND BASED GAMMA RAY ASTRONOMY

2.1 Introduction

The phenomenon of atmospheric Cerenkov radiation allows the exploration of a region of the electromagnetic spectrum that would otherwise be impractical to study. Energetic gamma rays (> 100s MeV) can be detected above the earth's atmosphere in spark chamber experiments. the most sensitive contemporary example is the Energetic Gamma Ray Experiment Telescope (EGRET) instrument on the NASA Compton Gamma Ray Observatory (CGRO) satellite. However, the celestial gamma ray spectrum approximates to a power law and consequently the collecting area of the largest spark chamber instrument that could be placed into earth orbit rapidly becomes inadequate to investigate the highest energy gamma rays (> 10 GeV). Atmospheric Cerenkov astronomy provides the facility to extend this astronomical window to higher energies. This chapter introduces the Cerenkov radiation mechanism and then describes the production of such radiation within the atmosphere.

2.2 Cerenkov Radiation

Production of light via the Cerenkov mechanism was proposed by Heaviside (1890), and it is probable that Marie Curie was the first to notice the bluish white light characteristic of Cerenkov radiation emanating from glass phials containing concentrated radium solution. Since this observation made around 1910, concomitant with the discovery of nuclear

radiation, Cerenkov light has been observed in various dielectric media in the vicinity of radioactive materials (eg Mallet, 1926). The prerequisite properties of particles to allow production of the radiation within a dielectric is that they are charged and very energetic. Cerenkov radiation can be viewed as an electromagnetic shock wave propagating within a dielectric medium in a manner directly analogous to an acoustic shock wave, the shock advancing as a conical wavefront with the perturbing particle at its apex. A fuller description of Cerenkov radiation is given in Section 2.3.

The early pace of investigation was slow with most effort being directed at the rapidly developing field of radioactivity, and the more conspicuous associated phenomena of fluorescence and phosphorescence. Ultimately though, it was through the study of these other forms of luminescence that Cerenkov radiation became recognised as an independent mechanism for production of electromagnetic radiation within the visible spectrum.

The first systematic study of the Cerenkov effect was made by Mallet (1926, 1928 and 1929) who was able to show that the spectrum was continuous, which distinguishes it from the spectra due to fluorescence. Cerenkov then conducted a series of experiments between 1934 and 1938 (Cerenkov, 1937) during which he demonstrated that the site of production of the radiation was modified by the presence of a magnetic field (Cerenkov emission in the vicinity of a source of uncharged ionising radiation must be due to charged secondary particles). The results of the experimental work of Cerenkov subsequently proved to be in excellent agreement with a theoretical electromagnetic treatment of the mechanism proposed by Frank and Tamm (1937). A natural progression was provided by Ginzberg (1940) who contributed a quantum mechanical treatment and also coined the expression Cerenkov radiation.

2.3 The Physical Basis of Cerenkov Radiation

A lucid, qualitative physical description of the Cerenkov effect has been given by Jelley (1967), and forms the basis of the following description.

As a charged particle moves through a dielectric the atoms of the medium in the locality of the particle become polarized. The distorted atoms behave as elementary dipoles, each aligned with its axis pointing at the particle. Figure 2.1 illustrates the instantaneous local polarization of molecules within a dielectric when traversed by, (a) a slowly moving negatively charged particle, and (b) the same particle moving relativistically.

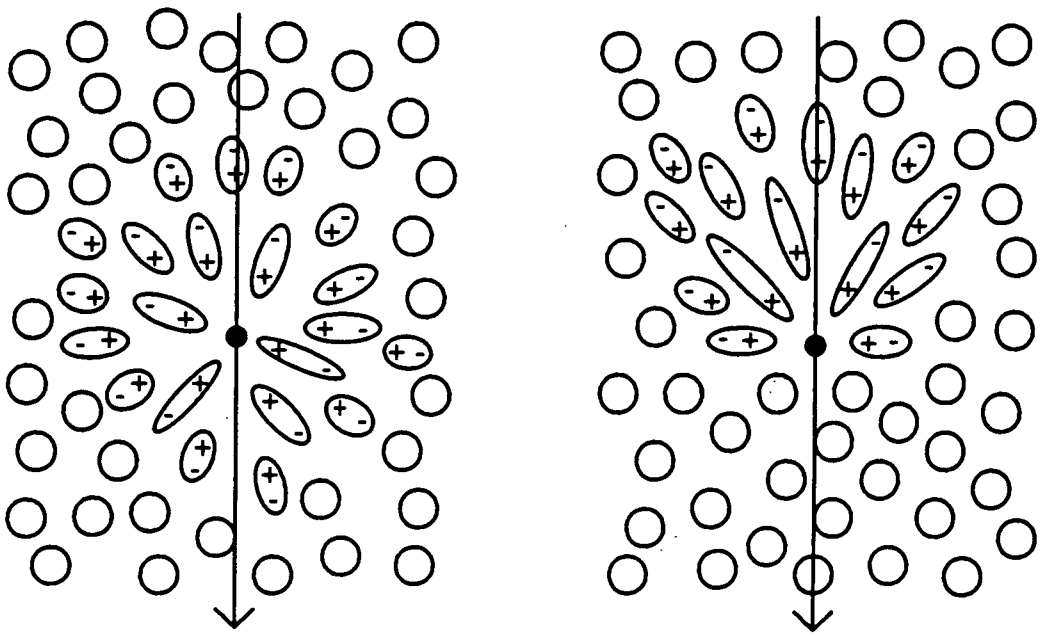

Figure 2.1: Polarization of molecules within a dielectric when traversed by a charged particle with a velocity, (a) less than the phase velocity, and (b) greater than the phase velocity of light in the medium.

If the particle is moving relatively slowly, the polarization field surrounding the particle is completely symmetric, both axially and azimuthally, and so there is no resultant field at distances significantly larger than the extent of

the local polarization. However, in the case of a very energetic particle moving with a speed comparable to the phase velocity of light in the medium, the axial symmetry is lost. At any point considered along the path of the particle there exists a resultant dipole field whose influence will be apparent away from the perturbing particle.

The electromagnetic pulse generated by the instantaneous dipole field can be understood as being due to a retarded electric potential. As the dipole field moves past each point within the dielectric the axial component of the polarization vector is perturbed, first in one direction relative to the path of the particle and then in the reverse direction, taking the form of the first derivative of a delta function with respect to time.

The electromagnetic pulses can then be imagined to propagate on a spherical wavefront from each point on the particle track. If the velocity of the particle is less than the phase velocity of light in the medium then the wavefronts interfere destructively at all angles to the particle path. If, however, the velocity of the particle exceeds the phase velocity of light then there exists a conical wavefront on which "wavelets" from each point on the particle track are coherent in phase, such that at a distant point there exists a resultant field. Figure 2.2 is a simple geometrical construction which illustrates each condition. From the figure it is evident that radiation will be observed exclusively at one angle to the direction of travel of the particle. That angle is given by;

$$\mathrm{Cos}\theta = \frac{1}{\beta n}$$

which is widely referred to as the "Cerenkov relation" with θ known as the Cerenkov angle. β is the ratio between the velocity of the particle and the

velocity of light ($\beta = v/c$) and n is the refractive index of the medium the particle traverses.

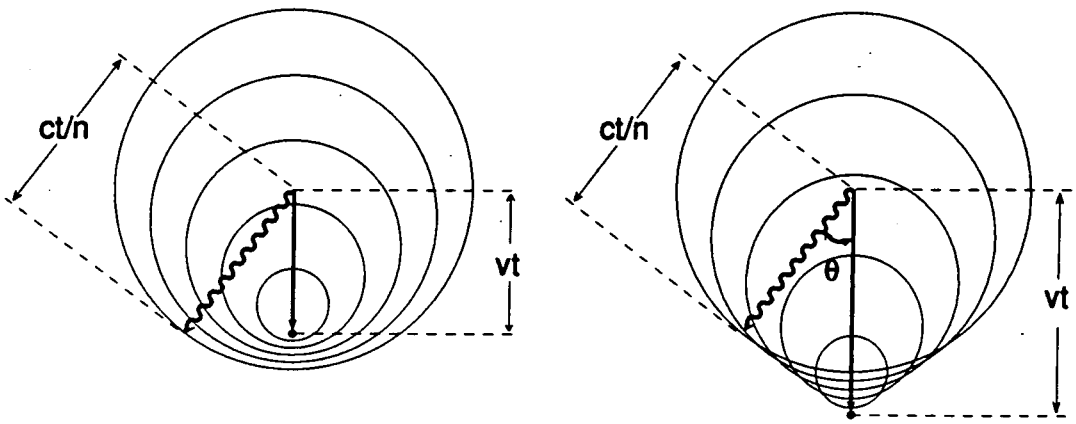

(a) v = 0.8 c/n (b) v = 1.25 c/n

Figure 2.2: The different physical environment which prevail for radiation emitted by a charged particle with a velocity, (a) less than, and (b) greater than the phase velocity of light in the dielectric medium.

The classical electromagnetic treatment due to Frank and Tamm, (1937) gives an expression for the energy radiated dE, at a frequency ω, in frequency bandwidth $d\omega$ (rad s^{-1}), from a path length dl, which in its most general form is given by;

$$dE = Z^2e^2\sin^2\theta.\omega.d\omega.dl / c^2$$

This equation and the Cerenkov relation above illustrate some of the constraints upon the characteristics of Cerenkov radiation. We can see that the spectrum of the radiation is proportional to $\omega d\omega$ for values of ω for which the Cerenkov relation is satisfied ($\beta_{min} = 1/n$ is the threshold velocity below which Cerenkov radiation ceases, this velocity is unattainable in the X ray region where n is less than unity). We would therefore expect most of the radiation to be emitted at higher frequencies (the blue end of the visible

spectrum). Quantum mechanical treatments give essentially the same results (Ginzberg, 1940).

2.4 Cerenkov Radiation in the Atmosphere

2.4.1 Introduction

Blackett (1948), during a study of the brightness of the night sky, was the first to recognise that Cerenkov radiation may be produced within the atmosphere. The refractive index of air in the atmosphere is everywhere >1 for visible light, taking the value 1.00029 at standard temperature and pressure (STP). As a consequence of this values proximity to unity, the associated parameters describing emission are severely constrained. The threshold energies of the particles are very high and the emission is strongly beamed (the maximum possible value for the Cerenkov angle within the atmosphere is 1.3° at STP). It is these features which give the effect its utility in ground based gamma ray astronomy.

2.4.2 Extensive Air Showers (EAS)

So far we have considered the Cerenkov effect on the basis of a single charged particle traversing a homogeneous dielectric. Cosmic rays and very high energy gamma rays which interact with the atmosphere do so catastrophically creating a cascade of daughter particles and energetic photons. These cascades are known as extensive air showers (EAS).

The evolution of showers is complex. The primary may be either a gamma ray, an electron or a nucleon. The first interaction of a gamma ray with the atmosphere involves electron-positron pair production in the vicinity

of an atomic nucleus. The electron pair, each with almost half of the energy of the incident gamma ray, emit further energetic gamma rays by the Bremsstrahlung mechanism as they encounter further atomic nuclei. As the interaction lengths for pair production and Bremsstrahlung are comparable, simplistically we can say that after n interaction lengths there are 2^n individual components to the shower, comprising electrons, positrons and gamma rays. Their average energy is $E_o/2^n$. This exponential growth continues until ionisation replaces Bremsstrahlung as the dominant energy loss mechanism of the electrons and positrons. This occurs when the particle energies fall below 84 MeV.

The early development of an extensive air shower with a nucleon as its progenitor is a succession of strong interactions as hadrons collide with air nuclei. An avalanche of secondary nucleons and mesons results, the development of which is arrested when the particle energy is insufficient to allow multiple pion production (< 1 GeV). Pions are the ultimate product of the nuclear cascade. Neutral pions decay almost instantaneously into gamma rays, each initiating an electromagnetic cascade. High energy charged pions, with protracted lifetimes due to relativistic effects, undergo further interactions. Lower energy charged pions decay into muons. The muons have a spectrum of energies, with the higher energy particles surviving to greater atmospheric depths. The muon decay products are electrons and positrons which may be the seeds for further low energy electromagnetic cascades. Muons which do decay will be at the lower end of the muon energy spectrum, thus few of the electrons and positrons produced as decay products will exceed the threshold for Bremsstrahlung radiation. Neutrino production is associated with both pion and muon decay and the neutrino flux forms an important hidden component of the shower.

The electron cascade initiated by a photon emanates from one point and

then develops and degrades in a predictable manner. In contrast, electromagnetic cascades in a hadron initiated shower emanate from the points of decay of many mesons created in the preliminary nucleon cascade. Figure 2.3 illustrates the complexity of a hadron initiated EAS.

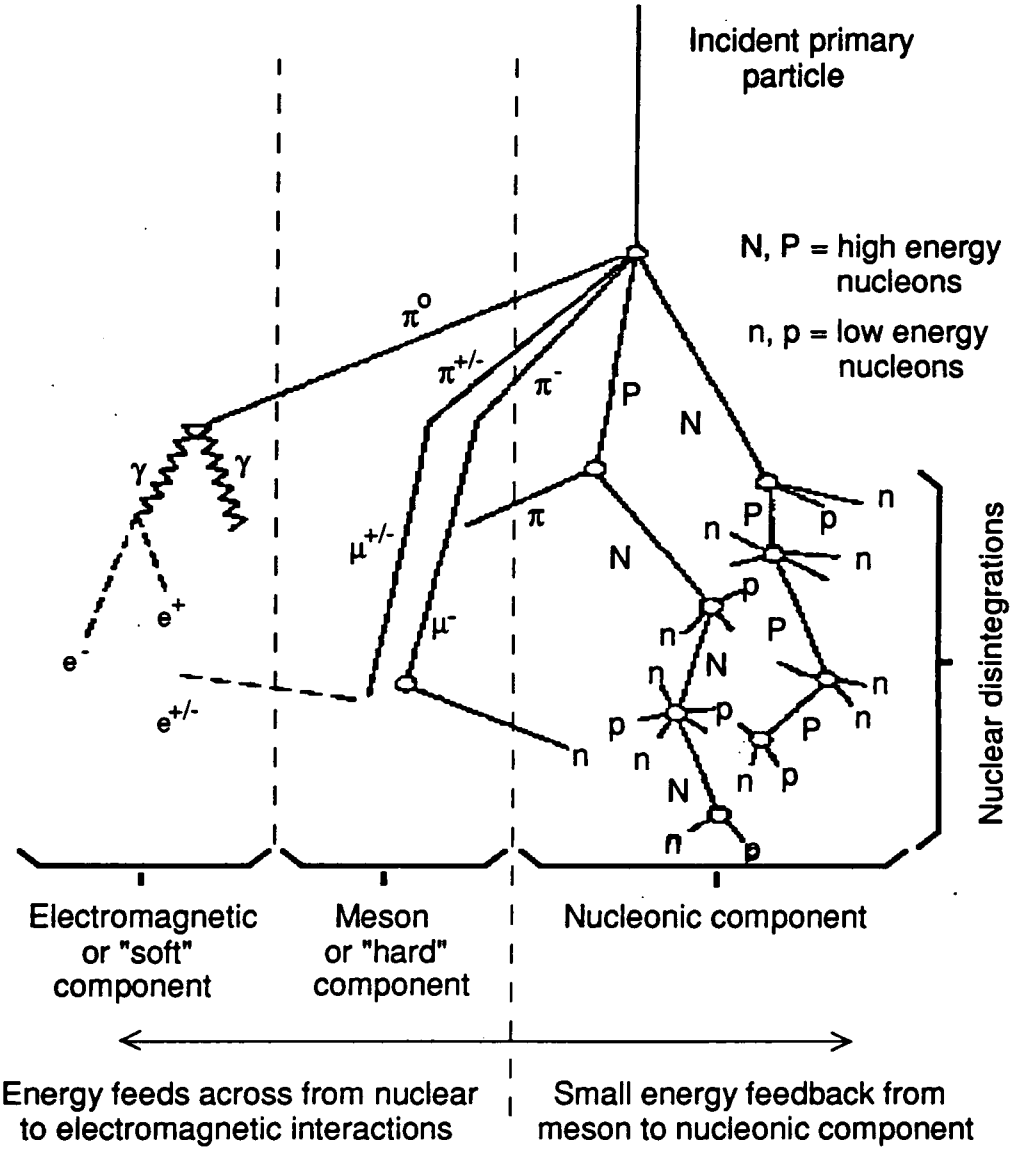

Figure 2.3: Schematic representation of hadron initiated EAS development.

(After Simpson, Fonger and Treiman, 1953)

Cerenkov light is produced by all of the charged components of the EAS

which have energy in excess of the threshold for Cerenkov radiation production. These threshold energies, which are a function of mass, are for an electron 21 MeV, a muon 4.4 GeV and a proton 39 GeV at sea level. Its occurrence in large numbers and its relatively low threshold energy conspire to make the electron the predominant source of Cerenkov light in an EAS (Boley, 1964).

The majority of Cerenkov radiation production then, occurs within a window in the shower's development bounded by the initiation of the first electromagnetic cascade, and the point at which the last cascade succumbs to ionisation loss. In the case of a gamma ray initiated shower this window is well defined. The maximum intensity of Cerenkov production is achieved just as the 84 MeV threshold is reached, at which ionisation supersedes Bremsstrahlung as the predominant mechanism of energy dissipation within the air shower. For a 300 GeV gamma ray this occurs after about 8 radiation lengths which corresponds to an atmospheric depth of 300 g cm^{-2} (Longair, 1992).

Atmospheric density decreases exponentially with height, thus by integrating from infinity (effectively the top of the atmosphere) down, we can show that for a vertically incident gamma ray this depth of maximum corresponds to a height above sea level of 10km (the total column density of the atmosphere is approximately 10^4 kg m^{-2}). The variation of the refractive index of air (η), with height (h), being proportional to density, is given by;

$$\eta(h) = 1 + (\eta_o - 1)\exp(-h/h_o)$$

where η_o is the refractive index of air at STP and h_o is the atmospheric scale height (~7.1km). Figure 2.4 illustrates trends in the characteristics of Cerenkov emission through the atmosphere.

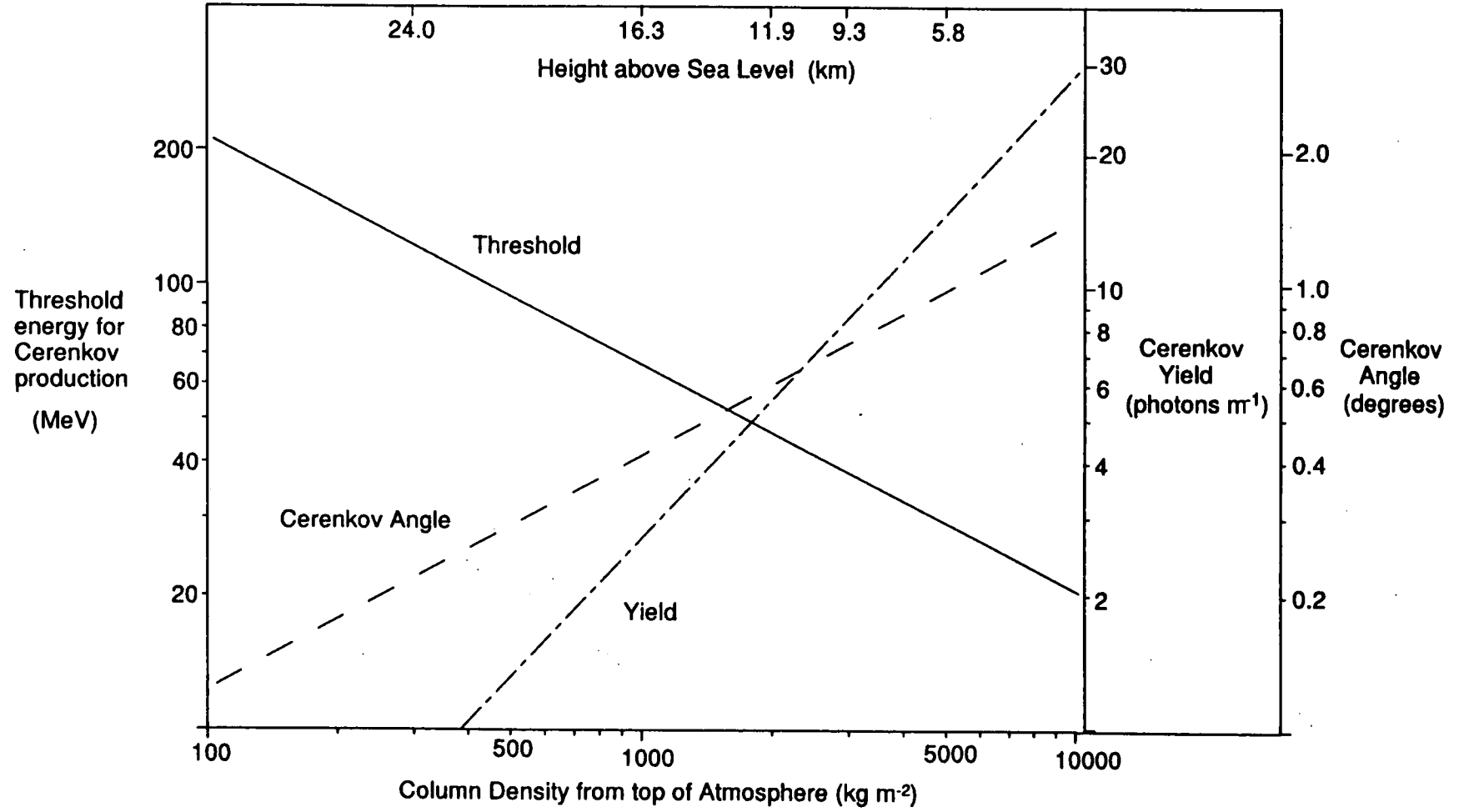

Figure 2.4: Parameters describing Cerenkov radiation production by relativistic electrons in the atmosphere. (after Ramana Murthy and Wolfendale, 1986)

The figure shows values for a vertically incident gamma ray, yield being related both to path length within the atmosphere and to the local refractive index (which is dependent upon the height above sea level).

2.4.3 The Cerenkov Light Pool on the Ground

2.4.3.1 Lateral Distribution

Secondary cascade particles are strongly beamed due to their extreme energies, and on average retain the directionality of the primary. As a consequence of the logarithmic density distribution of the atmosphere the cascade develops rapidly, with many interaction lengths traversed in a short time. This serves to constrain the secondary particles to a very thin disc (almost a plane wave), the lateral extension of which is due to the opening angles of the interaction processes and multiple coulomb scattering. Coulomb scattering dominates the electron distribution and thus is the predominant mechanism defining the form of the light pool produced by the purely electromagnetic, gamma ray initiated, cascade. Conversely an additional process of importance when considering the more massive hadrons is the angle of emission, more specifically the incipient transverse momentum of the pions. The opening angles of the nuclear processes are, in general, small on the scale of the electromagnetic cascade, thus the hadronic component of a cascade constitutes what is effectively a line source for particles which will initiate further electromagnetic cascades.

A gamma ray initiated shower is wholly electromagnetic and one might imagine a horizontal particle distribution around the axis which is Gaussian in section. If the atmosphere were of uniform density the Cerenkov radiation intensity on the ground would mirror this distribution. However, the

distribution in the Cerenkov light pool at ground level is modified by the variation of the Cerenkov angle with altitude. If one considers the cascade as lying close to the direction of beaming in comparison with the Cerenkov opening angle, then one can conceive of an intensity distribution which is deficient towards the axis and enhanced at a range of larger radii. For certain shower configurations this effect is quite marked (Hillas,1982). Figure 2.5 is a schematic illustrating this condition.

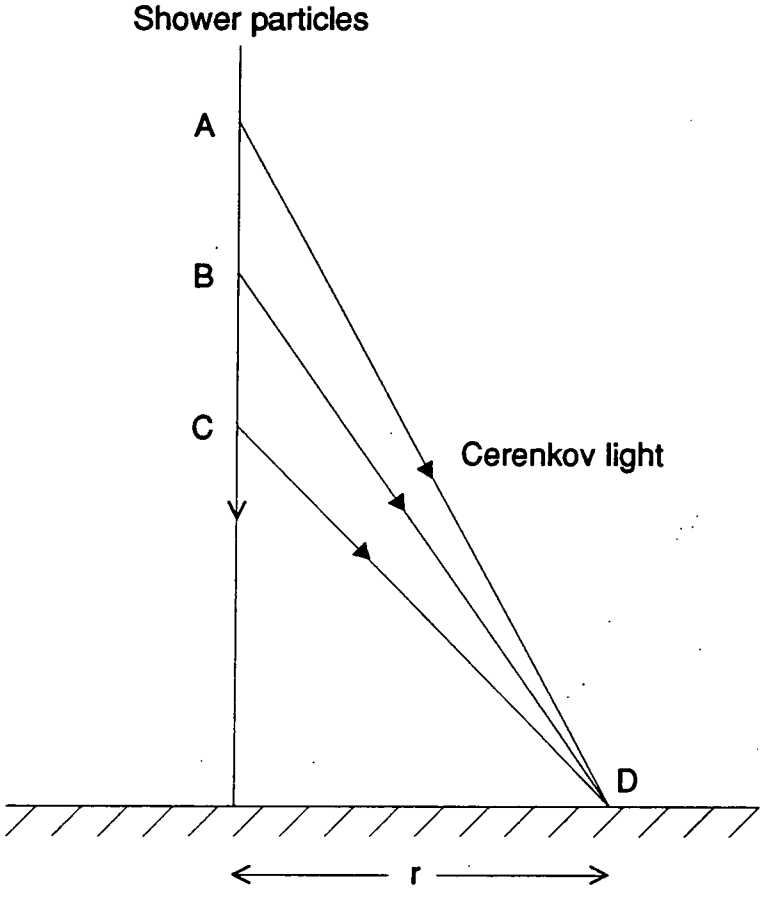

Figure 2.5: Schematic illustrating production of the "Cerenkov shoulder" in the gamma ray light pool. The increase in Cerenkov angle with refractive index of the atmosphere is compensated for by the reduced height of emission along the axis. This results in a deficiency of light close to the axis, and an annulus of enhanced intensity at a radius of about 150m.

In the case of a hadron initiated extensive air shower the energy in the electromagnetic component of the shower is concentrated more towards the shower axis, with the electromagnetic cascade continually replenished on the axis by the hadronic core. As a result, a proportion of the Cerenkov light from the electromagnetic cascade is produced lower in the atmosphere than for a cascade initiated by a gamma ray of similar energy. This gives a Cerenkov profile with a definite peak on the axis and a significant fall off in intensity with radius. Figure 2.6 shows the results of Monte Carlo simulations of the lateral distribution of Cerenkov light for gamma ray and hadron initiated extensive air showers at sea level. The gamma ray initiated event has a relatively flat plateau extending out to a radius of about 150 m, with a rapid fall off of intensity external to this area. There is evidence of the Cerenkov shoulder. In contrast, the nucleon initiated event has a profile with a narrow peak, with several randomly distributed subsidiary peaks. These smaller peaks are due to Cerenkov light from local penetrating muons, or sub showers initiated by the decay products of high transverse momentum charged pions.

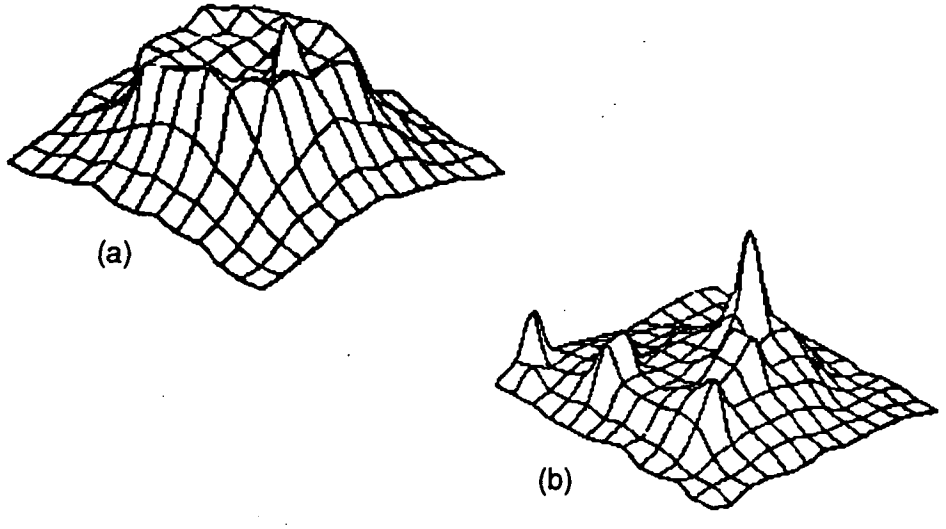

Figure 2.6: Cerenkov photon densities at ground level from Monte Carlo simulations of EAS initiated by, (a) a 320 GeV gamma ray, and (b) a 1 TeV hadron. Grid spacing is 50 m. (After Hillas and Patterson, 1987)

2.4.3.2 Temporal Distribution

If we consider a group of relativistic particles constrained to a region around the shower axis, then the intensity profile of the Cerenkov signal produced by these particles on the shower axis is a function of the refractive index of the atmosphere (assuming all the particles continue to travel at close to the speed of light). The Cerenkov light emitted closer to the ground arrives first, with the light emitted earlier being delayed by a time which is proportional to the column density of atmosphere traversed. Now consider moving away from the shower axis. The increasing path length for the Cerenkov light produced near the ground to the corresponding point on the light front serves to compress the time profile. Thus, for a gamma ray, the Cerenkov pulse width reaches a minimum at the radius corresponding to the Cerenkov shoulder, outside this radius the time sequence inverts with the light produced early in the shower arriving first. This is a simplistic picture which takes no account of the finite thickness of the shower front or the lateral extent of the shower, but nonetheless provides a useful illustration.

2.5 Summary

The gamma ray flux above a few GeV is so small as to render the collecting area of satellite borne instruments inadequate. However, at energies in excess of a few tens of GeV, the EAS precipitated in the atmosphere by the energetic gamma rays comprise particles with sufficient energy to radiate by the Cerenkov mechanism whilst traversing the atmosphere. Directionality of the primary is retained due to the narrow opening angle of the Cerenkov cone and so the atmosphere can be incorporated as an active component of instrument design. The efficacy of

the method is due to the extent of the light pool on the ground which defines the possible collection area of the telescope. For example, a Cerenkov angle of 1° defines a collection area of slightly less than 10^5 m^2 for a shower which maximises 10 km from the detector. This collecting area is 5 orders of magnitude larger than the most sensitive satellite borne spark chamber experiment, offering the potential to turn an intrinsically low flux into an acceptable count rate. The atmospheric Cerenkov technique therefore opens the window on the gamma ray spectrum from tens of GeV to tens of TeV.

At higher energies (> 50 TeV) substantial numbers of extensive air shower particles persist to ground level and are detectable by scintillator arrays. The atmosphere serves to dissipate the energy of the incident particle or photon amongst a multitude of daughter particles which collectively retain the directionality of the primary. The field of view of a scintillator array incorporates most of the sky and its collection area is limited only by the area of the array. Thus reasonable statistics can be obtained from the extremely small flux of primaries of these energies.

Chapter 3 introduces the instrumentation used in the detection of atmospheric Cerenkov radiation and considers the optimisation of such equipment to the application of ground based gamma ray astronomy.

CHAPTER 3

THE PERFORMANCE OF GROUND BASED GAMMA RAY TELESCOPES

3.1 Introduction

The physical basis of the phenomenon of Cerenkov radiation in general, and its production within the atmosphere in particular, has been outlined in Chapter 2. The aim of this chapter is to introduce the equipment which is used to detect atmospheric Cerenkov radiation in ground based gamma ray astronomy, and to discuss the relative merits of competing detection philosophies.

The chronological development of the telescopes operated by the Durham group is used as the central theme to this chapter. The group has been active in gamma ray astronomy for 15 years and its hardware development programme, evolving with the field, reflects the status of contemporary ground based gamma ray astronomy projects.

Initially, the broad properties of atmospheric Cerenkov radiation from EAS and the comparative brightness of the night sky will be discussed, and their bearing on the choice of photosensitive device and associated electronics considered. A brief account of the Dugway experiment, operated by the Durham group between 1981 and 1984, gives an indication of the operating conditions and performance of a simple atmospheric Cerenkov detector.

The leap in sensitivity gained in the progression from operation of the Dugway Mk.1 and Mk.2 detectors to the Mk.3 telescope in Narrabri demonstrates the merit of large flux collectors and introduces a simple method of noise rejection based on constraining the Cerenkov signature of

EAS to lie within a small aperture. The remainder of the chapter concentrates on more sophisticated rejection strategies based on the differences between the Cerenkov signatures of gamma ray and hadron initiated extensive air showers. These strategies were devised using data derived from detailed Monte Carlo models of extensive air showers (Turver and Weekes, 1977; Hillas, 1985).

3.2 Very High Energy Gamma Ray Detection From the Ground

3.2.1 A Ground Based Gamma Ray Telescope

An atmospheric Cerenkov detector comprises a photosensitive device at the focus of a reflector. The reflector, which serves to collect the Cerenkov flux and afford directionality, can be of several different forms, each with advantages in different detection strategies. Competing detection philosophies have evolved from this rudimentary detector, each with its own advantages and potential for signal enhancement.

3.2.2 The Photosensitive Device

The principal challenge in the telescope design is to effectively resolve the Cerenkov component of the night sky above the background of ambient starlight. This may seem like a difficult task when one considers that Cerenkov radiation contributes only 10^{-4} of the total integrated photon flux. However, as a consequence of the near parity of the phase velocity of light in the atmosphere and the velocity of the radiating charged cascade particles, and the fact that the shower develops and propagates as a well defined shower front, this energy is concentrated into very short bursts. The

rise time of the Cerenkov signal is typically a few nanoseconds, and close to the shower axis its duration rarely exceeds ten nanoseconds. This is much shorter than the characteristic duration of any other atmospheric or astrophysical process which produces visible light. Thus, by matching the time constant of the detection system to that of the Cerenkov flash, an acceptable signal to noise ratio can be achieved. The sample of light intercepted by the flux collector is typically of the order of a few tens or hundreds of visible photons per square metre. The requirement is then for a photosensitive detector with an exceptionally fast response and a high intrinsic gain. The photomultiplier (PM) tube is ideally suited to this application. It has a fast rise time (typically 2 ns), a high gain (of between 10^3 and 10^8, negating the need for significant further amplification), and the requirement for a suitable spectral response is easily satisfied. The rest of the electronic equipment making up a gamma ray telescope comprises fast analogue and digital electronics to select the Cerenkov signal and record the output of the PM tubes.

3.2.3 Photomultiplier Noise

Observation of the night sky is an unusual application for PM tubes in which they are subject to comparatively high illumination. If they are to be run in a state where individual photoelectrons can be resolved their gain will be very low. In practice the PM tubes are run with appreciable gain and operate in a condition of photoelectron 'pile up' in which the background flux is manifested as a DC offset in the tube output. Fluctuations in this background are Poissonian and the Cerenkov flashes are observed superimposed on this noise.

Consider a simple Cerenkov telescope comprising a single PM tube at the

prime focus of a flux collector. The number of photoelectrons due to the night sky background is the product of the effective Collector area A, the PM tube quantum efficiency ε, integration time τ, the solid angle subtended by the photocathode Ω, and the night sky background flux ϕ. The noise, N, in the system is the square root of this function.

$$N = (A\varepsilon\tau\Omega\phi)^{1/2}$$

The number of photoelectrons due to the Cerenkov radiation, the signal, is given by;

$$S = A\varepsilon\rho$$

where ρ represents the Cerenkov photon flux. This assumes that Ω and τ are both large enough to encompass the whole Cerenkov signal. The signal to noise ratio is therefore

$$\frac{S}{N} = \frac{(A\varepsilon)^{1/2}\rho}{(\tau\Omega\phi)^{1/2}}$$

The minimum detectable flux is proportional to the inverse of this function.

3.2.4 The Fast Coincidence Triggering Technique

The tenet that has underpinned the work of the Durham group has been the conviction to operate its telescopes at a high gain and consequently low energy threshold. In order to achieve this, a triple fast coincidence system has been adopted to allow the photomultiplier tubes to be operated with

high individual tube noise rates. Three independent paraxial flux collectors are used with photomultipliers at the prime focus of each viewing the same region of sky. A condition is imposed that for an event to be recorded the output of the tubes viewing each of the three dishes must each exceed a discrimination threshold within a narrow coincidence time interval. This fast coincidence technique formed the basis for the earliest observations and has been shown, by recent simulations, to be particularly efficient when combined with an appropriate field of view (Patterson and Hillas, 1989). The rate R (Hz), at which the noise from each PM tube will fulfil this three fold coincidence criterion by chance is given by

$$R = 3!\, n^3 t^2$$

where n is the count rate for a single PM tube in Hz and t is the coincidence gate width in seconds.

The choice of the number of independent flux collector / PM tube units to be used in coincidence, for a given area of available collector, is a compromise between the potential increase in gain and the reduction in individual flux collector area with increase in fold of coincidence. The optimum configuration is dependent upon the variation of noise with gain at particular illuminations of the PM tubes. In the case of the design of the Mk.3 telescope the performance from an n fold coincidence system was evaluated (with a constant low accidental rate) on the basis of empirically determined noise rates as a function of illumination and gain. Figure 3.1 shows the results with the expected telescope background count rate approaching a maximum value asymptotically (Brazier, 1991). The rate for a three fold coincidence system is within 15% of the maximum but is significantly greater than that for a two fold coincidence system. The rather

meagre improvement in performance achievable by the increase to four fold coincidence is offset by the accompanying increase in complexity in the electronics. The Durham group therefore chose three fold coincidence as a cost effective, compromise solution.

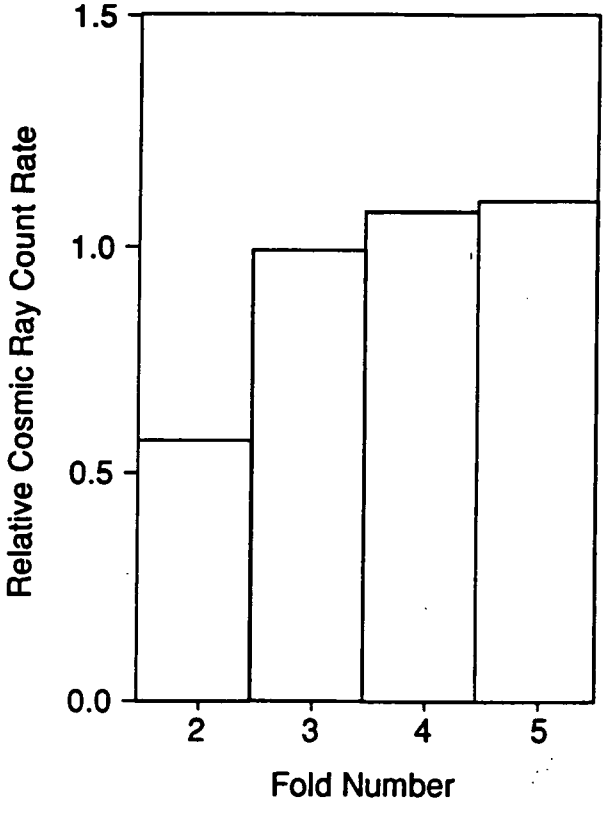

Figure 3.1: Estimated relative count rates versus number of detectors in coincidence for unit flux collector area (after Brazier, 1991).

A gate width of 10ns, comparable to the duration of the Cerenkov signal, would allow the tubes to be run with noise rates of 10 kHz with an accidental coincidence count rate of one per hour. This is negligible in comparison with the background counts due to the hadronic cosmic ray flux.

An additional advantage associated with the triple fast coincidence system is the suppression of background events due to local muons. Charged muons passing through the window material of the PM tubes will radiate Cerenkov light, in some instances of sufficient intensity to exceed the

discrimination threshold. An instrument which employs a single detector package, with a trigger requirement for two or more tubes to exceed threshold within a specified gate interval, will be troubled by spurious events generated by the passage of muons through the windows of adjacent PM tubes (Vacanti et al., 1993). A multiple coincidence telescope with separated detector packages will not suffer this problem.

3.2.5 Conclusion

The triple fast coincidence system has formed the basis for the telescope development programme of the Durham group, allowing the PM tubes to be operated at high gain giving the optimum energy threshold for a telescope of given flux collector area. This is believed to be important when seen in the context of possible soft gamma ray source spectra and a harder proton background spectrum.

3.3 A Brief Summary of the Dugway Telescopes

3.3.1 The Durham Facility at Dugway, Utah

The Dugway Proving Grounds (40.2° N, 112.8° W) are at an altitude of 1450m above sea level. An array of four telescopes was commissioned at this site in Utah by the University of Durham in May 1981, and operated until October 1984. The detectors were arranged at the apices and centre of an equilateral triangle of side 100m. This configuration was chosen, on the basis of computer simulations of the Cerenkov flash anticipated from 1 TeV gamma rays, as a compromise between effective area for multiple telescope response to individual Cerenkov showers and angular resolution of an array

of telescopes. A smaller separation between detectors would have given a larger rate of multiple responses but would have degraded the angular resolution of the array.

3.3.2 The Mk.1 Telescope

Each Mk.1 telescope comprised three paraxial 1.5 m diameter searchlight mirrors on a computer controlled alt-azimuth mount. Positional information was provided by incremental shaft encoders and drive by DC servo motors; the pointing accuracy was good to 0.1°. The f number of the searchlight mirrors of 0.43 defined a very small image scale at the prime focus and gave an inappropriate aperture for the large diameter (RCA type 4522) PM tubes available. A cassegrain system was adopted to overcome this limitation. Secondary mirrors with a diameter of 25 cm and focal length 115 cm were fabricated from aluminium and the PM tube was masked down to an aperture of 5cm, which defined a geometrical field of view of 2°. A complete description of the Mk.1 telescope and the Dugway array is given by Macrae (1985).

3.3.3 The Mk.2 Telescope

In 1983 an experiment in low cost mirror manufacture was made and one of the telescopes was remirrored with purpose-built, polished, solid Dural mirrors. Seven circular mirrors were arranged in a hexagonal pattern to form each collector. Each mirror facet, of spherical form, had a diameter of 60cm and a focal length of 2.21m. A 2" diameter RCA 8575 PM tube was placed at the prime focus of each collector, eliminating the need for the secondary mirror and defining a geometrical aperture of 1.1° for the

photocathode. Anode current response to a passage of a star through the field of view showed the physical aperture to a point source to be 1.3° at FWHM. Light transmission losses were significantly reduced due to the removal of the need for the second reflector. The Mk.2 telescope is described in detail in Dowthwaite (1987).

3.3.4 Performance of the Dugway Telescopes

A useful yardstick by which telescopes may be compared is their energy threshold, often derived from the response of the telescope to the isotropic and relatively well defined cosmic ray spectrum. For simple telescopes the relative energy thresholds are a function of count rate. For reliable comparisons of threshold to be made however, the count rate of any telescope must be qualified by specifying the field of view and the assumed collecting area of the telescope. As the intensity profile of the Cerenkov light pool produced by a proton shows a marked gradient away from the shower axis, the collecting area will be a function of primary energy. However, because of the steep integral spectrum for cosmic ray protons it is adequate to use an estimate for the collection area at the threshold of the telescope. In the case of the Dugway experiment this can be estimated from the observed single and multiple telescope responses of the array. A collection area of radius 45 m was assumed for the Mk.1 detectors (Dowthwaite, 1987). Computer simulations of 1 TeV gamma rays showed the aperture function for the telescope to be Gaussian in form with a FWHM of 2.2° +/- 0.2° (Macrae,1985). Once normalized for collection area and field of view, count rates can be compared with the cosmic ray flux to derive an energy threshold for cosmic rays. Dowthwaite (1987) has estimated the proton threshold of a Mk.1 detector to be about 2500 GeV based on a zenith

count rate of 16.9 counts per minute. In order to calculate the gamma ray threshold recourse must be made to computer simulations modelling the relative response to gamma ray and proton initiated Cerenkov events. Simulations have shown that above 1000 GeV gamma rays are twice as efficient as protons at producing Cerenkov photons (Zatsepin and Chudakov, 1962; Turver and Weekes, 1977). A gamma ray threshold of 1300 GeV has been quoted for the Mk.1 telescope. Following the same reasoning a threshold of 800 GeV was assigned to the Mk. 2 telescope (Chadwick et al., 1985).

	Mk.1	**Mk.2**
Collector Area	1.77m^2	2.04m^2
PM Tube Diameter	50mm	46mm
Focal Length	1.5m	2.21m
Geometrical Aperture	2°	1.1°
Reflectivity	35%	55%
Typical Count Rate	15 c.p.m.	11 c.p.m.
γ Threshold	1300 GeV	800 GeV

Table 3.1: Physical characteristics of the telescopes of the Dugway array.

3.4 The Mk.3 and Mk.4 Telescopes

3.4.1 The Narrabri Facility

The Dugway telescopes were very successful, with detections of TeV gamma rays being claimed for a number of isolated and binary pulsars. It became evident, though, that the fluxes involved were at the limit of

detectability, and that an instrument could be designed and built that would offer a significant improvement in sensitivity. Evidence from the results of the Dugway experiment, suggesting that the X-ray binary systems (which were an unexpected source type) had the highest luminosities, prompted the decision to make observations in the southern hemisphere. Also, objects such as the Vela pulsar and Centaurus A, for which early claims of emission were made (Bhat et al., 1980 and Grindlay et al., 1975 respectively), are available for observation. The southern skies, as well as containing the majority of X-ray binaries, also incorporate the galactic centre and the large and small magellanic clouds, all of which are of enormous astrophysical interest.

The site chosen for the new telescope was the Bohena Settlement, Narrabri, N.S.W., Australia. Having previously been occupied by the University of Sydney giant air shower array (SUGAR) the site fulfilled all logistical requirements. Narrabri is situated in a region favoured by optical astronomers because of the high proportion of stable cloud free nights (50% according to staff at the Anglo Australian Telescope, 100km south of Narrabri). Rainfall is infrequent and skies in this rural environment are dark and clear. The altitude is 260m above sea level and geographical position 149° 49' E, 30° 29' S. The Mk.3 telescope was installed during 1986 and is still in use today as a platform for an instrument of significantly enhanced optics and electronics.

3.4.2 The Mk.3 Telescope

3.4.2.1 Introduction

The design of the Mk.3 telescope is a simple evolution of the Dugway

telescopes with refined optics. It follows from the decision to use the largest practical area of mirror on the mount available. PM tube packages were placed at the prime foci of three tessellated dishes of approximately parabolic section. The packages differ from those used in the preceding Dugway experiment in that a number of peripheral, off-source monitoring, channels were incorporated surrounding the on source channel. These channels are important in the verification of results, being sufficiently far from the optic axis to preclude their being triggered by gamma rays from the source region and so provide a continuous measure of the background flux. They subsequently proved to be of value in narrowing the effective aperture of the telescope, enhancing sensitivity to gamma rays by rejecting 50% of the cosmic ray background by acting as a guard ring.

3.4.2.2 Flux Collectors

The specification of a flux collector is inevitably a compromise between engineering practicality and the concept ideal. The requirements were for a large collecting area with a field of view (defined by the physical aperture function) close to the empirically suggested optimum for this system which is 1.3° FWHM. In the light of experience gained with the Mk.2 telescope it was thought that the 46 mm diameter photocathode of the RCA 8575 PM tube viewing a mirror with a focal length of 245 cm would be appropriate. The solid Dural mirrors used for the Mk.2 telescope had the required shape and image quality but had a moderate reflectivity (55 %) and were heavy and laborious to produce. An alternative method was developed based on that used to manufacture the antenna sections for the James Clerk Maxwell millimetre wavelength telescope. A thin (0.5mm) anodised aluminium (Alanod) sheet forms the reflective surface, bonded to a honeycombed

supporting structure. The reflectivity, of about 80 % between 300 and 500 nm, is a significant improvement on that of the polished Dural. The Alanod skin was stretched over a spherically figured steel former before the honeycomb and a sheet aluminium backing plate were bonded using an epoxy resin. Individual mirrors suffered significant aberration off axis, image size increasing from 1cm on axis to 5cm when 200cm off axis; this effectively constrained the dish diameter to around 4m. The total complement was 130 mirrors, each of 60cm diameter, giving each collector an effective area of 11 m^2. There has been no noticeable change due to mirror degradation throughout the life of the experiment, which is now approaching 10 years, showing the mirrors to be very durable.

The physical aperture to a point source for a complete tessellated collector was found to be 1.5° +/- 0.2° FWHM which is close to the specification (Chadwick, 1987). The system offers a 5 fold increase in flux collector area and a 45% increase in reflectivity over the Mk.2 telescope.

Optic axis alignment was effected utilising the anode current response of the on axis PM tubes to a raster scan over a second magnitude star. Peak anode currents in each of the on axis tubes was noted relative to the position of the image of the star produced by an analogue camera. The required adjustment was achieved by manipulating the structure supporting the detector packages. The reflectors were subsequently shown to be paraxial to within one steering bit, which corresponds to less than a tenth of a degree.

3.4.2.3 Photomultiplier Packages

Four triple coincidence channels were operated initially. One channel was dedicated to the three PM tubes which lie on the optic axis and under

normal operating conditions view the region of sky which includes the target source. The three remaining channels were originally conceived as off source monitors. Three sets of PM tubes arranged at 120° intervals around the central tube, viewing adjacent regions of sky 2° removed from the source, A further nine PM tubes in three channels were added later to give coverage at 60° intervals around the source.

The count rate of the telescope is given by the area under the cosmic ray energy spectrum above the threshold energy of the telescope. Because the spectrum is so steep, with the majority of events being around threshold, the count rates of these instruments are very susceptible to changes in gain. Gain variations of a few percent cause a similar percentage increase in count rate at threshold and in ground based gamma ray astronomy this is of the same order as the signal excesses expected above background for quite a strong source. In order to achieve a stable PM tube gain an automatic gain control system was employed. This consisted of a green LED close to the face of each PM tube servoed to its anode current. The additional illumination provided by the LED, typically 10% of the total illumination, could be offset against a brightening sky (brighter region of sky or a decreasing angle to zenith) or the passage of a star through the field of view, without significant increase in the accidental rate.

3.4.2.4 The Telescope Platform and Steering

An alt-azimuth platform, which was developed from a Royal Navy surplus gun mount, forms the mechanical base of the Mk.3 telescope. The mount comprises a box structure, steerable independently in the vertical and horizontal sense, to which the superstructure which supports the dishes is fixed. Drive specification for the telescope was for a maximum slew rate of

$1° s^{-1}$, and the ability to achieve this from rest in 10 s (the greatest moment of inertia, of about 10^4 kg m^2, is about the azimuth axis). A D.C. servo motor with an output torque of 20 Nm and integral gearbox was chosen to achieve this. Attitude of the telescope is sensed to a resolution of 5 arc minutes in altitude and azimuth using orthogonal 12 bit shaft encoders. Configuration of the steering was performed after the optic axes had been aligned. The shaft encoders provide absolute position and were zeroed by noting the encoder values for a number of widely separated stars (centred on the field of view using the anode current response of the PM tubes to the increase in illumination) and solving for the angular offsets in altitude and azimuth. The offset of the telescope's azimuthal axis from local vertical can also be calculated, this is allowed for by the tracking software as an offset in geographical location. Positional information is recorded for each event within the data stream. Pointing accuracy is monitored using a CCTV sky camera mounted paraxial with the flux collectors.

3.4.2.5 Time Keeping

The specification adopted for the timing accuracy for the Narrabri facility was that it should be adequate to retain phase on a 1 ms pulsar over the nine or ten months which constitute the duration of one observing season (ie accurate to within 1 part in 3×10^9). A Rubidium atomic oscillator was chosen as the timing standard. The Efratom model FRK-L Rb oscillator provides a 10 MHz output signal allowing events to be time stamped to μs accuracy. A battery back-up power supply, sufficient to bridge a ten day interruption in mains supply, is provided and the unit has internal batteries to allow it to be transported to compare it with time standards. The Rb clock was first synchronised with an off air radio time signal in January of 1987

and a broadcast time signal has been used regularly to measure the systematic drift of the oscillator. The clock is very stable, having a constant drift rate. As an oscillator which loses its power and is restarted is prone to drift at a different rate such interruptions are avoided. It has only been necessary to restart the clock twice, in July 1990 and August 1993. Drift rate since the latest interruption has been 0.05287 +/- 0.00005 ms day^{-1} (Roberts, priv. comm.). A Global Positioning Satellite (GPS) system replaced the off-air radio signal as the reference time signal in April 1992. Figure 3.2 is a graph demonstrating the remarkably stable drift rate relative to the value of UT (Universal Time) received from the Global Positioning Satellite system.

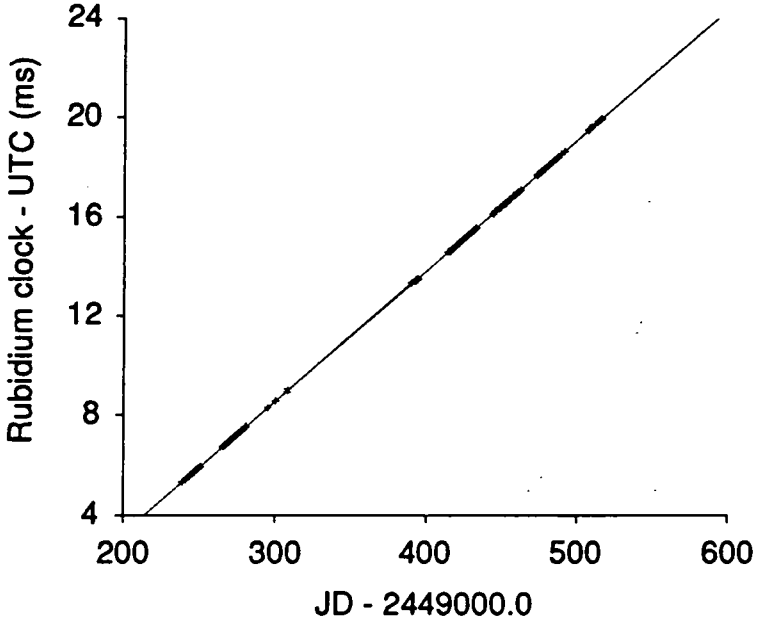

Figure 3.2: The drift of the rubidium clock delay measured relative to UTC.

3.4.2.6 Environmental Monitoring and Data Logging

The nucleus of the Mk.3 control electronics system is a Motorola 68000 based microcomputer. This computer was developed by the Durham University Microprocessor Centre which allowed its mode of operation to be

tailored for this application. As a result a very fast and versatile, high capacity logger / CAMAC electronics system was evolved. A low system dead time was considered paramount in the specification of the system and so the software was made interrupt driven, with a rank of priorities headed by data collection. This system, allied to the provision of 1 Mbyte of RAM buffer for data collection, facilitates the recording of transient bursts of intense activity. An event comprises; the arrival time to μs accuracy, the integrated charge from each of the PM tubes, a record of which of the 7 channels has achieved the condition for three fold coincidence, the target and actual zenith and azimuth pointing angles and the instantaneous anode current for selected PM tubes. The recording of this information occupies the processor for 350 μs. During this dead time the arrival times of a burst of 16 further events can be stored for recording, each with an individual dead time of 6 μs.

A Local Area Network (LAN), accessible to the 68000, is responsible for the control and monitoring of the telescope. One master microcomputer acts as the interface between the 68000 and the LAN, while 5 dedicated computers within the network perform the tasks of steering, telescope performance and environmental monitoring.

3.4.2.7 Overview of Telescope Electronics

The high voltage required for operation of the PM tubes is provided by a multi-channel LeCroy HV4032A E.H.T. unit. Every PM tube signal is passed to Automatic Gain Control (AGC) units which isolate the D.C. component of the analogue output of the PM tubes. The anode current of each PM tube is compared with a reference current generated by the 68000, and the error signal used to drive a LED in the servo loop which

stabilizes the anode current. The value of the measured anode current is passed to an analogue to digital converter. Anode current values of all 21 tubes are displayed at all times as these are an important measure of the operating condition of the telescope.

At the input of the AGC unit the signal from each PM tube is A.C. coupled to a VV100 amplifier within a LeCroy model 612A amplifier unit. After ten fold amplification the signal path is split. One of the signals goes to a voltage discriminator which has a peak voltage threshold which can be set by the 68000 via its CAMAC interface. The usual value is 50 mV. When this threshold is exceeded an output is generated and passed to a 3 fold coincidence unit. If the three signal paths which together constitute a coincidence channel each provide a signal within a narrow (10ns) gate then the channel is deemed to have fired. This generates an event signal. Each event signal initiates the charge to time converter (QT) units in the second signal path. The QT units are LeCroy model 2249A analogue to digital converters which digitise the charge integrals of the signals from all of the PM tubes during a 30 ns gate interval. The outputs of the QT units are scaled, and then logged by the 68000. An additional logic unit, the coincidence register, records which of the channels have fired for each event and its output is recorded in the event record.

3.4.3 The Mark 4 Telescope

This telescope is similar in design to the Mk.3 telescope, but with a reduced flux collector area of 3 x 6 m^2. Focal length and aperture are identical and the steering and electronics have similar specifications. The telescope was designed to be portable and was first deployed at the Observatorio del Roque de los Muchachos (18°E, 28°N, 2500 m above sea

level) on La Palma in the Canary Islands. It operated on La Palma from June to October of 1988 and 1989. In May 1990 it was assembled in Narrabri and operated in conjunction with the Mk.3 telescope until the summer of 1993.

3.4.4 Performance of the Telescopes

When the specification for the Mk.3 telescope was drawn up a count rate of 75 min^{-1} per channel was predicted based upon a model of telescope performance. This proved to be a faithful representation of initial count rate, lending weight to the telescope performance model. The collection area was predicted to be $1x10^4 m^2$, and single channel aperture 0.8 sq. degrees. With improvements to the optics and optimisation of the PM tube operating parameters this count rate has increased to almost 2 Hz. The count rate at the inception of the experiment translates to an energy threshold at zenith of 300 GeV (Brazier et al., 1989). This has been revised downwards to 250 GeV in light of the increase achieved in the count rate. This energy threshold is confirmed by results of simulations and it is believed that the uncertainty in this threshold is no greater than 50 GeV.

The count rate is a function of zenith angle, and in the case of the Mk.3 telescope this function has been shown to be of the form

$$N(\theta) = N_0 \cos^n \theta$$

where n is 2.3 +/- 0.5 (Chadwick, 1987). This is consistent with the response of the Dugway telescopes and is an inherent characteristic of the triple fast coincidence system. The index in the above function tends to differ widely between telescopes employing different detection strategies.

The corresponding function for the Whipple telescope, for example, with a trigger system relying entirely on the response within a camera viewing a single large collector, has an index of 0.9 (Punch, 1993).

The Mk.4 telescope has a count rate of about 60% of that of the Mk.3 telescope, a consequence of its reduced mirror area. An energy threshold to gamma rays of 450 GeV has been assigned (Bowden, 1993).

	Mk.3	**Mk.4**
Collector Area	11 m^2	6 m^2
Photomultiplier Diameter	46 mm	46 mm
Focal Length	2.45 m	2.45 m
Physical Aperture (FWHM)	1.5 +/- 0.2	1.5 +/- 0.2°
Reflectivity	80 %	80 %
Count Rate (at Zenith)	120 c.p.m.	70 c.p.m.
Gamma Ray Threshold	250 GeV	450 GeV

Table 3.2: Physical characteristics of the Mk.3 and Mk.4 telescopes.

3.4.5 Conclusion

The early gamma ray telescopes described above, which have been referred to as the first generation, had little or no capacity to differentiate between gamma ray and hadron initiated events on the basis of the detail of the Cerenkov light produced. The majority of the effort was directed towards optimising the spatial and temporal response of the telescope to the typical Cerenkov event, which has a characteristic size and duration. Aperture functions of the telescopes were adjusted to achieve maximum sensitivity (a compromise between rejection of night sky noise and loss of

Cerenkov light) and electronic integration times matched to the duration of the events.

A first generation system is therefore simply a counting device typifying a brute force approach to source detection. Long exposures to potential sources are performed in the hope of eventually revealing a periodicity within a strong background, and / or a small count rate excess over a control background rate. The count rate of the telescope is of paramount importance and these simple telescopes, requiring only that the trigger criterion is satisfied, count at a rate which is a function of the integrated flux above energy threshold. A modest decrease in telescope threshold energy produces a significant increase in count rate. Therefore, much attention was paid to maximising the system gain leading, in the case of the Durham group, to the adoption of the threefold coincidence system to minimise threshold energy. Even so, within the energy range over which these instruments are sensitive, the method is hamstrung by the hadronic background. Second generation systems have evolved to meet the challenge of discrimination between gamma ray and hadron initiated events.

3.5 Possible Enhancement of Response to Gamma Rays

3.5.1 Introduction

Prior to the advent of detailed Monte Carlo simulations of extensive air showers, insufficient information on the relative morphologies of gamma ray and hadron initiated showers was available to invoke rejection criteria based on the form of the Cerenkov events. However, one method which was adopted by the Durham group appeals to the directionality of the gamma rays (Brazier, 1991). A 'guard ring' of PM tubes surrounds the tube which

has the source at the centre of its field of view and effectively constricts the aperture of the central channel. This method appeals to the more compact and regular nature of Cerenkov images produced by on axis gamma rays, in comparison with their hadron initiated counterparts. This method also discriminates against showers which appear within the centre of the field of view but are due to off axis hadrons with a compensating perpendicular distance between detector and shower core (the impact parameter). These images will be extended in one dimension and so will be prone to trigger peripheral channels as well as the centre. This rejection strategy was operated in both hardware and software modes. In its simplest form only events which satisfy the discrimination threshold solely for the on source channel are accepted as emanating from the source direction. There has been evidence for the validity of this method from data recorded by both the Mk.3 and Mk.4 telescopes, with detections in the on source channel data always having no counterpart in the guard ring data. The guard ring was initially configured with a separation of 2° from the centre channel, with the proportion rejected being 40 % to 50 %. A reduction in separation to 1.5°, effected in March 1991, increased this proportion to 50 % to 60 %.

A limitation of the hardware rejection criterion is its inflexible response to events displaying a spectrum of energies. Small showers are less constrained in arrival direction as peripheral light partially incident on a guard ring tube is less likely to exceed the discrimination threshold. This effect is mirrored in the response to variation in zenith angle. Due to geometrical effects showers at larger zenith angles appear smaller and the proportion of rejected events decreases. In response to these deficiencies the method was adapted to reject events during analysis on the basis of the pulse integrals for each of the PM tubes. Rather than require that a guard ring tube exceeds a constant threshold, the condition is imposed that the

pulse integral of a guard ring channel must not exceed a specified fraction of that of the on source channel. This ameliorates the detrimental effects of the energy spectrum and zenith angle dependencies (Brazier, 1991).

Since the centroid of the image at the focal plane migrates away from the optic axis as the impact parameter increases, an aperture rejection criterion obviously constrains the axis of the shower to lie within a smaller radius of the detector than would otherwise be the case. This effect reduces the collecting area of the telescope, rejecting gamma rays with large impact parameters. However, the optimum collection area for gamma rays is obviously that defined by the extent of the flat lateral distribution of Cerenkov light at the altitude of the detector. Expansion of the collection area necessitates a wide field of view. The maxima of showers falling with impact parameters of up to 50 m will fall within the field of view of a 1° aperture instrument, defining a collection area of 10^4 m^2. This could be improved by almost an order of magnitude by increasing the extent of the detector package to a size which would confine events with impact parameters of up to 150 m. Whilst this increases the rate of collection for gamma rays it leads to an even more significant increase in the observed hadronic flux, due to the wide solid angle of acceptance. In order to make this detector configuration viable one must be able to discriminate between the Cerenkov signatures of gamma ray and hadron initiated air showers.

Early analytical simulations of the gamma ray cascade by, for example, Zatsepin (1965) failed to highlight differences between gamma ray and hadron initiated Cerenkov events which could be exploited in a rejection strategy. It took the rapid development in microcomputer technology and more optimistic Monte Carlo simulations, particularly by Browning and Turver (1975, 1977), to rekindle interest in the detailed shower characteristics. Simulations can provide information on the three principal

parameters of consequence to detection strategies.

- The lateral distribution of Cerenkov light as it is incident on the ground, defining the sensitive area of a telescope. It is also possible to estimate the photon flux within this light pool as a function of energy, providing a measure of the photon flux through the detector.

- The angular extent and distribution of the Cerenkov light on the sky relative to the optic axis of a detector, and the projection of this image onto a camera on the focal plane.

- The time profile of the Cerenkov event at specific points on the shower front, and the delay of the light front as a function of impact parameter.

Several observational strategies designed to exploit differences between parametric representations of gamma ray and hadron generated Cerenkov events have evolved in response to the results of these simulations. These can be grouped broadly into two categories, imaging and wavefront sampling, utilising spatial and temporal shower information respectively. Telescopes employing these more sophisticated strategies have been referred to as second generation instruments.

3.5.2 Imaging

This approach was pioneered by the Whipple collaboration in the early 1980's (Fegan et al, 1983). Discrimination between gamma ray and hadron events is achieved on the basis of the distribution of the Cerenkov light projected onto a pixellated camera system at the prime focus of the flux

collector. The details of the Cerenkov production processes are unimportant when considering the nature of this image. An event is viewed as a projection of the particle track over the distance during which it radiates. The image length is predominantly defined by geometrical perspective, with the aspect of the shower being progressively foreshortened as impact parameter decreases. With the optic axis aligned with the source, images of showers developing parallel to the axis possess a radial symmetry which is not displayed by the off axis background arriving from random directions.

The Whipple flux collector is a purpose built tessellated dish of 10 m diameter. It has 248 hexagonal facets of spherical section, each with a width of 61 cm. The optics are of an unorthodox (Davies Cotton) design. The individual mirrors are configured on a 7.3 m radius spherical surface, with the normal to the mirrors directed at a point 14.6 m along the optic axis (Cawley et al, 1990). The focal surface is at the centre of curvature of the dish. This system was adopted to minimise the detrimental effects of coma for images off the optic axis, these images only being marginally larger at FWHM than those on axis. Quoted FWHM point spread functions on axis and 1.25° off axis are 0.12° and 0.14° respectively. This advantage is achieved at the expense of the isochronicity offered by a collector of parabolic section. The spread of travel times is 6 ns, sufficient to mask any differences inherent in the time profiles of gamma ray and hadron initiated events.

The first imaging device to be deployed on the focal plane was a camera consisting of 37 hexagonally close packed two inch PM tubes with a pixel size of 0.5°. This defined an aperture of 3.5°. Simulations of the response of the 37 element camera to both gamma ray and hadron initiated events, within the framework of the Whipple optics and incorporating appropriate

night sky noise, were performed by Hillas (1985). In order to make comparisons the images were parameterised, using standard moment fitting procedures appealing to the elliptical nature of the images. Figure 3.3 is a schematic illustration of the Hillas parameterisation of the image on the focal plane. The parameters and their interpretations are listed below (adapted from Fegan, 1992).

WIDTH : The maximum rms spread of light along the axis perpendicular to the major axis of the image, a measure of the lateral extent of the cascade at shower maximum.

LENGH : The rms spread of light along the major axis of the image, a projection of the extent of axial cascade development.

MISS : The perpendicular distance between the major axis of the image and the centre of the field of view, a measure of shower orientation.

DISTANCE: The distance from the centroid of the image to the centre of the field of view, a measure of the displacement on the sky of the shower maximum from the source direction. For gamma rays, constrained to emanate from the source direction, distance translates to impact parameter.

AZWIDTH : The rms spread of light perpendicular to the line connecting the centroid of the image to the centre of the field of view, an amalgamation of size and orientation parameters.

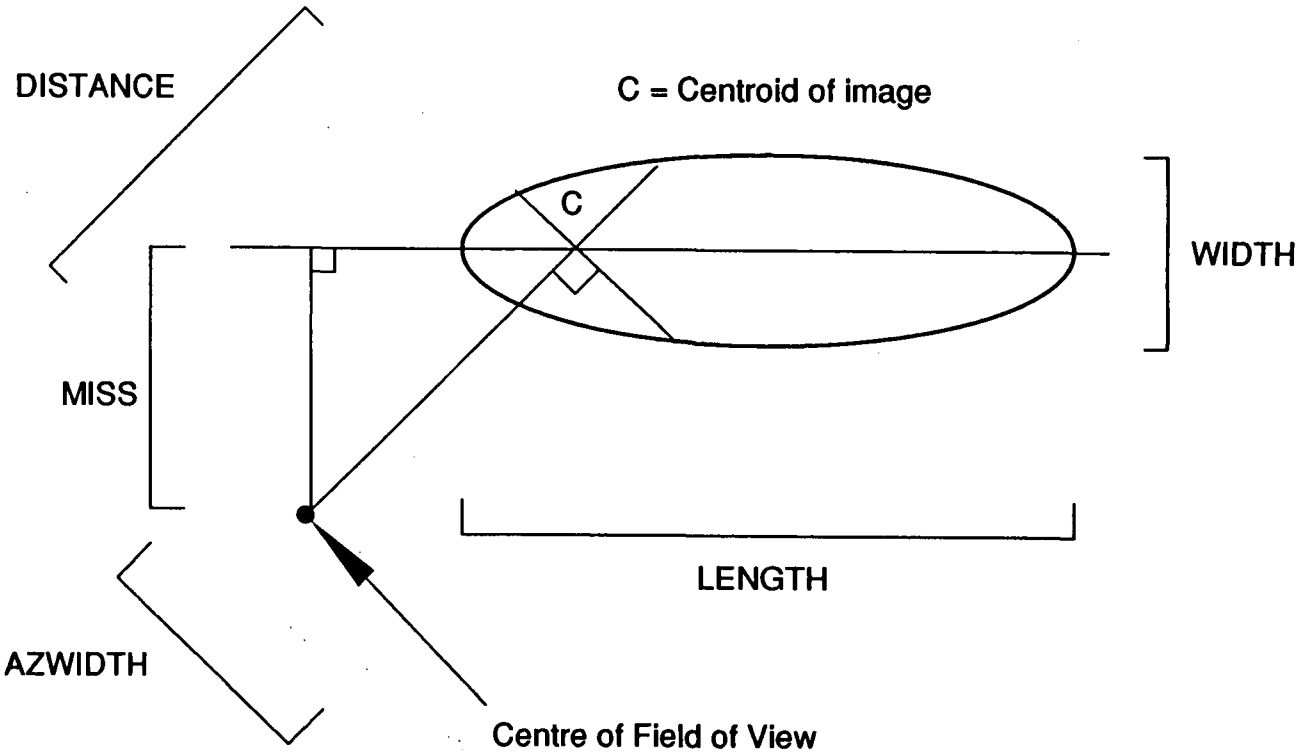

Figure 3.3: A schematic illustration of the parameterisation, of a focal plane image of the Cerenkov light from an extensive air shower developed by Hillas (1985)

ALPHA : $\alpha = \mathrm{Sin}^{-1}$ (Miss/Distance). The angle between the major axis of the image and the line joining the centroid of the image to the centre of the camera.

Significant differences were predicted between gamma ray and hadron initiated events, gamma events being almost a factor of two smaller and possessing the radial symmetry mentioned earlier. Multi-parameter cuts based on the data from simulations predicted that rejection of > 98 % of the background was possible whilst retaining 65 - 70 % of the signal. This confidence was borne out by a detection of the Crab Nebula at the 9σ significance level (Weekes, 1989). The 0.5° pixel pitch camera was replaced in 1988 with a camera with a similar field of view but with 0.25° resolution (Cawley et al.,1990). Flux sensitivity was increased by a factor of 3 and the Crab Nebula detected at a level of significance of 20 to 30σ.

A multi-parameter cut based on moment fitting of images is not the sole method applied to the data in order to discriminate between gamma and hadron initiated Cerenkov images. In order to be able to compare the various analysis techniques the Whipple collaboration have defined a quantity Q, the quality factor (Fegan, 1992), given by

$$Q = (n^{\gamma} / N^{\gamma}) (n^{h} / N^{h})^{-1/2}$$

where n^{γ} is the number of gamma rays passing the particular cut applied from an initial sample of N^{γ}, and n^{h} is the number of hadron initiated events surviving from a total of N^{h}. An indication of the achievable improvement in signal to noise can be gained from the Whipple collaboration's various efforts at background rejection, applied to their 1988-89 Crab Nebula dataset which are summarised in Table 3.3 (taken from Fegan, 1992).

Selection Method	Detection Significance (σ)	Q Factor	Reference
Azwidth	20.0	4.2	Vacanti et al. (1991)
Neural Network	24.5	5.6	Reynolds (1991)
Multiparameter Wedge Cut	27.2	6.6	Chilingarian and Cawley (1991)
Singular Value Decomposition	24.4	5.6	Danaher et al. (1993)

Table 3.3: A summary of the efficacy of the various hadron rejection techniques applied by the Whipple collaboration to their detection of the Crab Nebula in the data from the 1988 - 89 observing season.

3.5.3 Wavefront Sampling

Wavefront sampling has become the generic term which encompasses all experiments which use the temporal information within a shower front. They can be subdivided into two groups, one of which uses the relative arrival times of the shower at a number of distributed points to reconstruct the shower front and derive an arrival direction. This can be compared with the source direction, effectively improving the angular resolution of the detector. The other method relies upon intrinsic differences in the time profiles of gamma and hadron initiated events across the whole shower front, sampling the shower at a single point.

The Durham group was the first to achieve significant results using a distributed array of atmospheric Cerenkov telescopes. Two 15 minute bursts of pulsed emission were observed from the Crab pulsar (PSR0531+23) within 34 hours of data taken between 25th September and 2nd November 1981 (Gibson et al, 1982). A further 103 hours of exposure between September 1992 and November 1993 revealed steady emission with a narrow peak in the light curve, coincident with the main pulse at other wavelengths (Dowthwaite et al., 1984). It was demonstrated that the excess counts in the main pulse were concentrated around the source direction and that they had a disproportionate amount of multiple telescope responses, the aperture function of the array being narrower for such events. Applying a condition for multiple telescope response preferentially selects gamma rays as a result of their flat intensity profiles.

Multiple point wavefront sampling will not be considered further. However, pulse profile discrimination is being investigated by the Durham group for use both in a stand alone context and in conjunction with high resolution imaging.

The longitudinal development of the shower is represented by the range in arrival time of the Cerenkov photons. Photons from a gamma ray initiated event, having solely an electromagnetic cascade origin, are emitted predominantly from close to the core of the shower. A very narrow and uniform pulse profile results. In contrast, the nucleon and meson cascade which is the precursor to the electromagnetic component of a hadron initiated event gives these events much more structure. Photons emitted away from the core have a greater range of arrival times at any point of observation and are, in general, delayed relative to those produced near the core. The penetrating muon component emits Cerenkov light deep into the atmosphere which arrives in advance of light from the main body of the shower, accentuating the leading edge of the pulse profile. The parameterisation of the pulse profiles may prove more difficult than that of a two dimensional image on the focal plane. Parameterisation of the pulse shape is more subjective and probably a lot more sensitive to instrument design.

Turner et al. (1990), when observing near vertical showers from the direction of the Crab Nebula, characterised the showers on the basis of the number of secondary maxima on the pulse profile, the majority appearing on the trailing edge and on the offset of the trailing edge. This technique is very labour intensive, 3000 events taking 200 man hours to categorise, but led to a 4.2σ detection of the Crab Nebula from only 100 minutes of on source data. It is claimed that up to 95% of hadronic background can be rejected, which represents a quality factor of about 4 if all of the gamma ray candidates are included. A second measurement failed to confirm the result.

Roberts (1993) of the Adelaide group has parameterised time profiles in a less subjective manner, principally describing the profiles in terms of their

rise time, fall time and full width at half maximum. This method would appear to be more robust than that involving identification of secondary maxima, in that it is less sensitive to sky and electronic noise. The parameterisation is performed automatically. No results have been quoted but Monte Carlo simulations suggest Q factors of around 2 could be expected using a combination of pulse rise time and full width half maximum cuts, rejecting around 95 % of the hadron events whilst retaining more than 50 % of gamma rays.

3.6 Towards a Lower Threshold Energy

3.6.1 Introduction

The aim of this section is to describe the benefits of improving the sensitivity of telescopes to lower energy gamma rays and then outline how this might be achieved.

3.6.2 The Utility of a Low Energy Threshold

A reduction of energy threshold is important in the first instance because the cosmic ray energy spectrum falls steeply. Event yield increases dramatically as threshold decreases, with corresponding improvement in statistics and sensitivity. One reservation is that some observed gamma ray source spectra have been shown to be harder than the ubiquitous hadronic energy spectrum, making the move to lower energies less attractive than might otherwise be the case. However, gamma ray sources with steep energy spectra in the VHE region do exist, and a push to lower energy may reveal many such sources.

It has been assumed, on the basis of early work by Zatsepin and Chudakov, (1962), that above 1000 GeV gamma ray initiated showers are twice as efficient in production of Cerenkov radiation as those initiated by hadrons, and that light intensity normalized to the primary energy is a constant. Turver and Weekes (1977) have shown, through Monte Carlo simulation of extensive air showers, that below 1000 GeV the situation becomes markedly different as the energy decreases. Figure 3.4 shows the average lateral light intensity distributions from proton initiated air showers of energy 100, 1000 and 10,000 GeV normalized by energy.

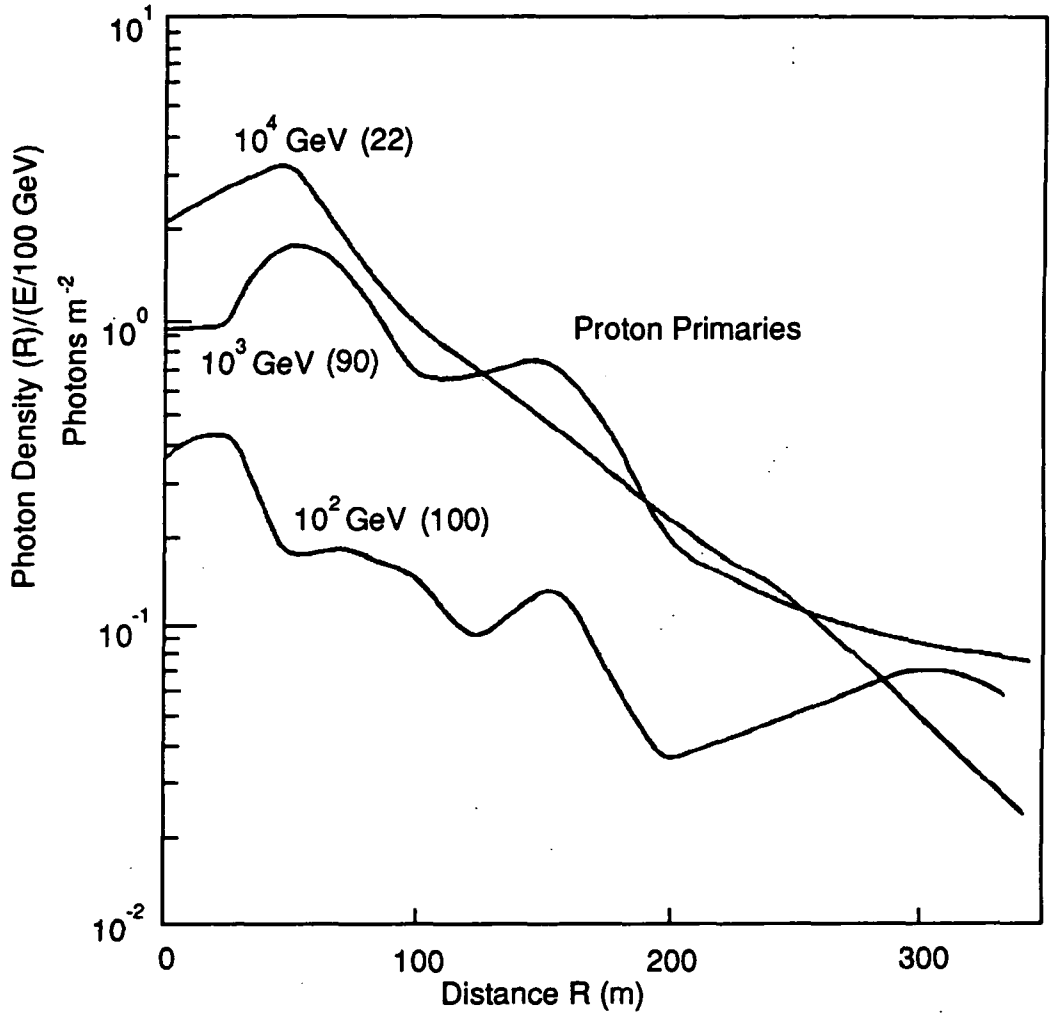

Figure 3.4: Average lateral Cerenkov photon density distribution of (n) Monte Carlo simulations of proton initiated extensive air showers of 10^2, 10^3 and 10^4 GeV. (after Turver and Weekes, 1977)

Figure 3.4 shows that the intensity distributions of the 1000 and 10,000 Gev showers are very similar but the 100 GeV average has suffered a five fold decrease in Cerenkov light production efficiency. Figure 3.5, which illustrates equivalent distributions for gamma ray initiated showers, shows no such severe degredation of intensity with energy.

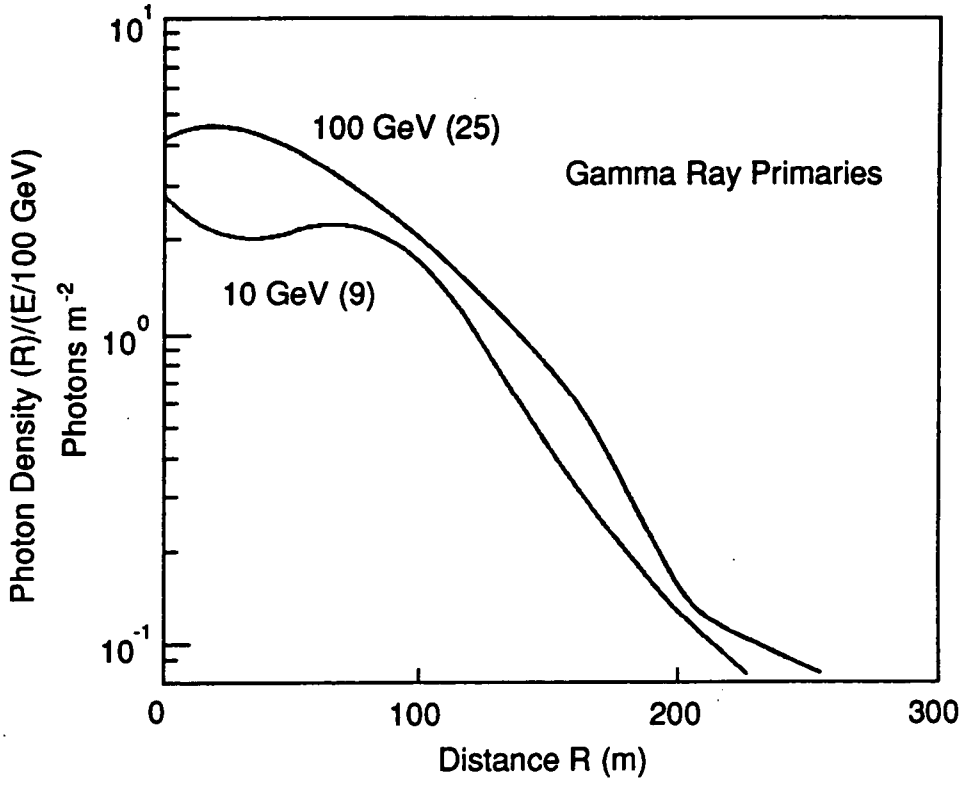

Figure 3.5: Average lateral Cerenkov photon density distributions of (n) Monte Carlo simulations of gamma ray initiated EAS of 10 and 100 GeV (after Turver and Weekes, 1977).

The physical explanation of this effect is bound up in the development of the nucleon cascade which generates the electromagnetic component of a hadron initiated extensive air shower. Energy is transferred to the secondary electromagnetic cascade via neutral pion decay, the decay product being a gamma ray. Charged pions are longer lived and their fate is subject to competing mechanisms, either decaying to charged muons or

undergoing further strong interactions with nuclei of the atmosphere. The latter interaction, which is preferred for higher energies, is the more efficient producer of Cerenkov light, producing more neutral pions. Due to relativistic effects lifetime to decay is longer at higher energies, thus favouring collision, production of further pions and hence electromagnetic cascading. As the energy decreases, however, more charged pions decay to muons and progressively more energy is lost to the production of low energy muons, whose energies fall below the threshold for Cerenkov radiation production. This results in a Cerenkov light deficit. Figure 3.5 demonstrates that even below 100 GeV, where the intensity of Cerenkov light from hadron initiated cascades is severely attenuated, gamma ray initiated showers are still very efficient producers of the radiation. The simulated 10 GeV gamma ray produces 50 % of the light anticipated by extrapolation from higher energies. This smaller deficit is due to an ever increasing proportion of the charged components of the electromagnetic cascade having lower energies and being produced in higher, less dense regions of the atmosphere where they are more likely to have energies below the Cerenkov threshold. The results of these early calculations have been supported by more recent work. Figure 3.6 shows the Cerenkov yield for EAS with gamma ray and proton primaries as a function of energy (Pare, 1993). Below 1000 GeV the Cerenkov light production of EAS with proton primaries decreases dramatically and the effects of the problematic cosmic ray background should decrease significantly.

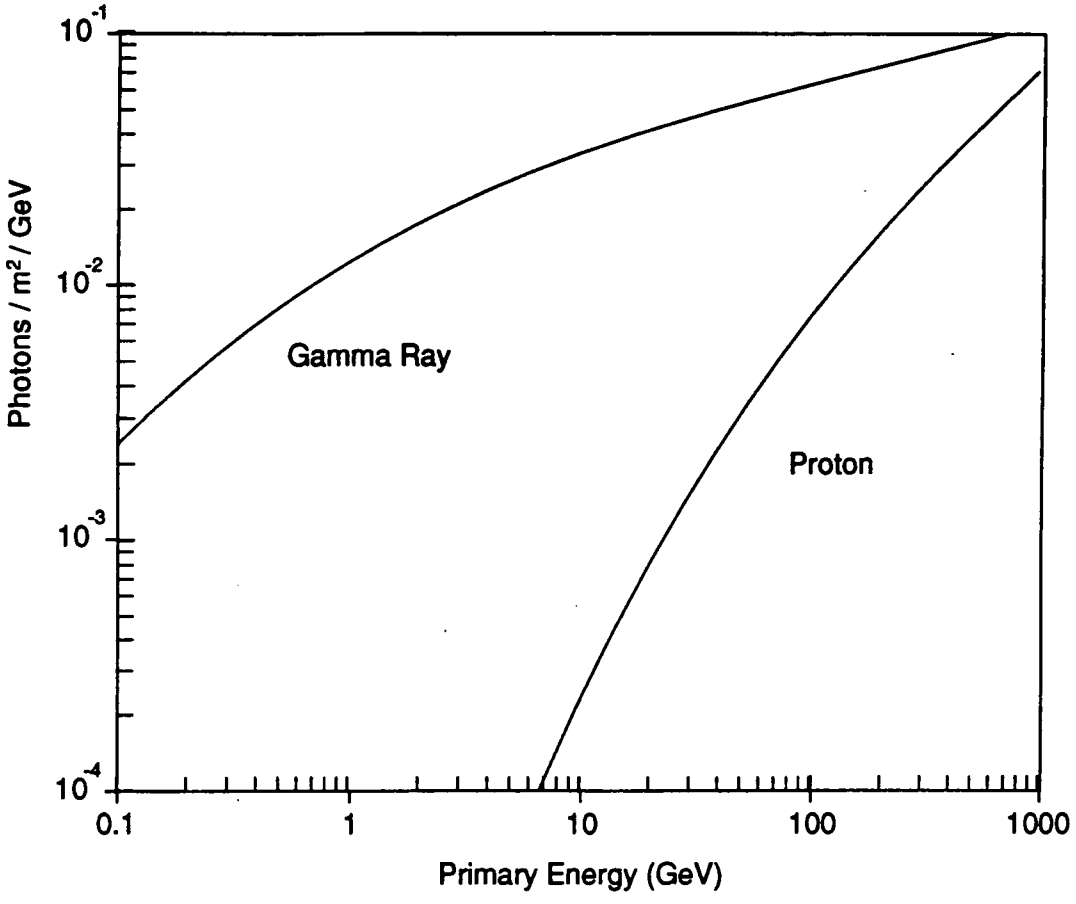

Figure 3.6: Cerenkov yield of EAS with gamma ray and proton primaries as a function of energy (after Pare, 1993).

3.6.3 The Optimisation of the Design of a Low Energy Telescope

3.6.3.1 Introduction

The energy threshold of a Cerenkov telescope is limited, ultimately, by the size of the flux collector. However, given a flux collector of a particular area, the lowest possible threshold is achieved by the optimisation of all design parameters. Factors such as the efficiency of the optics, effective collection area, choice of PM tube, suppression of background light, trigger efficiency and bandwidth of electronics can be considered independently and all have a bearing on instrument performance.

3.6.3.2 Optics

Ground based gamma ray astronomy using the atmospheric Cerenkov technique requires flux collectors of large area, with good reflectivity and adequate optical quality. The detector package is usually placed at the prime focus of a flux collector, minimising light loss by requiring the light to undergo only one reflection. An appropriate choice of reflective surface is important and is dictated by the Cerenkov light emission spectrum. The light intensity is proportional to λ^{-2}, increasing to shorter wavelengths until absorption within the atmosphere becomes important. This absorption is about 50 % at 300 nm and approaches 100 % asymptotically at around 280 nm. It is important then that the reflective surface has a high specular reflectivity from the near ultraviolet through the blue end of the visible spectrum. Silver, the material traditionally used as the reflective coating for glass mirrors, becomes progressively more absorbent below 400 nm making it a poor choice for the collection of Cerenkov light. Aluminium has a reflectivity (of between 80 % and 90 %, which it retains throughout the wavelength range of interest) but is unstable in air, forming an oxide coat almost immediately. This oxide coat forms as an amorphous crystal layer, which protects the Aluminium from further oxidation but is translucent, offering only very diffuse reflection. In order to achieve a stable reflective surface the aluminium may be subjected to an anodising process during which aluminium oxide is laid down on the metal in a regular lattice, forming a highly reflective surface. The optimal thickness of oxide layer is a half wavelength of the desired peak reflectivity. This thickness is about 100 nm for maximum reflectivity at a wavelength of 400 nm (as the refractive index of Aluminium oxide is near 2). The layer will be most absorptive at 200 nm, which is within the regime of atmospheric absorption, and 600 nm, which is

above the Cerenkov emission region and fortuitously at the maximum of the starlight background.

A further consideration in mirror design arises from the requirement for an efficient trigger for the telescope. In order to achieve the lowest threshold, the specifications for the image must match the characteristics of the photosensitive device and associated electronics as closely as possible. Considering the three fold coincidence system favoured by the Durham group, the optimum image size of a gamma ray initiated event at the focal plane is that which matches the photosensitive area of the triggering PM tubes. Gamma ray initiated events have been shown to be about a factor of two smaller in lateral extent than hadronic events, the optimum triggering pixel size being approximately 0.5° (Hillas, 1985). Similarly, the duration of the Cerenkov pulse must be kept to a minimum to achieve the maximum illumination of the photocathode within the response time of the PM tube, as this translates to the peak voltage at the discriminator. Integration of the charge in the pulse is also best done over as short a time as possible to reduce sky noise in the measurement. The light front from a parabolic flux collector is isochronous and so this is the ideal surface in this respect.

3.6.3.3 Photomultiplier Tubes

The PM tube is still the preferred photosensitive detector for the detection of atmospheric Cerenkov radiation. Avalanche photo-diodes would offer a significant improvement in quantum efficiency (perhaps by a factor of three) but solid state detectors such as these are still in the concept stage of design for this type of application, the major problem being suppression of noise (Lorenz, 1993).

Choice of suitable PM tubes is of paramount importance as these devices

can have quite widely differing operational parameters. Most of the gain of the recording system is provided by the PM tube, being determined by the voltage across each of the dynodes. A higher voltage per stage produces a larger accelerating field for the photoelectrons, these electrons then reach the next dynode with more energy and hence greater capacity to liberate further electrons. The rise time of the tube is important and should match as closely as possible the rise time of the Cerenkov pulse, little more than a few ns. Rise time is strongly dependent upon the voltage per stage of the device requiring the gain to be manipulated by constraining the number of stages used. The photoelectric current is proportional to the product of the illumination of the photocathode and its quantum efficiency. Yields quoted for the most sensitive devices can be as high as one electron for three light quanta, a quantum efficiency of 33%. Photocathodes are usually composed of the alkali metals, with the wavelength of peak response being dependent upon the work function of the particular metal. The peak response migrates to progressively longer wavelengths as one moves down the group in the periodic table. Even though the lighter metals, Lithium and Sodium, have peak response within the Cerenkov emission spectrum, the majority of the commercially available tubes have bi-alkali photocathodes consisting of complexes of the heavier transition metals with Antimony. The RCA 8575 tube used extensively by the Durham group in the past has the complex K_2CsSb as its photocathode with peak response at 420 nm and a quantum efficiency of 24 %. Ideally the windows of the tubes would be 100 % transmissive of UV light, the best approximation to this is a quartz window, but such tubes are prohibitively expensive. Pyrex and lime glass windowed tubes are more common.

3.6.3.4 Reduction of Ambient Background Light

Background light may originate from a variety of sources. The most significant source is the night sky reflected in the flux collectors. This background arises from specular reflection of the sky within the field of view of the detector and diffuse reflection from the whole of the sky in front of the detector. The sky noise is the Poissonian fluctuations in the D.C. illumination of the PM tube. This background illumination is minimised with respect to the Cerenkov signal by matching the field of view of the detector to the lateral extent of the signal, and the bandwidth of the electronics to the duration of the pulse. In reducing the aperture of the telescope to optimise the signal to noise we arrive, empirically, at a compromise between the night sky flux through this aperture and the proportion of the Cerenkov signal encompassed. This background flux cannot be eliminated. A certain proportion of the off axis light which has suffered diffuse reflection could be removed using collimators beyond the focal plane, but this light is of secondary importance to the on axis background and engineering considerations preclude this. With three paraxial flux collectors, however, diffuse and specular reflection from adjacent mirrors will augment the light noise from the flux collector dedicated to each particular detector package. This problem can be remedied quite easily by screening all angles of view between collectors. If a cylinder is placed around the camera with extension from the focal plane towards the collector, and a complementary cylinder is placed around the collector extending towards the focal plane, all angles of view external to the dish will be shielded, eliminating light from adjacent dishes and the ground albedo.

3.6.3.5 Optimisation of the Event Trigger

As indicated earlier it is the belief of the Durham group that the best compromise between coincidence fold number and individual flux collector area is to use three flux collectors. This judgement was originally based upon a configuration of three identical PM tube packages at the prime foci of three identical flux collectors. In the case of a system of signals from two dedicated triggering packages, combined with the signal from a higher resolution imaging camera, the situation becomes more complicated. The third required signal for coincidence can be generated by any one of a number of strategies which will be more or less stringent than for one further identical package. Trigger strategy is inextricably linked to the combined noise rates, and hence operational gain of the imaging tubes.

A cluster of a number of the smaller imaging tubes of the camera will have a field of view corresponding to one channel of the triggering electronics. Additional electronic logic is required to provide a signal for the coincidence unit in the event of one or more of the outputs of these tubes achieving the discrimination threshold. The larger the cluster of tubes providing the trigger, the higher the combined noise unless gain is sacrificed. As a consequence of this gain constraint and the dissipation of light in the images between tubes, the camera may become the component of the system which defines the threshold. However, as the image scale on the focal plane is large compared with the pixel pitch of the camera, each image will be represented in the output of a number of adjacent camera PM tubes. This allows the imposition of a camera coincidence trigger, supplementary to the three fold coincidence trigger. If the condition is imposed that coincidence is required between two camera PM tubes (within a cluster of seven), in addition to the corresponding left and right triggering PM tubes

then the imaging tubes could be run at a much higher noise rate and consequently higher gain. Many permutations of trigger can be envisaged but all are subject to the compromise between gain and accidental rate. The optimal solution will depend upon the gain and noise characteristics of components of the particular detector.

3.6.3.6 Optimisation of Discriminator Threshold

The output of a PM tube is represented by the instantaneous voltage across a resistance at its anode. This signal is passed, via an operational amplifier, to the voltage discriminators. This voltage will be proportional to the instantaneous anode current which is given by

$$I_a = LQGe$$

where L is the luminescence at the photocathode, Q is the quantum efficiency, e is the charge on the electron and G is the gain.

The discriminator threshold is defined by the acceptable noise rate above threshold. If the resolving time of the electronics is τ then the number of photoelectrons produced at the photocathode within this time is

$$N_\tau = LQ\tau$$

and the statistical fluctuation, obeying Poissonian statistics, is

$$\sigma_\tau = (LQ\tau)^{-1/2}$$

thus the anode current is uncertain by

$$\sigma_i = (LQ\tau)^{-1/2}eG/\tau$$

From the above it is evident that at constant illumination, anode current is a direct measure of gain and that the deviation from the mean is proportional to the gain. For a triple fast coincidence selection system, the choice of a tolerable accidental coincidence rate will define the acceptable single fold noise rate. An increase in gain pushes more of the tail of the instantaneous voltage distribution above the threshold, so increasing the PM tube noise rate. A corresponding increase in threshold can be made to reduce the noise rate to its previous value, but the increase in gain may not compensate for the required increase in threshold. The optimum gain and threshold combination for constant noise rate that which gives the highest three fold coincidence count rate, indicating a lower energy threshold.

At the inception of the Mk.3 telescope experiment the three fold coincidence count rate close to the zenith was noted for different voltage discriminator thresholds at a constant single fold noise rate. The results are presented in Table 3.4. A similar experiment was performed on the centre channel of the Mk.5 telescope in March 1993. The signal from the centre cluster of seven one inch tubes was used for the trigger in the camera, the trigger requirement being that at least one of the seven PM tubes achieve threshold. Noise rate for the centre cluster (CC-C6) is approximately the sum of the single fold noise rates of the seven tubes. The results of this test are displayed in Table 3.5. These tests demonstrate that the three fold count rate is relatively insensitive to discriminator threshold if compensation is made in tube gain.

	Discriminator threshold					
	50 mV			30 mV		
	Left	Centre	Right	Left	Centre	Right
Tube noise (kHz)	30	30	30	30	30	30
Tube Voltage (V)	1865	1910	1885	1725	1785	1760
Anode Current (μA)	11	20	17	7	14	12
3 Fold count rate		70 c.p.m.			68 c.p.m.	

Table 3.4: Sensitivity of the telescope count rate to voltage discriminator threshold for the conventional Mk.3 telescope three fold coincidence.

	Discriminator Threshold					
	50 mV			100 mV		
	Left	CC-C6	Right	Left	CC-C6	Right
Tube noise (kHz)	28	200	31	23	200	24
Tube Voltage (V)	1550	1150	1550	1650	1325	1650
Anode Current (μA)	21	25	16	37	55	27
Accidental Rate (Hz)		10^{-1} Hz			5×10^{-2} Hz	
3 Fold count Rate		89 +/- 4 c.p.m.			83 +/- 4 c.p.m.	

Table 3.5: Sensitivity of a Mk.5 telescope coincidence channel count rate to discriminator threshold. CC-C6 represents a cluster of 7 camera PM tubes.

In an effort to evaluate the level of amplifier noise on the system, 1000 V was applied to the tubes on the centre channel of the Mk.3 telescope at zenith, and the discriminator threshold progressively reduced in increments of 5 mV. The single fold noise rates proved to be negligible down to the minimum threshold of 15 mV suggesting that the night sky is the

predominant source of noise in the system.

3.7 A Design for a New Telescope

Within the preceding discussion of telescope performance a number of competing themes can be identified. It is obvious that in order to make progress in the field of atmospheric Cerenkov astronomy the next generation of instruments will have to discriminate actively against hadron initiated events. The three most promising concepts would appear to be;

- imaging of the event using a high resolution pixellated camera,

- pulse shape analysis utilising flash ADCs (or a commercially produced oscilloscope) to digitise the time profile of the Cerenkov pulse to nanosecond accuracy,

- operating at extremely low threshold energies to take advantage of the deterioration in efficiency of Cerenkov radiation production suffered by proton initiated EAS at low energy.

Each of these discrimination policies, while not being mutually exclusive, stress different aspects in telescope design. Adoption of the parabola as the section of the flux collector, in order to achieve isochronous arrival of the wavefront at the detector package, compromises off axis image quality due to coma. Dissipation of the Cerenkov signal between tubes of a high resolution camera has a similarly deleterious effect on the threshold energy of the telescope. Thus, if we wish to appeal to all of these rejection policies, telescope design is necessarily a compromise.

CHAPTER 4

A PROTOTYPE LOW ENERGY THRESHOLD TELESCOPE

4.1 Introduction to the Mk.5 Telescope

4.1.1 Prototype for a New Telescope

4.1.1.1 The Mk.6 Telescope Concept

The design of the Mk.6 telescope, which is the subject of Chapter 7, was prompted by the diminishing returns from the "first generation" systems of comparatively low sensitivity, typified by the Mk.3 telescope. A simple qualitative specification for the Mk.6 design is for a telescope with large flux collector area (and consequently a low threshold energy), with the capacity to exploit sophisticated background rejection techniques.

The scale of the Mk.6 telescope, 114 m^2 total reflector area, allows the telescope to operate in an energy regime (< 100 GeV) in which the gamma ray signal is enhanced relative to the hadronic background due to the fall off in Cerenkov radiation production in hadron initiated EAS. With better quality optics and fast electronics the Mk.6 telescope will also to be able to discriminate between higher energy gamma ray and hadronic initiated showers utilising spatial and temporal disparaties between their respective Cerenkov signatures.

4.1.1.2 The Mk.6 Telescope Prototype

The design of the Mk.6 telescope represented a significant advance in

technology for telescopes operated by the Durham group, and the need was felt for a testbed for a number of facets of the project.

The role of the Mk.5 telescope, as a half scale prototype, is to assess the viability of:

- Developments in the process of mirror fabrication.

- A new mechanical design and steering configuration for the alt-azimuth mount.

-The operation of an imaging camera comprising a close packed array of PM tubes.

- Incorporation of an imaging device into a fast coincidence triggering system.

- Fast sampling of the Cerenkov pulse shape.

4.1.2 The Scientific Potential of the Mk.5 Telescope Project

While its principal objective is proof of concept, the Mk.5 telescope represents a large improvement in sensitivity in comparison with the Mk.3 instrument. For example, the camera of the Mk.5 telescope possesses sufficient resolution to allow simple parameterisation of images of Cerenkov showers. This allows the imposition of event rejection criteria, providing the facility to reject those events which are obviously due to hadronic background.

An additional signal enhancement strategy utilising the medium resolution

imaging capacity of the telescope to target gamma ray like events is possible with the provision of a second telescope of similar resolution to the Mk.5 telescope. "Stereoscopic imaging" of Cerenkov showers, an analysis of the longitudinal cascade development, has the potential to increase sensitivity at energies insufficient to allow accurate higher moment parameterisation of images. Discrimination between gamma ray and hadron initiated events requires only the evaluation of the lower moments of the light distribution. Putting this into effect required the upgrade of the Mk.3 telescope to a similar level of performance to the Mk.5 telescope but provided a useful signal enhancement technique, for which the information provided by medium resolution imaging is perfectly adequate. The upgrade of the Mk.3 telescope to provide a complement to the Mk.5, and an account of the Durham stereo imaging programme is the subject of Chapter 5.

4.2 An Overview of the Mk.5 Telescope Design

4.2.1 Introduction

The Mk.5 telescope operates as a triple fast coincidence instrument in the mould of its predecessors and indeed, for a brief period during commissioning, it functioned as a conventional Durham atmospheric Cerenkov telescope, with three identical PM tube packages of seven close packed 2" tubes. It did, however, introduce several innovations in design and operation of the Durham telescopes.

A photograph of the Mk.5 telescope is presented in Figure 4.1.

Figure 4.1: The Mk.5 Telescope.

4.2.2 The Flux Collectors

The flux collectors (described in Section 4.3) are composite paraboloids configured from 12 individual mirror sectors. Each flux collector has an area of 10 m^2 and a diameter of 3.50 m. This aperture, together with the focal length of 3.32 m, defines an f number of 0.95. The non reflective area within the aperture of the dish has been minimised to give optimum flux collection for the given focal length / aperture ratio. The mirror sectors are the first large area mirrors produced by the Durham group, and the first with parabolic section. The development of these mirrors has been a major part of the prototyping of the new large telescope.

4.2.3 The Telescope Mount

The alt-azimuth mount of the Mk.5 telescope is the first such large mount to be built by the group. The telescope can be moved independently in altitude and azimuth under computer control, with independent positional information provided by absolute shaft encoders on each axis. The design was evolved to incorporate the capacity to scale the mount to a size appropriate to the proposed Mk.6 telescope dimensions

4.2.4 Incorporation of a Camera Response into the Trigger System

Provision of an imaging capacity for the central collector within a telescope incorporating triple fast coincidence requires the introduction of additional logic into the digital electronics defining the telescope event trigger. The Mk.5 telescope provided an insight into to this problem, and a measure of the efficiency of the new trigger relative to the conventional one.

4.2.5 Inception of the Telescope Performance Monitoring System

The Mk.5 telescope was the first to benefit from an independent comprehensive real time performance monitoring system. Instantaneous values of telescope operating conditions (anode currents and noise rates for every PM tube) and environmental conditions are displayed on monitors dedicated to the telescope. The values are updated every three seconds and each minute a complete set of values are recorded as "housekeeping" blocks for later analysis. These minute by minute readings are also displayed graphically through the microcomputers on the local area network allowing trends to be identified in real time during telescope operation.

4.2.6 A New Data Logger

The data logger of the Mk.5 telescope is based upon a standard commercial microcomputer in contrast to the purpose designed 68000 processor logger of the Mk.3 telescope. This development was possible because of the improvement in data handling rates and capacity of modern microcomputers. This use of commercial equipment increases the flexibility of the system and reduces dependency on complicated in house designed equipment.

4.2.7 The Mk.5 Telescope Pulse Profile Experiment

A fourth, smaller area (6 m^2), flux collector was included in the design of the Mk.5 telescope sited above the three large flux collectors. At the prime focus of the collector an RCA 4522 PM tube (12.5 cm diameter) defines an aperture on the sky of a little more than 2°. This mirror / PM tube

combination is independent of the trigger but has its output gated and electronics logged in response to any trigger provided by the seven triggering channels. The purpose of this additional mirror / PM tube system is to provide the facility to investigate pulse profile analysis as an additional method of hadronic background rejection, without affecting the operation of the telescope. The "timing dish" of the Mk.5 telescope is mounted above the three conventional flux collectors (see Figure 4.1).

4.2.8 The Central Control Room - The Annex

Prior to the introduction of the Mk.5 telescope at the Narrabri observatory, the telescopes were operated from control rooms housed in their respective shipping containers. These control rooms incorporated the processing electronics, which are necessarily close to the telescope to avoid transmission losses in the signal cables. As a result the Mk.3 and Mk.4 telescopes, separated by 100 m, were operated as two independent telescopes. For ease of operation remote monitors in the Mk.3 container also displayed steering information, and the PM tube anode currents and single fold noise rates from the Mk.4 telescope.

The increase in number and complexity of operational telescopes on the observatory site made it impractical to operate all of the telescopes independently and monitor their performance from the Mk.3 telescope control room. A control room dedicated to the monitoring of the performance of all of the telescopes was commissioned concurrently with the construction of the Mk.5 telescope. This control room has become known as the Annex.

Each telescopes operation is controlled by a Local Area Network (LAN) of computers. These LAN are interconnected site wide to provide a Wide Area

Network (WAN) over which data can be transferred. Within each LAN one computer is dedicated to the monitoring of telescope performance. Data displayed on each telescope performance monitor is echoed to a computer in the Annex over the WAN.

It is possible to switch off power to the EHT and steering of each telescope from the Annex control room. Site wide facilities such as the timing standard and weather station are also monitored from the Annex.

4.3 The Mk.5 Flux Collectors

4.3.1 Introduction

The mirrors of the Mk.3 telescope have been in service in Narrabri for more than eight years following exposure in Durham for 2 years. They have suffered negligible degradation of reflectivity and have retained structural integrity despite being constantly subject to the elements, including significant diurnal thermal cycling. This has engendered a great deal of confidence in the materials and method of manufacture used. The requirement for a significant improvement in optical quality for the mirrors of the Mk.5 telescope, however, places constraints upon the configuration of a new composite flux collector.

The Mk.5 telescope is seen as a platform to test a number of signal enhancement techniques as well as prototyping a telescope of very low energy. One background rejection strategy employed is based upon the time structure of the Cerenkov signal. This time structure is only preserved if an isochronous paraboloidal surface is used for the flux collectors. In addition to facilitating this technique the signal produced is narrower allowing a shorter, more stringent gate to be used in the fast coincidence

and producing higher instantaneous voltages at the discriminators. Both of these factors have positive implications for the effort to reduce the energy threshold.

A tessellated, approximately isochronous surface, comprised of mirrors of spherical section, would necessitate the batch production of a large number of mirrors with differing focal lengths. This complicates the production and lengthens the process significantly and a viable alternative was sought.

The solution adopted was to produce a paraboloidal surface composed of a number of identical sectors of parabolic radial section. The fabrication of such flux collectors requires the machining of only a single former of the required shape. In addition to the improvement in ease of manufacture, the sectors are flush fitting, minimising the proportion of non-reflective surface within the area of the flux collectors.

4.3.2 Mirror Specification

An improvement in optical quality was required in order to utilise the more sophisticated background rejection techniques envisaged for the telescope, in particular the imaging technique. Generally, an improvement in performance requires a change of technology and associated increase in cost. However, in this case a proven method of manufacture was believed to have significant further potential. The reflectivity of the Mk.3 telescope mirrors was excellent and the material cost of manufacture acceptable. The only requirement which remained to be satisfied was that the large area mirror sectors could be produced quickly, reproducibly and to a specified optical quality.

In the case of Atmospheric Cerenkov Astronomy the image quality required is quite modest, the smallest structure within the Cerenkov images

being on the scale of tenths of degrees. The focal length of 3.32 m, which was chosen for the Mk.5 telescope optics, defines an image scale of 5.8 cm deg^{-1} at the prime focus. For complete coverage of the potential collecting area of the telescope, an imaging camera with an opening angle of > 2.5° is required to encompass images from showers with the largest impact parameters likely to trigger the telescope. The choice of pixel size is determined by scientific requirements, cost and logistical considerations. In this case the sensitive area can be covered, with limited but acceptable resolution, by a close packed (3 cm pixel pitch) hexagonal array of 19 1" PM tubes. In turn, the extent of the Cerenkov light in the image and the pixel pitch defines the specification of the mirror point spread function, resolution much better than pixel pitch being redundant. A point spread function at FWHM of 2.5 cm on the focal plane was defined as the specification for optical performance of the flux collector.

4.3.3 Fabrication

4.3.3.1 Background to Technique

The method of manufacture of the mirrors is an adaptation of that developed for the production of the flux collectors for the James Clerk Maxwell millimetre wavelength telescope by staff at the Rutherford Appleton Laboratory. In essence, the technique involves forming the thin reflective surface over an accurately figured die and then applying a rigid back plane to maintain the form. Any shape or size of mirror could, potentially, be produced by this method. The decision to fabricate mirrors in the form of sectors of the complete flux collectors minimises the dead area and requires production of only one former. The irregular shape of the mirror sectors and

their size does, however, present additional problems to those encountered in the manufacture of the circular mirrors of the Mk.3 telescope. The symmetry in the form of the circular mirrors allowed the reflective surface to be pulled uniformly down over the die using a relatively small jig. Significantly more force would be required to form a surface over one of the mirror sectors and unequal residual stresses would inevitably result.

4.3.3.2 Former manufacture

The former for the mirrors employed on the Mk.3 telescope, circular in section, was turned on a lathe from a mild steel blank and then polished. This method produced a very durable former, accurate in section, but it is not a practical possibility for the large radius mirror sectors of the Mk.5 telescope. Enquiries were made into having the former made commercially using a computer controlled machine, but cost and the lack of availability of a suitable milling machine proved prohibitive. It was decided to produce the former in the Physics Department workshop using simple manual techniques.

Several alternatives to steel were considered for the material of the former in an effort to make the finishing less laborious. Materials were compared in terms of their strength, workability, damage resistance, availability and cost but no serious substitute for steel emerged.

A steel former, representing a 30° sector of the complete 3.5 m diameter paraboloid, was cut from a 1" steel plate and pre-rolled into a parabola in the radial direction along the centre line of the former. The pre-rolled plate was fixed to a horizontal jig with the axis of the centre line parabola vertical. The centre line parabola was accurately finished first and would subsequently act as the reference template for the rest of the paraboloid.

Measurements were made relative to a horizontal optical bench bisecting the sector. The optical bench is fixed to a hub at the centre of the paraboloid and is free to rotate in a horizontal plane. The measuring device at a particular radius therefore describes circular arcs across the former.

The former surface was worked to a condition where residual relief above the specification paraboloid was no greater than 0.1 mm. The whole surface was then progressively smoothed using a large area sanding tool with fine grain emery paper until all measurable relief was removed. Systematic errors in the measurement system represent the limit to the accuracy of the former and estimates of these errors are considered in the section describing mirror testing.

The temperature of the room was kept stable during working periods to minimise effects of thermal expansion of components of the measuring system and the former itself. Heat generated during working of the surface was allowed to dissipate before further measurements were made of the surface.

4.3.3.3 Mirror manufacture

The reflective surface of the mirror is a 0.5 mm thick sheet of anodised aluminium (trade name Alanod 410G3, manufactured by Aluminium-Veredlung GmbH & Co.). The total reflectivity is quoted at 88 % of which diffuse reflection represents 8-13 %. Specular reflectivity has been measured to be greater than 75 % throughout the wavelength range of interest (Weekes, private communication). This thin, flexible sheet of aluminium is pressed onto a rubber seal on the former, which is external to the area on which the mirror sector will be laid down. A vacuum pump is used to evacuate the space between the aluminium sheet and the former.

Atmospheric pressure forces the aluminium sheet to take up the shape of the former. The sheet has enough elasticity to avoid kinking.

All surfaces to be bonded are abraded to increase the contact surface area and then cleaned with acetone. CIBA GEIGY Redux 420A/B two component epoxy resin adhesive is applied to the reverse surface of the reflective skin and a 6 mm thick perimeter frame, with sides 5 cm deep is applied to the surface. The frame defines the boundary of the mirror sector. An aluminium honeycomb material (CIBA GEIGY Aeroweb 3003) with a hexagonal cell size of 0.8 cm is then pressed onto the surface across the whole area within the frame. The paraboloidal shape is taken up quite easily as the foil thickness of the honeycomb is only 0.04 mm allowing some flexibility. The back of the honeycomb is plated with 1.6 mm thickness aluminium sheet, loaded with lead and left for a period to allow the adhesive to cure. The manufacturers specification indicates that cold curing leads to a significantly stronger bond, with full mechanical strength achieved after seven days at room temperature. The structure can, however, be separated from the former after 24 hours without compromising the integrity of the structure. Applying heat during curing would not reduce the curing time sufficiently to allow production of two mirrors per 24 hour period without a potentially damaging reduction in the ultimate bond strength and variability in the quality of the mirror surfaces.

After the complete mirror is lifted from the former the border of reflective material required to form the vacuum seal is trimmed flush with the mirror frame. The border frame forms a perfect watertight seal with the Alanod surface as the adhesive is applied generously to this area. The back surface, however, is applied internal to the mirror frame and cannot be sealed with adhesive. In order to prevent the potentially damaging ingress of water, each mirror sector is sealed with an elastic car body filler. When

set, this surface is finished with sandpaper and the reverse surface of the mirror sector is painted white to minimise the heating effect of direct sunlight and thus reduce diurnal temperature variations.

The mirror sectors are light (14 kg m^{-2}) and relatively cheap (£150 m^{-2}) to produce and, in the light of the evidence from the Mk.3 telescope mirrors, should prove to be effective and very durable.

4.3.4 Individual Mirror Sector Testing Procedure

Assuming that the mirror sectors can be aligned optimally, the limit to the flux collector performance is the point spread function of the individual sectors. Prototype mirrors were made during the finishing of the former to get an idea of the degree of improvement between iterations of the finishing technique. Crude measurements were made of the focal length and point spread function of these prototype mirrors using a distant light source. Although these tests demonstrated that acceptable images were produced at distances comparable to the specification focal length, it was difficult to define the optic axis of the mirror. In order to achieve a reliable measure of the point spread function at FWHM a system using parallel laser beams was devised.

A laser is directed through a series of beam splitters on a horizontal optical bench. Mirror sectors to be tested are fixed to a sector of flux collector superstructure which is free to rotate about a hub whose rotation axis is horizontal, and perpendicular to the optical bench. The test apparatus is arranged such that the beam from the first beam splitter is in the same horizontal plane as the centre of the flux collector and is on the rotation axis. The beam from the first beam splitter is adjusted so that impinges on the centre of the collector, about which point the collector

rotates. A target board, marked at intervals corresponding to the intervals between the beam splitters, is then placed on the detector superstructure parallel to the optical bench, with the first mark at the centre of the collector and the board horizontal. The laser beams are then all adjusted to fall at their appropriate positions on the aiming board, producing a series of parallel beams of light which can be used to sample points on a radius of the mirror sector. The collector superstructure can now be rotated to bring the bisecting arc of a mirror sector into the horizontal plane incorporating the laser beams. The resulting image is brought to the focus of the dish which is defined as being at the specification focal length from the centre of the paraboloid, along the line defined by the principal laser beam. Upon the completion of this procedure we have defined a principal laser beam colinear with the optic axis of the mirror sector, and a number of other beams parallel to this. A plan view of the test apparatus is given in Figure 4.2.

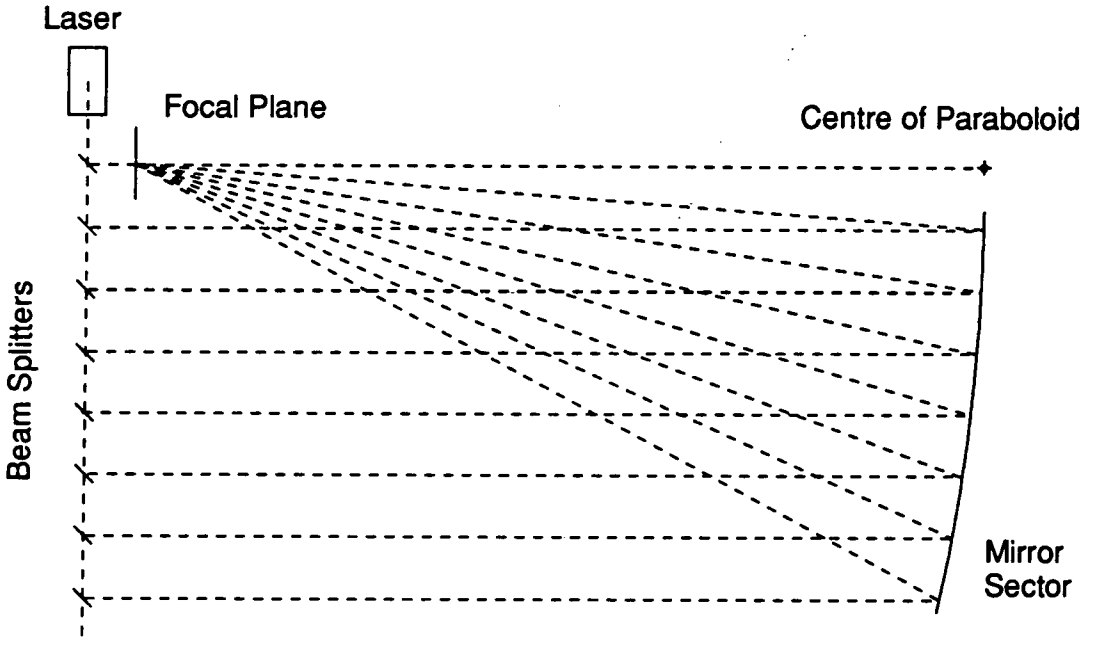

Figure 4.2: A schematic diagram of the mirror testing apparatus. Eight parallel beams of laser light sample the mirror surface along tangential arcs.

4.3.5 Performance of an Individual Mirror Sector

The objective was to derive an estimate of the intensity profile of an image on the focal plane assuming uniform, on axis illumination of the mirror sector. The laser beams sample points on the mirror surface. Assuming radial symmetry, the intensity profile is given by the number density of the laser beams at the focal plane within annuli around the focus.

The maximum number of parallel beams that could be produced was limited by the fall off in beam intensity at each successive beam splitter. Eight beams were used to sample the mirror surface along each radius. The distance of each beam splitter from the principal beam defining the optic axis was chosen so that each sample point represents an equal area of the mirror surface. The mirror was sampled on 15 radii equally spaced at 2° intervals. Measurements were taken of the deviation of the beams, reflected at each sample point, from the focus. A polar plot of these measurements is shown in Figure 4.3.

One can imagine that a composite image of 12 of the plots shown in Figure 4.3, each displaced by 30° from the preceding one, would be symmetrical about the focus. An approximate FWHM of 2.4 cm was inferred for the point spread function using the number density of points in successive 0.4 cm annuli as a representation of intensity. This hypothetical image size assumes that the mirror sectors are configured ideally using the image produced by the bisecting radii. On the evidence of Figure 4.3 it is obvious that the beams reflected from the majority of sample points fall below the focus. This suggests that the image produced from the bisecting arc of the mirror sector does not best represent the "centre of gravity" of the image produced by the whole sector. It is clear that the composite image could be improved by pushing the centroid of the distribution of points of

each sector to the focus, as shown in Figure 4.4.

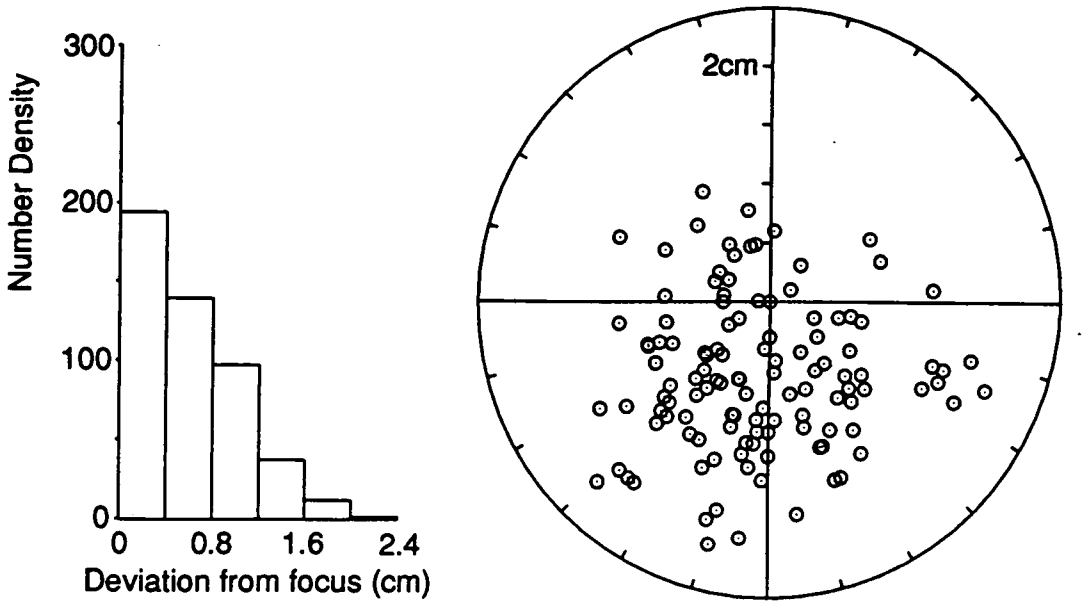

Figure 4.3: The points of the polar plot represent the position on the focal plane to which each of the laser beams were reflected from each sample point on the mirror surface. The bars of the histogram represent the number density of points within successive annuli of the polar diagram.

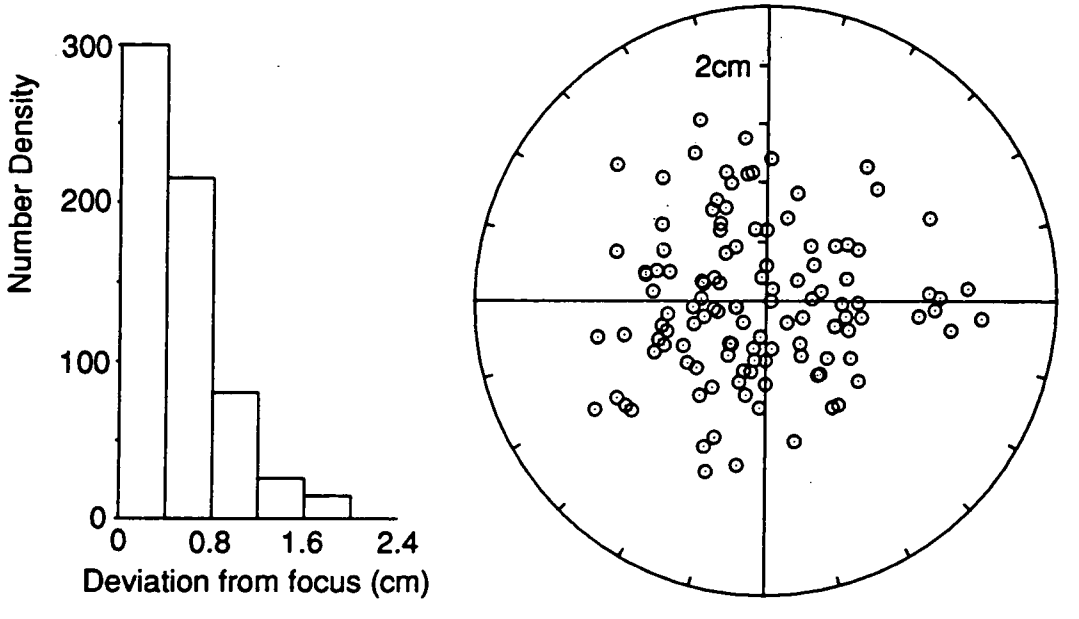

Figure 4.4: A revised number density histogram derived from the polar plot shown, which has had its centre adjusted to the centre of gravity of the distribution of points.

The estimated FWHM of the revised number density distribution is 2.0 cm corresponding to an aperture on the sky of 0.34°.

The data described above have also been used to estimate the accuracy of machining of the former. During the course of testing each laser beam describes an arc across the mirror surface at a particular radius. The circular arc sampled by the beam lies in a vertical plane normal to the optic axis. Any vertical displacement in the beam from the focus is due to there being a local deviation in the normal to the mirror surface from the horizontal. This deviation suggests extension of the arc on the mirror out of the vertical plane. A gradient in the arc can be inferred and is an error of manufacture. The tangential gradient at each sample point is calculated from the vertical displacement of the beam from the focus in the focal plane. The whole of the element of arc represented by the sample point is assumed to have this gradient. We can calculate each sample point's displacement normal to the arc assuming the change in gradient of the surface of the mirror is continuous, and does not change on a length scale which is short in comparison with the distance between sample points. Evidence that the change in gradient is continuous is provided by the observation that the beams can be seen to track across the focal plane with no discontinuities in their loci, save for those caused by local imperfections in the surface.

Surface deviations above or below the paraboloid have been calculated for each sample point, and the deviations from each arc have been plotted in Figure 4.5, with the ordinate axis representing a displacement from the bisecting radius along the arc. This figure suggests a gradient along each arc relative to the perpendicular to the plane of the parabola on the bisecting radius. The mean gradient of the best fit straight lines to these data sets is 0.001 (with a standard deviation of 0.0004). This would translate to a 1 mm

step between adjacent mirror sectors at the circumference of the flux collector. Steps such as these have been seen during alignment of adjacent sectors (configuration of flux collectors is described in Section 4.3.6).

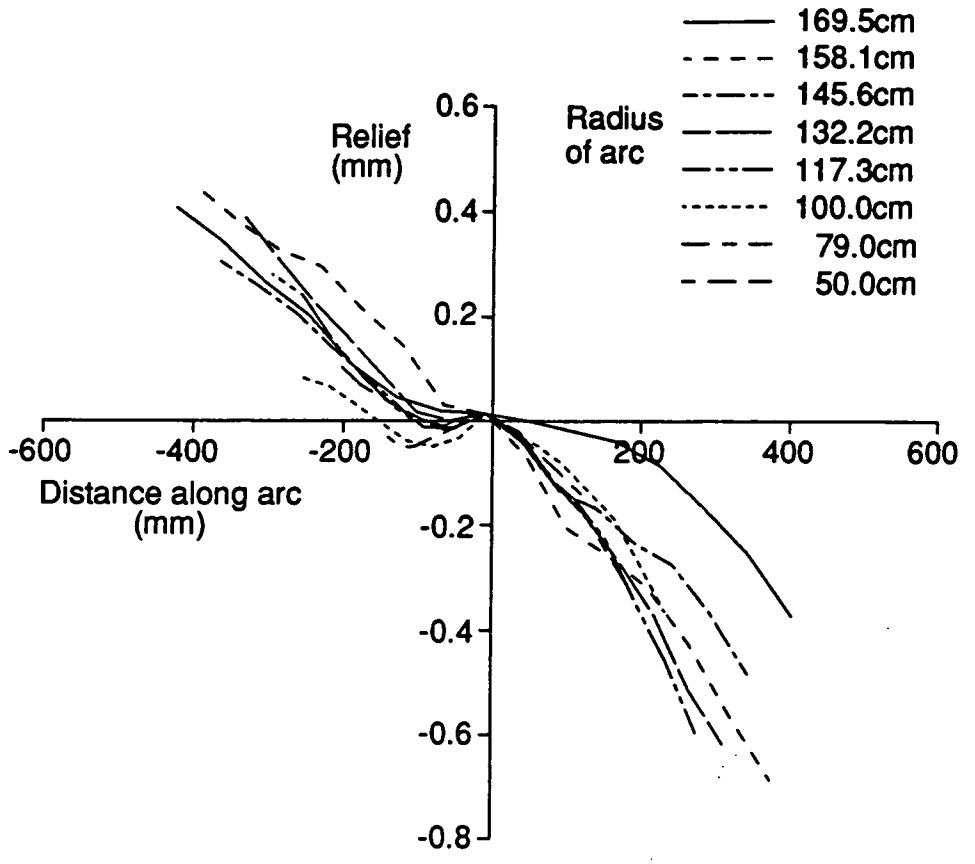

Figure 4.5: The vertical axis of this graph represents the relief of the surface of the former above the specification paraboloid. This relief, along arcs tangential to the sector radius, is calculated using data provided by the laser testing procedure applied to an example mirror sector.

On the evidence of Figure 4.5 it would seem that the reference horizontal used during the manufacture of the former was in error by approximately 3 minutes of arc. This systematic error has no effect on the ultimate performance of the mirrors. It simply causes the parabola to be "open" by a negligible amount.

Assuming that the gradient across the mirror is a genuine systematic error in the method of manufacture then we can subtract this gradient from the data and calculate the residual errors. Figure 4.6 is a plot of this residual relief.

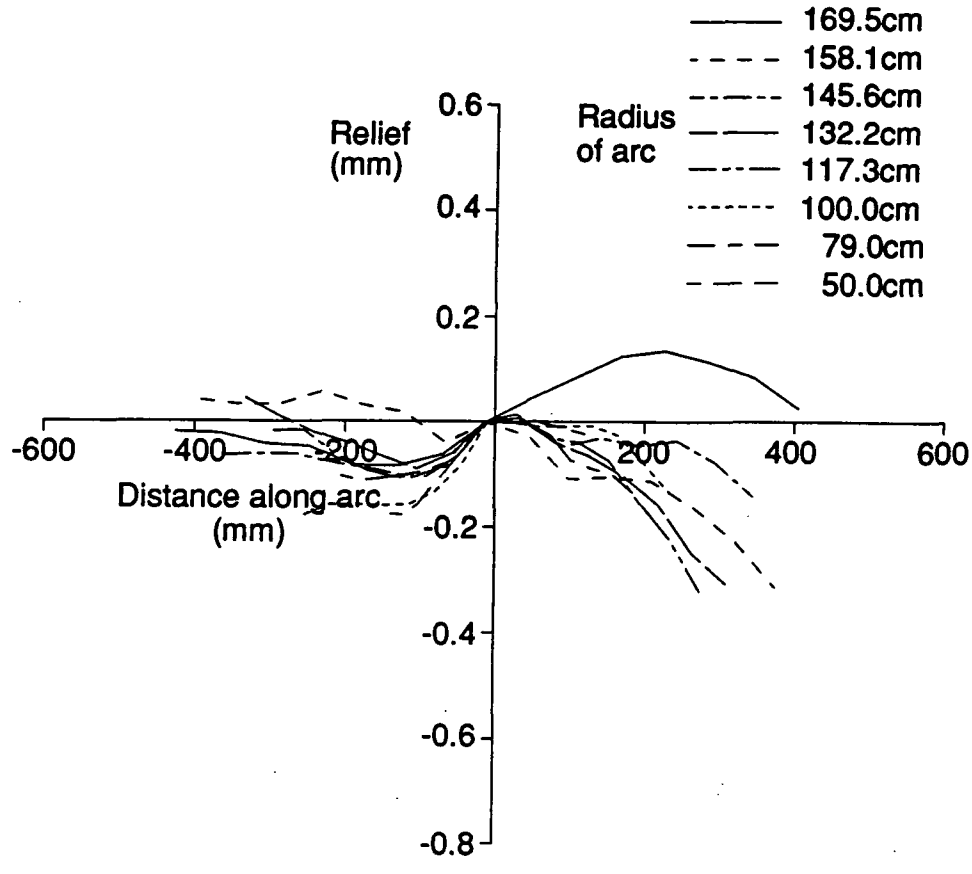

Figure 4.6: This graph represents the residual relief, after subtraction of the systematic gradient evident in Figure 4.5, along tangential arcs on the former surface, This is effectively the relief above the "best fit" paraboloid.

A contouring algorithm has been applied to these corrected data and the resultant contour plot of the residual relief is shown in Figure 4.7.

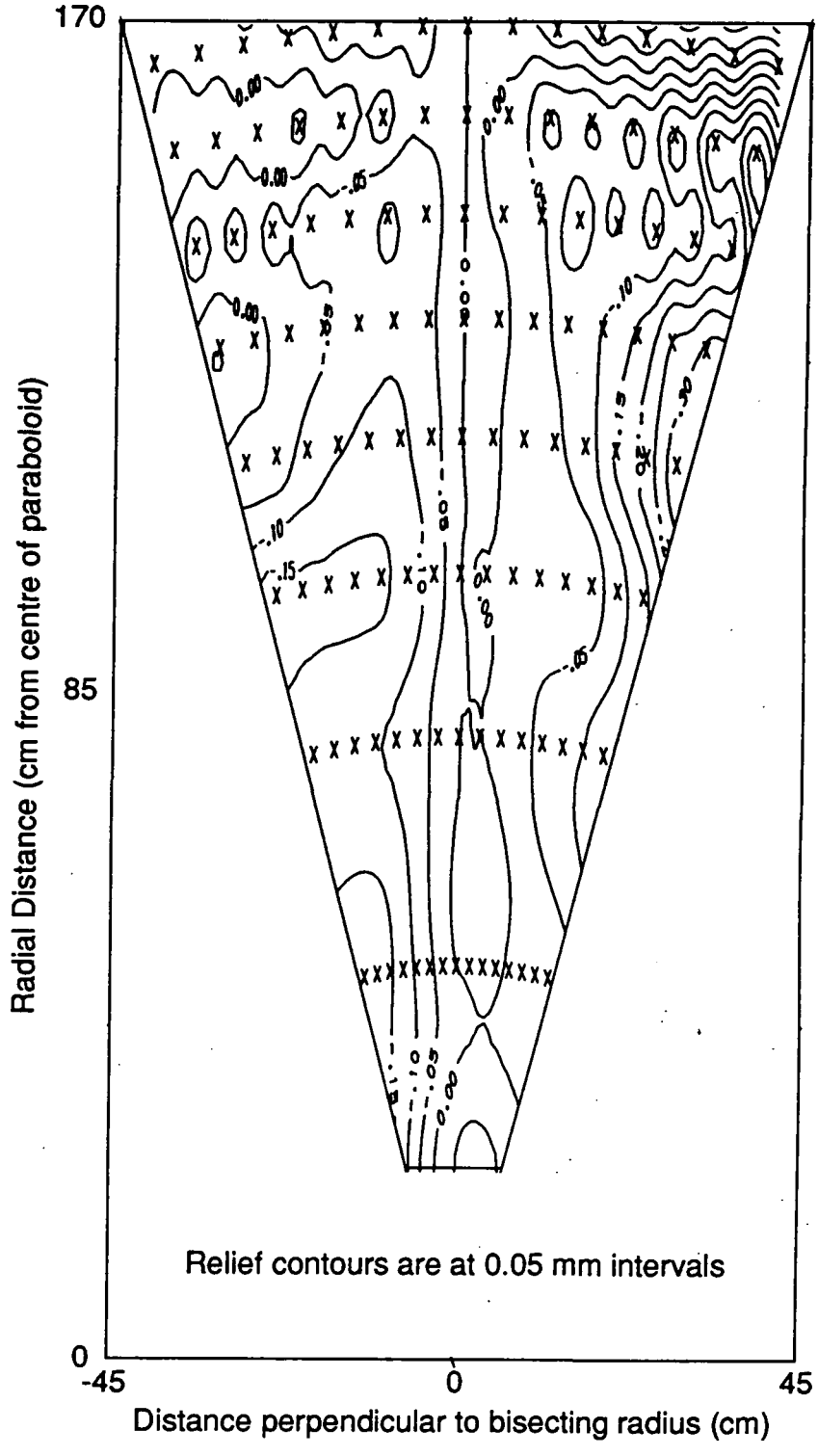

Figure 4.7: A contour plot representing the relief of the former surface above the "best fit" paraboloid. Relief on the centre line, which constitutes the reference arc, is constrained to be zero. Sample points are denoted x.

4.3.6 Configuration of Composite Collectors from Individual Sectors

Each identical mirror represents a 30° sector of a composite flux collector. The mirrors are fixed to the superstructure at three points, two at the circumference of the collector and one at the centre. All three support points have adjustment parallel to the optic axis. The requirement for accurate field configuration of three flux collectors, each comprised of 12 of these large area sectors, necessitated the development of a new method of mirror alignment. The solution arrived at was a development of the mirror testing equipment. A system of parallel laser beams was required which could be swept over each mirror sector in turn, imitating a distant light source. Obviously it was impractical to rotate the flux collectors as had been done in the laboratory, so a self contained, rotating laser system was developed within a 4 m length of aluminium channel. A centre point was defined within the channel and the channel fixed to a rotating hub with the centre point on the rotation axis. The axis of the hub was then aligned parallel to a heavy steel plate fixed to a tower which was adjustable in the vertical. A 5 mW solid state He/Ne laser was aimed down the axis of the channel through a series of regularly spaced beam splitters, including one on the rotation axis of the channel. Figure 4.8 is a photograph of the laser alignment system in the field.

The beam defining the rotation axis of the channel was set first. As the channel was rotated the beam from the beam splitter on the optic axis described a circle on a target board. The centre of this circle is on the rotation axis and the beam was adjusted to fall at the centre of the circle. Once the principal beam had been adjusted to define the optic axis the other beams were set parallel to this using a vertical aiming board.

With the beams set parallel, the relative attitudes of the spin axis of the

Figure 4.8: The mirror alignment system facing the Mk.6 telescope

laser system and the nominal optic axis of the flux collector were adjusted until the axes were colinear. The principal laser beam passes through the focus, which is at the centre of the cradle which supports the detector package at the focal plane, and impinges on the centre of the flux collector. Once this condition has been achieved the mirror sectors can be adjusted successively to bring their individual foci to the collective focus of the flux collector.

4.3.7 Composite Flux Collector Performance

The mirror sectors of the flux collectors on the Mk.5 telescope were aligned by adjusting the mirrors such that the centre of the cluster of laser spots at the focal plane fell on the optic axis. The bisecting radius of each mirror was used as the reference. An image size at FWHM was estimated in Section 4.3.4 for optics configured in this manner. The response of one and two inch PM tubes to the passage of a star across their field of view is consistent with this and Figure 4.9 shows a CCD image of a star projected onto a screen at the centre of the focal plane. Figure 4.10 displays the CCD pixel values across two perpendicular sections through the image. The width of the point spread function at FWHM is 2.5 cm demonstrating that the configuration of the mirror sectors was close to optimal, using the centre line of the sector as the reference.

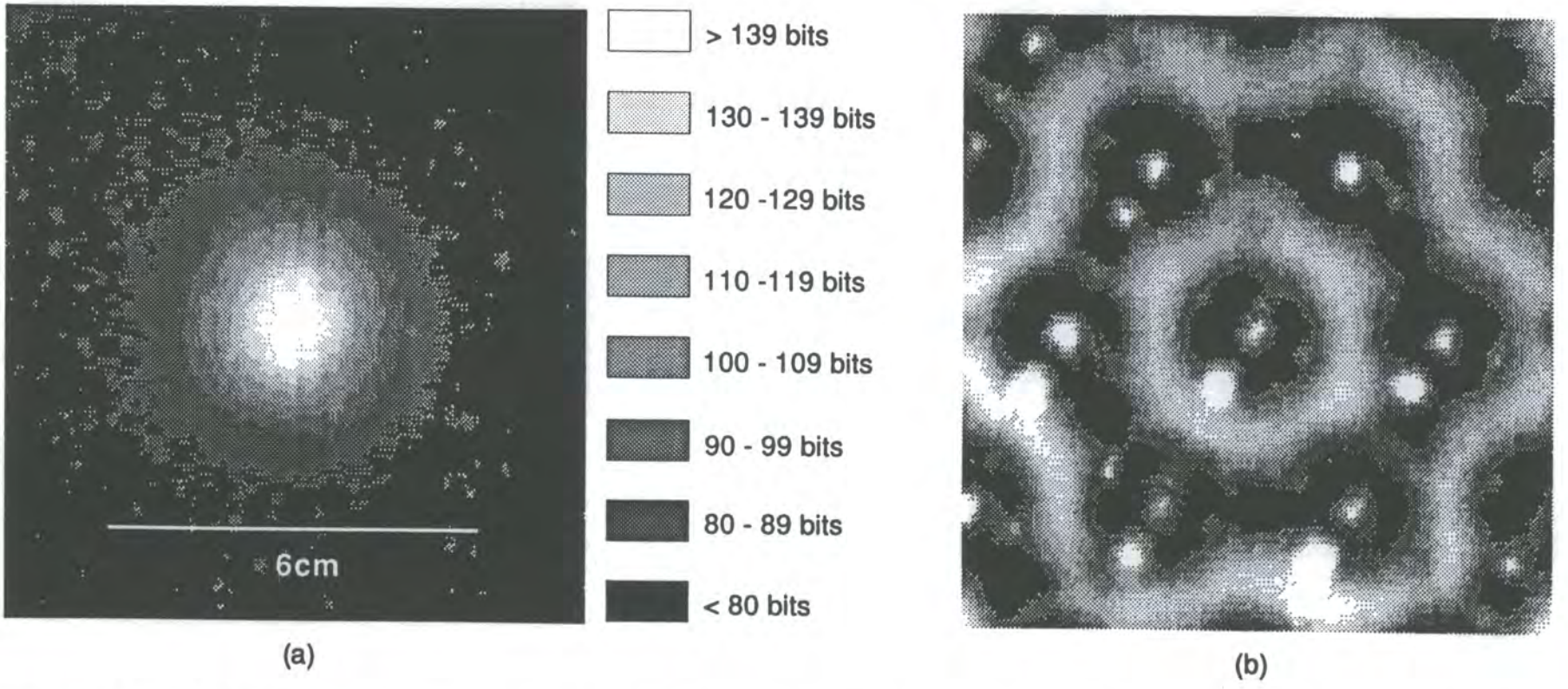

Figure 4.9: (a) A CCD exposure of a star image focussed onto a plain white target at the focal plane. The grey scale has been adjusted such that each band represents one eighth of the signal range. The background pixels average 73 bits while the largest pixel value is 150 bits. (b) A CCD image of the PM tube assembly at the focal plane of the same scale.

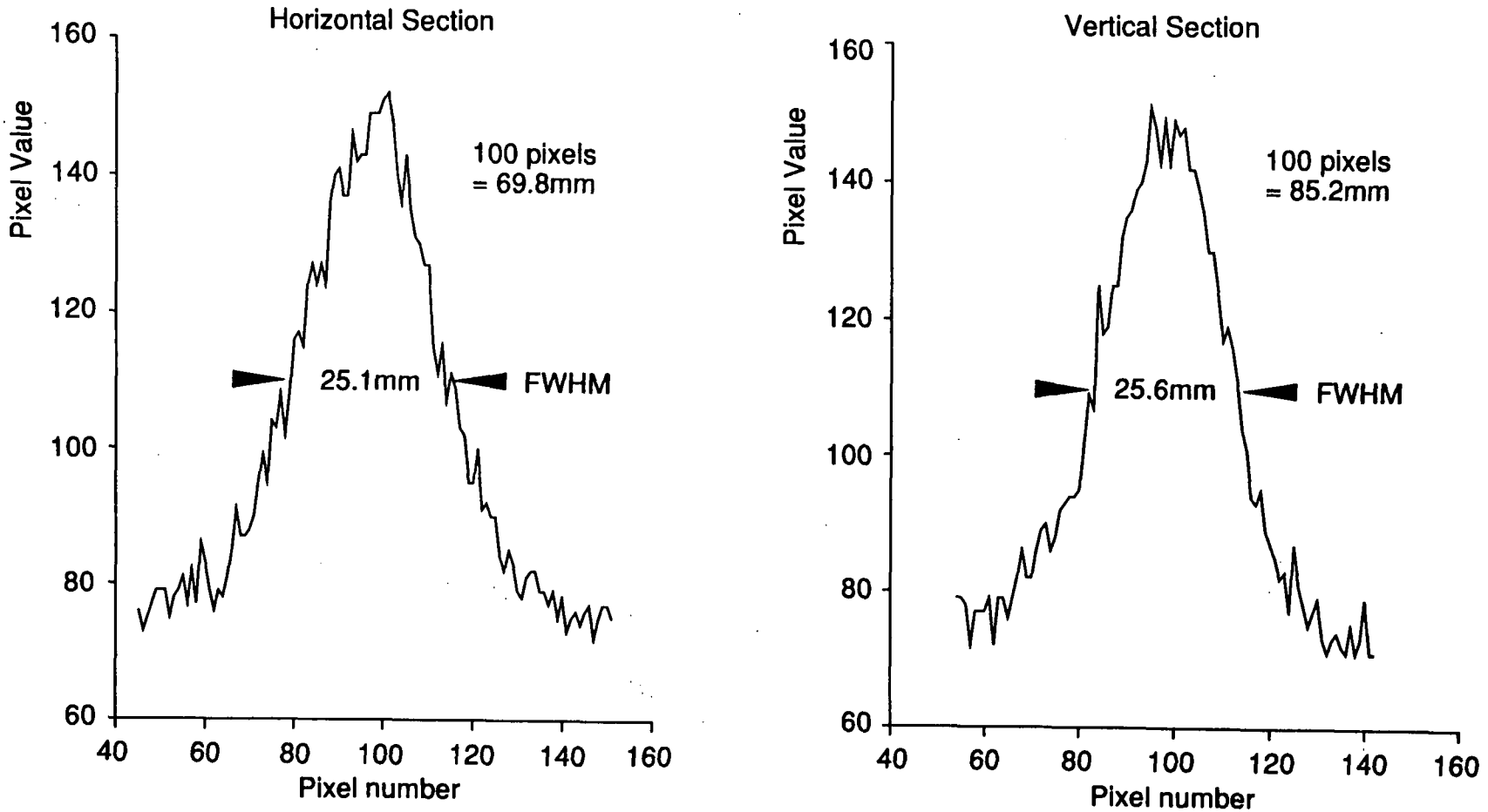

Figure 4.10: Intensity profiles for two orthogonal sections through the CCD exposure to the star image shown in Figure 4.9

The CCD response to light intensity is linear therefore the median pixel value represents the half maximum light intensity.

4.3.8 Co-alignment of the Optic Axes of the Flux Collectors

During the telescope build, the hexagonal cradles which support the detector packages have their centres plumbed vertically above their respective collectors. Thus the nominal optic axes are accurately paraxial. After alignment of the mirrors, the optic axis alignment is checked using the anode current response of PM tubes to the passage of a star through the focal plane. Minor adjustment can be made to the tripod support of the detector package to accommodate small errors.

4.3.9 Conclusion

The mirror manufacture technique proved to be very successful with the shape of the former being faithfully reproduced in every mirror surface. The limit to the utility of the technique appears to be the accuracy to which the former can be machined. Mirror form remains stable even without the added rigidity provided by the sector perimeter frame suggesting that larger area mirrors could be fabricated using the same method. The mirrors are cheap (£150 m^{-2}), light (14 kg m^{-2}), durable and have the required optical quality.

4.4 Telescope Mechanics

4.4.1 Introduction

The Durham group have traditionally used an alt-azimuth mount for their telescopes. This is due to the use of ex-military engineering components as the platform for the early instruments, and the ease of twin axis steering

using microcomputer technology. The increase in scale to that proposed for the Mk.6 telescope necessitated the production of a purpose built mount. With this increase in scale, and a clean sheet for design, the opportunity existed to consider an equatorial system.

The most significant advantage presented by the equatorial mount is that system rotates at constant angular velocity around a single axis whilst tracking. The angular velocities around orthogonal zenith and azimuthal axes in an equivalent alt-azimuth system are constantly changing within a large dynamic range. Unfortunately, this presents the possibility that drive velocities may coincide with resonant frequencies in the mechanics of the telescope. No serious problems in this area have been encountered with previous telescopes operated by the group and it was felt that any resonances could be suppressed by adjustment of the time constant of the drive. Ultimately, though, the use of an equatorial mount for the Mk.5 telescope was not a practical possibility due to the extension of the telescope in the equatorial plane. The provision of complete sky coverage would require a heavily engineered mount incorporating a large counterweight. This solution was precluded by cost and lack of access to heavy engineering facilities.

4.4.2 Alt-Azimuth Mount

In contrast to the adapted gun mount used for the Mk.3 telescope the mount for the Mk.5 telescope was purpose built. The three dishes which comprise the optics are rigidly connected and are supported on a cradle by two bearings on a horizontal axis. The relative positions of the collectors are configured such that the structure is approximately in balance at all zenith angles. Free to move from 90° to 0° in zenith, the structure is driven

by a DC servo motor with integral gearbox, through a gear quadrant of 18" radius. The cradle is bolted on top of a 4' diameter, 1" thick circular steel plate on which the motor sits to drive the quadrant. This plate, supported by a number of pylons around its periphery, faces a similar plate. Each pylon is fixed to the upper plate and incorporates a brass wheel at its base which is in contact with the lower plate. The wheels are arranged tangentially and allow the plates to rotate relative to each other. The plates are centred by a thrust race bearing. The lower plate defines the azimuthal plane and in construction is set to the local horizontal. This plate is stationary and is fixed rigidly to the plinth. A ring gear is fixed to the lower plate concentric to the thrust bearing and a motor fixed to the top plate, with its axis radial to the plate, drives the top plate against this ring.

4.4.3 The DC Servo Motors and Integral Gearbox

The Mk.5 telescope is driven by Electrocraft permanent magnet DC servo motors. Drive is transmitted through a Gysin gearbox with a reduction ratio of 196:1. An additional gear train in the zenith drive, with a ratio of 2:1, increases the final drive ratio to 400:1 and the final drive gear diameter of 4" meshing with the quadrant of radius 18" increases the mechanical advantage to 1800:1. In the Azimuthal axis the final drive of the gearbox drives the telescope against a 27" diameter bevel ring gear. The total reduction ratio in the azimuthal axis is 3528:1.

When a continuous current is passed through the windings of a DC motor a continuous torque is produced and the motor will accelerate until the torque matches the friction force. For effective drive and attitude control of the telescope the velocity of the motor and the position of the telescope must be sensed and provided as feedback for the motor controller. The

motor current is regulated in response to the feedback in such a way that the correct amount of torque is generated to effect the required movement. Telescope positional information is provided by absolute optical shaft encoders, which sense the attitude of the telescope in the azimuthal and zenith planes and provide positional feedback to the steering program. The telescope is driven independently in these planes. Motor angular velocity feedback is provided by tacho generators which produce a signal proportional to speed. The steering computer generates a velocity command signal, based upon the positional error in the encoder readings, indicating a required motor speed. This drive signal is passed to the servo amplifier which compares this with the feedback from the tacho generators and the resulting error is amplified to produce the drive current in the motors. Velocity changes are effected gradually to avoid placing undue stress on the drivetrain. The motor control boards also incorporate the facility for directional limit switches. At the limit the switches take a high resistance, passing a limit input of 0 V which reduces the motor current to a low value.

4.4.4 Shaft Encoders

The encoders (BEI model M25D-X-H4096N) used on the Mk.5 telescope are the same specification as those on the Mk.3 telescope. The zenith encoder is fixed to the cradle which supports the driven superstructure and provides the absolute position of a shaft passing through one of the zenith bearings, relative to a reference zero. This position is encoded as a 12 bit word. The azimuth encoder is fixed to the top one of the pair of circular steel plates which comprise the azimuth turntable. Its angular position is measured relative to a shaft which passes through the thrust bearing and is

clamped rigidly to the telescope plinth. Both encoders provide absolute positional information to one part in 4096 of a complete revolution, this translates to a resolution of slightly better than 0.09°.

4.5 Telescope Steering

4.5.1 Introduction

The format of the steering package has not changed during the evolution of the Durham telescopes. This section will address the interface of the computer steering program with the motor control loop, routine steering checks and developments towards improved tracking resolution.

4.5.2 The Steering Computer and CAMAC Steering Interface

The telescope steering is controlled by a BBC microcomputer. Target azimuth and zenith positions are calculated from the source R.A. and declination every six seconds. The attitude of the telescope is sensed to an accuracy of 0.09°. This angle is represented by one shaft encoder bit which corresponds to the least significant bit in the steering program. Shaft encoder readings are passed to a CAMAC steering interface which converts the encoded grey scale 12 bit word into a binary word. This positional information is read continuously by the microcomputer and compared with the current target position. If the telescope position is in error compared with the target position the steering computer generates an appropriate drive voltage. The magnitude of the drive voltage passed to the steering interface is a function of the error, though the program contains drive constraints to prevent mechanical damage. Drive voltage is ramped up and

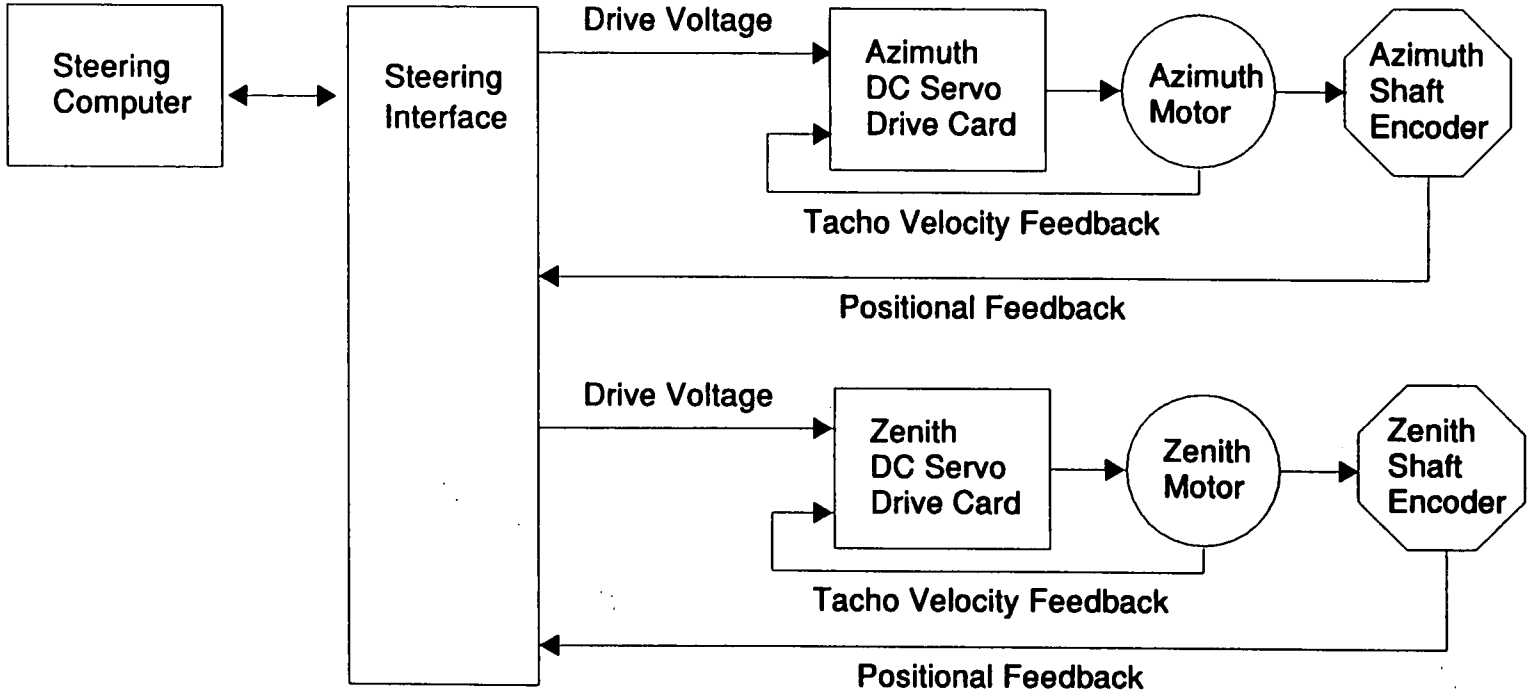

Figure 4.11: A schematic diagram of the motor control system.

down to large values, restricting the maximum rate of change of drive. Figure 4.11 is a schematic representation of the motor drive control system.

During tracking the updated target position rarely differs from the previous one by more than one bit. Thus, if the tacho gain and time constant of the motor controller are adjusted such that the telescope achieves the new desired pointing direction inside the six seconds then the telescope moves in a series of well mannered steps, reducing the probability of mechanical resonances within the structure.

4.5.3 A Routine Check of the Steering Integrity

The steering integrity of the telescopes is checked regularly using an automated "starcheck" procedure. A CCTV camera is mounted paraxial with the optic axes of the telescope and views the same region of sky as the detector packages. The anode current response to a star within the field of view of the central PM tube of the camera is used to define an isophote contour at half the maximum light intensity. For the Mk.5 telescope this contour is a circle of a diameter corresponding to a 0.5° aperture. This countour is marked on the CCTV monitor and is used as the reference for the "starcheck". The telescope is pointed at 12 stars, chosen to exercise the telescope over the whole of its range of movement, and the positions of each of these stars in the field of view of the CCTV camera are compared with the direction representing the axis of the central PM tube. The results of a typical "starcheck", performed at 11:00 UT on 30th November 1994 are presented in Figure 4.12.

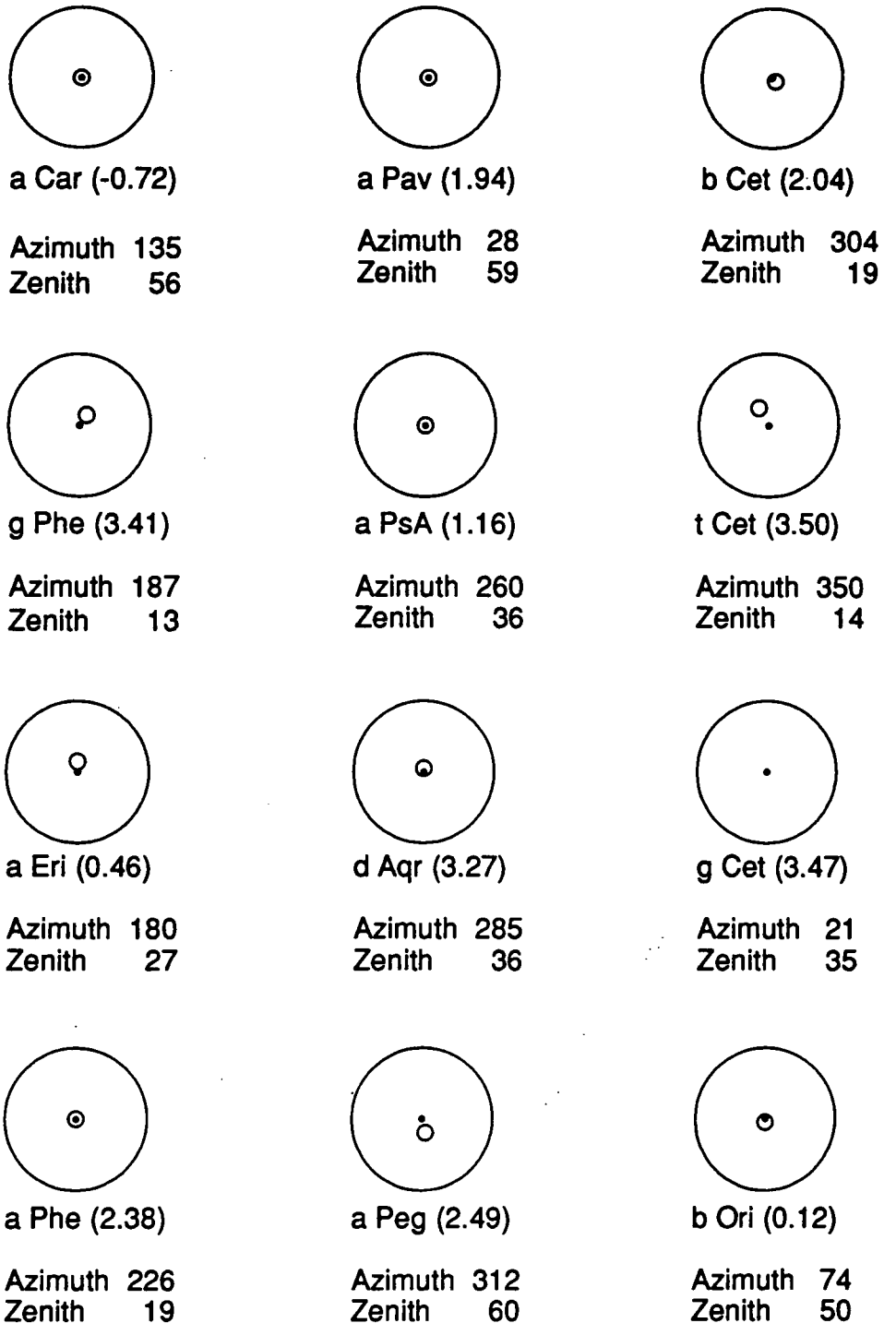

Figure 4.12: The results of a typical check of telescope pointing accuracy. The positions of 12 stars relative to a reference circle on the monitor of the CCTV camera. The reference circle represents the effective aperture of the central PM tube of the camera and defines an opening angle of 0.5°. The smaller open circle marks the position of the star in each case.

4.5.4 The CCD Camera

The improvement of optical resolution associated with the advent of the imaging technique within the Durham group has challenged the accuracy of the steering. The resolution of 0.09° provided by the 12 bit shaft encoders is barely adequate. However, rather than replace these with expensive 14 bit encoders, an astronomical CCD camera has been fitted to the telescope to observe the sky and provide an equivalent four fold increase in accuracy of position sensing. The sensitive area of the CCD is 2.54 mm^2 comprising 165 x 192 pixels, which translates to arc second accuracy when used with a f/1.4 50 mm lens.

At the start of an observation a full frame image of the field of view of the CCD camera is recorded. The minimum magnitude star visible after the typical exposure of between 1 and 5 seconds seconds is 7th to 8th magnitude. The position and brightness of the brightest star within the field of view is then tracked and recorded as a five bit word within the event data for each event. During the pre-processing of data this position is compared with the predicted position of the brightest star within a star catalogue subset containing the stars within the field of view of the CCD camera for the target source. CCD integration time during observation is reduced to allow frequent measurement but allows tracking of 5th or 6th magnitude stars. The actual attitude of the telescope is reconstructed to an accuracy of 1arc minute and the Cartesian deviation, on the focal plane, of the projected source direction from the centre of the detector package is calculated. The encoder values of azimuth and zenith pointing angles are overwritten in the data file and the x, y deviations are recorded elsewhere within the event data record. Figure 4.13 is a composite of a full frame CCD exposure and the locus of the star in the field of view during an observation.

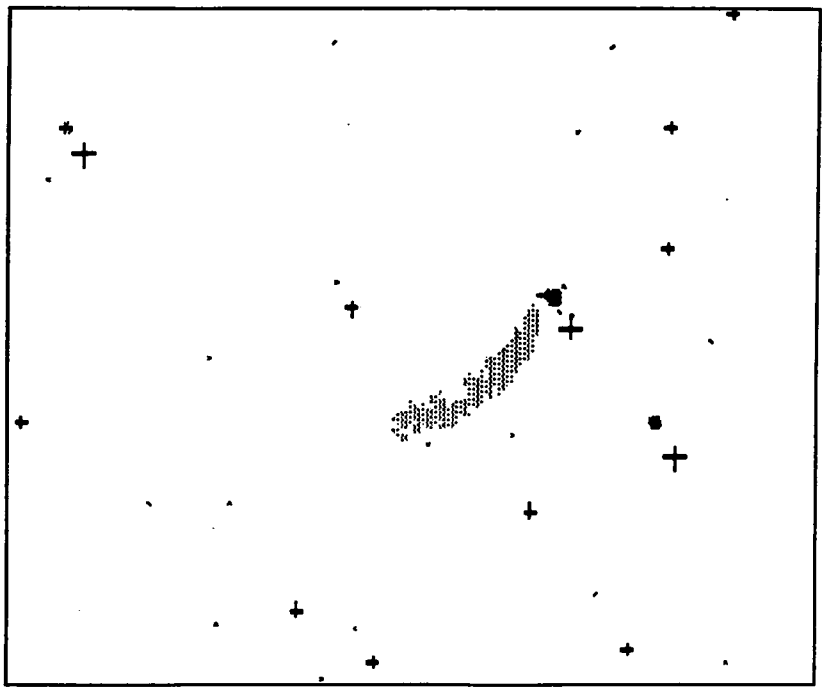

Figure 4.13: The above diagram represents the field of view of the CCD camera at the start of an observation of Vela X-1. A number of stars are evident in the full field exposure. The crosses represent the predicted fiducial star positions at the start of the observation. The brightest star is chosen by the software and its position recorded for each event. The locus of the star position through the field of view during an observation is indicated by the plotted position of the star for each event of the data file.

4.6 Camera PMT Detector System

4.6.1 Introduction

In order to be able to exploit the spatial disparities between the Cerenkov signatures of EAS initiated by gamma ray and hadron primaries in a signal enhancement technique, a detector is required with a resolution comparable to the scale of the relevant structure in the image. In the context of the function of the Mk.5 telescope as a half scale prototype for a genuinely high

resolution detector the resolution is dictated by the optics. The point spread function of the Mk.5 telescope flux collectors at FWHM is 2.5 cm at the focus, which equates to an angular resolution of 0.43°. The latest Monte Carlo simulations of EAS predict Cerenkov images with a typical angular size of 0.5° for gamma ray primaries and somewhat larger for hadrons. Images of showers with axes displaced from the optic axis will have extension in one dimension as described in Section 3.5.2. A detector package with granularity on a somewhat smaller scale would then be able to appeal to parameters such as image shape and directionality of the shower axis in a background rejection strategy.

4.6.2 Photomultiplier Tubes

4.6.2.1 Sensitive Area and Pixel Size

Assuming the radius of the Cerenkov light pool produced by a gamma ray initiated EAS to be 130 m and that every shower develops and degrades somewhere between 13,000 and 6,000 m above the telescope, then the whole image of every shower from the source direction would be contained within the field of view of a telescope with an opening angle of 2.5°. The focal length of 3.32 m of the Mk.5 telescope flux collectors defines an image scale on the focal plane of 0.17° per cm, thus the required sensitive area of the focal plane has a diameter of approximately 15 cm. This area can be covered by a hexagonally close packed array of 19 one inch photomultiplier tubes, with a pixel pitch of 3 cm, to provide a camera with resolution on the half degree scale. A peripheral ring of 1.5" PM tubes has been added to the camera, external to the triggered area, in order to provide intensity information on the extremities of images whose centroids are close to the

edge of the camera.

4.6.2.2 Choice of Photomultiplier

The PM tube of choice since the inception of the Mk.2 telescope programme has been the 2" diameter RCA (subsequently Burle) 8575. This tube was designed for pulse counting applications, displaying high quantum efficiency, high gain, good noise characteristics and good temporal performance. These are the characteristics desired for the one inch PM tubes which will form the pixels of the camera, with an added requirement that the tubes have a good energy resolution. The Burle S83062E 1" diameter PM tube has been designed with fast applications in mind and its manufacturers specifications for the tube characteristics compare favourably with those quoted for the 8575.

The ring of PM tubes peripheral to the 1" tube array does not contribute to the trigger. Twelve Burle C7151Q 1.5" tubes were used for this ring. These tubes have a rise time of 2.2 ns, which is comparable to the S83062E 1" tubes, and sensitivity over a similar spectral range.

4.6.2.3 Comparison of the Burle S83062E and 8575 PM tubes

The spectral responsivity of these tubes is very similar, the sensitivity of both peaking in the blue and extending well into the important ultra violet region. The typical photocathode spectral responsivity characteristics are reproduced in Figure 4.14. The rise time of the tube is quoted to be 2.3 ns for a potential difference of 1500 V over the whole dynode chain, which is adequate for the intended application.

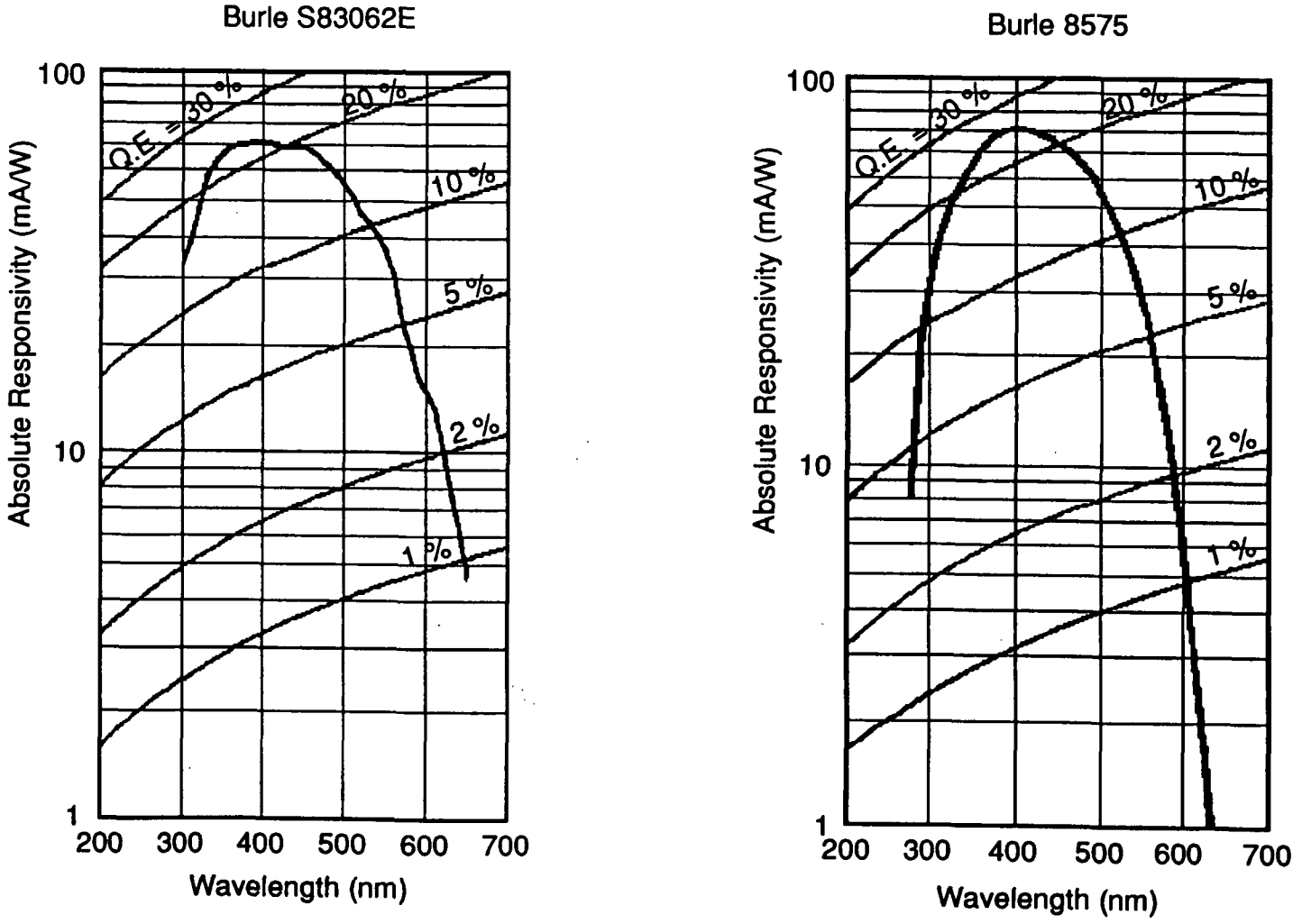

Figure 4.14: Spectral response of the Burle S83062E and 8575 photomultiplier tubes

A series of tests were performed to compare the noise and gain characteristics of the 8575 tube with the S83062E. A considerable amount of experience has been gained in the operation of the Burle 8575 PM tube during several years of use under night sky conditions in the telescopes operated by the group. A Burle 8575 PM tube of known telescope operating conditions was placed in a dark box. Light from a yellow LED, in series with a variable resistor and 5 V supply, was reflected from a piece of white card to simulate the starlight of the night sky. The anode current and noise rates of the control Burle 8575 tube and the test Burle S83062E tube were recorded for illuminations varying over two orders of magnitude around a simulated average night sky brightness. The results of these tests are displayed in Figures 4.15 and 4.16.

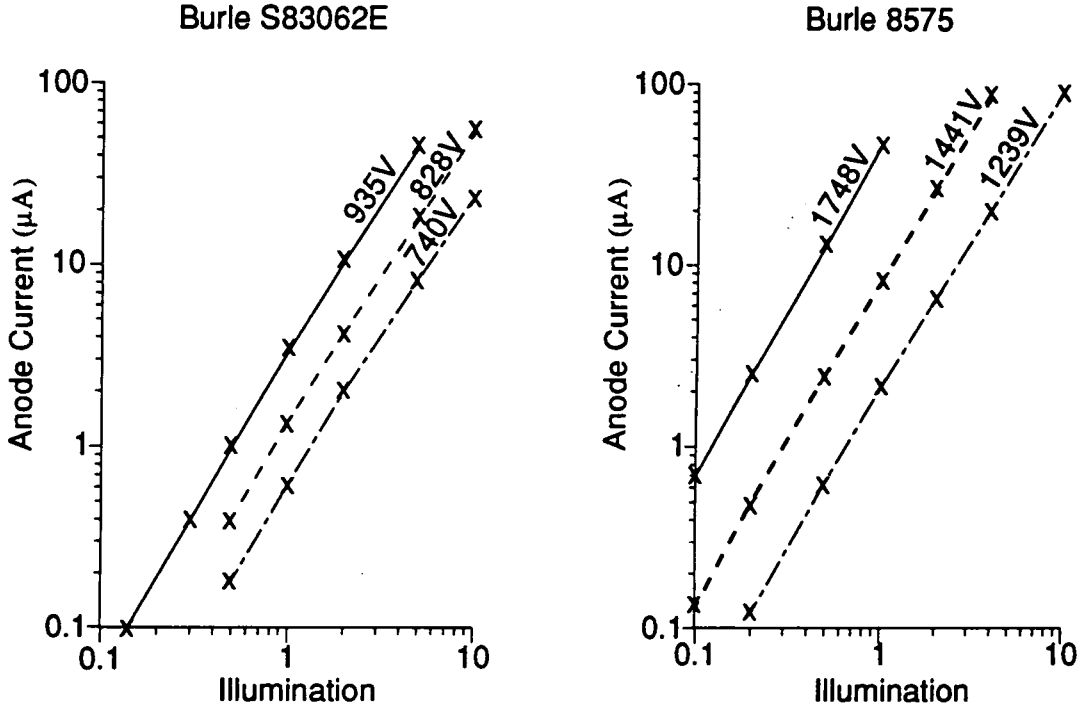

Figure 4.15: Comparison of the gain characteristics of Burle S83062E and 8575 PM tubes. Tests were performed at three voltages under varying illuminations. Illumination is normalised to a typical night sky brightness.

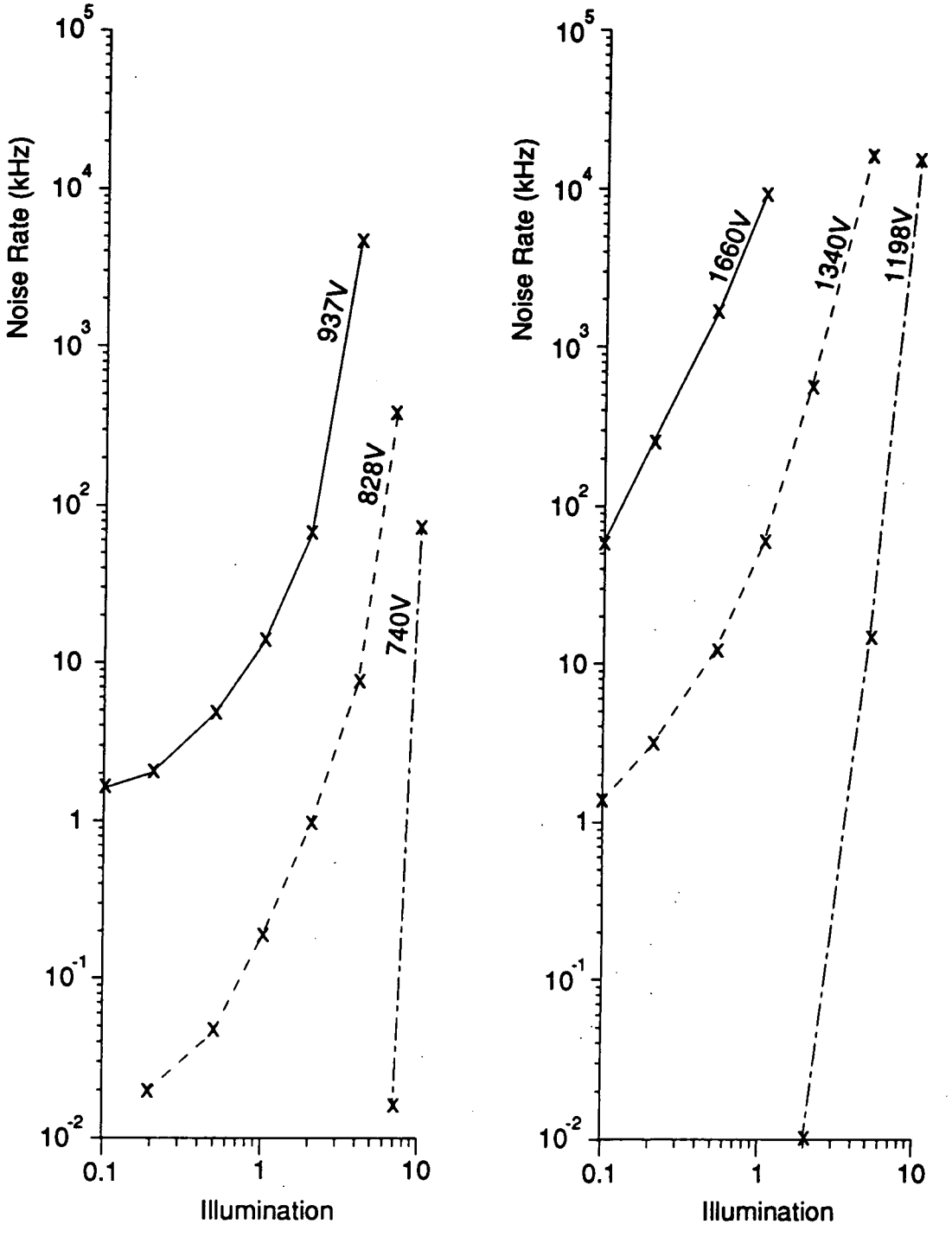

Figure 4.16: Comparison of the noise characteristics of the Burle S83062E and 8575 PM tubes. Illumination is normalised to a typical night sky brightness.

The tests were performed at three tube voltages in each case. A 50 mV discrimination threshold was used, after amplification by a factor of 10, to define the noise rate in order to simulate the Narrabri tube operating conditions.

Tube anode current is plotted against illumination in Figure 4.15 and Log_{10} (Anode Current) is seen to increase linearly with Log_{10} (Illumination). The gradient of the relationship is very similar in each case demonstrating that the tubes have similar gain characteristics (anode current being approximately proportional to gain at constant illumination). The illumination scale has been normalised to an average night sky brightness. Figure 4.16 in which the tube noise rates are plotted against illumination, shows the tubes to have remarkably similar noise characteristics.
These graphs together demonstrate that these tubes are compatible insofar as voltages exist at which the tubes can be operated with similar gains and acceptable noise rates.

4.6.3 Mechanical Construction

The PM tube array is housed in a hexagonal section aluminium cage which mates with an aperture in the cradle supported at the focal plane by the tripod legs. Countersunk circular holes are drilled in a polyethylene front plate, which forms one end of the cage, to accommodate the windows of the PM tubes. The tubes are also supported near their bases by a similar plate which is lodged in the aluminium cage in a plane parallel to the front plate. The EHT wires and coaxial signal cables are led from the bases of the tubes to connectors on a third plate which forms the back plate of the camera package. The coaxial signal cables connect through individual BNC connectors so that a continuous shield is maintained to prevent cross talk

between channels. For convenience the EHT leads converge and are accomodated by two multiway connectors.

Each individual PM tube is magnetically shielded along the length of the dynode chain by the use of a μ-metal cylinder held at the potential of the cathode. An envelope of non conducting heat shrink material is then used to electrically insulate the μ-metal.

4.6.4 Baffles

The application of baffles to exclude extraneous light which adds to the noise may allow the photomultiplier tubes to be operated with higher gain with a consequent reduction in threshold energy, and thus in the case of the camera a more well defined image.

A reflector tessellated with circular mirrors has a dead area of 21% of its surface, thus the light noise from the source direction is augmented by albedo of this dead area. The irregular perimeter shape and design of the superstructure of a tessellated flux collector, such as those used for the Mk.3 telescope, also makes screening at the perimeter of the dish difficult. In contrast, the flush fitting composite mirrors of the Mk.5 telescope lend themselves to screening of background albedo in that the detector package views a complete, approximately circular, reflective surface. In addition, extraneous light from a direction exterior to the mirror surface has been eliminated by the use of a cylinder projecting towards the focal plane from the perimeter of the dish, and a complementary baffle extending from the focal plane towards the reflector. The geometry of this system is illustrated in Figure 4.17. A photograph of the Mk.5 telescope, complete with this albedo protection, can be seen in Figure 4.1. Fitting of the baffles resulted in a 15 % reduction in background current and allowed a corresponding

increase in gain.

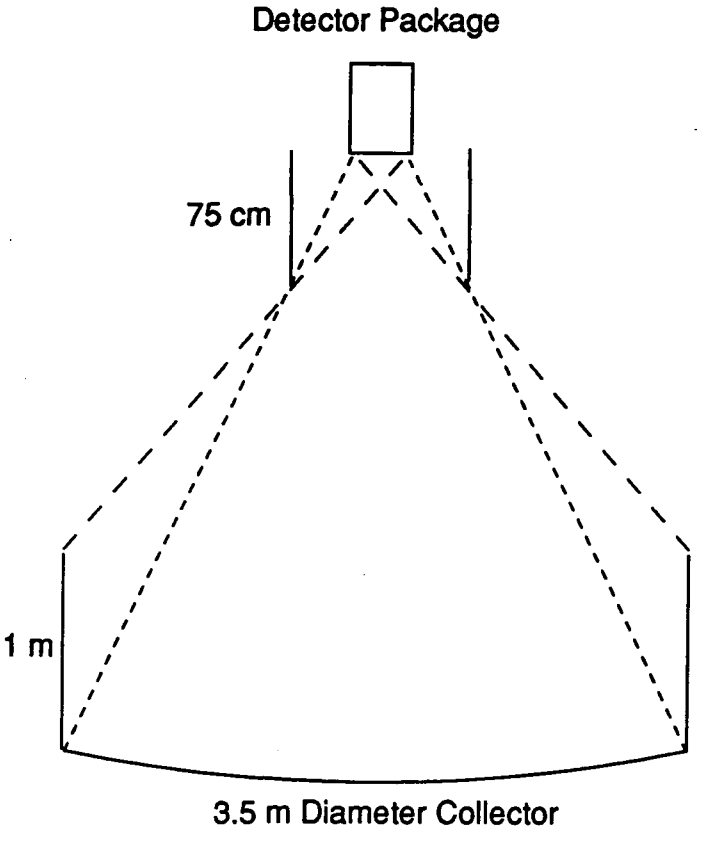

Figure 4.17: Schematic of the albedo protection of the Mk.5 telescope. The combination of the baffles projecting from the focal plane and the cylinder surrounding the mirror exclude all background light while allowing all of the PM tubes in each detector package to view the whole of the reflective surface.

4.6.5 Light Gathering Cones

In general the fast response PM tubes favoured in atmospheric Cerenkov astronomy have circular photocathodes and this, allied to the wall thickness of the tubes, restricts the proportion of area on the focal plane which is photosensitive to about 56 % for hexagonally close packed circular tubes. This dead area on the focal plane has differing effects on the telescope

trigger and the capacity of the camera to form an image. In both cases the effect is to the detriment of telescope sensitivity.

The triggering tubes viewing two of the three flux collectors should have a field of view approximately matched to the size of the gamma ray initiated Cerenkov event. Thus, images which fall on the axis of one trigger channel will fall wholly onto a photosensitive surface, while images falling between channels will lose the majority of their energy to the dead area. Projected onto the camera the image is distributed over several tubes; thus a similar proportion of each event's energy is lost to the dead area, reducing the efficacy of the camera both within the trigger and in its capacity to reproduce the form of the image above the night sky noise.

It is, therefore, important that the amount of Cerenkov light lost to dead areas within the focal plane is minimised. One solution to this problem is the application of light collecting cones to the front of the photomultiplier tubes. These are reflective funnels which have a circular aperture at the face of the tube which matches the size of the photocathode and a hexagonal aperture to the dish with a width, flat to flat, equal to the pitch of the pixels. The cones are designed such that light from any point on the dish which would have fallen peripheral to the photosensitive area will suffer only one reflection before falling on the photocathode. Assuming 80% reflectivity and complete coverage of the focal plane the proportion of light gathered could be increased to 91% giving a corresponding decrease in telescope energy threshold. A test involving the addition of cones fabricated from Alanod resulted in a 15 % increase in background count rate.

4.6.6 Conclusion

A camera detector package has been developed using a close packed array of PM tubes with the capacity to provide spatial information on the Cerenkov images from EAS. The 1" PM tubes chosen for the pixels, which are new to the group, have been shown to have very similar operational characteristics to the familiar Burle 8575 tubes which comprise the triggering packages of the instrument. Pixel pitch in the camera approximately matches the characteristic size of the smaller gamma ray initiated Cerenkov images, offering the opportunity to experiment with imaging background rejection techniques at a resolution with which the Whipple collaboration had success. The shielding of the detector package from background albedo has been effected on the telescope, and plans are in hand for the application of light gathering cones to the camera detector package at the focal plane to maximise the collection efficiency.

4.7 Telescope Event Trigger

4.7.1 Introduction

The ultimate goal of the project is the provision of a telescope of very low energy threshold (< 100 GeV) which is prototyped by the Mk.5 telescope. This goal is unattainable without the use of a very stringent event trigger criterion to allow operation of the PM tubes at high gain without causing pollution of the data with accidental events. Three fold coincidence is retained for the Mk.5 telescope as this represents the best compromise between electronic complexity and optimum performance.

4.7.2 PM Tube Packages Devoted to Event Trigger

The detector package of seven close packed 2" tubes defines a field of view for the telescope of 9 square degrees, each PM tube channel having an aperture of slightly more than one degree on the sky. This field of view matches the opening angle required for the camera defined in Section 4.6. Three identical packages of 2" tubes were initially installed at the focal planes of the three flux collectors of the Mk.5 telescope, and the telescope operated briefly as a conventional three fold coincidence instrument with seven independent channels.

4.7.3 Incorporation of the Camera Tubes into the Event Trigger

After tests which demonstrated that the Mk.5 telescope operated with a conventional event trigger had a equivalent count rate per channel to the Mk.3 telescope, the central detector package was replaced by a camera composed of hexagonally packed 1" PM tubes. The mapping of the camera pixels onto the triggering tubes in the left and right flux collector packages is illustrated in Figure 4.18.

It is evident that the field of view of seven of the camera tubes is wholly contained within the field of view of the corresponding trigger channels. The remainder, however, fall between two triggering channels and are important in the trigger of each. Grouping of the tubes into clusters in a selective trigger is impractical as the majority of tubes would each be active trigger elements in two adjacent clusters and the cost and complexity of the electronics required to effect this precludes this in the Mk.5 telescope. The trigger criterion was, then, relaxed to require coincidence between the two corresponding 2" tubes and one of the 19 camera pixels. This trigger is

easy to implement but requires the camera tubes to be operated at less than optimum gain to restrict their combined single fold noise rate to 20 - 30 kHz (ie 1 - 2 kHz per pixel PM tube). Nevertheless, the count rate with the camera incorporated into the trigger is the same as that achieved with the conventional three fold coincidence, demonstrating the energy threshold to be defined by the Left/Right triggering units. This observation vindicates the choice of trigger logic but suggests improvements are possible to the left and right triggering tubes.

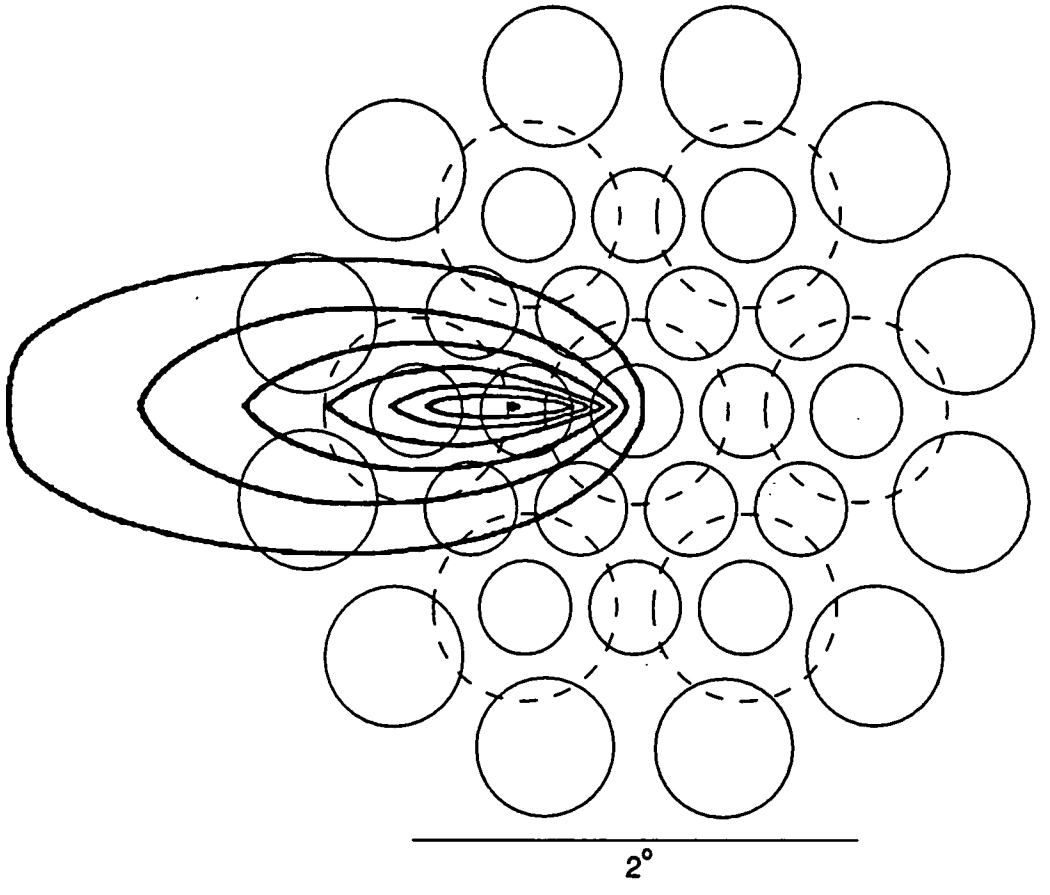

Figure 4.18: Relative field of view of camera tubes (solid circles) and trigger package tubes (dashed circles). Superimposed on the diagram is a representation of the Cerenkov image produced by a 0.1 TeV photon with an impact parameter of 100 m (after Rieke, 1969). Successive isophotes represent a factor of $(10)^{1/2}$ reduction in intensity.

4.7.4 Typical Event Rate and Inferred Threshold Energy

The trigger requires corresponding pairs of 2" PM tubes in the left and right flux collector detector packages and 1 of the 19 1" PM tubes of the camera to achieve the discrimination threshold within an 8 ns gate. At the zenith the aggregate count rate for the 7 independent channels approaches 150 cpm. This count rate is accidental free and is comparable to the count rate of the Mk.3 telescope from which we infer an energy threshold to gamma rays of around 250 GeV.

4.7.5 Conclusion

Incorporation of a simple camera into the trigger of a conventional three fold fast coincidence telescope proved to be successful. Event rate was not degraded by the simple camera trigger criterion indicating that it is the left and right flux collector PM tube packages which define the lower limit to signal detectability. This suggests that the signal should be well represented in the camera pixels even for events with energies near the energy threshold of the telescope. Improved left / right PM tubes would lower the threshold energy, but the camera images at threshold would be less well defined. This problem could be offset by the provision of additional logic within the camera trigger which would allow an increase in camera pixel gain restoring image definition.

4.8 Calibration Routines

4.8.1 Introduction

A prerequisite for any reliable interpretation of image data is knowledge of relative pixel gain. The response of the camera to a "flat field" is dependent upon the relative PM tube gain, and of the pedestal and gain of the digitising electronics. The large number of PM tubes in the Mk.5 telescope introduces a requirement for quick, repeatable and appropriate pedestal and gain calibration procedures.

4.8.2 Digitizer Pedestal Determination

The pedestal values of the charge to time converters (digital readout for zero signal input) are measured by artificially triggering the telescope under normal operating conditions during observation. The trigger is generated at random intervals at an average rate of 5 per minute. The RMS deviation from the average value of the pedestal, for a number of these events, represents a measure of the night sky brightness. The pedestals of the charge to time converters are set to be about 3 standard deviations above the noise to avoid bias introduced by truncation of downward fluctuations of such noise.

4.8.3 Gain Calibration and Flat Fielding of the Camera

Normalisation factors representing the relative gains between PM tubes are derived from their response to a calibration light source. During the early life of the experiment the light source has been a plastic scintillator

impregnated with the radioactive isotope Americium 241.

The scintillator is housed in a shallow well in a length of wooden dowel of of a diameter which matches the diameter of the outside aperture of the holes in the polyethylene front plate of the detector package. Therefore, the position of the calibration source relative to the photocathode is uniquely defined thus repeatable. Alpha decay of the Americium 241 generates, on average, 300 photons within the scintillator per event, and the average decay rate is 700 events per second. The PM tube signal is passed through the usual electronics with the trigger adjusted to operate from the relevant tube. A distribution of charge integrals is built up over a typical period of 10s, giving a sample of approximately 7000 events. The mean is calculated for the distribution of each tube and the appropriate pedestal value subtracted.

4.8.4 An Example of Calibration

The scaled output of the charge to time converters (QT-ADC units) for all of the camera PM tubes is recorded in the event record for every event. The integrated charge in each camera tube is displayed in Figure 4.19, initially raw and then after each of the two stages of camera calibration.

The raw values indicate the magnitude of the mean Cerenkov signal from the PM tube, superimposed on the pedestal of the digitising electronics. The first step of the image processing is the subtraction of the pedestal, the measurement of which is described in Section 4.8.2. The pedestal subtracted values are a measure of the signal from the individual tubes. The camera is then "flat fielded" by normalization of tube gains to the centre tube using normalization factors derived from the response of the tubes to the scintillator light.

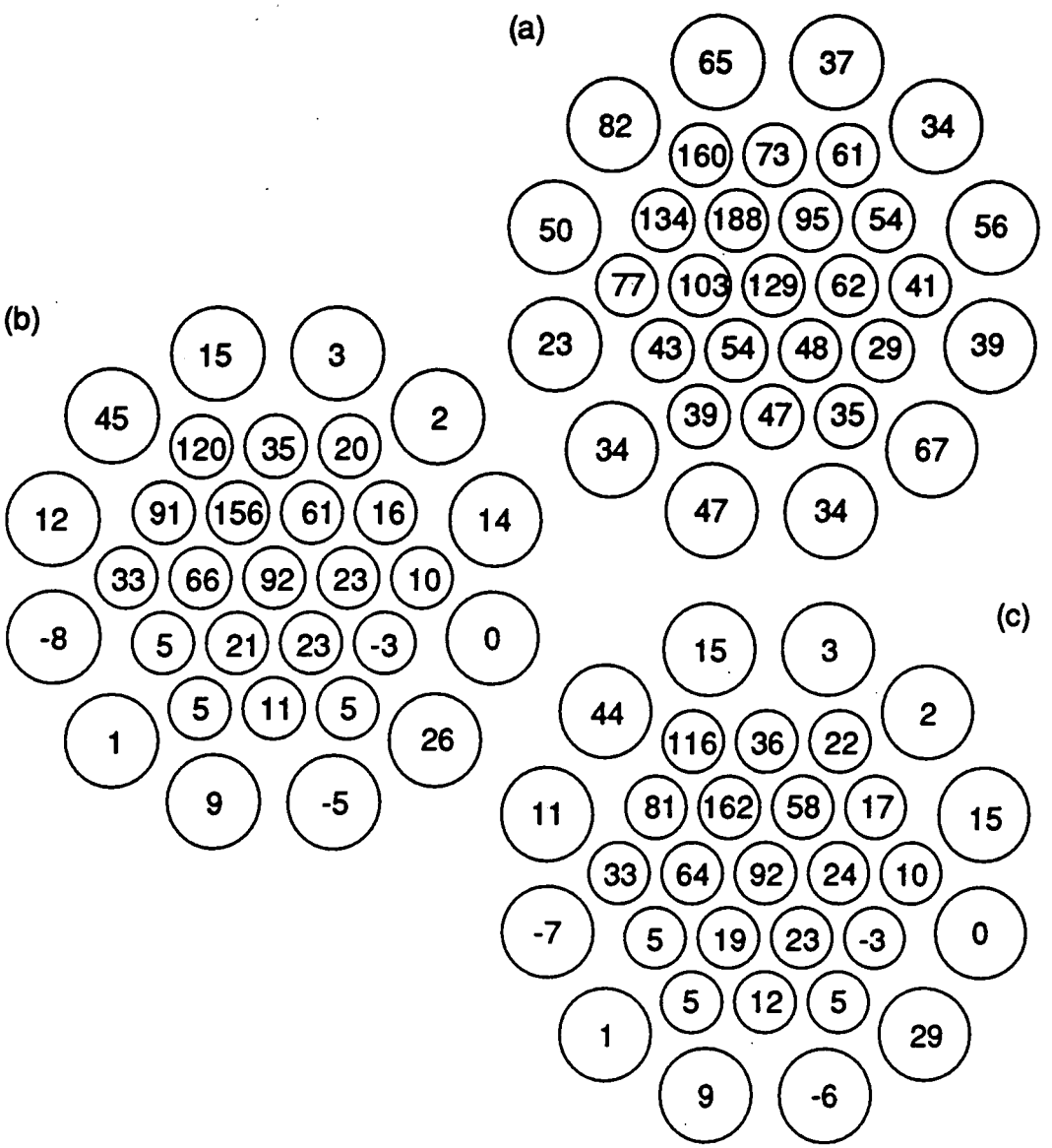

Figure 4.19: An example of the calibration of a typical medium resolution image: (a) Raw pixel values; (b) pedestal corrected pixel values; (c) pedestal and gain corrected value.

4.8.5 Effect of Stars in Field of View

The improvement in resolution of the optics and increase in granularity of the detector packages has introduced potential problems with stars in the field of view of the PM tubes. The majority of light from a star at the centre of the field of view of a 1" PM tube will be focused onto the photocathode of

that tube, increasing background illumination and tube noise dramatically. This effect will become even more marked in the Mk.6 telescope with the four fold increase in flux collector area and two fold increase in pixel resolution. The increase in PM tube noise results in an appreciable accidental rate in the channel whose field of view encompasses the star. These accidental events are, however, easy to identify and discriminate against during data processing and so are tolerated in the data stream except in extreme circumstances. In the case of a observations made of a target with a very bright star within the field of view of the telescope, the accidental rate may increase to such an extent that the dead time of the electronics begins to compromise the genuine count rate. Under these conditions the noisiest camera PM tube can be removed from the event trigger, reducing the accidental rate appreciably. A number of PM tubes in one ring of the camera will be successively removed from the trigger as the sky rotates in the field of view. The option also exists to turn off the EHT to individual PM tubes if the maximum allowable anode current is exceeded, although this results in loss of image information.

4.9 Electronics and Data Logging

4.9.1 Introduction

The data logging and performance monitoring of the Mk.3 telescope is performed by the 68000 operating a very fast but highly complex hierarchical interrupt system. The system was highly labour intensive to program and is not amenable to development. In an effort to simplify the system the tasks of data logging and performance monitoring were separated and assigned to independent commercial microcomputers.

4.9.2 Digital and Analogue Electronics of the Mk.5 Telescope

The signal path of the Mk.5 telescope is identical to that of the Mk.3 telescope with the exception that additional logic is employed in the event trigger to provide a logic output of 1 if any of the 19 1" PM tube discriminator thresholds is exceeded. This signal is then compounded with the 2 fold coincidence signal from the left / right PM tube packages to form the event trigger.

4.9.3 The Telescope Performance Monitoring System (TPMS)

The TPMS is based on an Archimedes microcomputer. Environmental conditions, steering information and instantaneous values of the anode current and noise rate of every PM tube are displayed via a graphical user interface designed to alert observers to irregularities in the operation of the telescope. The displayed values are updated every three seconds and each minute a complete set of telescope performance data are recorded on the network file server. All of the recorded values are the instantaneous readings except those for steering residuals and wind speed for which the maximum value of the previous minute is taken.

4.9.4 The Mk.5 Telescope Data Logger

The logger of the Mk.5 telescope is based on a commercial BBC Master microcomputer. When interrupted by an event the computer interrogates the electronics via the MHz bus. The data recorded in each event record is listed below.

- An event time, recorded from the CAMAC clock.

- The charge integrals from the ADC (QT) units for each of the PM tubes.

- A "fire pattern" denoting which of the channels has exceeded the discrimination threshold and satisfied the coincidence criterion.

- The coordinates and brightness of the brightest star in the field of view of the CCD camera.

The dead time of the logger is approximately 10 ms which restricts the maximum resolvable burst rate to 100 Hz.

4.10 Images From a Medium Resolution Camera

4.10.1 Conventional Parameterisation of Medium Resolution Images

The medium resolution images produced by the 31 pixel camera of the Mk.5 telescope are of the same resolution as the 37 pixel package on which the Whipple collaboration first achieved success with the imaging technique. Initially, to take advantage of the experience gained by the Whipple collaboration, the Whipple image parameterization technique was adopted by the Durham group.

After the pixel values have been pedestal corrected and "flat fielded" to compensate for variation in digitiser offset and PM tube gain each tube is flagged as an "image tube", a "border tube" or a "noise tube" according to the following definitions. A tube is labelled as a image tube if the integrated charge in the signal is greater than 5 times the RMS background noise of

the tube. A tube with a signal of 2.25 RMS noise is defined to be a border tube if it is adjacent to an image tube. A tube which satisfies neither of these categories is assumed to contain no signal and its value is set to zero. The standard Hillas image parameters (Hillas, 1985) are calculated from the zeroth, first and second order moments of the light distribution.

Distributions of image parameters are not dissimilar to those obtained by the Whipple collaboration while operating with a camera of similar resolution. Exploitation of the AZWIDTH parameter proved to be the most successful method of signal enhancement for the Whipple collaboration (Weekes et al., 1989) and so was chosen to assess the efficacy of the technique when applied to Durham data. An optimisation of the Q factor (defined in Chapter 3) for signal enhancement using the AZWIDTH parameter was performed on data from AE Aquarii. This data, which is the subject of Chapter 6, contains a burst of periodic emission. A dataset comprising events with an AZWIDTH between 0° and 1.0° was progressively reduced in size by constraining maximum AZWIDTH to successively smaller values. If it is assumed that the pulsed events in the sample are gamma rays and that the Rayleigh strength represents the gamma ray fraction of the dataset, then the proportions of gamma rays and hadronic background events remaining in the dataset can be estimated. A maximum Q factor of 1.5 was obtained for an AZWIDTH selection of AZWIDTH < 0.2.

4.10.2 The Concept of Simple Shape Parameters

The limited success achieved in signal enhancement using the Hillas parameters is an indication of the level of improvement possible using medium resolution cameras in imaging. The resolution is inadequate to allow identification of gamma ray images with any certainty therefore effort

has been directed towards the rejection of images which clearly display the characteristics of hadron initiated events. A target requirement of rejection of 75 % of the hadronic events with retention of the whole of the gamma ray fraction of the dataset was adopted. This requires a median cut on each of two parameters representing measures of shape and orientation of the image. A simple measure of the angular extent of the light pool has been developed, representing the angle subtended by the image at the centre of the camera. This parameter has been given the name SPAN. Gamma rays from the source direction produce small elliptical images with their major axes aligned radially on the camera and therefore have small values of SPAN. In contrast the larger, lumpier and randomly oriented hadron events are characterized by large values of SPAN. A cut at the median value of the distribution reduces the data set by half and it is hoped that all of the gamma ray signal will be retained. Examples of large SPAN and small SPAN events are reproduced in Figure 4.20.

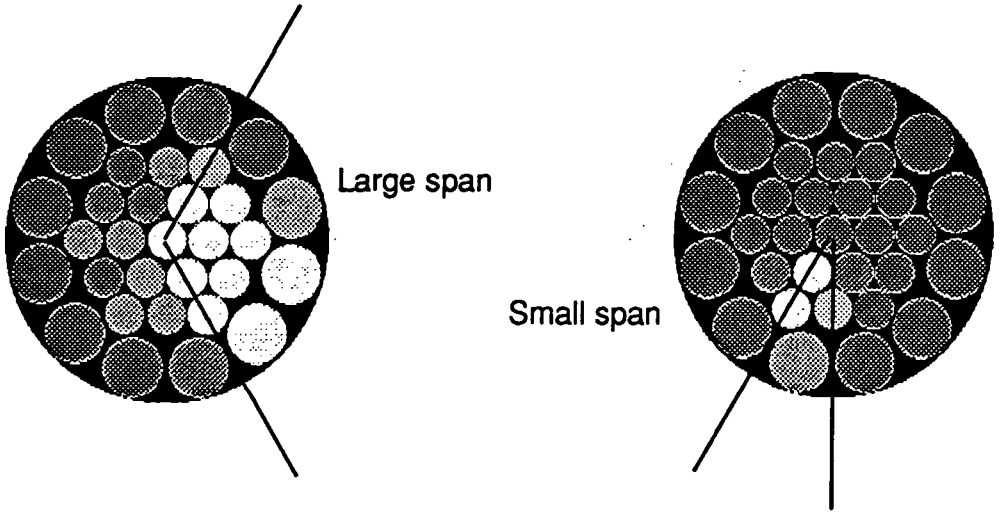

Figure 4.20: Examples of events with large and small values of the SPAN parameter. Relative tube charge integrals are denoted by the grey scale.

The second rejection criterion is based on the traditional Hillas parameter describing the orientation of an image, ALPHA. Events with values of

ALPHA greater than 45° are rejected as being hadron like giving a further 50 % reduction in the dataset. Chapter 6 details the analysis of a burst of periodic emission from AE Aquarii which includes event selection based on parameterisation of medium resolution images in terms of SPAN and ALPHA. The selection applied resulted in an enhancement of the dataset equivalent to a Q factor of greater than 1.5 suggesting that the majority of gamma rays were retained. If the ambition to reject 75 % of the hadrons while avoiding rejection of any gamma rays is eventually realised, then the Q factor of 2 this represents should transform typical hints of signal in the data into worthwhile detections (a 2 % periodic signal in a dataset of 10000 events with a Rayleigh probability of chance occurrence of 10^{-2} translates to an 8 % signal with a probability of chance occurrence of 10^{-8}).

4.11 Summary

The Mk.5 telescope has been a successful element of the progression of the Durham group from a fast timing narrow aperture detection philosophy, to observation with a wide field of view incorporating a background rejection strategy based upon imaging of the Cerenkov event. In its role as a prototype the Mk.5 telescope shed light on many of the areas critical in the design of the Mk.6 telescope.

- The large area mirror concept was proved in terms of structural integrity and resolution.

- The operational characteristics of small PM tubes were examined at the level of night sky background illumination projected for the Mk.6.

- A camera comprising a hexagonally close packed array of PM tubes was built and incorporated into a three fold fast coincidence system.

- A novel "in house" designed and built alt-azimuth mount and its associated drive and position sensing equipment was proved.

The medium resolution imaging capacity of the Mk.5 telescope provides it with a signal enhancement capacity represented by a Q factor of up to 2. This represents a significant advance in sensitivity over the previous telescopes operated by the Durham group. The development of its potential as one component of a stereoscopic imaging pair of telescopes is the subject of Chapter 5.

CHAPTER 5

STEREOSCOPIC RECORDS FROM A PAIR OF TELESCOPES

5.1 Introduction

5.1.1 Stereoscopic Imaging of Extensive Air Shower Development

Stereoscopic imaging of Cerenkov light offers the potential to discriminate between gamma ray and hadron initiated EAS, enhancing the sensitivity of medium resolution telescopes, which would have limited ability in this respect when operated in isolation. The basis of identification of the nature of the primary to be described here is a measure of the height of origin of the light, and disparities in the magnitude of fluctuations in this height between showers initiated by gamma ray and hadron primaries.

5.1.2 The Concept of the Narrabri Stereo Facility

High resolution cameras such as the one operated by the Whipple collaboration on Mount Hopkins, Arizona (Punch et al., 1992) reproduce the light intensity distribution faithfully, lending credence to the parameterisation and interpretation of the images in terms of the higher moments of the light distribution. These statements must be qualified with the proviso that the Cerenkov light is of sufficient intensity to produce a well defined image above the background. Thus the threshold energy for effective discrimination between hadron and gamma ray initiated events is higher than the simple trigger threshold of the instrument. If, however, we have the facility to observe Cerenkov events in two telescopes simultaneously we

may be able to appeal to the information contained in the lower moments of the intensity distribution in our rejection strategy. Due to the predictable nature of its electromagnetic cascade the Cerenkov light generated by a gamma ray will show;

- a uniform brightness out to the Cerenkov shoulder,

- a circularly symmetric intensity profile around the impact point,

- an origin at a fixed atmospheric depth.

Thus the position of the centroid of the image and its intensity, quantities available from measurements made with a telescope with only moderate resolution optics providing poorly defined images, will correlate well between telescopes. The more haphazard hadron initiated events will show no such correlation. The energy threshold at which this method of hadron rejection ceases to be viable will be lower than for an equivalent, independent, high resolution imager with the same flux collector area. This statement must be qualified to a certain extent as the average energy of stereo events is slightly higher than single telescope threshold energy, although this increase in energy requirement is probably less marked for gamma rays than for hadronic events due to their uniform light pool intensity.

The Mk.5 telescope was never envisaged as an effective stand alone imager, nor was it seen as merely a prototype for a low energy detector. It has fulfilled a pivotal role for the Durham group in the transition between the first generation detectors and the more complex imaging devices. In proving the efficacy of the medium resolution camera in the context of three

fold coincidence (with a similar energy threshold to the simple Mk.3 telescope) it broke the ground for the upgrade of the Mk.3 telescope to identical imaging optics to provide the capacity for medium resolution stereo imaging of showers. The Mk.5 telescope was assembled 100 m east of the Mk.3 telescope, a distance small enough for the footprint of a significant proportion of gamma ray events to encompass both telescopes, and yet with sufficient separation to provide adequate parallax for image interpretation.

5.2 Other Observatories with Multiple Cerenkov Telescopes

5.2.1 Introduction

In addition to the observatory of the Durham group, four further facilities exist which currently have, or will shortly develop the capability of recording images, in separated telescopes, which represent views of an extensive air shower from different aspects.

5.2.2 The GRANITE Project of the Whipple Collaboration

The observatory of the Whipple collaboration is situated on Mt. Hopkins, Tucson, Arizona (32° N, at 2300 m asl). The GRANITE (Gamma Ray Astrophysics New Imaging TElescope) experiment comprises a pair of telescopes with a baseline of 140 m in a North/South direction. Each telescope has a single flux collector, one of 11 m diameter and the other 10 m. The 10 m flux collector is of a Davies-Cotton design with a focal length of 7.3 m (Cawley et al., 1990). The point spread function of the optics at FWHM is < 0.14° over the whole of the sensitive area at the focal plane.

The 11 m diameter flux collector is composed of hexagonal mirrors mounted to form an approximately paraboloidal surface of area 66.3 m^2 with a focal length of 7.6 m (Schubnell et al., 1992). The point spread function at the centre of the field of view is 0.18°. Identical 91 PM tube cameras are deployed at the prime focus of each flux collector producing a well matched pair of telescopes. The trigger requirement of the telescopes is that 2 of the 91 tubes within the camera exceed a specified level (about 40 photoelectrons). This defines an energy threshold of 300 GeV for the telescopes operating independently (Cawley et al., 1990). The event rate for two telescope response, hence stereo energy threshold are not yet reported.

5.2.3 The HEGRA Collaboration

The HEGRA (High Energy Gamma Ray Astronomy) collaboration operate at the Roque de los Muchachos observatory on La Palma (29° N at 2200 m asl). An array of 5 telescopes is under construction at the observatory, with a separation of 80 m between telescopes. Each telescope will consist of a high resolution (< 0.25°) camera at the focus of a single flux collector of area 8.5 m^2. The telescopes will be triggered independently employing a trigger strategy similar to that used by the Whipple collaboration.

The first telescope with a 5 m^2 flux collector of Davies - Cotton design was commissioned during 1992. A 37 pixel camera at the focus of the flux collector has a pixel pitch of 0.4°, and an energy threshold of 1.5 TeV has been estimated for the telescope operating in this configuration. The 37 pixel camera of this telescope will be replaced with a 127 pixel package to give resolution of 0.25°. The array is due to be completed during 1995/96

5.2.4 The Crimean Astrophysical Observatory

The Crimean Astrophysical Observatory (45° N at 2100 m asl) consists of a pair of telescopes located on a North / South line with a baseline of 20 m. Each telescope has a flux collector area of approximately 13.5 m^2 and is triggered when 2 of the central 19 PM tubes of a 37 pixel camera exceed threshold. The energy threshold of each telescope triggering independently is estimated to be 2 TeV (Vladimirsky et al., 1989).

Preliminary results presented in Kornienko et al. (1993) indicate that the two telescope event rate varies between 55 % and 76 %.

5.2.5 The CANGAROO

The telescopes which comprise the stereo imaging system at The International Astrophysical Observatory at Woomera, South Australia (27° S 160m asl) are independent instruments operated by different research groups. The CANGAROO (Collaboration between Australia and Nippon for a GAmma Ray Observatory in the Outback) experiment utilises images from cameras of both the BIGRAT (BIcentennial Gamma RAy Telescope), and the Dodaira telescope for simultaneous observations of the Cerenkov light from EAS.

The BIGRAT, operated by the University of Adelaide (Clay et al., 1989), is a triple fast coincidence instrument. Packages comprising 3 Burle 8575 PM tubes are deployed at the focus of two of the three 13 m^2, 2.66 m focal length flux collectors, with the third flux collector viewed by a high resolution camera. The camera consists of 37 13 mm x 13mm square Hamamatsu photomultipliers which have a geometrical aperture to the sky of 0.15° for the photocathode. Pixel pitch is 0.3° giving a total camera aperture of 2.5°.

The telescope has operated in this configuration since September 1992. The energy threshold is estimated to be about 600 GeV.

The second component of the stereo system is the Dodaira telescope operated by a Japanese collaboration (Hara et al., 1993). This telescope has a very high resolution camera at the prime focus of a single flux collector of 3.8 m diameter. The original purpose of the Dodaira mirror was lunar ranging and thus it has much better angular resolution than the mirrors typically used for Atmospheric Cerenkov astronomy. To do justice to the mirror quality a highly granular camera comprising 220 PM tubes is employed to give a 2.7° field of view. An energy threshold of about 1 TeV is estimated from the vertical triggering rate of 1 Hz. The rate of stereo events is estimated in early observations to be 10 to 15 % of the BIGRAT triggering rate (Roberts, 1993).

5.3 The Modifications to the Mk.3 Telescope to Provide a Component of a Stereo Pair

5.3.1 Introduction

The Mk.3 and Mk.5 telescopes employ flux collectors of similar size and have been shown to have similar count rates, normalized for field of view, demonstrating that they have similar energy thresholds. In order to provide the capability for stereo imaging the Mk.3 telescope required upgrading to produce images of comparable quality to the Mk.5 telescope.

Figure 5.1 is a photograph of the upgraded Mk.3 telescope.

Figure 5.1: The upgraded Mk.3 telescope

5.3.2 Upgrade of the Optics

5.3.2.1 Introduction

The pre-upgrade configuration of the Mk.3 telescope is described in detail in Chapter 3. The flux collectors, comprising three tessellated dishes of area 11 m^2, were manufactured to a specification for an event counting device, requiring only limited optical quality. The point spread function of the optics was too large to preserve any characteristics of an image, a point exacerbated by serious off axis aberration due to the spherical mirror section. In order to achieve images of similar quality to the Mk.5 telescope a new flux collector was required.

5.3.2.2 Replacement of the Flux Collector

The centre flux collector was replaced by a flux collector of the type developed for the Mk.5 telescope, furnishing the Mk.3 telescope with identical imaging optics (see Figure 5.1).

The upgrade was effected during April 1993. With the telescope supported rigidly pointing at the zenith, the central tessellated flux collector and associated superstructure was lifted, in its entirety, from the two parallel U section steel girders to which it was fixed. A rectangular steel frame was then bolted to the girders to provide the required rigidity for support of the replacement flux collector. A prealigned Mk.5 type flux collector was lifted onto the steel frame and bolted into place (prealignment of the flux collector was necessary because of the inability of the Mk.3 telescope to point horizontally, rendering the field laser alignment system unworkable). The alignment was performed in the lab by an equivalent method to the field

laser alignment system described in Chapter 4 but using a fixed array of parallel laser beams and rotating the flux collector about a hub. The whole flux collector and detector package support was aligned and then marked. The detector package and supporting tripod was disassembled in such a way that accurate reassembly was possible. Co-alignment of the optic axes was effected by manipulation of the whole of the flux collector and superstructure, successive adjustments being made in the packing between the steel frame and the original girder supports.

5.3.2.3 Replacement of the Triggering PM Tube Packages

The left and right flux collectors were retained without modification as triggering elements. However, due to the shorter focal length of the original Mk.3 telescope flux collectors, an array of close packed 2" tubes at the prime foci of the triggering flux collectors would have defined a field of view larger than that of the Mk.5 telescope, and larger indeed than the field of view of the camera. The ratio of focal lengths between Mk.3 and Mk.5 telescope optics of 3:4 defines the optimum trigger tube diameter to be 1.5". Replacement triggering packages were, then, made up of close packed arrays of Burle C7151Q 1.5" tubes which define the same triggering field of view of 9 square degrees as do 2" PM tubes in the Mk.5 telescope. Figure 5.2 displays the relative noise / gain characteristics of the two types of PM tube when subject to night sky illumination in their respective telescopes. Flux through the tubes is similar, as the 1.5" at the focus of a Mk.3 telescope tessellated flux collector has the same geometrical aperture to the sky as a 2" tube at the focus of a paraboloidal Mk.5 telescope flux collector. These measurements suggest that the C7151Q tubes are slightly noisier than the 8575 tubes for a given gain, and thus will cause the upgraded Mk.3

telescope to have a slightly increased threshold.

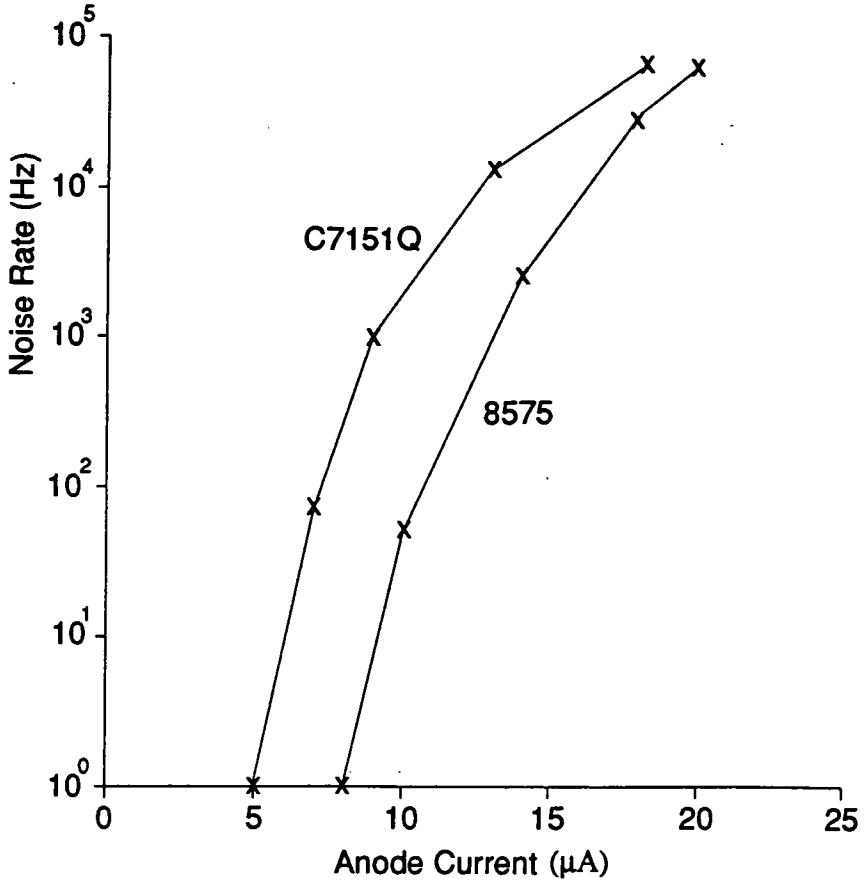

Figure 5.2: A comparison of the noise / gain characteristics of the Burle C7151Q and 8575 PM tubes under Narrabri night sky illumination. The level of illumination remained stable whilst EHT was varied in each case.

5.3.3 Installation of Camera and Associated Electronics

The Mk.3 telescope camera is identical in every respect to the camera of the Mk.5 telescope. Its complement of 31 tubes represents an increase of 24 over the detector package it replaced, so an additional 24 channels of fast electronics were required. Two further 12 channel commercial Le Croy NIM amplifiers and three 8 channel NIM discriminator units were added. The output of the discriminators is passed to an additional digital logic unit, which constitutes the camera element of the revised trigger of the telescope.

Two supplementary fast ADC (QT) CAMAC units digitise the output of the amplifiers for the additional channels. The output of the QT units is scaled and recorded by the reprogrammed 68000 logger in the new data stream. Additional slow ADC units and scalers are dedicated to the monitoring of PM tube anode current and single fold noise rates respectively. The output of these units is monitored by an Archimedes microcomputer and forms the Telescope Performance Monitoring System (TPMS) of the new components of the upgraded Mk.3 telescope. The TPMS information is echoed to the Annex control room.

5.3.4 Steering Information from a CCD Camera

In order to exploit fully the potential of stereo imaging it is desirable to know the position of the telescope to an accuracy of perhaps +/- 0.025°. This problem was addressed in Section 4.5.4 in connection with the improvements to positional accuracy required for effective medium resolution mono imaging. This improvement in positional information, desirable for medium resolution imaging, is essential if the relative position of centroids of the images are to be compared between cameras. The upgraded Mk.3 telescope was, then, provided with an identical CCD system to that employed on the Mk.5 telescope providing telescope attitude information good to arc minute accuracy.

5.4 Data from a Stereo Pair of Telescopes

5.4.1 Introduction

The telescopes are located 100 m apart on an East - West line. This is

the preferred configuration for the telescopes as the baseline of the system is constant for all objects at culmination. The distance between the telescopes is a compromise between the overlap of the sensitive areas of the telescopes and the degree of parallax afforded by their separation. The effective separation varies with azimuthal pointing angle of the telescopes.

5.4.2 Typical Stereo Data

Examples of pairs of stereo events recorded at a zenith angle of 30° are displayed in Figure 5.3.

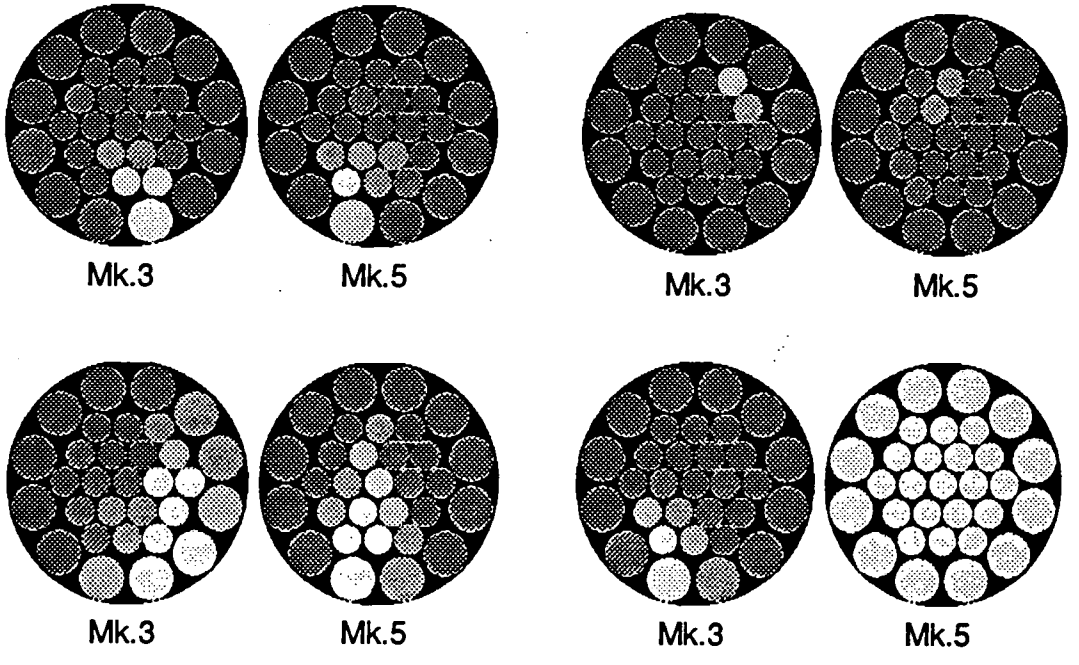

Figure 5.3: Example pairs of stereo events. The signal within the PM tubes of each of the cameras is represented as a linear grey scale with maximum intensity representing a signal of 5σ above noise. The bottom right example appears to be an event whose shower axis passes close to the Mk.5 telescope, while that top right is a small shower falling between the two. The images on the left are of typical intensity.

5.4.3 Inter-telescope Gain Calibration

As the telescopes are to be operated in tandem, with direct comparisons being made of Cerenkov light intensity at the focal planes of the two detectors, it is important that the relative gain of the cameras and digitising electronics is known. During routine flat fielding of the cameras the gains of the PM tubes are normalized to the central tube using the scintillation source (see Section 4.8). This source was also used to provide a gain factor to normalize one camera to the other. The signal from the central tube of the camera of the Mk.5 telescope was passed through a coaxial cable to the Mk.3 digitising electronics, where its pulse height spectrum was recorded. Vice versa for the central PM tube of the Mk.3 camera. The response of the PM tubes through their own electronics was also recorded. Comparison of the means of all of these pulse height spectra allow the affects of attenuation within the cable between the telescopes to be eliminated and the relative gain to be established. The response of the central PM tube of the Mk.3 telescope and its associated electronics was found to be approximately 20 % higher than that of the Mk.5 telescope.

5.4.4 Proportion of Single Telescope Events With a Stereo Counterpart

Recognition of a common (stereo) event is effected at the data analysis stage by matching of the microsecond time (taken from the CAMAC clocks of the respective telescopes) in the event record. These clocks are slave clocks of the site wide time standard which is checked daily to microsecond accuracy against the signal from a GPS receiver. The telescopes are very similar in terms of field of view and triggering requirements; thus the count rates, which are similar, imply that the telescopes have much the same

energy threshold. The proportion of events at zenith in each telescope which have a stereo counterpart in the other is about 45 %. This fraction roughly corresponds to a single telescope sensitive area to hadronic events of radius 110 m.

5.4.5 Parameterisation of Stereo Images

5.4.5.1 Introduction

The limited resolution afforded by cameras of the Mk.3 and Mk.5 telescopes is barely adequate to allow parameterisation of Cerenkov images in terms of the Whipple parameters which are derived from the zeroth, first and second order moments of the light distribution. They are however identical detector packages viewing identical flux collectors. In this respect they are ideally suited to provide information on the lower moments of the Cerenkov light distribution in an EAS, viewed from two different aspects. These lower order moments, the intensity of the light and the position of its centroid, are sufficient to allow analysis of the longitudinal development of the extensive air showers based upon trigonometric information from stereoscopic measurements.

Three stereoscopic measures relating the light distributions within the two cameras have been chosen as representing quantities which will be different for events with gamma ray primaries compared with those with hadron primaries.

5.4.5.2 Height of the Cerenkov Light Maximum, H_c.

This parameter is the simplest and most robust. The position of the

centroid of the light distribution defines uniquely a direction to the peak intensity of Cerenkov light in the shower, relative to the optic axis of the telescope. The height of Cerenkov maximum of the shower, H_c, is derived directly from the intersection of lines (in practice the distance of closest approach) from each of the telescopes projected from the centroids of their respective images. This procedure makes no assumptions about shower development and so calculation of this parameter does not require recourse to simulation data. Figure 5.4 shows the anticipated distributions in height of Cerenkov maximum derived from Monte Carlo simulations performed by Orford (Chadwick et al., 1995). The distributions are composed of 250 gamma ray and 800 hadron primaries.

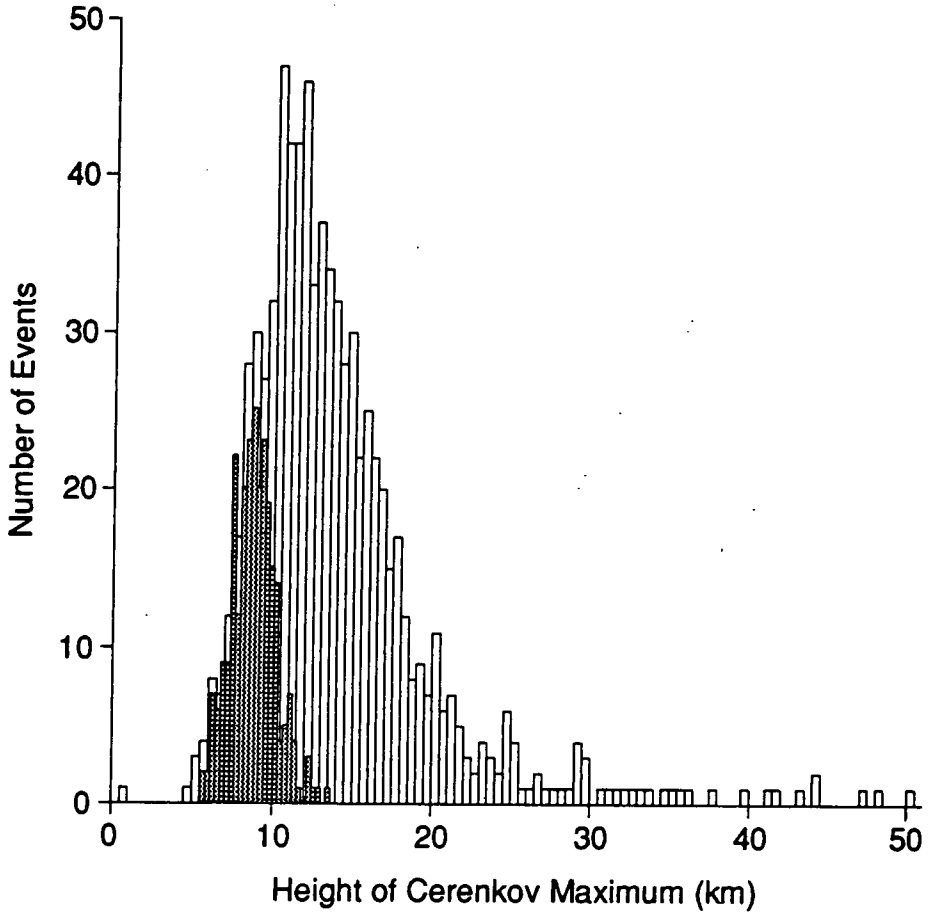

Figure 5.4: Distributions of H_c for simulations of EAS with gamma ray (shaded) and hadron primaries.

The utility of H_c in a background rejection strategy is based on the uniformity of development of the electromagnetic cascade of gamma ray initiated showers. Such showers at a particular energy will maximise, with little variation, around a similar height. The same is not true of hadron initiated showers where large scale fluctuations in the transverse and longitudinal shower development are introduced by the hadronic cascade. The gamma ray candidates are therefore constrained to lie within a thin band and can be removed from the dataset, so rejecting a large proportion of the hadronic events.

5.4.5.3 A Spatial Correlation Parameter : D_{miss}

If the assumption is made that the Cerenkov light from gamma ray initiated showers originates from a well defined atmospheric depth then we can locate the position of shower maximum in space using the position of the centroid of the light distribution in one camera. This position can then be projected onto the camera of the second component of the stereo system and compared with the position of the centroid of the light distribution as detected by that camera. The discrepancy between predicted and observed positions for the centroid is termed D_{miss}.

D_{miss} should be small for gamma ray initiated events, position correlating well between telescopes, while hadron initiated events will display a broad range of values. Simulated distributions of D_{miss} for populations of gamma ray and hadron primaries are displayed in Figure 5.5.

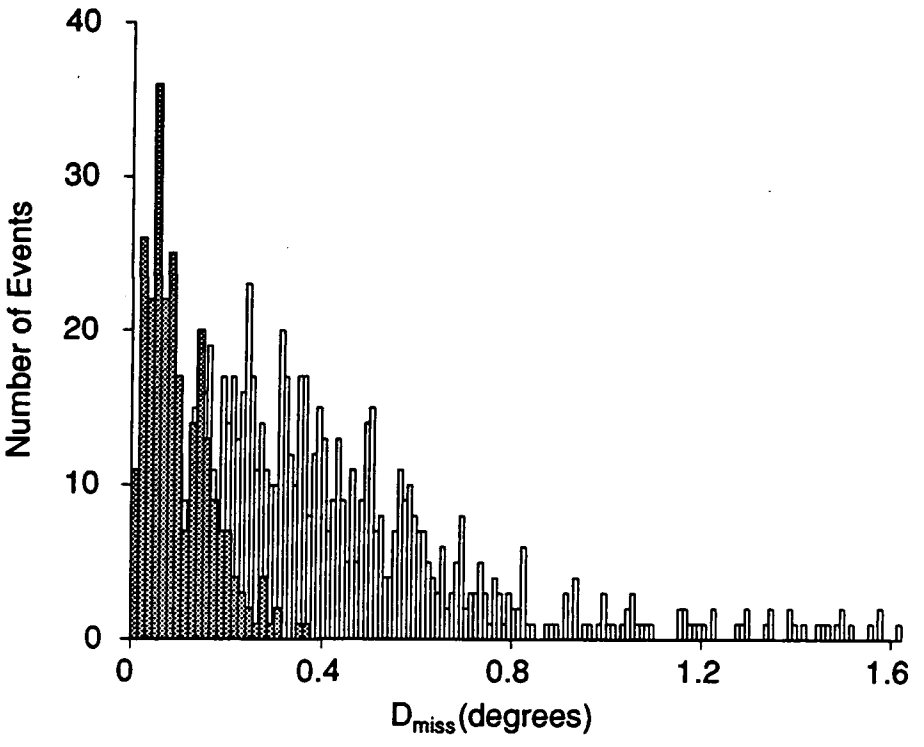

Figure 5.5: D_{miss} distributions for simulations of EAS with gamma ray (shaded) and hadron primaries.

5.4.5.3 The Brightness Ratio, R_{ep}

A further measure of the correlation between the images from each telescope, which appeals to the well ordered and predictable development of a shower initiated by a gamma ray primary is the ratio of estimated primary energies, R_{ep}. Estimation of the energy of the primary is dependent upon simulation data based predictions of the characteristics of the Cerenkov light from the electromagnetic cascade initiated by a gamma ray. The Cerenkov signature of a gamma ray primary is assumed to reflect the form of the cascade and display;

- a well defined image due to the well ordered and circularly symmetric shower development,

- a good correlation between the impact parameter and the position of the centroid in the field of view, and

- a continuous and predictable lateral intensity distribution for the Cerenkov shower front.

Given these characteristics a relative value of primary energy can be estimated with reasonable confidence. The ratio between estimates of two separated telescopes should be close to unity for a gamma ray primary. Figure 5.6 displays the distributions of primary energy ratio for the Monte Carlo simulations of gamma ray and hadron initiated EAS.

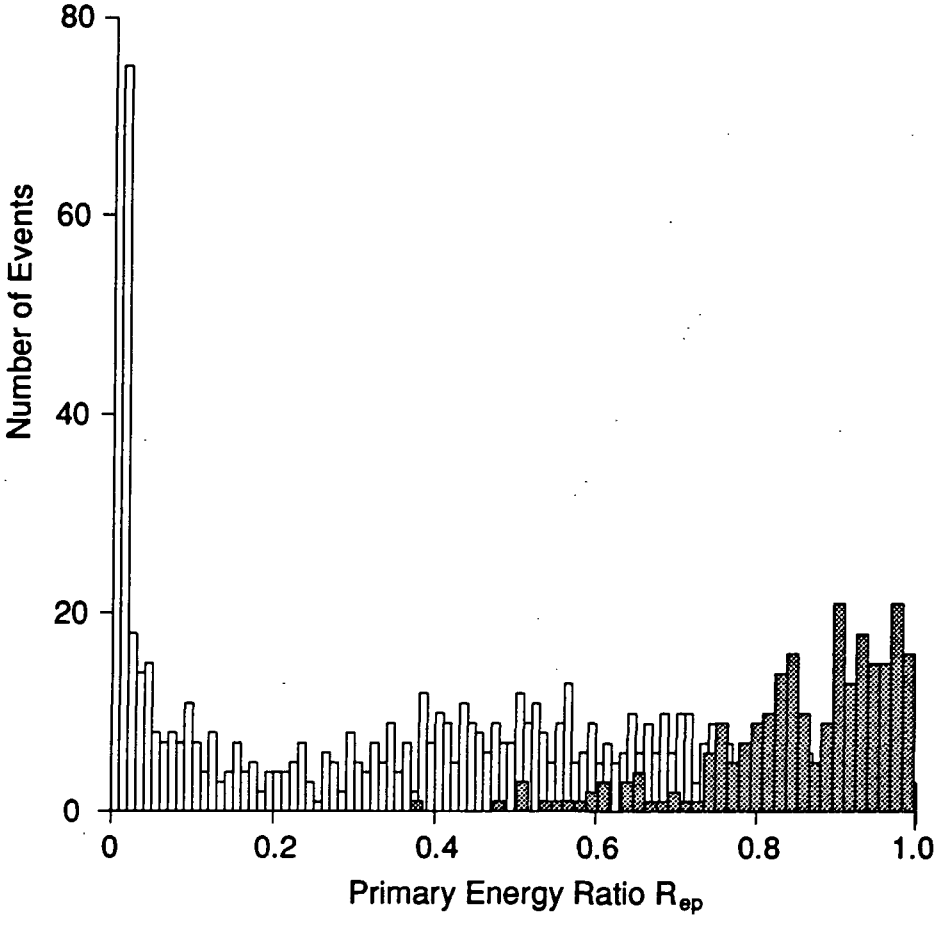

Figure 5.6: Distribution of the primary energy Ratio, R_{ep}, for simulations of EAS with gamma ray (shaded) and hadron primaries.

For hadronic cascades the position of the centroid of the image does not correlate with impact parameter as the arrival direction is not known. This, allied to the haphazard nature of the development of these cascades, renders primary energy prediction imprecise and will cause the primary energy ratio to have a wide range of values. The large peak in the smallest bin of the hadron distribution represents those simulated events whose lateral extent does not encompass both telescopes.

5.5.5 Background Rejection Criteria

It is evident from comparison of the distributions of the parameters H_c, D_{miss} and R_{ep} for hadron and gamma ray primaries that gamma ray regimes exist within each of the parameter distributions which are not heavily populated with the hadron background events. It is anticipated that a region will exist in the parameter space described by these measures of the light distribution which encompasses almost all of the gamma ray events whilst excluding the vast majority of the hadronic background.

Use has been made of these stereo parameters in background rejection during the analysis of an AE Aquarii dataset which contains a short burst of periodic emission. This analysis, described in Chapter 6, demonstrates the efficacy of the stereoscopic imaging technique.

CHAPTER 6

ANALYSIS OF DATA FROM THE MK.3 AND MK.5 TELESCOPES

6.1 Introduction

VHE gamma ray data is characterised by the arrival times of a stream of events with an apparently random time distribution. The majority of the events are due to charged components of the cosmic ray flux and are spatially and temporally homogeneous. A small supplementary flux of gamma ray initiated events is anticipated from the direction of VHE gamma ray sources. It is expected that both extended and discrete sources of VHE gamma rays exist, and that the emission may be pulsed or continuous. A number of different observation strategies may be used, each with optimum sensitivity for a particular source type. The two generic modes of observation are described in Section 6.2.

Section 6.3 describes a series of corrections to the arrival times of the events, which are carried out as routine preprocessing of the data before analysis takes place. Analysis of the dataset which comprises statistical tests for periodicity and / or a D.C. excess is outlined in Section 6.4.

The efficacy of the medium resolution and stereoscopic imaging signal enhancement techniques is then examined in Section 6.5, in the context of a pulsed burst of VHE gamma ray emission from AE Aquarii.

6.2 Modes of Observation

6.2.1 Introduction

Choice of the observational strategy for a given object is dependent upon the type of VHE gamma ray signal anticipated. In the case where continuous emission is expected a background count rate is required, which may then be compared with the count rate from the source direction. If a periodic signal is predicted, sensitive tests for periodicity can be applied to the dataset and measurement of a background count rate is of secondary importance.

6.2.1 Chopping

This method of providing a control background count rate involves periodically displacing the telescope pointing away from the source direction. The telescope observes the source and background region alternately, with the background region being sufficiently distant from the source region to ensure that the source is entirely removed from the telescope's field of view.

The chopping method used by the Durham group has evolved in response to constraints imposed by the telescopes operated by the group. The original cycle involved observing the source for two minutes and then a background region at the same zenith angle, displaced 2° right of the source on the sky, for the same period. This operation was then adapted to compensate for effects of the Earth's magnetic field, with the background region being alternately 2° right and 2° left of the source (Bowden et al., 1992). This method of chopping to alternate sides of the source region also

helps to negate the effect of large scale gradients in the sky brightness (Historically the light noise in the PM tubes was padded using an Automatic Gain Control (AGC) system. An LED close to the face of each PM tube was servoed to the anode current of the tube. However, with the increase in tube numbers this procedure has lapsed). At small zenith angles, achieving a 2° displacement from the source requires a large azimuth angle movement which can take a large proportion of the observing interval. Observations of sources which culminate at small zenith angles precipitated the change to chopping in zenith.

One problem associated with the use of this method, for a telescope on an alt-azimuth mount, is that the control regions of sky constantly change as the region of the sky viewed rotates around the source.

6.2.2 Tracking of a Phantom Object

The method used to provide the background count rate for the Whipple experiment is to track a phantom object at an R.A. and declination which appears at the same point in the sky as the start of the source observation a specified period of time later. This object is then tracked for the same period of time as the source. The Whipple observation technique is described by Lang (1991). The data take the form of pairs of observations with the same locus in azimuth and zenith, one containing the source and the other providing the background count rate. The time separation between source and background observation is chosen such that the two regions of sky are similar. For the Crab Nebula the separation is 30 minutes with the duration of each observation being 28 minutes. The time allowed to steer the telescope between the source and background region, and vice versa, is 2 minutes.

The relative merits of the two methods are largely subjective. Chopping, with its short cycle, gives a reasonable guarantee of similar sky conditions on and off source. Tracking the source and then a "phantom object" for longer periods of time, however, minimises the time spent steering between the two observed regions.

6.2.3 Source Tracking

This mode of observation is the simplest in operation and has the advantage that all of the time is spent observing the source, maximising sensitivity for periodicity searches. The source is tracked continuously throughout the observation, avoiding the introduction of discontinuities in the event record which complicate the process of periodicity searching.

In the simple first generation atmospheric Cerenkov telescopes this method of observation was restricted to the search for periodic emission from potential sources, save for intense bursts of activity which could be identified above the ambient count rate. However, as confidence in the parameter distributions of high resolution images of Cerenkov light from EAS grows, then D.C. excesses in the gamma ray regimes of these distributions can be inferred.

6.3 Corrections to Gamma Ray Arrival Times

6.3.1 Introduction

Observations lasting typically 2-3 hours with count rates of 2 to 3 Hz generate data files comprising several thousand events. A number of corrections to the arrival times of these events must be made before any

test for periodicity can be applied. These corrections are discussed below.

6.3.2 Correction for Clock Drift Rate

The event times stamped on each event record are supplied by the CAMAC clock dedicated to each telescope. These clocks are slaved to a highly accurate Rubidium oscillator, the accuracy of which is checked daily against the time supplied by a GPS receiver. The Rubidium clock is shown to have a very stable linear drift rate, which allows the event time to be corrected to UT by removal of the accurately determined clock delay. The site wide time standard is described in Section 3.4.2.5.

6.3.3 Adjustment of Event Times to the Solar System Barycentre

The time of arrival of the event at the telescope must be transformed to an equivalent arrival time at the Solar System barycentre to eliminate the effects of the motion of the telescope relative to the barycentre. This transformation is effected by the application of three corrections;

- translation of the events times to the centre of the Earth,

- translation of the event times to the Solar System barycentre,

- application of relativistic corrections.

The translation of the event times to the centre of the Earth eliminates the Doppler effect inherent in making observations from the surface of a rotating Earth, and corrects for the absolute position of the observatory relative to its

centre. This correction requires that the observatory's geographical location is accurately known, information which is provided by the GPS system. The maximum correction will be approximately 0.021 seconds, the time taken for light to traverse a distance equivalent to the radius of the Earth.

Correction of the event times to the Solar System barycentre accounts for the same effects introduced by the Earth's orbital motion around the Sun, and includes a small effect due to the orbit of Earth around the barycentre of the Earth / Moon system. The corrections are performed using the JPL DE200 Earth ephemeris (Standish, 1982), and can be as large as 500 seconds, the time taken for light to travel from the Sun to the Earth.

A correction is required to allow for the relativistic effects on the observers timescale introduced by the Earth's motion, and the difference in gravitational environments between the surface of the Earth and the Solar System barycentre. This correction can be as much as 3 milliseconds (Mannings, 1990).

6.3.4 Adjustment of Event times to the Barycentre of a Binary System

In the case of the potential source being a member of a binary system a correction is required to compensate for the effects of orbital motion of the source object around the centre of mass of the system. The masses of the binary companions can be many times that of the Sun and consequently their orbital angular velocities can be very large. The Doppler effect due to these large angular velocities is significant, which makes the process of event time correction important. This correction requires knowledge of a set of parameters which describe the binary system. This is known as the orbital ephemeris and is usually derived from radio, X-ray or optical measurements. The correction is made on the assumption that the site of

the VHE gamma ray emission is coincident with that of the emission region at other wavelengths. For a full description of this correction the reader is referred to Carraminana (1991).

6.4 Data Analysis

6.4.1 Introduction

The substantiation of a signal within the noise is a matter of achieving a statistically significant D.C. excess of counts from a source direction (over a control background from a direction containing no such source), or demonstrating that periodicity exists within the dataset at a period associated with emission from the potential source.

6.4.2 Searching for a Count Rate Excess Above A Control Background

In the case where emission is expected to be continuous, or there is no known period to test, analysis is reduced to testing the significance of an on source excess over a control background in identical time intervals. A maximum likelihood method is used to test the significance of the on source excess. The test is described in detail by Gibson et al. (1982b) and Dowthwaite et al. (1983).

6.2.3 Phase Sensitive Analysis

6.2.3.1 Introduction

A large proportion of the candidate VHE gamma ray sources studied by

the Durham group comprise or contain neutron stars. The majority of these are pulsars, which are isolated rotating neutron stars, or X-ray binaries in which a neutron star forms one component of a binary system. These source types may show periodicity in one or more of the radio, visible, X-ray or low energy gamma ray regions of the electromagnetic spectrum. Data recorded in the VHE region of the gamma ray spectrum is then subjected to tests for periodicity at the known neutron star rotation period. This, of course, assumes that the VHE gamma ray emission is associated with the neutron star. Periodicity within a highly noise contaminated dataset is easier to detect than a small count rate excess, using techniques of phase sensitive analysis. This point is particularly pertinent when one considers the difficulty in achieving a reliable background count rate with changing sky conditions. Thus periodicity searching facilitates the detection of gamma ray emission from periodic sources, allowing these sources to be tracked continuously. A further advantage is that no observation time is lost to the determination of background count rate.

6.2.3.2 Epoch Folding

In cases where the period of the source is known with confidence from observations made in other regions of the electromagnetic spectrum, a dataset can be tested for periodicity by binning the arrival times of the events by period phase. This process is known as epoch folding. Poincare's theorem is adopted as a null hypothesis (Mardia, 1972): a random time series of sufficient length, folded at an arbitrary period, results in a uniform phase distribution. The events are consigned to phase bins, folded at the test period to produce a histogram, and Pearson's χ^2 test for uniformity applied (Leahy, Elaner and Weisskopf, 1983). Uniformity of the

phase distribution is taken as an indication of the absence of periodicity at the test period within the dataset.

Several problems exist with this method when applied to VHE gamma ray data. Generally the light curves of the sources are unknown, making the bin width arbitrary and hence the number of bins a free parameter. In addition, if absolute phase is not known then the bin origin is also arbitrary. The statistical significance of any detection is reduced by these limitations of the method.

In circumstances where the precise period and absolute phase are not known circular statistics are preferred. The Rayleigh test, which is a statistical method derived specifically for use with cyclical phenomena, is described in the next section (Rayleigh, 1894).

6.2.3.3 The Rayleigh Test

This test is the most prevalent for periodicity searching in VHE gamma ray astronomy. It has been described in detail by Mardia (1972), and more recently by Batschelet (1981). It was introduced to gamma ray astronomy by Gibson et al. (1982b). The data are folded circularly with a radial vector describing the phase of a cyclical period (see Figure 6.1).

The null hypothesis states that in the absence of periodicity at the trial period the distribution of events around the circle is random and uniform. Binning is not required and absolute phase is irrelevant. Periodicity at the trial period will be manifest as a preferred direction within the event distribution, which will allow rejection of the null hypothesis if the bias can be shown to have attained a predetermined level of significance.

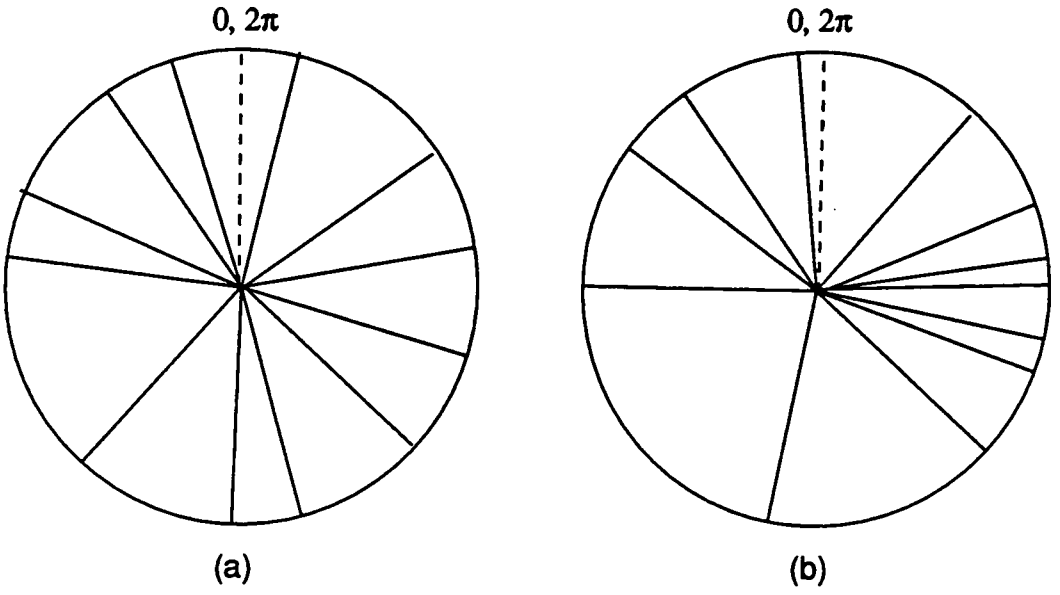

Figure 6.1: In the above diagrams the relative phase of each event of a dataset, folded at a trial period, is represented as a unit vector in phase space. Diagram (a) shows a circular phase distribution, which appears to be consistent with a random probability density while (b) shows a preferred direction.

The Rayleigh test is based upon the magnitude of the resultant (R) of the unit vectors which represent the phase of each event distributed on the perimeter of the circle. Figure 6.2 illustrates this using the distribution shown in figure 6.1.

The Rayleigh test effectively determines the degree of correlation between a sine wave and the time series at the test period, hence it is most sensitive to broad peaked light curves. When n, the number of events, is large, which is invariably the case in VHE gamma ray astronomy, then the product nR^2 has a χ^2 distribution with 2 degrees of freedom. The probability of nR^2 exceeding a value P_n by chance is $P(>P_n) = \exp(-P_n)$.

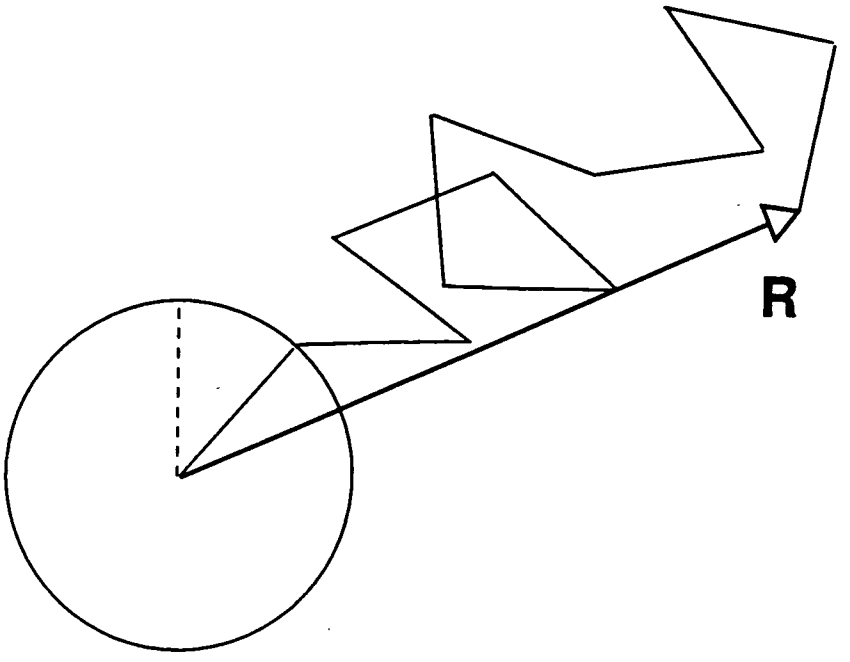

Figure 6.2: An illustration of the resultant of the unit vectors representing event phase for each event for the hypothetical data displayed in Figure 6.1(a).

It is clear that the Rayleigh test would be insensitive to a bimodal distribution. However, periodicity in light curves displaying an interpulse at opposite phase to the main pulse would be evident in the first harmonic. As the ratio of signal in the pulse and interpulse is variable it is common to test for periodicity at both the period and half period.

6.2.4 A Comparison of the Sensitivity of the Rayleigh Test with a Test for D.C. Excess

If we consider a dataset which includes a fraction which is pulsed at a known period, we can compare the sensitivity of the Rayleigh test to the pulsed fraction with its D.C. significance.

For a D.C. excess to be significant at the 3σ level we would require a signal strength, $R_{D.C.}$ such that $3(n)^{1/2} = R_{D.C.n}$ or

$$(R_{D.C.})^2 = 9/n$$

The equivalent 3σ Rayleigh probability is 1.348×10^{-3}. The Rayleigh probability is given by $\exp(-nR_{Rayleigh}^2)$, thus we have $1.348 \times 10^{-3} = \exp(-nR_{Rayleigh}^2)$ which can rearranged to

$$(R_{Rayleigh})^2 = -(1/n).\mathrm{Log}_n(1.348 \times 10^{-3})$$

The value of $R_{Rayleigh} / R_{D.C.}$ is approximately 0.855 demonstrating that, even assuming that no observing time is lost to establishing the background rate, a lower flux of periodic emission can be detected than a D.C. excess of similar significance. If we assume that determination of the background count rate halves the data rate for a D.C. observation then the ratio becomes, $R_{Rayleigh} / R_{D.C.} = 0.604$.

6.5 A Burst of Pulsed VHE Gamma Rays From AE Aquarii

6.5.1 Introduction to AE Aquarii

AE Aquarii is a DQ Her type magnetic cataclysmic variable. The magnetic white dwarf is in a tight binary orbit with a K type red dwarf from which it accretes via an accretion disk. The object is known to emit at radio (Bookbinder and Lamb, 1987), optical (Zinner, 1938) and X-ray wavelengths (Patterson et al., 1980). Periodic emission in the radio and optical regions has been associated with the white dwarf spin frequency which, at 33.08 s, is short for objects of this class. The system is prone to frequent optical and radio flaring, with outburst durations of minutes to hours. The quiescent accretion luminosity is around 10^{32} ergs s^{-1} which can increase to a few times 10^{33} ergs s^{-1} during outburst. Optical observations during outburst exhibit quasi periodic oscillations (QPO) at a frequency lower than that of the spin frequency (Patterson, 1979).

The orbital period of 9.88 hours has been derived both from optical absorption and emission lines (Chincarni and Walker, 1986; Robinson et al., 1991) and optical and X-ray pulse timing measurements (Patterson, 1979; Patterson et al., 1980; Meintjes et al., 1993).

6.5.2 Previous VHE Gamma Ray Detections of AE Aquarii

VHE gamma ray emission has been detected by two independent groups. Periodicity at the frequency of the quasi periodic oscillations during outburst was first identified by the University of Potchefstroom group working at Nooitgerdacht, South Africa (Meintjes, 1992). Within a dataset of 374 hours spanning five years periodicity was found in the period range 33.08 s to

33.44 s, consistent with the optical QPO period during outburst (Meintjes, 1993). Figure 6.3 shows the Rayleigh power spectrum in a frequency range which encompasses the spin and QPO frequencies.

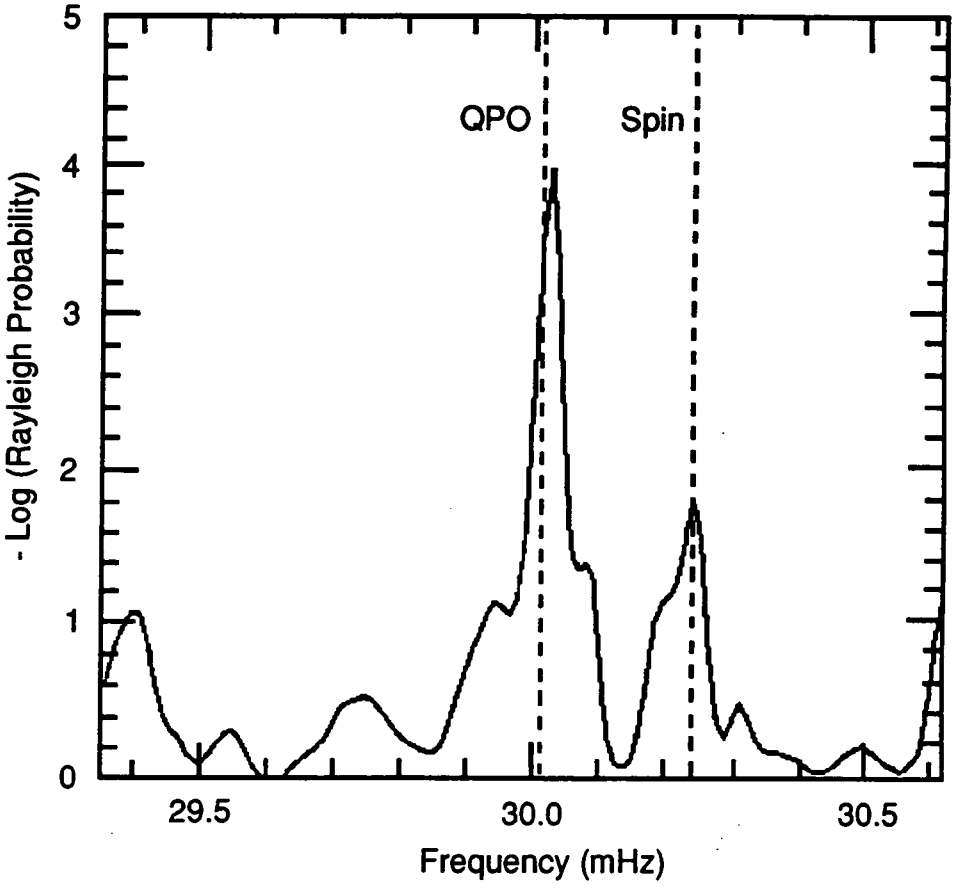

Figure 6.3: The power spectrum in a range of frequencies which brackets the white dwarf spin frequency and the QPO frequency of AE Aquarii. The spectrum represents a non-coherent analysis of 374 hours of data obtained over a 5 year period (after Meintjes et al., 1993).

The Durham group reported the detection of a VHE gamma ray flare with a duration of 1 minute at the 6σ level of statistical significance (Bowden et al., 1992a). The burst, on the 13th October 1990, was seen as an excess in the count rate of two independent telescopes, and displayed a 33 s periodic pulse structure. The light curve during the event was double peaked, an emission pattern corroborated by data taken by the Potchefstroom group

during the same period (Meintjes, 1992). Optical flares with a similar time structure to the gamma ray burst claimed are present in the archival data (De Jeger and Meintjes, 1993).

6.5.3 The Recent Observations

Observations of AE Aquarii were made using the Mk.3 and Mk.5 telescopes on 5 nights between the dates 7th October and 12th October 1993. An observing log is given in Table 6.1.

	Mk.3			Mk.5			
Date	**Start (UT)**	**End (UT)**	**No. of Events**	**Start (UT)**	**End (UT)**	**No. of Events**	**Zenith Angle**
Oct 7th '93	09:30	13:44	18221	09:26	13:46	14261	30° - 65°
Oct 8th '93	09:30	13:25	16813	09:23	13:36	14137	30° - 61°
Oct 9th '93	09:22	13:21	17792	09:32	13:21	16248	30° - 61°
Oct 11th '93	09:25	12:51	15993	09:34	12:53	14379	30° - 55°
Oct 12th '93	09:24	11:37	12363	09:24	11:38	12193	30° - 41°

Table 6.1: Log of the October 1993 observations of AE Aquarii. The date refers to the UT date at the start of the observations.

6.5.4 Periodicity in the Raw Dataset

6.5.4.1 Introduction

The JPL DE200 earth ephemeris (Standish, 1982) is used to correct all event times to the Solar System barycentre. Corrections to the event times

to allow for the motion of the gamma ray source region within the binary system are made using the orbital ephemeris of Welsh et al., (1993). The assumption is made that the gamma ray emitting region is co-located with the white dwarf. The data are divided into three independent datasets:

- events registered solely by the Mk.3 telescope (Mk.3 "mono")

- events registered solely by the Mk.5 telescope (Mk.5 "mono")

- events registered by both the Mk.3 and Mk.5 telescopes ("stereo")

Unfortunately, when the data were recorded the Mk.5 telescope had developed a fault. A voltage line regulator had failed on a voltage supply line to the charge digitizers and the unregulated voltage, which had a large 50 Hz component, caused the pedestal of the digitizers to oscillate. This problem precluded background rejection on the basis of imaging of the events, but has no bearing on the analysis of the raw dataset. Stereo analysis using the height of Cerenkov maximum and D_{miss} measures was also unimpaired as the pedestal values oscillated in phase, leaving the position of the centroid of the light unaffected.

6.5.4.3 Periodicity in the Total Dataset

The series of observations of each of the three independent datasets were combined and tested for persistent periodic emission using the Rayleigh test at periods close to the QPO period and its first harmonic. The data were tested both with and without the assumption of phase coherence between observations. If phase coherence is assumed the data are merged into a

gapped dataset and the Rayleigh test applied to the whole, otherwise the Rayleigh probabilities of individual observations are combined using the formula of Eadie et al. (1971).

No evidence was found for persistent periodic emission at either the pulse period or its first harmonic in any of the datasets, combined with or without use of phase information.

6.5.4.4 Periodicity in Individual Observations

No strong periodicity was evident in any of the datasets over the timescale of a single observation (2-4 hours). However, the data from the observation made on 11th October 1993 did show some evidence for pulsed VHE gamma rays at a period within the range of QPO periods reported by the Potchefstroom group, with a chance probability of occurrence of 10^{-3}.

6.5.4.5 Short Term Periodicity Within Observations

In order to test for transient bursts of periodicity over smaller timescales the data from each night in each independent dataset were tested for periodicity in blocks of 4200 seconds rolling forwards by 600 seconds. Significant periodicity was revealed within one 4200 second block (09:36:25 UT- 09:46:25 UT). The results of phased and unphased periodicity searching on the relevant section of data within the three independent datasets is displayed in Table 6.2. There is evidence to suggest that all of the pulsed signal is contained in this time interval.

	Mk.3 "Mono"	"Stereo"	Mk.5 "Mono"	Unphased	Phased
No. of Events	5007	2784	5659	13450	13450
Rayleigh strength	3.7 %	4.5 %	2.1 %	3.3 %	2.2 %
Rayleigh prob.	1.1×10^{-3}	3.3×10^{-3}	7.2×10^{-2}	4.4×10^{-5}	1.4×10^{-3}
Period (+/- 0.065 s)	16.477	16.456	16.469	16.464	16.464

Table 6.2: Results of the analysis of mono and stereo data during the active 4200 second interval on the 11th October 1993.

The burst of pulsed gamma rays reported in Bowden et al., (1992a) had a duration of only about 60 s. The 1993 data was therefore searched, in a similar fashion to the analysis applied to the 4200 s intervals, for episodes of pulsed emission on a timescale of 66 s which represents two cycles of the white dwarf rotation. None was revealed.

6.5.5 Improvement in Signal to Noise Ratio

6.5.5.1 Introduction

The recent progress made in atmospheric Cerenkov astronomy have been made as a result of the development of efficient background rejection strategies based upon the high resolution (0.25° pixel size) imaging of the Cerenkov light from EAS using a single telescope (eg Reynolds et al., 1993). This degree of resolution was not available to the Durham group when these observations of AE Aquarii were made. However, the group has developed simple critera for background rejection based on imaging at a resolution comparable to that successfully employed by the Whipple

collaboration (0.5° pixel size) prior to the of their high resolution camera (Weekes et al., 1989). The concept of Durham medium resolution imaging is described in Section 4.10 of this thesis. In addition to this single telescope approach the group has developed a background rejection strategy based on data provided by an pair of telescopes making stereoscopic observations of the development of EAS. The "stereo" method is described in Section 5.4.

6.5.5.2 Medium Resolution Imaging

The medium resolution images of the Mk.3 telescope were parameterised in terms of the SPAN and ALPHA parameters described in Section 4.10. SPAN is a measure of the angle subtended by the light pool at the centre of the camera. Events which have a SPAN value in excess of the median, typically 1 - 1.5 radians are rejected as being hadron-like. ALPHA, defined as the angle between the major axis of the image and the radius from the centre of the camera through the centroid of the image, has been shown to be a reliable measure for discrimination between hadron and gamma ray events (Vacanti et al., 1991, Punch et al., 1992, Kifune et al., 1995). In our analysis images with ALPHA > 45° are rejected as hadronic, this is again around the median value resulting in rejection of approximately 50 % of the remaining events.

Calculated values of ALPHA are only reliable if the image is largely confined within the field of view of the camera. Thus only images which display maximum light intensity internal to the outer ring of PM tubes are acceptable for parameterisation in terms of ALPHA. Therefore a DISTANCE cut is applied to remove all events whose centroids are within 0.4° of the centre of the field of view, as these events are not amenable to

discrimination. This is effectively an aperture restriction constraining the region of maximum intensity to within 1.25° of the optic axis of the telescope.

The unconfined subset of data is not necessarily gamma ray poor, due to the limited angular extent of the camera and is retained in the analysis. However, the only measure of the image which can be applied is the SPAN cut. The event selection criteria described above were applied to the 4200 second segment of Mk.3 telescope data from the 11th October 1993 which had shown evidence of periodicity in the raw data, and each subset tested for periodicity at the first harmonic of the white dwarf rotation period. The results of these background rejection cuts are presented in Table 6.3.

	Confined			Unconfined		
	No.	**R(%)**	**Prob.**	**No.**	**R(%)**	**Prob.**
a. No selection	3851	2.7	5×10^{-2}	1156	8.0	5×10^{-4}
b. 0.4° < DIST < 1.0°	2723	3.2	6×10^{-2}	not applied		
c. b + SPAN < median	1283	7.6	5×10^{-4}	552	11.9	4×10^{-4}
d. c + ALPHA < 45°	707	11.6	7×10^{-5}	not applied		

Table 6.3: Results of the Rayleigh test for periodicity, applied to subsets of the Mk.3 telescope "mono" dataset selected on the basis of SPAN and ALPHA parameterisation of the medium resolution images of the events.

The amalgamated dataset comprising the selected confined and unconfined images contains 1259 events. This dataset shows evidence for periodicity at the first harmonic of the white dwarf rotation period with a probability of chance occurrence of 6×10^{-7}, with a Rayleigh signal strength of 10.7 %. The data rejected by the background rejection criteria show no such periodicity. The periodograms for the selected and rejected data are

both presented in Figure 6.4.

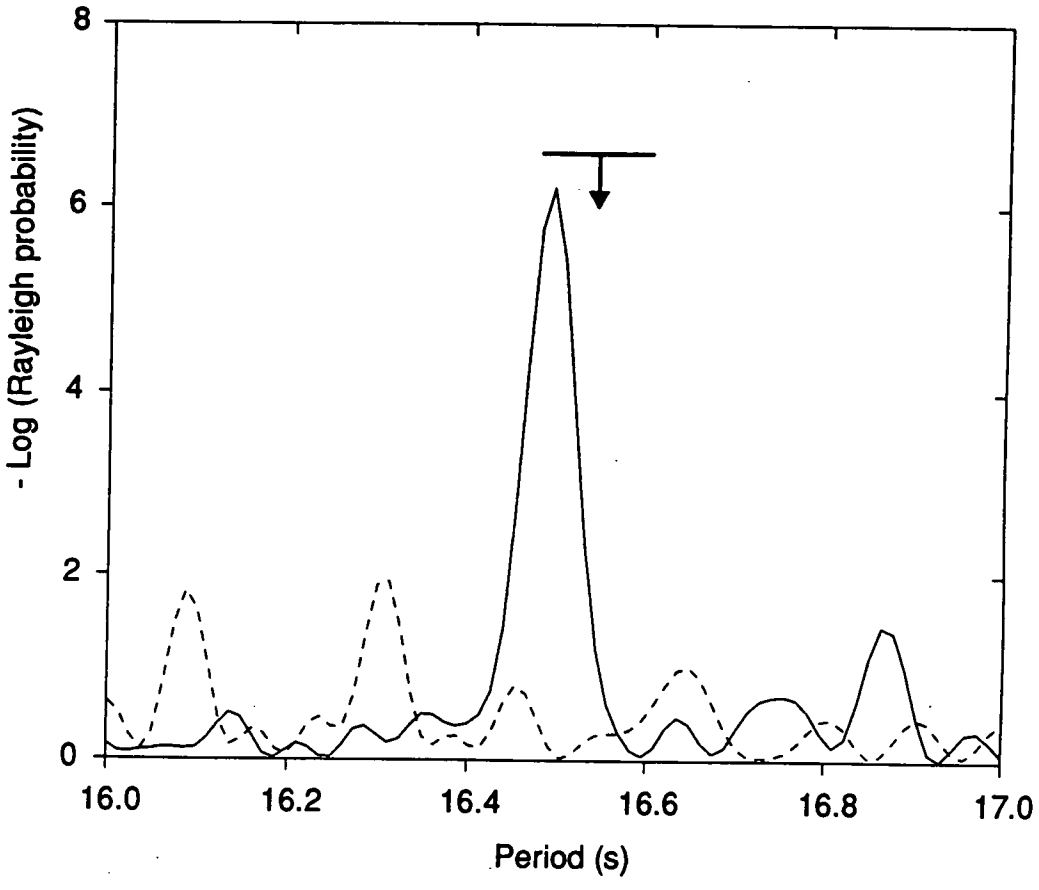

Figure 6.4: Superimposed periodograms showing the results of the Rayleigh test for periodicity over a period range which includes the first harmonic of the white dwarf rotation period (indicated by the arrow). The solid line represents data selected with SPAN < median and ALPHA < 45°. The broken line represents the rejected data. The bar indicates the period resolution of the test.

6.5.5.3 Stereoscopic Measurements

This background rejection technique, based on stereoscopic measures of the development of EAS, developed by the Durham group utilizes the two lowest moments of the light distribution, the brightness of the image and the position of its centroid. The medium resolution cameras of the Mk.3 and

Mk.5 telescopes have sufficient granularity to give a reliable measure of these moments. The height of Cerenkov maximum H_c, and the spatial correlation parameter D_{miss} were used in this analysis. Use of the primary energy ratio was precluded by the problem with the Mk.5 digitisers.

The independent stereo dataset from the period 09:36:25 UT and 10:46:25 UT on 11th October 1993 contained 2786 events. These "raw" data showed evidence for 16.5 s periodicity with a probability of chance occurrence of 3×10^{-3}.

The height of Cerenkov maximum parameter H_c is derived from the positions of the centroids of the images in the two cameras using simple trigonomotry. A broad acceptance range in H_c is imposed prior to selection on the basis of the D_{miss} parameter. Calculation of the parameter D_{miss} is more dependent upon Monte Carlo simulations but allowance can be made for the systematic change in the depth of shower maximum with energy. The basis of the utility of the parameter D_{miss} is the large fluctuations in light intensity from hadron initiated EAS. The random errors in the position of the centroid of an image in each telescope will be approximately Gaussian, thus distribution of D_{miss} will be a Rayleigh distribution. The background D_{miss} distribution is a broad Rayleigh distribution in contrast to the small values of D_{miss} anticipated for gamma ray events. A cut in the D_{miss} distribution of $D_{miss} < 0.4$ was chosen on the basis of detailed Monte Carlo simulations as appropriate to retain most of the gamma ray events whilst rejecting 75 % of the hadrons. No optimisation of the D_{miss} selection threshold has been performed.

The periodogram of the for the Rayleigh analysis of the cut dataset is presented in Figure 6.5 along with a comparable cut to select events unlikely to be gamma rays. The probability of chance occurrence of the periodicity is reduced from 3×10^{-3} to 6×10^{-5} (see Table 6.4).

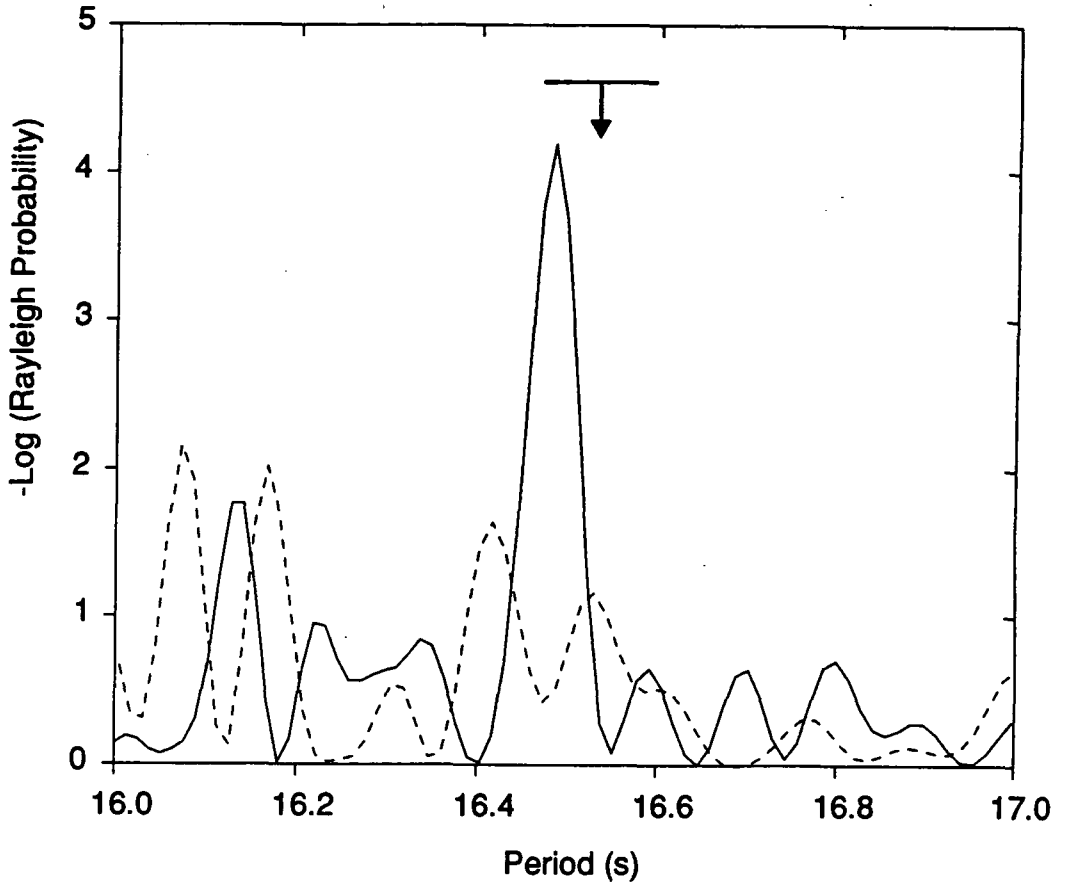

Figure 6.5: Periodograms displaying the results of testing for periodicity (using the Rayleigh test) within the dataset selected on the basis of the parameter D_{miss}. The solid line represents the data with values of $D_{miss} < 0.4$. The broken line represents a similarly sized dataset which satisfies $0.4 < D_{miss} < 0.8$. The first harmonic of the white dwarf rotation period is marked by the arrow.

	No. of Events	R(%)	Probability
Uncut "stereo" events	2784	4.5	3×10^{-3}
$D_{miss} < 0.4°$	787	11.2	6×10^{-5}
$0.4° < D_{miss} < 0.8°$	891	3.0	3×10^{-1}

Table 6.4: Results of the Rayleigh test for periodicity applied to subsets of the stereo data, cut on the basis of the stereo parameter D_{miss}.

6.5.5.4 The Enhanced Dataset

The amalgamated dataset comprising the events selected on the basis of medium resolution imaging and stereoscopic background rejection criteria contains 2080 events. A Rayleigh test of this data reveals periodicity at a period of 16.483 +/- 0.065 s with a chance probability of occurrence of 1.0 x 10^{-10}. The periodogram of this result is shown in figure 6.6. The corresponding light curve folded at this period is illustrated in Figure 6.7.

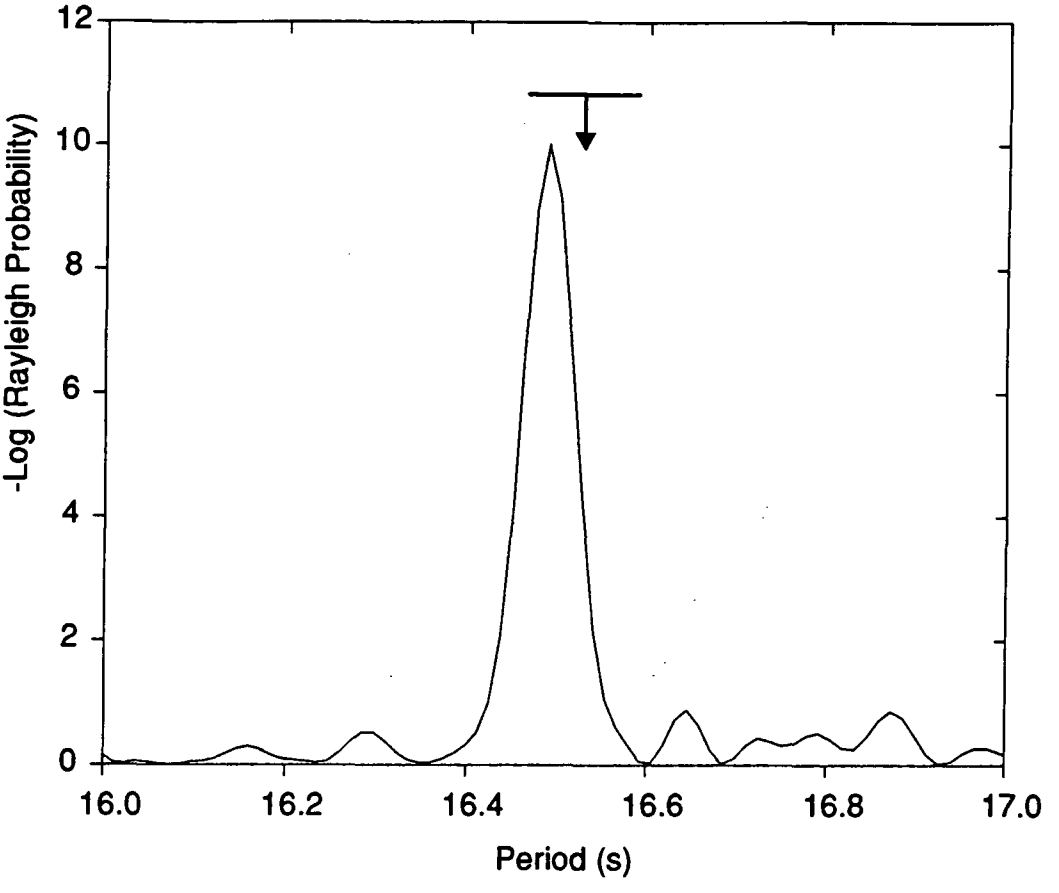

Figure 6.6: The periodogram representing the results of the Rayleigh test for periodicity at the first harmonic of the white dwarf rotation period, within the dataset comprising all of the "mono" and "stereo" selected candidate gamma ray events.

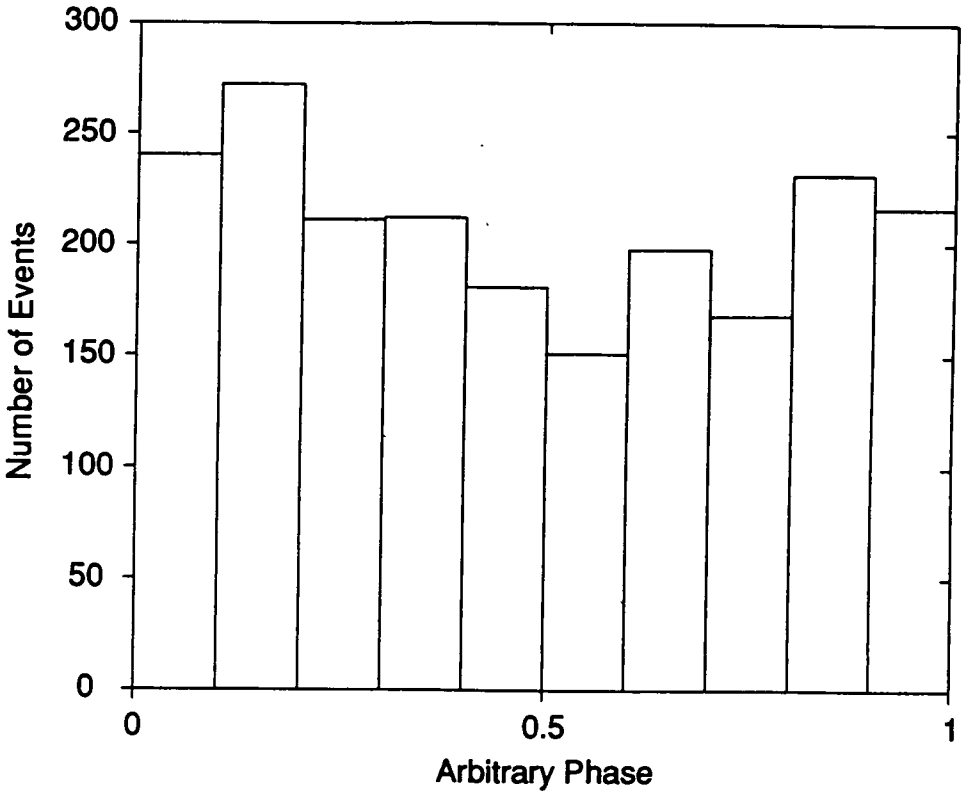

Figure 6.7: The light curve produced by folding the enhanced dataset at a period of 16.483 s.

6.6 Conclusion

Evidence of an outburst of gamma ray emission from AE Aquarii was revealed as periodic emission within a 4200 second segment of data taken on 11th October 1993. Background rejection criteria were applied to two of the three independent datasets. The Mk.3 "mono" dataset was cut using the SPAN and ALPHA image parameters devised for data taken using the medium resolution cameras of the Mk.3 and Mk.5 telescope (the Mk.5 "mono" data was not used in the analysis due the the problem with the digitisers). The "stereo" dataset was cut on the basis of the D_{miss} parameter. In each case the signal to noise ratio was significantly improved, with an associated decrease in Rayleigh probability.

CHAPTER 7

A LOW ENERGY (< 100 GEV) GROUND BASED GAMMA RAY TELESCOPE

7.1 The Mk.6 Telescope Concept

7.1.1 Introduction to the Mk.6 Telescope

The principal objective of the Mk.6 telescope was to provide the facility to make measurements of gamma rays at low energies (< 100 GeV). This would effectively bridge the gap between previous atmospheric Cerenkov telescopes and the highest threshold energy satellite instruments (currently the EGRET experiment on the NASA Compton Gamma Ray Observatory. See Kanbach et al., 1988). A division has developed in the field of ground based gamma ray astronomy between the use of purpose designed instruments of relatively modest size (CANGAROO, HEGRA, GASP, Nooitgedacht, SHALON - ALATOO, Beijing, THEMISTOCLE, CAT) which are confined to TeV energies, and the utilization of the vast flux collection areas provided by solar concentrators (eg Tumer et al., 1993). Solar concentrators are effective large area flux collectors but are not optimised for Cerenkov astronomy. For example, large path differences across the wavefront result in temporal dissipation of the Cerenkov signal. The Mk.6 telescope however, with 114 m^2 of flux collector, in conjunction with efficient PM tube operation, could hypothetically allow detection of photon densities of ~3 m^{-2} which corresponds to gamma ray primary energies of 60 GeV, while retaining the facility of imaging showers produced by gamma rays of higher energy.

There are excellent physical reasons for confidence in the utility of ground based Cerenkov astronomy at these energies, not least the increase in effective collection area provided by utilisation of the atmosphere as a medium to disperse the energy of the primary over a large area on the ground. The effective area of the EGRET instrument, a function of the cross section of the spark chamber, is 0.16 m^2 for gamma rays of energy 500 MeV. This compares with the lateral extent of the Cerenkov light pool on the ground which is reasonably stable with energy and has an area of approximately 9×10^4 m^2, providing an effective collection area more than 5 orders of magnitude larger at energies typically 1000 times larger.

The increase in effective collection area presents the potential for a huge improvement in sensitivity. However, this potential is still subject to the constraints imposed by the all pervasive hadronic background, a background eliminated in the EGRET experiment by the use on an anti-coincidence scintillation dome. Fortunately, though, Cerenkov radiation production by hadron initiated EAS is significantly reduced below 100 GeV, due to the mechanism outlined earlier in Section 3.6.2. Thus a potential improvement in the ratio of signal to noise events within the raw data sample is inherent in the reduction of energy threshold.

In a slightly higher energy regime the cascades yielding the Cerenkov light have sufficient density to provide relatively well defined images at the focal plane. Signals produced by the PM tubes are significantly above the sky noise. The Mk.6 telescope is provided with a high resolution camera with which to exploit the spatial differences between images of gamma ray and hadron initiated EAS, in a hadron background rejection strategy.

The Mk.6 telescope has been assembled at Narrabri on the same East-West line as the Mk.3 and Mk.5 telescopes, adjacent to the Mk.3 telescope. This provides for operation of the Mk.5 and Mk.6 telescopes as an

enhanced stereo imaging system with a separation of 80 m. Figure 7.1 is a schematic diagram illustrating the layout of the Narrabri site.

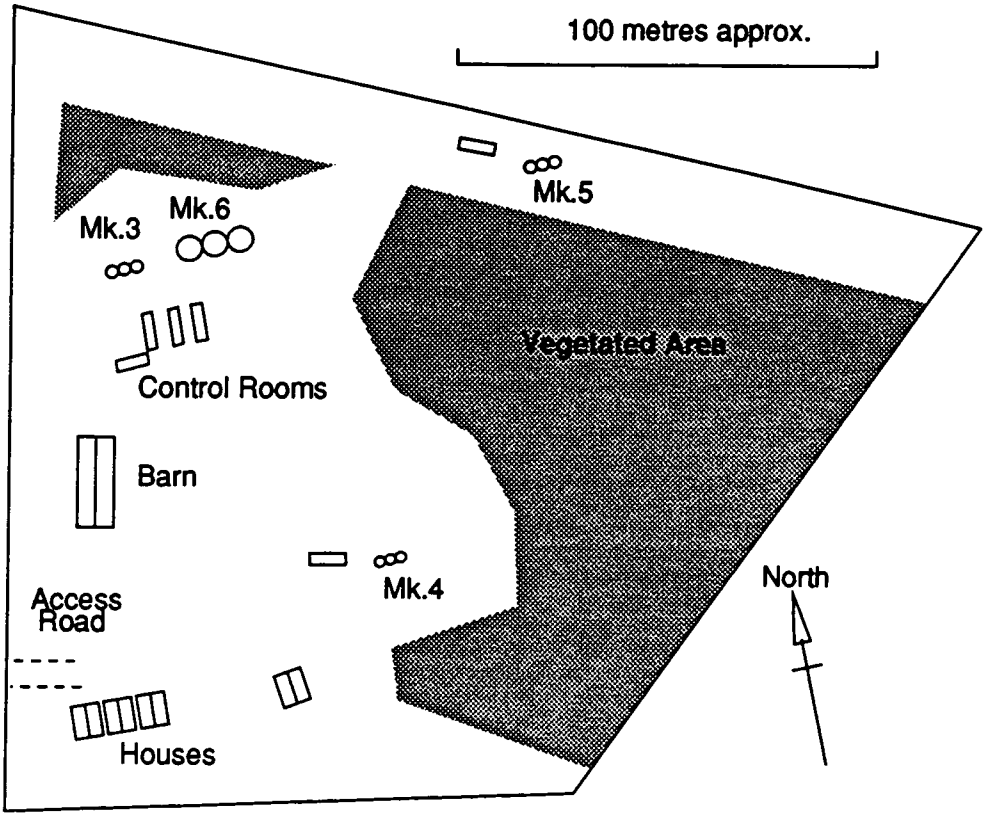

Figure 7.1: Plan view of the Narrabri observatory site (after Bowden, 1993).

7.1.2 A Low Energy Threshold Ground Based Telescope

By maximising the flux collection capacity of the Mk.6 telescope, the Durham group intends to exploit the advantages of observations made at low energies outlined in the previous Section.

The Mk.6 telescope has a total flux collector area of 114 m^2 equally divided between three paraboloidal dishes. This represents the largest area of mirror which could be presented to the sky, on a single mount, using the existing Durham mount technology. Once the flux collector area is so defined, the emphasis is switched to the optimisation of all other

components which have bearing on the performance of the telescope. Some important design considerations are listed below.

- Optimisation of signal collection: Use of hexagonal PM tubes or light gathering cones at the focal plane, and flush fitting mirror sectors to minimise light loss.

- Light noise suppression: Albedo protection using baffles and a reflective surface with high specular reflectivity.

- PM tube choice: Use of tubes which display the characteristics of high gain, high QE, fast response and low noise, with sensitivity over an appropriate spectral range (matched to Cerenkov light).

- Electronics: Provision of a stable system with adequate bandwidth and a large data handling capacity.

- Effective event selection trigger: Optimisation of PM tube field of view to the size of a gamma ray initiated Cerenkov event.

With rigorous attention to all areas in which potential improvements in sensitivity can be made, it is believed that an energy threshold can be achieved which will narrow the gap in the energy spectrum between space based (EGRET) and ground based gamma ray astronomy.

Figure 7.2 is a photograph of the Mk.6 telescope.

Figure 6.2: The Mk.6 telescope.

7.1.3 A High Resolution Imaging Telescope

The high resolution imaging telescope operated by the Whipple collaboration has proved the concept of the atmospheric Cerenkov imaging technique, establishing the Crab nebula as the northern hemisphere standard candle of the field of VHE gamma ray astronomy (Weekes et al., 1989, Vacanti et al., 1991 and Reynolds et al., 1993). In light of this success, a camera with an equivalent resolution to the Whipple camera was specified for the Mk.6 telescope in order that use could be made of the high resolution imaging technique. The design of the camera is considered in Section 7.2.4.

The high resolution camera will be operated as a component of a three fold fast coincidence system. Design of appropriate triggering packages is described in Section 7.2.5 and the incorporation of the camera into the trigger is considered in Section 7.2.7.

7.1.4 Enhanced Stereoscopic Observation of Cerenkov Light from EAS

The separation of the Mk.5 and Mk.6 telescopes is slightly less than that of the current Mk.3 and Mk.5 telescope stereo system (80 m vs 100m). The Mk.6 telescope will provide a high resolution / low energy threshold component to the Mk.5 / Mk.6 pair of telescopes. Statistics for stereo events should improve significantly, with almost all of the Mk.5 telescope events having a stereo counterpart in the Mk.6 telescope, approximately doubling the present stereo event rate. The threshold energy for stereo events, previously higher than that of the independent Mk.3 and Mk.5 telescope thresholds, will be defined by the energy threshold of the Mk.5 telescope. In addition to the reduction in energy threshold, the improvement

in resolution will provide better definition of the centroid of the image in one component of the stereo system.

7.2 The Design and Construction of the Mk.6 Telescope

7.2.1 The Mk.6 Telescope Mirrors

7.2.1.1 Introduction

The mirrors for the Mk.5 telescope proved to be successful and so the manufacturing method was extended to the provision of the mirrors for the Mk.6 telescope. The commitment to observations at low energies (below 100 GeV) necessitates the use of very large flux collectors. A paraboloidal flux collector of nominal focal length and aperture of 7 m was specified due to the following considerations:

- Three 7 m diameter dishes were seen as the maximum possible flux collector area for a single mounted telescope using the available Durham technology.

- An isochronous surface was required in order that pulse profile experiments could be performed.

- f/1 is the aperture limit if seriously debilitating aberrations are to be avoided. This focal length / aperture ratio also facilitates the effective application of albedo protection and flux collecting cones at the focal plane.

7.2.1.2 Specification

The specification for the FWHM of the point spread function of the mirrors was defined by the image scale required at the focal plane. A resolution was sought which would allow the higher moments of the image to be reliably measured, to form a basis for background rejection. This requires that the image on the focal plane extends over a number of pixels. A two fold improvement in resolution over that of the Mk.5 telescope was considered to be adequate, corresponding to the pixel size of the Whipple telescope.

The Mk.6 telescope has been designed to have twice the linear dimensions of the Mk.5 telescope retaining the focal length to aperture ratio of 1. Thus, pixels with the same pitch on the focal plane (3 cm) equate to the desired improvement in resolution to 0.25°. This image scale also defines the required tolerance of manufacture to be half of that achieved for the Mk.5 telescope. If achieved this would result in the point spread function matching the pixel pitch of the camera. It was believed that, with the benefit of experience gained from production of the mirrors for the Mk.5 telescope, this was not an unreasonable objective.

7.2.1.3 Manufacture

The first requirement for the production of the Mk.6 telescope mirrors was the manufacture of a former with the requisite focal length. Each flux collector is divided into 24 mirror sectors, rather than the 12 of the Mk.5 telescope. The dimension of the base of a mirror sector is constrained to be somewhat less than 1 m, as this is the maximum available width of the anodised aluminium reflective surface. The base of a 15° sector at a radius

of 3.5 m is 91 cm which leaves adequate overlap for the vacuum seal required in fabrication. This size of mirror doubles the number of individual mirror sectors in the production run but has the advantage of being only twice the area of a Mk.5 mirror sector rather than the four fold increase if the dimensions were simply scaled. This, in turn reduces the work involved in machining the former.

Steel was again used for the former but 3/8" sheet was used to allow some manipulation of the shape of the surface before machining. The steel was pre-rolled in the radial direction and the spine of the surface which represented the reference parabola was welded to steel pylons fixed at intervals to a reinforced steel table. The plate was then forced down onto other pylons distributed at intervals over its whole area. This resulted in an approximately paraboloidal surface which was then finished in the same manner as the mirror sectors for the Mk.5 telescope (see Section 4.3.3). The production process was identical to that employed for the Mk.5 telescope mirror production and the cold curing routine required the same turn around time of 24 hours.

7.2.1.4 Mirror Sector Testing

The parabolic section of the mirror was initially proved using the testing procedure developed for the Mk.5 telescope, using parallel beams of laser light. The best focus was achieved somewhere between 7.15 and 7.20 m. The uncertainty in the determination of the best focal length was partially due to the rather diffuse laser images at the focus. The light within each beam tended to diverge over the longer distance that each is required to travel, producing poorly defined points of light at the focus.

A method was required to give a better estimate of the best focal length

and derive a measure of the point spread function of the mirror sectors at this distance. The method involving statistical treatment of a number of nominally parallel beams of laser light which formed the basis for early estimates of the point spread function of the Mk.5 telescope mirrors was rejected. This method has been shown to be at the limit of its utility due to the dispersion of the laser beam after its passage through successive beam splitters when projected over the distances involved. Ideally what one would like to achieve is illumination of the whole surface of the mirror sector with light parallel to the optic axis, effectively imitating an infinitely distant light source. The best workable approximation of this condition was achieved by arranging two of the mirror sectors facing each other with an incandescent light source at the provisional focus of one and a target screen at the corresponding focus of the other (see Figure 7.3).

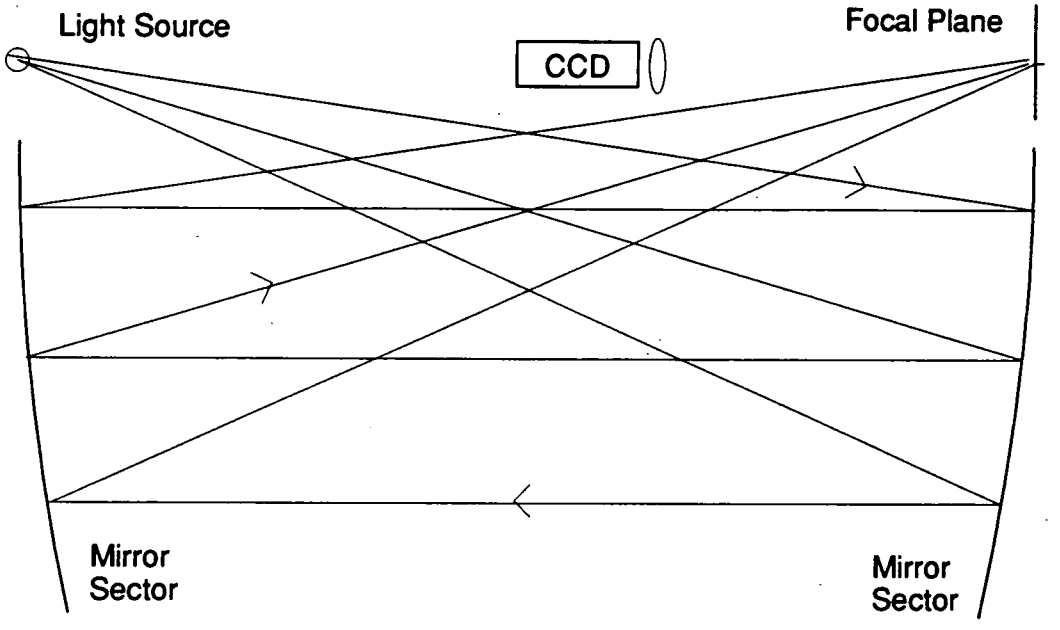

Figure 7.3: A schematic diagram of the Mk.6 mirror testing apparatus.

In preparation, a single beam of laser light was projected from one focus and the mirrors manoeuvred so that the beam, successively reflected by both mirrors, impinged upon the focus of the other mirror. This, together

with other tests demonstrating that the beam is constrained to one horizontal plane, ensures that the optic axes of the two mirrors are parallel. The axes could be made colinear by constraining the laser beam to be near the outer edge of each mirror sector. A number of different apertures for the light source were used, the one ultimately chosen, as a compromise between size and illumination, was 6 mm. This aperture gave a uniform illumination of the mirror, with sufficient intensity to allow meaningful measurements to be made in a dimly lit environment.

A CCD camera was used to digitise a series of images from various tests performed. A Mylar filter (a few % transmissive) was used in front of the camera lens to attenuate the light to a level appropriate to the CCD. This filter has no effect on the contrast of the image but allows a convenient integration time for the camera to be used. In order to ascertain their optimum focal length test exposures of images from inner and outer portions of the mirror sector were taken over a range of focal lengths. These images were diffuse but the centroid and half maximum contour were well defined in each case. For the case where the foci were arranged to be at 717 cm, the images from the large radius and small radius portions of the mirror fell at the same point on the focal plane. This focal length was adopted for subsequent tests.

7.2.1.5 Mirror Sector Performance

The result of an exposure of the whole mirror surface at a focal length of 717 cm is reproduced in Figure 7.4. The maximum value of light intensity within a pixel in this image is 116 bits, with the background being represented by a level of 51 bits. The grey scale in the image shown is linear, thus the boundary between the fourth and fifth bands is the contour

of half maximum intensity. It is evident that there is some extension in the image radially with respect to the mirror sector, which is not surprising given the mirror geometry.

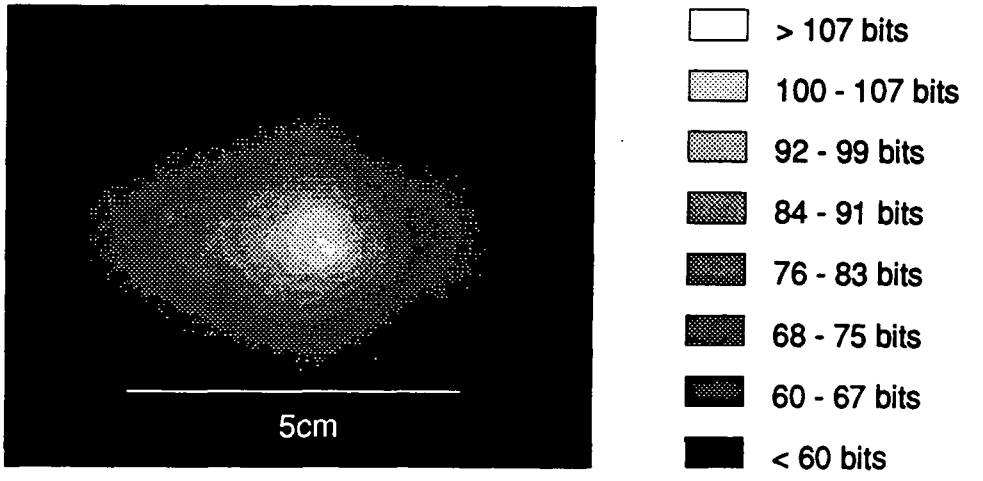

Figure 7.4: A CCD exposure of the image at the focus of a mirror sector, of nominally parallel light from the surface of a second mirror sector with a light source at its focus. The test arrangement is illustrated in Figure 7.3.

A composite of 24 such images successively rotated through 15° will be circularly symmetric and thus will introduce no systematic bias into images of Cerenkov light from EAS. Intensity profiles of sections through the image, both radially and tangentially (with respect to the mirror sector) are plotted in Figure 7.5. The full width half maxima for these sections are 28 mm x 22 mm. Obviously the image is the result of two successive reflections from the geometrical surface under investigation. The intensity profile achieved will therefore be the product of the individual point spread functions and the FWHM of the observed image will be a factor of $(2)^{1/2}$ larger than that for single reflection. Thus one can infer a FWHM for the point spread function of a single mirror sector of 20 mm x 16 mm. This is within the specification.

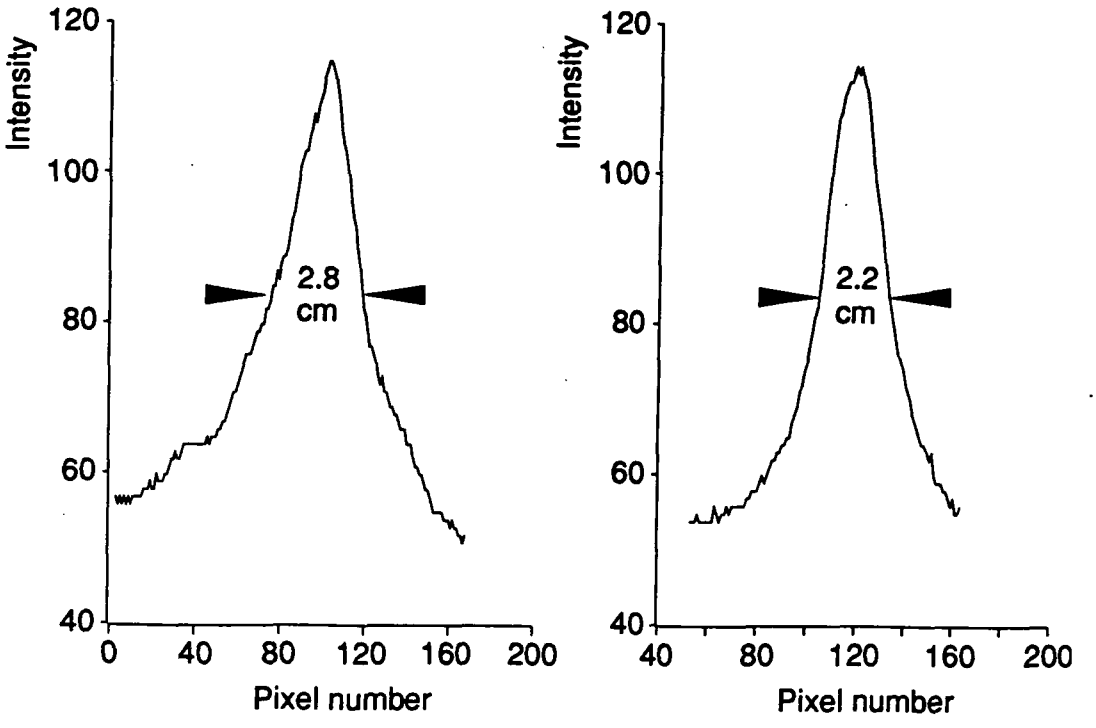

Figure 7.5: Orthogonal light intensity profiles along horizontal and vertical sections through the image shown in Figure 7.4.

A reservation one might have with this reasoning is that systematic errors in the mirror surface might be compounded by the successive reflections. In order to eliminate this concern the test was performed both with the optic axes colinear, and separated but still parallel. The image achieved with the optic axes separated was indistinguishable from that shown in Figure 7.4.

7.2.1.6 Flux Collector Configuration

In the field, the alignment of the mirror sectors was effected using the same method and equipment employed for the Mk.5 telescope mirror alignment. The mirror surface was sampled at intervals from close to the inner edge of the mirror sector out to a radius of 175 cm giving coverage over half of the radius of the dish. It had been shown in the laboratory tests

that images from the inner half of the mirror and outer half were coincident at a focal length of 717 cm. The cradle which supports the detector package at the focal plane was therefore set to be this distance from the centre of the paraboloid. A development incorporated in the Mk.6 telescope design was a common mount for the apices of the mirror sectors at the centre of the flux collector. This mount consists of a 2' diameter steel ring with 24 studs projecting radially into the mirror sectors. The ring has adjustment along the optic axis to allow fine tuning of the focus after alignment, by moving every sector simultaneously at its inner edge.

7.2.1.7 Flux Collector Performance

A CCD camera was used to digitise an image of a star formed at the focal plane. This image is reproduced in Figure 7.6.

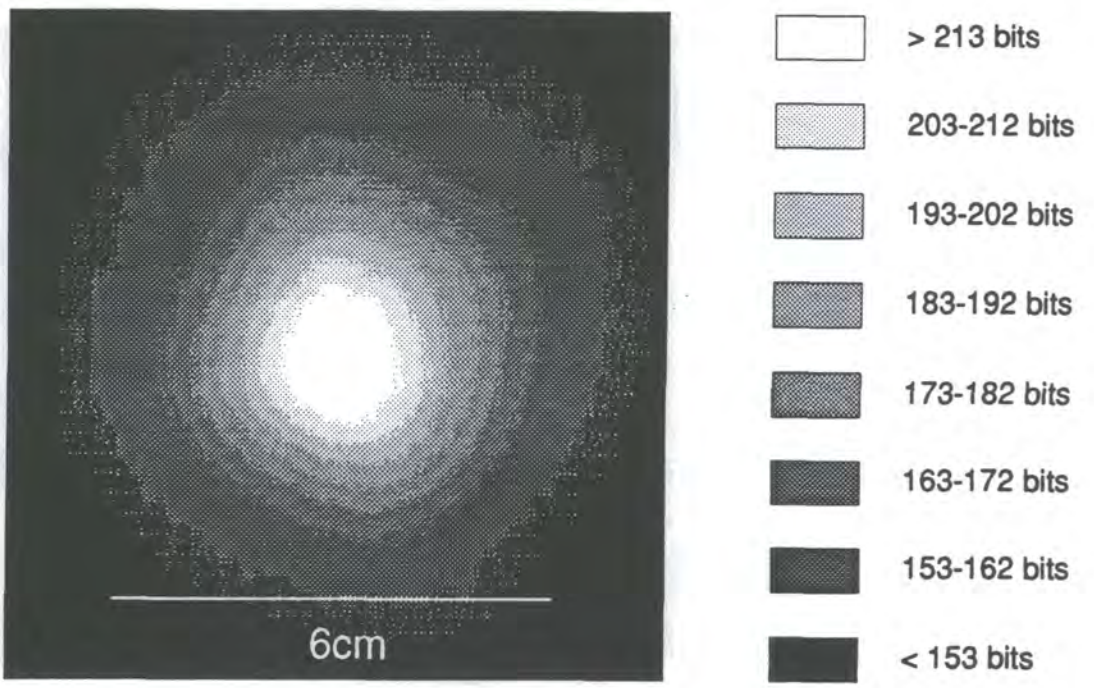

Figure 7.6: A CCD exposure of a star image at the focal plane of a Mk.6 telescope flux collector. The border between the 4th and 5th shades of grey represents the half maximum of the light intensity.

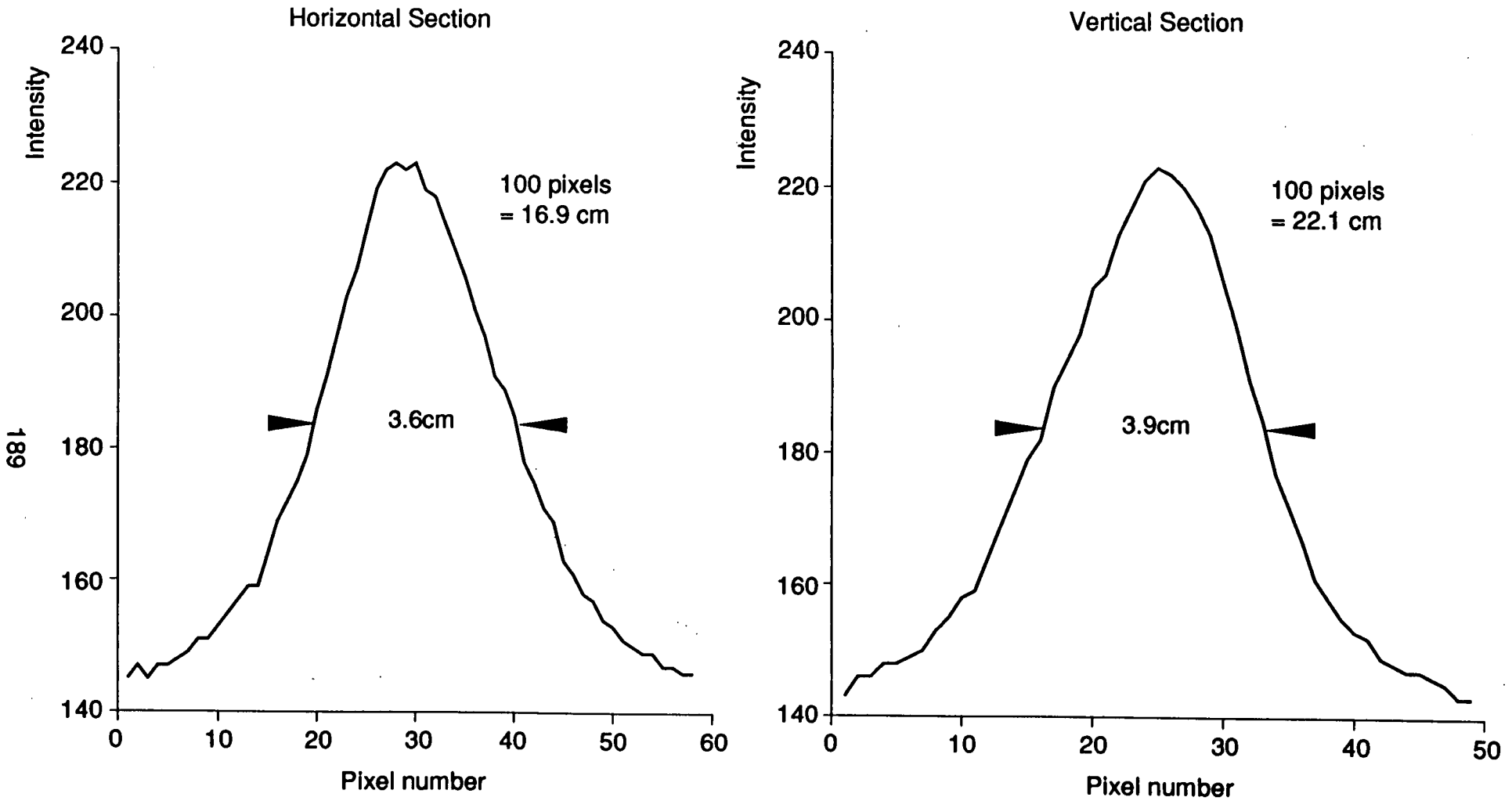

Figure 7.7: Intensity profiles of orthogonal sections through the star image shown in Figure 7.6.

Intensity profiles of orthogonal sections through this image are plotted in Figure 7.7. The actual FWHM of the point spread function is slightly less than 4 cm. This is poorer than anticipated, the shortfall in performance perhaps due to less than ideal mirror configuration, as the laser alignment method was at the limit of its utility on this scale.

7.2.2 Telescope Mount

7.2.2.1 Introduction

The Mk.6 telescope alt-azimuth mount is a scaled version of that employed on the Mk.5 telescope. The linear dimensions of the Mk.6 telescope are a factor of two larger but in light of the experience of the Mk.5 telescope an increase in turntable diameter of 25 % was deemed sufficient. Although the diameter of the two steel plates which comprise the rotating turntable is increased to 5' the diameter of the ring gear against which the telescope is driven remains 27".

7.2.2.2 Mechanical Design

The concept of the Mk.6 telescope mount is identical to that of the Mk.5 telescope. The telescope superstructure is supported by a cradle through two horizontal bearings and is free to move through 90° from the horizontal to the zenith. The cradle sits atop a 5' diameter, 1" steel plate which rotates relative to a similar plate supported by wheeled pylons at its perimeter.

The increase in linear dimension was not too problematic, telescope rigidity proving as good if not better than previous telescopes constructed by the Durham group. The spine of the telescope was shown to flex by only

about 1 cm under the load of the mirrors and superstructure. This corresponds to a maximum divergence in the optic axes of less than 0.03°. Sag associated with the detector packages was shown to be negligible over the operating range of the telescope.

7.2.3 Steering

7.2.3.1 Introduction

Mechanically, the most significant difference in the Mk.6 telescope from the Mk.5 telescope is its increased mass and concomitant increase in moment of inertia. The mass of the steered component of the telescope is between a factor of three and four times greater than that of its prototype. This engineering consideration is exacerbated by the doubling of linear dimensions giving a 12 to 16 fold increase in moment of inertia. Moment of inertia only limits the acceleration of the telescope and in normal stable operating conditions does not feature in its operating characteristics. The huge moment of inertia of the telescope (estimated to be approximately 4 x 10^5 kg m^2) may even afford some protection to the gearbox from the effects of short gusts of wind. It was evident from the start that the Mk.6 telescope would be operated only in stable weather conditions and so the motor drive system was lightly engineered. The mass of the telescope is large in comparison with the manufacturers specification for the D.C. servo motors and gearbox, thus it is important that the telescope is very close to neutral balance at all attitudes. This is easily achieved in the azimuthal plane due to the symmetry of the telescope but adjustment was necessary in the zenith. The solution to the problem of imbalance was to incorporate two counterweights in the design of the telescope. These comprise aluminium

cages which project forwards from either side of the central flux collector. The cages are loaded with lead until a neutral balance is achieved at all angles to the zenith.

7.2.3.2 D.C. Servo Motors and Gearbox

The gearbox and motor chosen to drive the Mk.6 telescope represent an upgrade in the specification of torque compared with those used on the Mk.5 telescope. The motor is an Electrocraft S26-1AT permanent magnet DC servo motor. The motor has a stall torque of 2.1 Nm, a peak torque of 75 Nm and a maximum speed of 2500 RPM. The motor controller is from the Digiplan HFC range and has the capacity to provide a continuous motor current of +/- 12 A at 50 V. Torque is transferred through a Gysin gpl 90.3 gearbox with a reduction ratio of 161:1. The maximum continuous torque is rated at 75 Nm. In the zenith an additional gear train affords a further 6:1 reduction to a final drive gear of 8" diameter this drives a quadrant of 4' diameter giving a total reduction ratio in the zenith of 5796:1. The reduction ratio for drive in azimuth external to the gearbox is the same as the Mk.5 telescope at 18:1 which gives an overall reduction ration of 2898:1. In response to a number of azimuth drive shaft breakages due to the effects of wind, a torque limiter has been introduced between the gearbox and the final drive to allow slippage under potentially damaging wind loading.

7.2.3.3 Shaft Encoders

The shaft encoders are BEI Electronics Inc. M25D absolute position encoders and are mounted in the same way as on the Mk.5 telescope. These encoders provide positional information accurate to 14 binary bits.

The accuracy of positional feedback provided for the steering computer is maintained at the same level as for the Mk.5 telescope. However, the additional two bits of accuracy in sensing of the attitude of the telescope are recorded in each event record.

7.2.3.4 The CCD Camera

Provision is made on the Mk.6 telescope for the tracking of stars in the field of view of the telescope to provide accurate pointing information. A CCD camera identical to those employed on the Mk.3 and Mk.5 telescopes is fixed to the central detector package and provides, for each event record, the position of the brightest star within its field of view to arc minute accuracy.

7.2.4 A High Resolution Imaging Camera

7.2.4.1 Introduction

The benchmark for detectors using high resolution imaging as a background rejection technique in atmospheric Cerenkov astronomy is the telescope operated by the Whipple collaboration on Mount Hopkins, Arizona. The Crab nebula has been detected repeatedly with high significance by this instrument. A 109 element array of PM tubes is used as the photosensitive package at the focal plane. 91 of these tubes form a hexagonally close packed camera with a pixel pitch of 3.2 cm. The radius of curvature of the Davies Cotton design flux collector is 7.3 m, defining an image scale on the focal plane of 0.078° cm^{-1}. Thus the pixel pitch of 3.2 cm equates to an angular resolution of 0.25° (Cawley et al., 1990).

7.2.4.2 Field of view

The resolution of the Whipple camera was adopted for the specification minimum angular resolution of the imaging camera of the Mk.6 telescope. A 3 cm pixel pitch at the flux collector focal length of 720 cm defines an angular resolution for the detector package of 0.24°. The geometrical aperture to the sky for the whole width of the close packed area of the camera (across opposite vertices) is 2.64° for an array of 91 tubes. The configuration of the camera is illustrated in Figure 7.8.

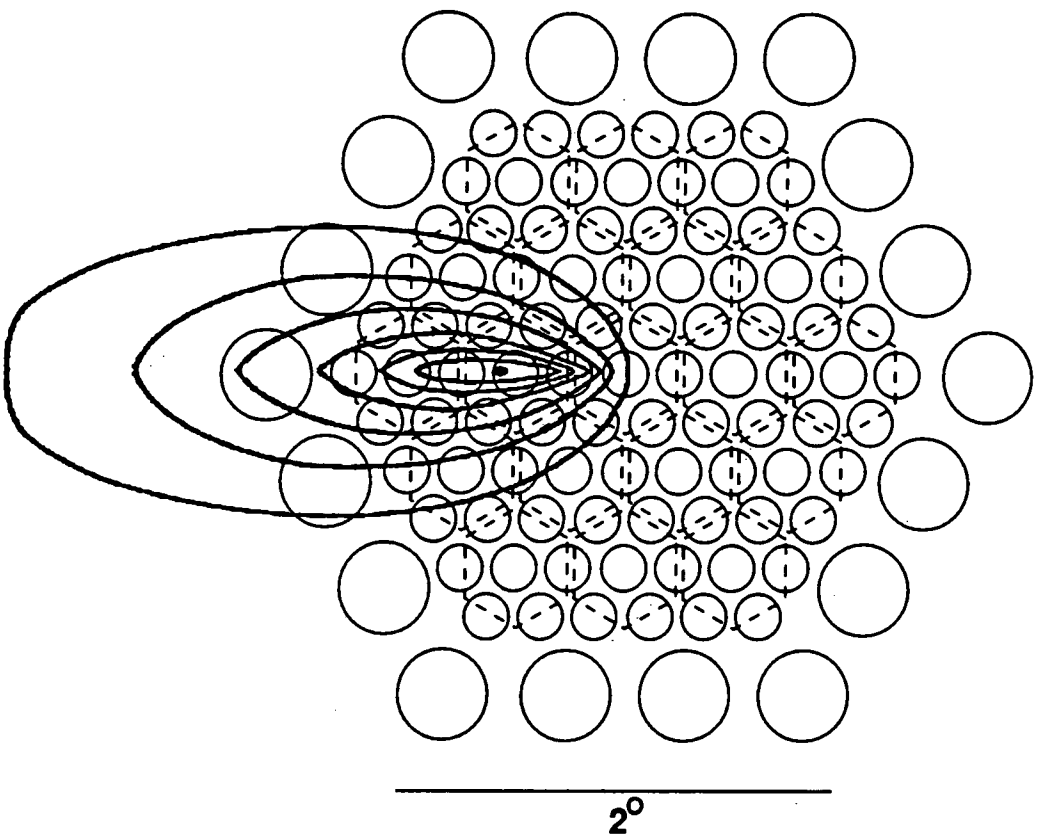

Figure 7.8: Configuration of the Mk.6 telescope camera. The mapping of the camera pixels onto the hexagonal PM tubes of the triggering packages is illustrated. The isophote plot of a Cerenkov pulse produced by an EAS produced by a 0.1 TeV photon primary is again superimposed. (after Rieke, 1969). Successive isophotes represent a reduction in intensity of $(10)^{1/2}$.

A peripheral ring of 2" tubes extends the photosensitive area of the camera beyond the triggered area in order to provide data which will confine images close to the edge of the higher resolution area.

7.2.4.3 Choice of Photomultiplier Tube

Choice of PM tube is restricted to the available 1" diameter tubes by the specified pixel pitch. The use of electromagnetic shielding and insulation along the length of the tubes, which adds to their diameter, precludes the use of 1.125" tubes. The Burle S83062E 1" PM tubes have performed well in the medium resolution cameras of the Mk.5 telescope and the upgraded Mk.3 telescope. However, an alternative make of 1" PM tube (the Hamamatsu R1924) was identified and one unit purchased to test in comparison with the Burle S83062E.

Typical values of pertinent operational characteristics of the tubes, as presented in the manufacturers specification documents, are tabulated for comparison in Table 7.1 below.

	Hamamatsu R1924	Burle S83062E
Rise Time	2.0 ns	2.3 ns
Electron Transit Time	19.0 ns	23.0 ns
Spectral Response	300 - 650 nm	300 - 650 nm
Peak Response	420 nm	420 nm
Quantum Efficiency	26 %	28 %
Photocathode Diameter	21 mm	22 mm

Table 7.1: Comparison of the manufacturers specifications for the Hamamatsu R1924 and Burle S83062E 1" diameter PM tubes.

It would appear that there is very little to choose between the tubes in terms of their specified technical performance. Logistically, though, the Hamamatsu PM tube presented several possible advantages. It is approximately half the length and weight of its Burle counterpart, requires significantly less voltage between the anode and photocathode and is supplied with an appropriate small plug-in base. The Hamamatsu tubes are slightly cheaper per tube, substantially so if the cost of the bases is considered, offering a considerable cost saving for 100 units. The Hamamatsu R1398 tubes (similar to the R1924) operated by the Whipple collaboration have performed well under night sky illumination and have proved to be durable.

The Hamamatsu tubes became the preferred choice because of the practical considerations mentioned but as a final check of their suitability the test tube was incorporated in the camera assembled for the upgrade of the Mk.3 telescope. The test Hamamatsu PM tube was exposed to the Narrabri night sky at the focus of a 3.32 m paraboloidal flux collector in exactly the same environment as the Burle tubes in the camera. The noise/gain characteristics of the two tubes are plotted in Figure 7.9. Both tubes were initially supplied with 770 V and then the voltage incremented in steps of 10 V. In the camera of the Mk.3 telescope an acceptable single fold noise rate is approximately 2 kHz. Both types of tubes draw an anode current of 8 μA when operating at the voltage which produces this noise rate, indicating that their gains are similar. Background starlight photon flux through the tube should be similar in the Mk.6 telescope camera as the increase in flux collector area is offset by the reduction in geometrical aperture of the tube. The introduction of additional logic into the trigger of the Mk.6 telescope may allow the PM tubes to operate at a slightly higher noise rate. If the tubes are gated into clusters of 7 tubes the upper limit on individual noise

rates could be relaxed by a factor of three relative to that of the Mk.3 and Mk.5 telescopes. The noise/gain characteristics of the tubes in the region defined by anode currents between 8 μA and 14 μA are very similar. This region, spanning an order of magnitude in noise rate, encompasses all probable operating conditions for the Mk.6 telescope. The Hamamatsu test tube has been left as an operational tube within the camera of the Mk.3 telescope to provide further information on the relative performance of the Burle and Hamamatsu tubes in the longer term.

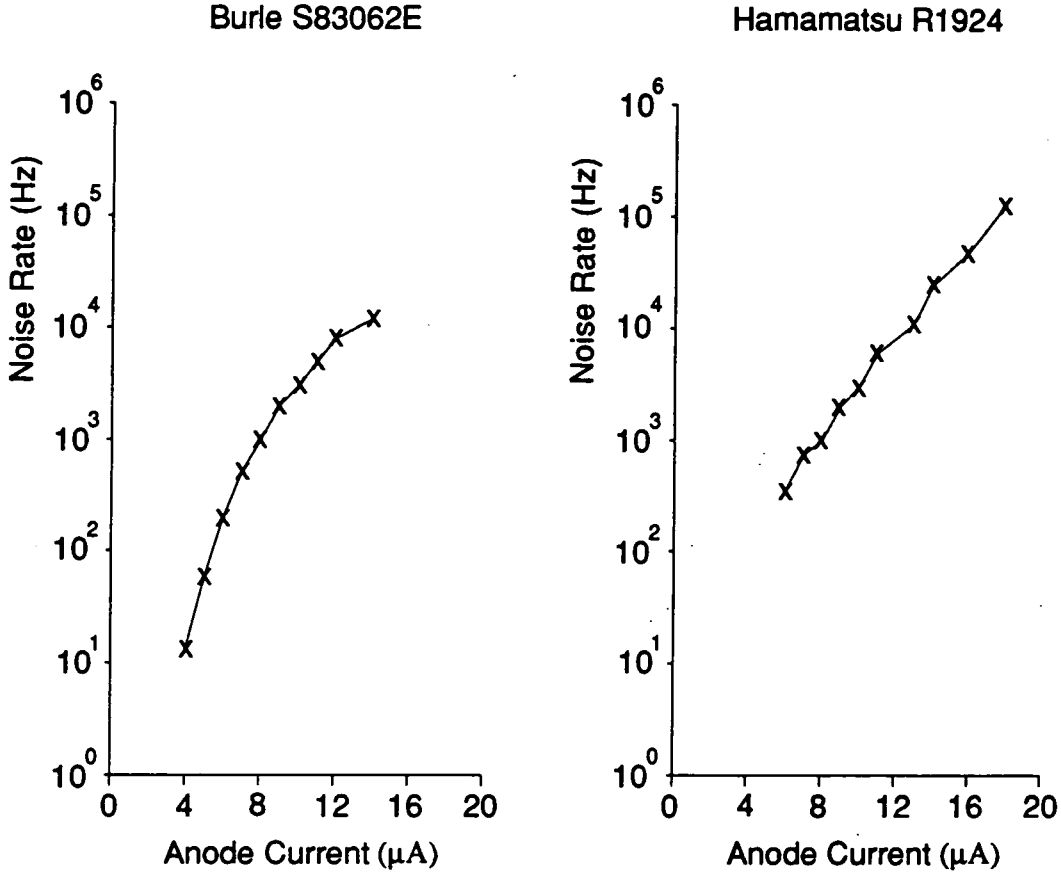

Figure 7.9: Comparison of noise / gain characteristics of Burle S82063E and Hamamatsu R1924 PM tubes when exposed to the night sky. The data were taken at constant illumination for a range of EHT settings.

100 Hamamatsu tubes were purchased and bases assembled and fitted. The tubes were found to be excessively noisy when new until subjected to a period of "burning in". All of the tubes were run, at a nominal operating voltage, under low level illumination for a period of three hours after which the tubes conformed to a reproducible and relatively short warm up characteristic.

7.2.4.4 Construction of Photomultiplier Package

91 1" PM tubes are to be packed into a hexagonal array with a pixel pitch of 3 cm. The Hamamatsu R1924 tubes are only 43 mm in length and so the twin plate method employed to mount the longer Burle PM tubes was deemed unnecessary. The solution adopted was to lodge the tubes in a deeper polyethylene front plate drilled to the configuration of the array. A μ-metal shield was applied to the length of the dynode chain and the tube then insulated with heat shrink material. Self amalgamating tape was then wrapped around the neck of the tube until it formed a tight fit in the countersunk front plate. Once assembled in this manner the tubes were held very firmly in place but could still be replaced individually if required.

The signal from each tube is passed to an individual BNC connector on the back plate of the detector package. EHT is supplied to the 1" tubes via three 37-way high voltage multiway connectors. The EHT required for the 2" tubes is too high to pass reliably through multiway connectors and so is supplied through 18 individual EHT BNC connectors.

The signal is passed from the detector package to the electronics in the control room via 50 m of 75 Ω coaxial cable (type CT100) which has an adequate bandwidth whilst still being sufficiently flexible and light.

7.2.4.4 Light Collecting Cones

A matrix of light collecting cones have been fitted to the front of the detector package to funnel light, which would otherwise be lost to dead areas of the focal plane, onto the photocathodes of the PM tubes of the camera. The concept of these cones is described more fully in Section 4.6.5. Preliminary tests suggest an increase in gain of 25 - 30 %, with corresponding reduction in energy threshold.

7.2.5 Triggering Detector Packages

7.2.5.1 Introduction

The sensitive triggering area of the detector packages at the focal plane of the left and right flux collectors must match that of the camera. This area has an angular extent of 2.64°. The image scale on the focal plane is 12.5 cm per degree, therefore a triggering tube pitch of 6 cm would define triggering channels with a geometrical aperture of slightly less than 0.5°. This aperture matches the size of Cerenkov images from gamma ray initiated EAS and is, therefore, the optimum size for a triggering channel. This pixel pitch is double the pixel pitch of the camera and is a pitch compatible with the common 2" PM tube diameter. The natural choice of PM tube was the Burle 8575 as a sufficient stock of these tubes was held, and their operational characteristics are very familiar to the group. However, a number of Philips XP3422 hexagonal tubes, whose dimensions are the optimum at 6 cm flat to flat, were made available to the group. An array of hexagonal tubes would eliminate the need for light collecting cones for optimisation of signal collection.

7.2.5.2 Choice of Photomultiplier Tube

The Philips XP3422 PM tube has a hexagonal bialkali photocathode with a minimum size of 56mm across the flats. The tubes can be packed with a pixel pitch of 6 cm giving a dead area on the focal plane of only 13 % of the total area. The spectral responsivity of the tube is very good, extending below 300 nm with peak response at 400 nm. The close packing facility provided by hexagonal tubes is usually achieved at the expense of tube bandwidth, however the Philips XP3422 PM tube has an acceptable pulse rise time of less than 3 ns. The noise / gain characteristic of the hexagonal tube and the Burle 8575 PM tube are compared in Figure 7.10.

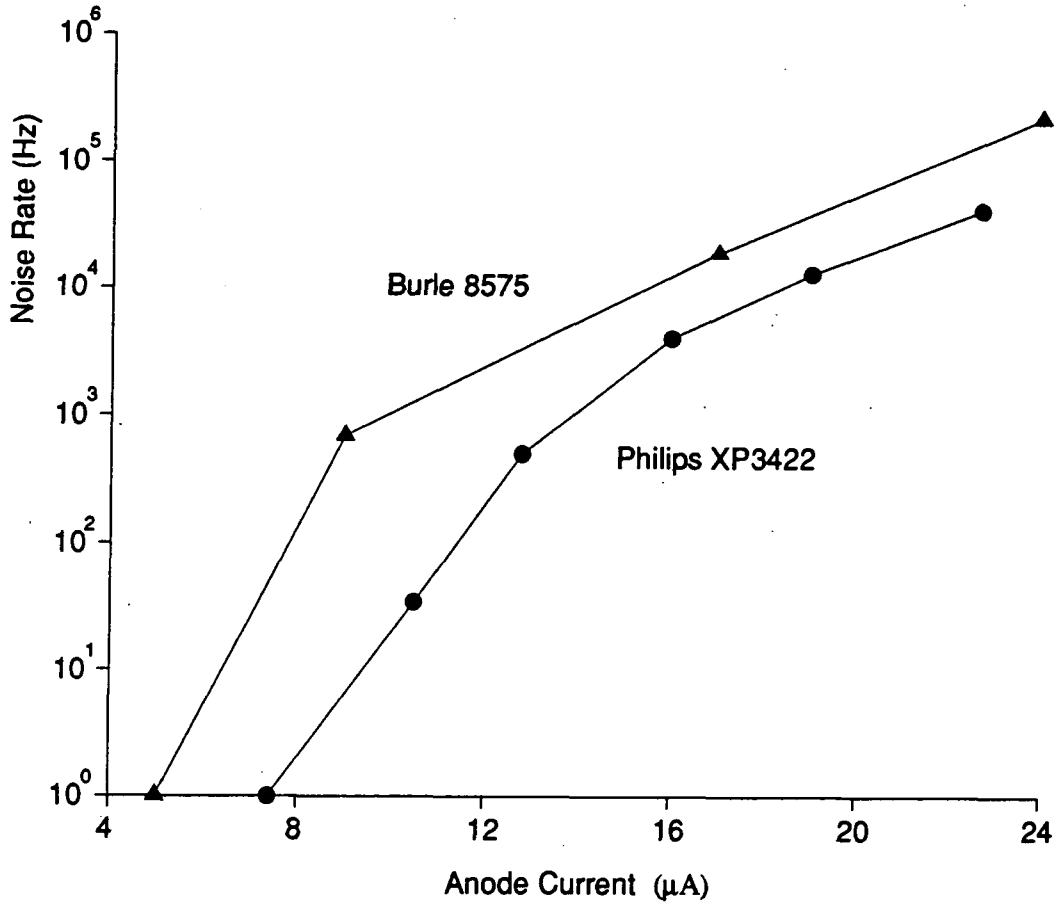

Figure 7.10: Noise / gain characteristics of the Burle 8575 and Philips XP3422. The data are taken at constant illumination as EHT is varied.

All of the data were taken under operating conditions at the Narrabri observatory. The graph demonstrates the Philips tube to have a remarkably low noise rate. Using the radioactive scintillator the relative gain between the tubes and the speed of tube response was measured at a nominal operating single fold noise rate of 10 kHz. The results of these tests are presented in Table 7.2 below.

	Philips XP3422	**Burle 8575**
EHT (V)	1200	1800
Amplitude (mV)	157	63
Area (nC)	1.36	0.84
Rise Time (ns)	2.2	3.2
Pulse Width (ns)	7.0	8.6
Fall Time (ns)	4.6	5.4

Table 7.2: Relative performance of the Philips XP3422 and Burle 8575 PM tubes in response to the radioactive pulser scintillation source. The EHT values used were those which corresponded to a 10 kHz tube noise rate when the tubes were exposed to the Narrabri night sky.

The data above show that the Philips tube to proved to be 1.6 times more sensitive to the pulser than the Burle 8575 and had a faster response. on the evidence that the Philips XP3422 is superior to the Burle 8575, two triggering packages of 19 Philips tubes were constructed. The single channel count rate improvement as a result of this upgrade is considered in Section 7.3 detailing the performance of the telescope.

7.2.6 Calibration

7.2.6.1 Introduction

The current method of calibration is the same method described for calibration of the Mk.5 telescope. Determination of pedestal values presents no problem as this is possible from random events recorded during observation. However, gain calibration using the radioactive scintillator is a highly time and labour intensive process necessitating a significant period of down time for the telescope. Alternative methods of calibration have been considered with the intention of developing a calibration routine capable of providing relative gain information "in flight". An experimental system has been implemented using scintillation light excited by an ultra violet laser.

7.2.6.2 Digitiser Pedestal Determination

Values of the digitiser pedestals are derived from the average tube response to artificially generated random triggers of the telescope recording electronics. The random events are recorded at a rate of a few per minute and provide a measure of the pedestal values throughout an observation.

7.2.6.3 Gain Calibration of Camera PM Tubes

The gain calibration procedure developed for the Mk.5 telescope involves illuminating the photocathode of each PM tube with a radioactive scintillation source and recording a pulse height spectrum through the electronics dedicated to each particular tube. This is obviously a very time consuming

process, which restricts the frequency of repetition of calibration of the telescope. However, it has the attraction that the mean number of photons in the light pulse is known and this allows absolute calibration of the telescope response. The problem of the infrequency of gain calibration can be circumvented by the provision of a light source to flood the camera with a uniform blanket of light at random intervals during observation to provide real time relative gain calibration . The light source which has been implemented is a scintillator excited by the signal from a pulsed nitrogen laser (VSL Model 33700). The laser produces a short duration (3 ns) 40kW pulse of UV light of 378 nm wavelength. This light impinges on the scintillator and a sample of the resulting visible blue light is piped to each collector using optical fibres. The lengths of the optical fibres are adjusted so that the telescope is triggered by the light, allowing the gain calibration measurements to be incorporated into the data stream. Figure 7.11 shows a single event before and after gain calibration. Gains of all camera tubes are normalized to the gain of the central pixel PM tube which is the subject of extensive absolute calibration using the radioactive pulser scintillation source. It is not possible to assess the effectiveness of the calibration system on the basis of single events so an average response to the cosmic ray beam was sought. Figure 7.12 illustrates the average camera response to 1000 unselected events, before and after gain calibration using the laser technique derived gain normalization factors. Before calibration the variation in PM tube response to the average Cerenkov intensity was up to 200 % whilst afterwards the range was no more than 30 % of the central pixel response.

(a)

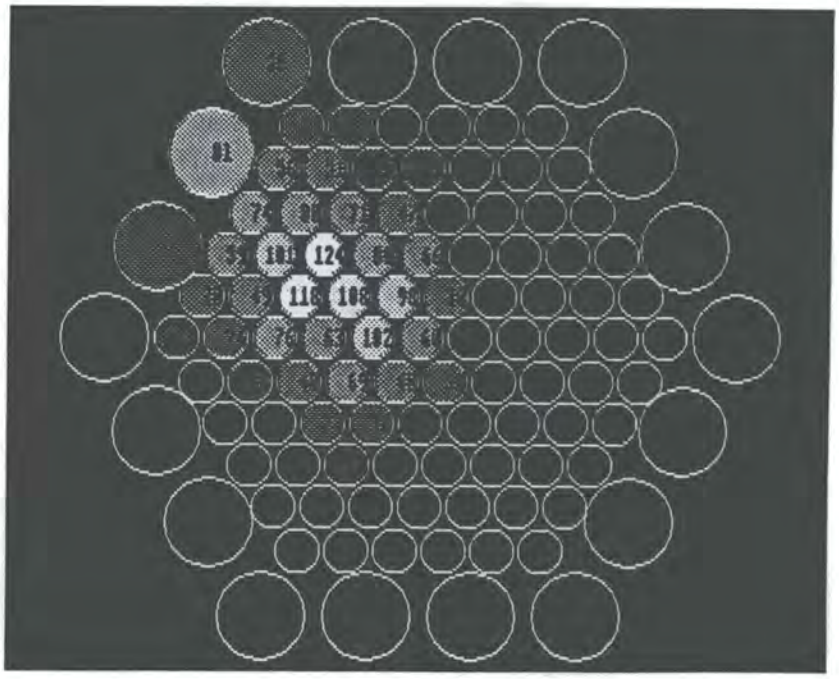

(b)

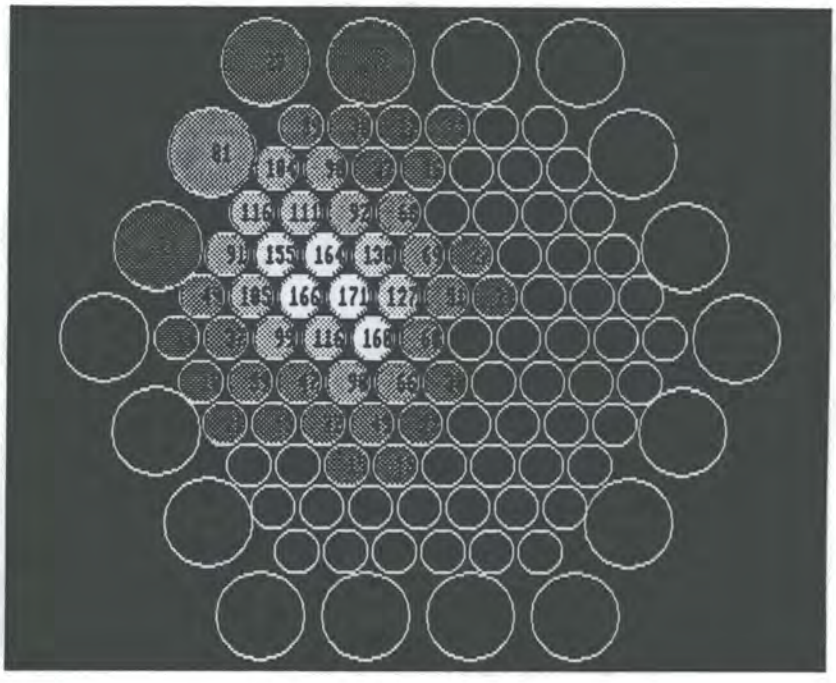

Figure 7.11: An example event (a) before and (b) after gain calibration of the camera using normalization factors derived from the laser calibration procedure.

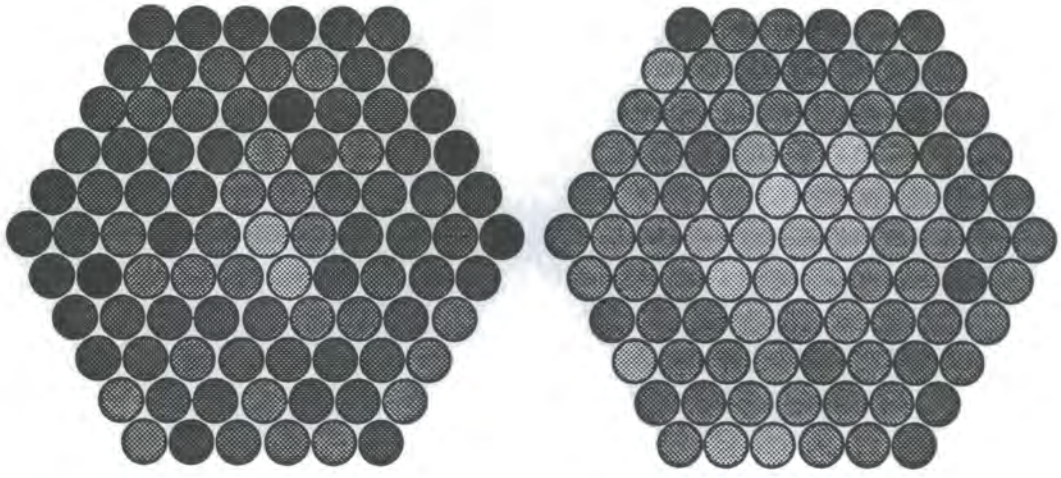

(a) (b)

Figure 7.12: The average response of the camera to 1000 unselected cosmic ray events (a) before and (b) after gain normalization using data provided by the laser calibration system. The grey scale represents the average response of each PM tube. Eleven greys represent the full range (5-15 bits above pedestal) of average charge digitizer values for each pixel.

7.2.6.4 Calibration of the PM Tube Packages Dedicated to the Event Trigger

It is desirable to have as even a response as possible in the triggering energy threshold over the whole field of view of the camera. Calibration of the triggering tubes in the detector packages at the focal planes of the left and right flux collectors is also performed using the radioactive scintillation source pending the introduction of the laser calibration method. Of greater importance, however, is the response of the telescope to the isotropic cosmic ray flux. Triggering PM tube gain is adjusted to give an even trigger rate over the 19 triggering channels. The individual coincidence channel count rates are presented in Table 7.3 below.

	Zenith Angle					
Channel	**10°**	**20°**	**30°**	**40°**	**50°**	**60°**
1	116	106	98	73	40	28
2	109	110	98	70	45	30
3	100	97	92	72	38	25
4	117	100	93	70	46	24
5	100	96	100	68	44	26
6	87	94	81	70	36	22
7	132	111	108	84	58	34
8	92	110	72	57	30	20
9	126	87	94	78	40	24
10	106	104	84	70	40	20
11	115	98	102	78	46	30
12	118	103	97	72	53	25
13	124	108	108	82	48	31
14	135	106	112	82	52	28
15	136	119	108	90	53	34
16	140	80	114	98	53	32
17	110	86	96	62	46	22
18	117	80	98	62	56	26
19	100	79	81	56	46	27

Table 7.3: Individual single channel count rates (counts per minute) for each of the coincidence channels, for a range of zenith angles. Trigger response is demonstrated to be quite uniform.

7.2.7 The Event Selection Trigger

7.2.7.1 Introduction

Three independent flux collectors were specified in the design of the Mk.6 telescope, so that the detectors at their foci could be operated at high gain within a three fold coincidence system. After gain optimisation, the aperture of the individual PM tubes within the coincidence channels becomes the dominant influence on sensitivity. The signal to noise ratio within a PM tube was considered in Section 3.2.3 and shown to decrease linearly with increase in aperture, beyond the aperture which includes the whole of the signal. The optimum aperture is, then, the one which matches the extent of the Cerenkov flash. The aperture of the triggering channels of the Mk.6 telescope, at 0.5°, are optimised to the size of the Cerenkov signature of a gamma ray initiated EAS. The lowest possible energy threshold configuration for the telescope therefore, comprises three identical 19 pixel detector packages at the prime foci of the flux collectors. Pixel aperture is optimised to the image size, and the conventional three fold coincidence, with gate length matched to the duration of the Cerenkov pulse allows the PM tubes to be operated with with the highest possible gain.

Incorporation of a high resolution imaging camera into coincidence introduces complications. The individual pixels do not have the optimum signal to noise ratio, and so individually offer an inferior triggering threshold and telescope energy threshold is compromised. However, the fact that a number of camera pixels correspond to the field of view of each triggering channel presents a number of possible logic combinations for the camera contribution to event selection. If, by introducing further logic requirements into the camera trigger, the sensitivity of the central detector package can

be restored, then it may be possible to make low energy and high resolution observations simultaneously. The triggering regimes currently under investigation are described below. Relative performance of the various configurations are presented in Section 7.3.2.

7.2.7.2 A Conventional Three Fold Fast Coincidence Trigger

Tests have been performed using three similar detector packages, each of 19 hexagonal tubes, at the foci of the flux collectors. This should constitute the ultimate low energy threshold configuration of the telescope, each PM tube being matched to the image size giving the optimum signal to noise ratio. Individual single fold noise rates are constrained to be less than 30 kHz to provide practically accidental free data.

7.2.7.3 Incorporation of a Camera into Three Fold Coincidence

The number of tubes in the camera of the Mk.6 telescope makes it impractical to implement a similar trigger requirement to that which allowed the incorporation of the camera of the Mk.5 telescope into its event selection. The simplest solution requires that the two corresponding triggering tubes in the detector packages at the focus of the left and right flux collectors achieve discrimination threshold coincidentally with one of the seven 1" tubes of the camera whose field of view is wholly or partially enclosed by these triggering tubes. A combined noise rate of 15 kHz for each triggering cluster of 7 camera pixels ensures an effectively accidental free three fold trigger rate, constraining the individual PM tube noise rates to 2-3 kHz.

7.2.7.4 A Four Fold Coincidence Trigger

The preliminary tests of this trigger condition were performed in January 1995. The logic unit which defines the "any one from seven" condition for the clusters of seven tubes in the camera is replaced with a hard wired unit to specify a condition of "any two from seven" for each of the clusters of seven camera tubes which correspond to each triggering channel. The noise rate form the cluster of 7 is again held at 15 kHz, however the additional logic requirement allows an increase in individual PM tube noise rates to 200-300 kHz.

7.2.8 Electronics

7.2.8.1 Introduction

Despite a significant increase in the number of PM tubes the signal path is almost identical to the Mk.5 telescope, the only difference being the addition of trigger logic for the camera. A schematic diagram of the electronics is displayed in Figure 7.13.

7.2.8.2 The Telescope Performance Monitoring System

The TPMS system employed by the Mk.5 and Mk.3 telescopes has been extended to provide full telescope operating conditions for the Mk.6 telescope. The operating condition of the telescope is defined by the anode currents and single fold noise rates of the 147 PM tubes. Anode currents are provided by purpose designed ADC units while Durham-designed fast scalers monitor the single fold rates and coincidence rates. The ADCs and

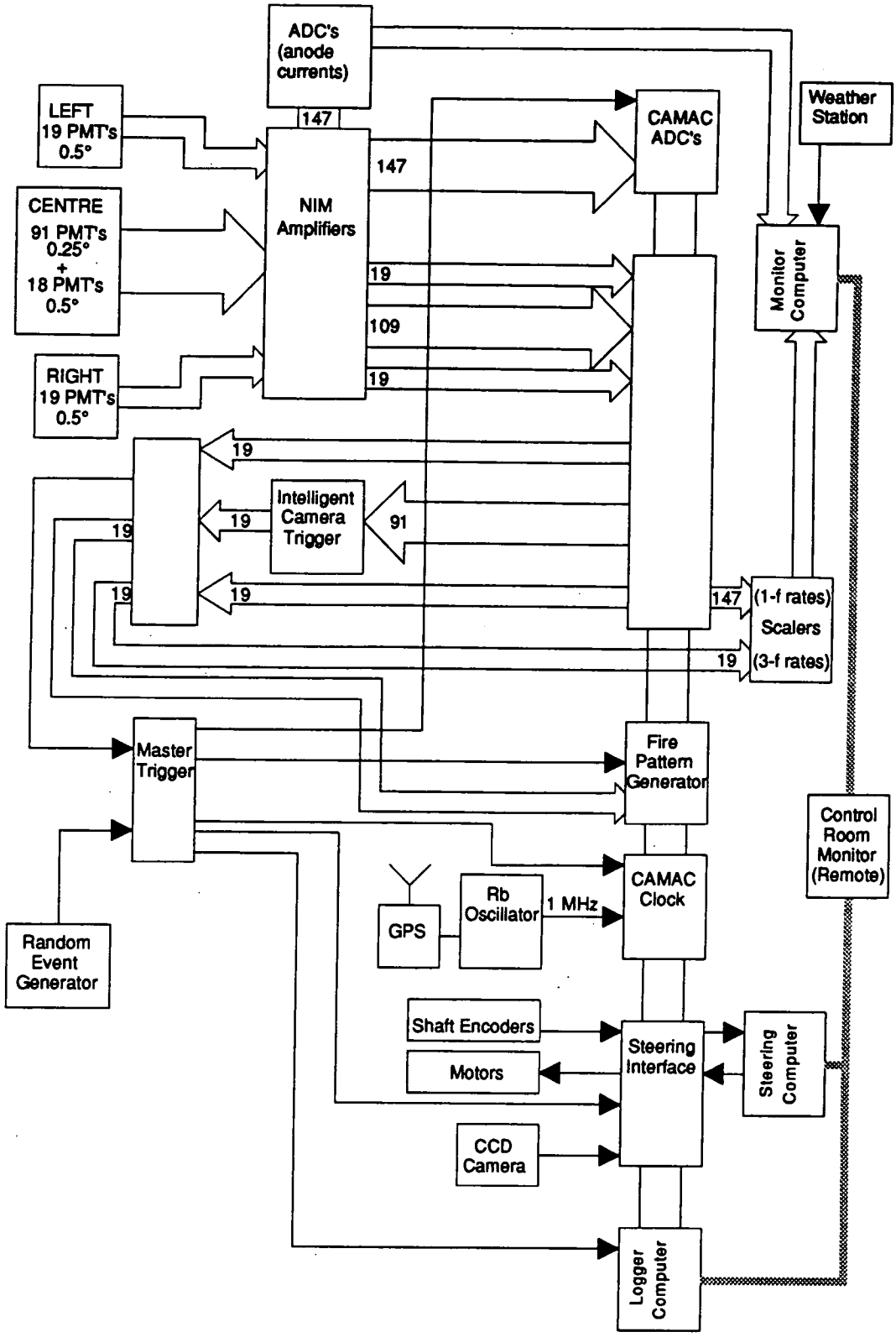

Figure 7.13: Schematic diagram of the Mk.6 control and logging electronics.

scalers are interrogated by an Archimedes microcomputer which also receives steering information and weather information from dedicated microcomputers on the telescope's LAN. Visible and audible warnings are created in the event of predetermined operating ranges being exceeded.

Signals from the PM tubes are passed to the control room via 50 m of CT100 coaxial cable. Inside the control room the cable is spliced onto a length of RG179 cable which is trimmed to adjust for signal transit time differences. The signal then enters an AGC unit which changes the impedance of the signal path from 75Ω to 50Ω. The anode current is converted to a voltage for monitoring and the analogue signal is AC coupled for subsequent processing. AGC output is then amplified by a factor of ten by a LeCroy Model 612A amplifier which has two outputs. One amplifier output is passed to a LeCroy voltage discriminator the other is delayed by an appropriate amount and fed into a fast charge digitiser (LeCroy model 2249A ADC). Each voltage discriminator channel has two ECL outputs. One output is passed to a scaler via an in house designed ECL - TTL converter and provides the single fold noise rate for each PM tube. The second output is passed to a LeCroy coincidence logic unit. The signals are grouped into channels which produce an output when a signal is registered from each of the corresponding left, right and camera inputs to the unit, within a narrow gate interval (10 ns). The coincidence and logic system as been designed to be flexible in order to accommodate the developments planned for the event selection trigger. The ECL outputs of the logic units are passed to a Durham designed coincidence register which determines which of the individual channels has achieved coincidence for each event. This "fire pattern" is latched for subsequent recording. Each channel is also scaled in a similar way to the single folds to provide the three fold coincidence count rate for each channel. The output of each of

the coincidence channels is ORed and combined with a site wide random trigger at a voter coincidence unit, to provide a master trigger for the telescope. This master trigger is fanned out to provide;

- an interrupt to signal an event to the logging computer,

- signals to latch the coincidence registers, the telescope steering information from both the shaft encoders and the CCD star tracker,

- gate pulses for the charge digitisers.

The logger of the Mk.6 telescope is based on an Archimedes commercial microcomputer. The logging system is interrupt driven, communicating with the CAMAC electronics via HyTec CAMAC interfaces. 1kByte of data is recorded to the hard disk of the computer for each event. The system is very efficient, operating with a dead time of 1 - 2 ms.

7.3 Performance of Mk.6 Telescope

7.3.1 Introduction

The preliminary commissioning of the Mk.6 telescope was completed by the end of 1994 and tests of the operational characteristics of the telescope have been performed in the early months of 1995. A summary will be given below to illustrate the performance of the telescope as a low energy threshold telescope and as a higher energy imager.

7.3.2 Minimum Energy Threshold

7.3.2.1 Introduction

As stated earlier in Section 7.2.7, it was anticipated that the ultimate low energy threshold configuration of the Mk.6 telescope may comprise three identical 19 pixel detector packages at the prime foci of the flux collectors. Operation of the telescope in this configuration would, however, produce only medium resolution images of the more energetic events which are amenable to high resolution image parameterization. It would be very desirable to be able to operate at very low energies with the high resolution camera incorporated into the trigger. Tests have been performed with the telescope operating with different triggering regimes, in order to assess the relative efficiency of the different detector packages and coincidence requirements.

7.3.2.2 Relative Performance of Differing Telescope Configurations

Table 7.2 summarises the relative performance of various configurations of the central PM tube assembly. The event rates quoted are for a single left / right / centre coincidence channel with a geometrical aperture of 0.5°.

	Central Detector Configuration	**Event Rate (c.p.m.)**
(a)	"1 of 7" Trigger	51 +/- 5
(b)	"1 of 7" + Light Cones	68 +/- 5
(c)	"2 of 7" + Light Cones	72 +/- 5
(d)	19 Hexagonal PM tubes	75 +/- 5

Table 7.2: Relative single channel coincidence count rates achieved from various configurations of the central PM tube assembly of the Mk.6 telescope. For case (d) the detector package was identical to the left / right triggering packages. The data were taken at 30° to the zenith.

The above count rates demonstrate that the telescope performance was initially constrained by the camera response - configuration (a). The addition of the light collecting cones to the focal plane of the camera however, resulted in an improved count rate, consistent with that achieved for the three identical detector packages - configuration (b). Also, it would appear that imposition of the "2 of 7" event selection criterion for the camera PM tubes gives only a marginal improvement in count rate. This suggests that the energy threshold of the telescope is now defined by the response of the left / right triggering packages. Thus, the "2 of 7" camera logic does not offer any further reduction in energy threshold. It does, however, allow the

PM tubes of the camera to be run with a slightly higher gain. This results in a better representation of the image in the camera, which will reduce the energy threshold at which high resolution imaging is viable.

The count rate of the telescope has been improved since the data shown in Table 7.2 were recorded. This has been achieved by the application of simple baffles to the focal plane to exclude a proportion of the background albedo. The increased albedo protection has allowed the EHT on the PM tubes of the central camera of the Mk.6 telescope to be increased to the extent that their operating conditions are now similar to those of the Mk.5 telescope. As the night sky flux through the corresponding camera tubes of the Mk.5 and Mk.6 telescopes is identical, due to the compensating reduction in aperture and increase in flux collector area, this suggests that the tubes in the two telescopes are operating with similar gains. If this is the case, then the Cerenkov signal in an event will be increased four fold for the Mk.6 telescope relative to the Mk.5 telescope. Conversely, the Mk.6 telescope should be sensitive to showers of four times lower intensity.

7.3.2.3 Estimation of Energy Threshold

Historically, the Durham group has assigned gamma ray energy thresholds to their telescopes by reference to a semi-empirical model linking telescope performance to that of the original telescopes of the Dugway array. Count rate, for a given aperture, is a function of the energy threshold for hadron events and the effective collection area of the telescope. A detailed analysis of the response of the Dugway array yielded a well defined collection area for each component of the array, and the energy threshold for the array components was calculated using Monte Carlo simulations of EAS. This energy threshold has been used as the baseline for estimation of

thresholds for subsequent telescopes.

The effective energy threshold of the telescope can be varied by adjustment of the discriminator threshold, and by so doing the integrated count rate above energy threshold can be shown to conform to a power law spectrum. The index of this spectrum is a function of the cosmic ray energy spectrum, and the variation with energy of the lateral distribution of Cerenkov light from hadron initiated EAS. This spectrum can be used to infer an approximate energy threshold for the Mk.6 telescope, relative to that of the Mk.5 telescope, by comparison of the count rates of the Mk.5 and Mk.6 telescopes. Figure 7.14 shows the variation of Mk.6 telescope count rate with voltage discriminator threshold.

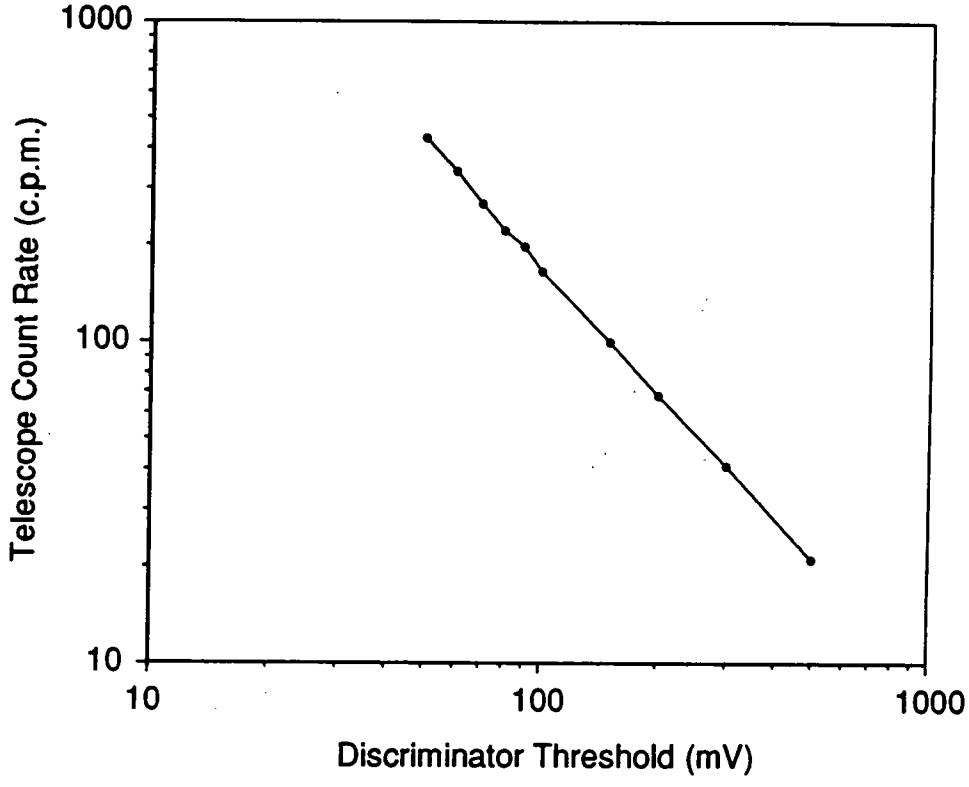

Figure 7.14: Mk.6 count rate variation with voltage discriminator threshold as threshold is increased from its operating value of 50 mV to 500 mV. The tests were performed with the telescope pointing at 30° to the zenith.

The index of the power law spectrum shown in figure 7.14 is -1.32. The count rate at the zenith for the Mk.6 telescope is 500 c.p.m., thus its estimated energy threshold to gamma rays, extrapolated from that ascribed to the Mk.5 telescope, is given by,

$$R_6 / R_5 = (E_6 / E_5)^{-1.32}$$

where R_6 and R_5 are the count rates of the Mk.6 and Mk.5 telescopes and E_6 and E_5 represent their respective energy thresholds. Thus,

$$-1.32 \ \log_n (E_6 / 250) = \log_n (500 / 150)$$

The inferred energy threshold of the Mk.6 telescope in its current configuration is ~100 GeV. Estimation of energy threshold, however, is fraught with difficulties. An alternative approach to extrapolating the threshold of the Mk.5 telescope to achieve an estimation of the Mk.6 telescope threshold is to compare the measured photon densities for events between telescopes. The smaller events recorded by both telescopes show similar integrated photon flux, suggesting that the threshold events of the Mk.6 telescope are a factor of four lower in energy than those recorded by the Mk.5 telescope. Further small improvements to the Mk.6 telescope are planned which will reduce the energy threshold still further (see Section 7.4).

If the anticipated degradation of telescope response to EAS with hadron primaries with energies of 200 GeV and below occurs, an equivalent count rate spectrum to that shown in figure 7.14 should show a deficiency of events at low energies. Thus estimation of telescope energy threshold to gamma rays, based on an extrapolation of the integrated count rate above

threshold, becomes invalid. In order to establish the energy threshold recourse must be made to simulations. The count rate variation with energy threshold can be modelled and compared with that achieved by variation of the voltage discriminator threshold. The point at which the count rate begins to deviate from the power law spectrum will define a known energy threshold for the telescope. The ultimate low energy threshold can be derived from this point.

Energy threshold is obviously a function of zenith angle, the optimum threshold only achievable close to the zenith. Figure 7.15 shows the zenith angle dependency of the count rate for the Mk.6 telescope. Beyond a zenith angle of 30° the count rate begins to deteriorate dramatically suggesting that the lowest energy measurements will be restricted to less than 30° to the zenith.

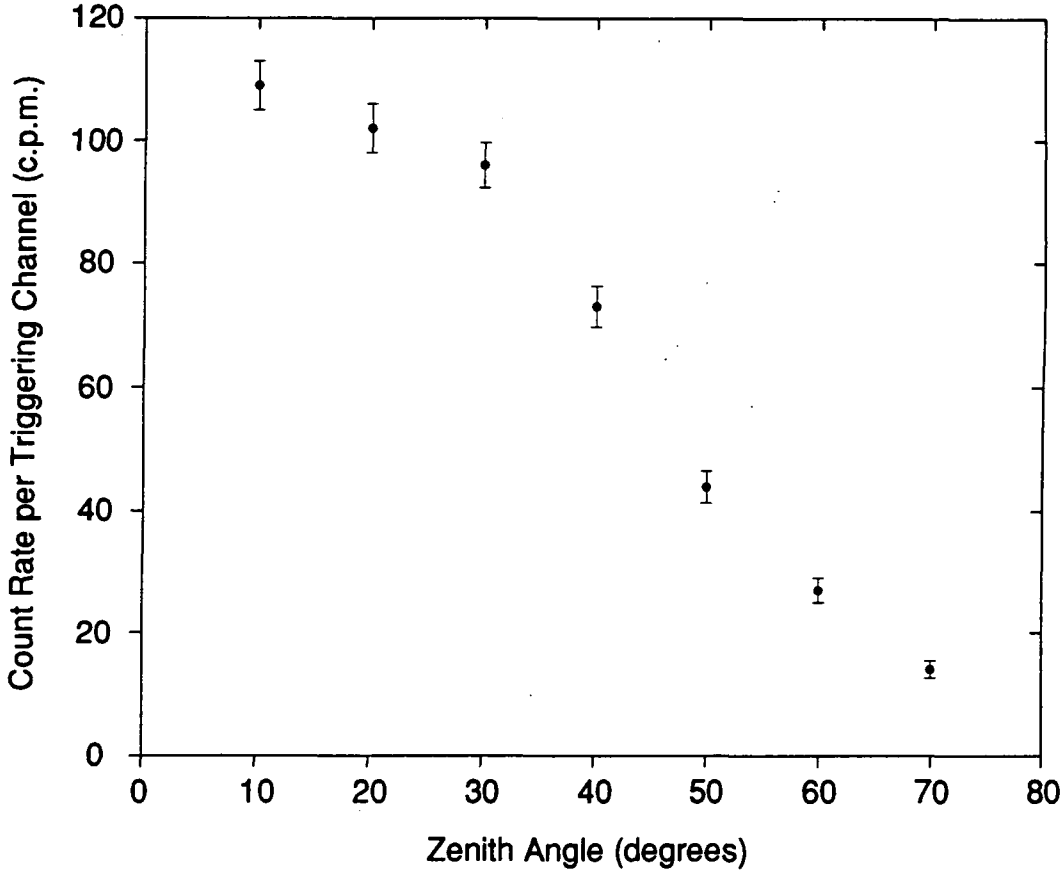

Figure 7.15: Zenith angle dependency of single channel count rate.

7.3.3 High Resolution Imaging Configuration

7.3.3.1 Introduction

The Durham camera has an equivalent pixel resolution to that of the telescope operated by the Whipple collaboration. The contemporary, well established, Whipple analysis procedure as described by Fegan (1994) has, therefore, been adopted for the treatment of the preliminary data. These are engineering data taken at a fixed angle to the zenith of 20°.

7.3.3.2 High Resolution Images

The standard calibration procedure described in Section 7.2.6 has been applied to the data. Digitiser pedestals have been subtracted from the response of each PM tube, and the gain of each pixel normalized to the response of the central pixel using relative gains derived from the laser calibration system. Following the procedure developed by the Whipple collaboration, each PM tube is labelled as;

- an "image" pixel if the signal within the tube exceeds 4.25σ of noise within the tube,

- a border pixel if the signal exceeds 2.25σ of noise if it is adjacent to a signal tube, or

- a background pixel, set to zero, if neither of the above criteria are satisfied.

Figure 7.16 illustrates a typical image classified in this way.

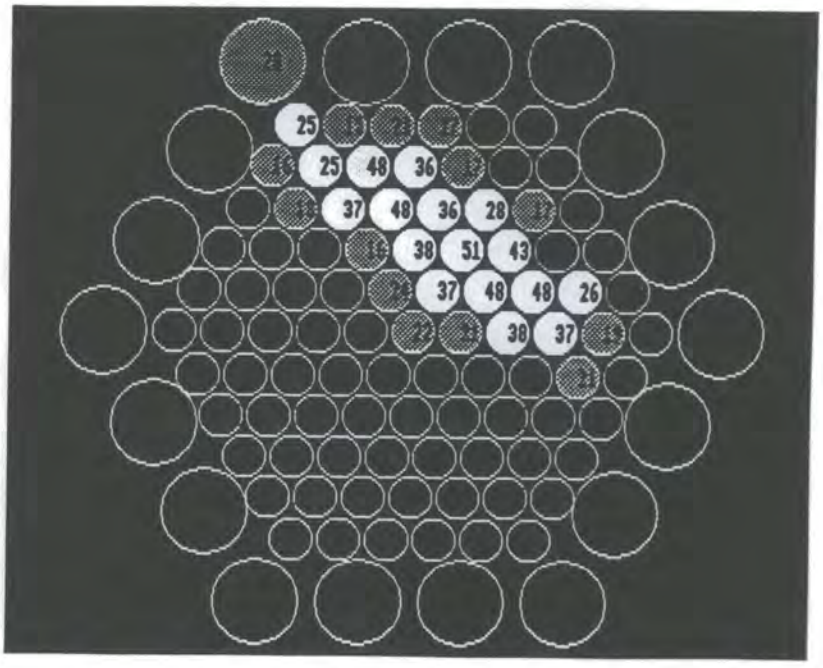

Figure 7.16: An example image demonstrating the classification of PM tubes as image (white), border (grey) and background (black) pixels. the average noise of the response of the tubes was +/- 6 bits.

The charge integrals in the image and border pixels are used to calculate the standard parameters, introduced in Section 3.5.2, which describe the shape and orientation of the image (Hillas, 1985). The values of these parameters for the image in figure 7.16 are presented in Table 7.2.

Parameter	**Value**	**Parameter**	**Value**
Distance	0.58°	Width	0.25°
Azwidth	0.53°	Length	0.57°
Alpha	63.7°	Miss	0.52°

Table 7.2: Image parameters values which describe the image presented in Figure 7.16.

7.3.3.3 Parameter Distributions

Distributions of the image parameters, for the data taken at the constant 20° zenith angle, are displayed in Figure 7.17. These data were taken using a trigger involving the "1 of 7" camera event selection described in Section 7.2.7.3. No image parameter cuts have been performed on the data. The residual count rate of 100 c.p.m., for events which have sufficient signal to satisfy the requirements for image parametisation, implies an energy threshold for high resolution imaging of approximately 400 GeV, similar to the threshold of the Whipple telescope. It is encouraging to note that the parameter distributions are similar to those achieved using the telescope of the Whipple collaboration which has an equivalent resolution, with some allowance made for the altitude difference of the two observations. The variation of these parameters, over a wide zenith angle range, is shown in figure 7.18. The figure shows that even at large zenith angles the average value of azwidth is significantly larger than that of width. This demonstrates that the parameterization of the hadronic images retains a significant amount of image orientation information. If this is also true for the gamma ray candidates, then discrimination between hadronic and gamma ray primaries by high resolution imaging of EAS will be possible over a wide range of zenith angles. Even if the parameterization of the gamma ray images becomes unreliable at large zenith angles, due to their reduced size, some background rejection will be still be possible on the basis of image extent.

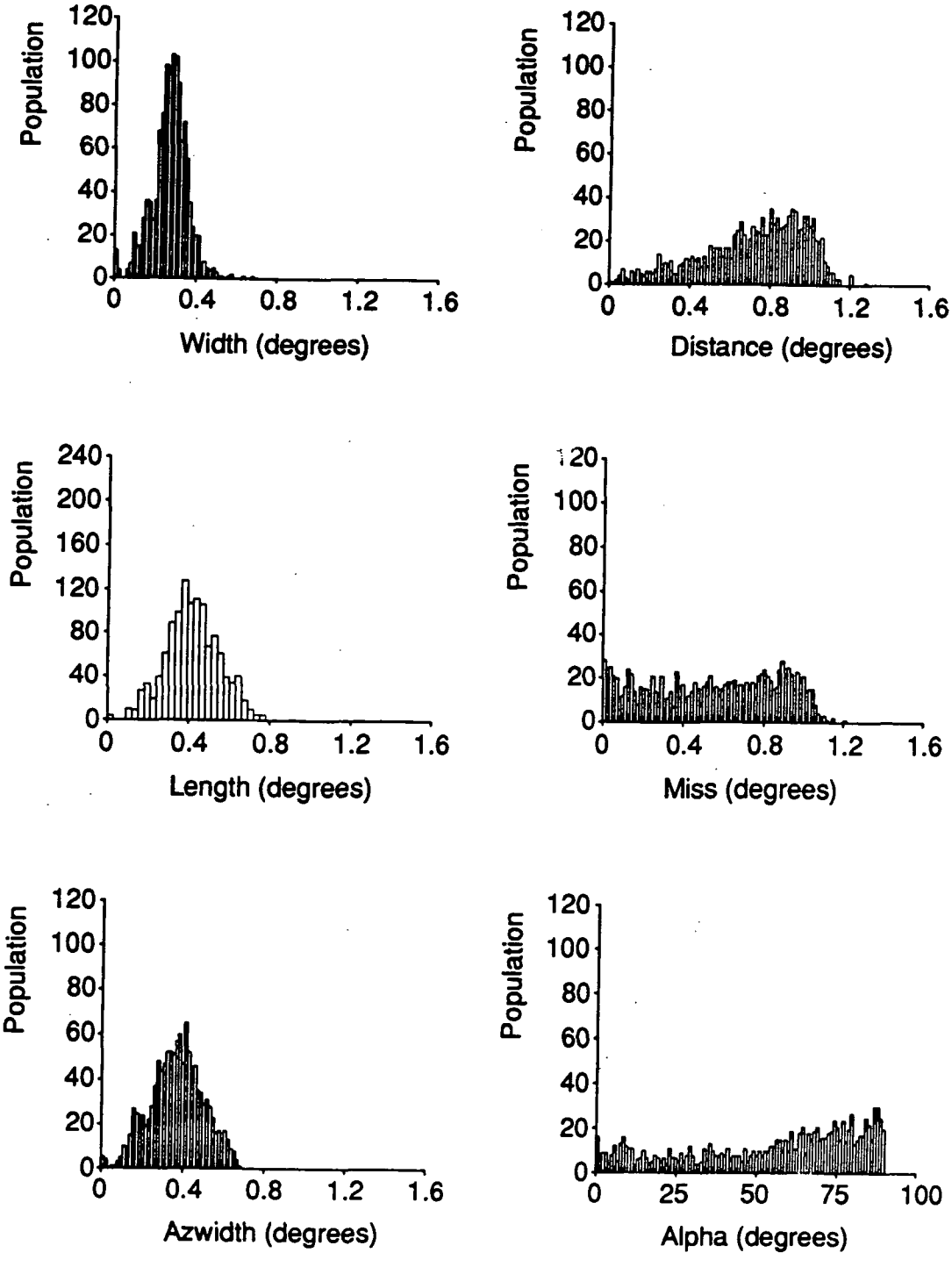

Figure 7.17: Hillas parameter distributions for 1501 hadronic background events observed by the Mk.6 telescope at a zenith angle of 20°. These parameter distributions are not dissimilar to those achieved by the Whipple collaboration from data treated in a similar way (Fegan, 1989).

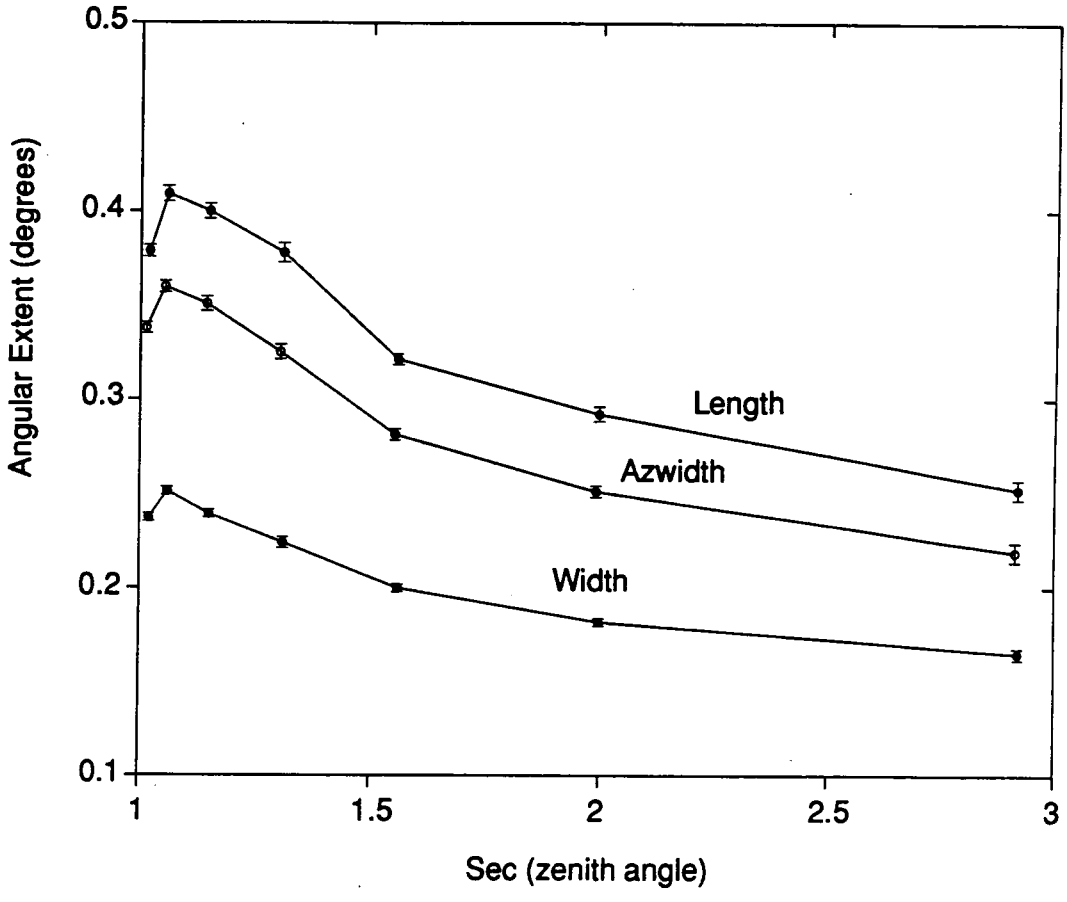

Figure 7.18: Zenith angle dependence of the parameters which describe the size of an images.

7.4 Future Developments

The energy threshold of the telescope is now approaching the optimum for the size of flux collectors deployed. It has been demonstrated that the response of the left / right triggering packages are now the limiting component in the telescope event trigger. In an effort to force down the energy threshold still further, comprehensive albedo protection will be applied to the left and right flux collectors and further small improvements to the PM tube bandwidth may be possible. It is acknowledged that when this has been effected the gain of the tubes will be maximised and all of the

potential energy sensitivity of the telescope realised.

With the sensitivity of the telescope maximised, effort will be redirected to exploiting fully the potential of the data. The data provided by the Mk.6 telescope is unique in many respects. Its low energy capability affords it an exceptional data collection rate with the Cerenkov signature of each event being represented in three independent detector packages measurements.

The medium resolution images provided by the left / right triggering packages provide a very interesting insight into the fluctuations of the lateral distribution of the Cerenkov light within the shower. The work with the Mk.5 telescope has shown that a 0.5° resolution image can provide reliable values for the total light signal and the centre of gravity of the signal. The Mk.6 triggering PM tubes will, therefore, provide two independent measures of these two quantities. These quantities should correspond well between flux collectors for showers with gamma ray primaries and poorly for hadronic events. This provides a further method of discriminating between gamma ray and hadron initiated EAS. Figure 7.19 is an example of the data available from the triggering packages. The figure shows the multiplicity of triggering coincidence channel responses as a function of zenith angle and is an example of the wealth of information which is yet to be tapped in the data of the Mk.6 telescope. Completion of the commissioning of the Mk.6 telescope will now allow the release of effort towards the gathering and exploration of this extremely interesting data.

Chapter 8 outlines the contemporary state of gamma ray astronomy and serves to place the potential of the Durham observatory in context.

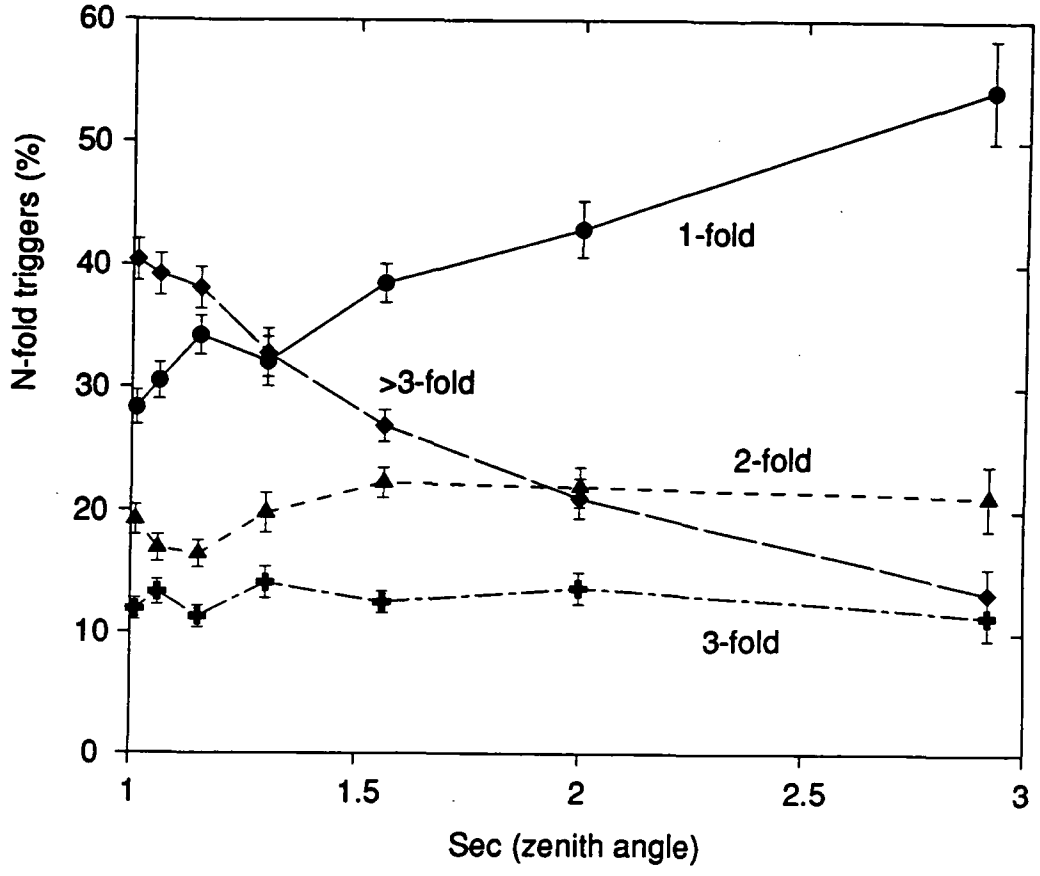

Figure 7.19: Multiplicity of coincidence channel response as a function of zenith angle.

CHAPTER 8

SUMMARY AND FUTURE WORK

8.1 Introduction

The gamma ray region of the electromagnetic spectrum represents a vibrant region of astrophysical research. Further impetus has been provided by the spectacular success of the CGRO, which has sensitivity over the whole of the range of energy from 10's of keV to 30 GeV (At the time of writing the CGRO is still fully operational). Above 30 GeV coverage of the electromagnetic spectrum is fragmentary and incomplete. The atmospheric Cerenkov technique, which provides the next window on the spectrum and is the subject of this thesis has obvious potential which is yet to be fully exploited. Detection with high statistical significance of the Crab Nebula and the AGN Markarian 421, together with more marginal detections of accreting binaries and isolated pulsars demonstrate the breadth of utility of the method. However, if the atmospheric Cerenkov technique is to prove its worth as an astronomical tool then the sensitivities of the instruments must be improved to such an extent that the statistical significance of detections is unquestionable and the energy spectra of sources can be determined.

This thesis describes the rapid progress made by the Durham group over the past four years towards the provision of a gamma ray observatory comprising "second generation" atmospheric Cerenkov telescopes employing sophisticated background rejection strategies and low energy capabilities. The three telescopes at the Durham Observatory in Narrabri, operated in a number of different configurations, provide a facility with useful sensitivity in the energy range 75 - 2000 GeV.

8.2 The sensitivities of the Durham Telescopes

The sensitivity of the small, simple event counting devices that were the first generation of atmospheric Cerenkov telescopes is constrained by the hadronic background that dominates the cosmic ray flux. Source detections were of marginal statistical significance offering little return in terms of elucidation of the production mechanisms of cosmic rays. The recent commissioning, at the Narrabri Observatory, of telescopes with the capacity to employ sophisticated background rejection strategies has increased the sensitivity of the facility dramatically. Efficacy of the background rejection strategies, expressed as the quality factor Q, for the medium resolution Mk.5 and Mk.3 telescopes is tentatively estimated to be 2 for the stereoscopic imaging method and 1.5 for medium resolution "mono" imaging. The large count rate of the Mk.6 telescope afforded by its low energy capability offers a two fold improvement in flux sensitivity over the raw data from the smaller telescopes, and its capability as a high resolution imager should prove equivalent to the Whipple collaboration telescope, offering Q factor improvements of greater than 4.

8.3 Candidate Sources of VHE Gamma Rays

8.3.1 Introduction

Historically the principal astrophysical objects of interest to VHE gamma ray astronomers have been highly compact bodies. TeV gamma ray emission has been associated with the extreme magnetic fields in the vicinity of rotating neutron stars, which exist both as isolated pulsars and in accreting binary systems. The gamma ray flux from such objects is

inherently time variable, emission being beamed and subject to periodicities introduced by the neutron star rotation and binary orbit. The detection, by the Whipple collaboration, of non-periodic TeV gamma ray emission from the direction of the Crab Nebula has broadened the spectrum of potential sources, and the net must be cast still wider to encompass the Active Galactic Nuclei (AGN) identified by the EGRET experiment on board the CGRO.

8.3.2 Accreting Systems: X-Ray Binaries and Cataclysmic Variables

Chapter 6 of this thesis presents further evidence of VHE gamma ray signal from the cataclysmic variable AE Aquarii. This signal was detected as a short burst of periodic emission pulsed at the first harmonic of the white dwarf rotation period, consistent with previous detections of emission from this binary system (Bowden et al., 1992a). This result is the first achieved using data recorded by the Mk.5 and upgraded Mk.3 telescopes, and as such is the first to benefit from background rejection based upon imaging of Cerenkov showers by the Durham group. It is encouraging to note that analysis of the data using the medium resolution "mono" imaging and "stereo" imaging of Cerenkov showers resulted in enhanced datasets in both cases. It is hoped that a similar enhancement to the datasets for projected observations of sources for which marginal detections have been claimed in the past, will result in detections with high statistical significance.

AE Aquarii is unusual in being a "white dwarf pulsar", the more conventional binary objects of promise in the Narrabri observing programme are the X-ray binaries Vela X-1, Cen X-3 , Cyg X-3 and Her X-1 (Chadwick, McComb and Turver, 1992). The X-ray binary source group is sub-divided into high mass and low mass systems on the basis of the size of the

companion to the neutron star. Vela X-1 and Cen X-3 are high mass X-ray binaries (Bowden et al., 1992b, Bowden et al., 1993). Accretion by the compact companion is believed to occur via an accretion disk in the case of Cen X-3 and by a stellar wind mechanism in Vela X-1. The neutron stars in the low mass X-ray binary systems Cyg X-3 and Her X-1 accrete via Roche lobe overflow from the companion into an accretion disk. Each of these mechanisms is unstable and results in significant variability in emission. The high cout rate and sensitivity of the Mk.6 telescope is invaluable for the study of the transient emission typical of these sources.

8.3.3 Isolated Neutron Stars

Five of the seven isolated pulsars detected by the CGRO (Fierro et al., 1993): the Vela pulsar, PSR1509-58, PSR1706-44 PSR1055-52 and the Crab pulsar are visible from the Narrabri Observatory. In contrast to the binary systems, whose VHE gamma ray emission is powered by the release of gravitational potential energy by the accreting matter, the energy source for emission from an isolated pulsar is the rotational energy of the neutron star. Models have been proposed for gamma ray emission in the outer magnetosphere of rotating magnetised neutron stars (for example Cheng, Ho and Ruderman (1986). Emission is predicted to be beamed, therefore a pulsed flux is anticipated from isolated neutron stars. The Durham group reported a weak periodic signal from the Crab pulsar, manifest as a narrow pulse in the light curve coincident with the main pulse at other wavelengths (Dowthwaite et al., 1984). This evidence was supported by further detections of pulsed emission (Tumer et al., 1985; Bhat et al., 1986). Subsequently, however, the pulsed VHE gamma ray flux from the direction of the Crab pulsar has been shown to represent less than 10 % of the total

flux at these energies (Reynolds, 1991).

The production of GeV gamma rays within supernova remnants powered by pulsars was suggested as an explanation for the coincidence of a number of plerions with gamma ray sources within the COS-B source catalogue (Weiler and Panagia, 1980). This provides a mechanism to explain the unpulsed flux from the direction of the Crab pulsar. The Crab nebula is now accepted as a source of TeV gamma rays, D.C. signals having been detected by a number of independent groups. Searches for periodicity within the Whipple and ASGAT data at the pulsar period has shown the pulsed component of the signal to be less than 10 % of the total in contrast to the 50 % pulsed fraction for energies of a few GeV (Clear et al., 1987). This suggests that the production site for the majority of TeV gamma rays is in some region of the nebula rather than close to the pulsar.

The CANGAROO collaboration working in the southern hemisphere reported a detection of a DC signal from the direction of the pulsar PSR1706-44 (Ogio et al., 1993), and suggested that there was evidence also of emission from the direction of the Vela SNR and W28. The common feature to all of these three potential sources is the plerion-like association of a SNR with an active pulsar. A more complete description of these sources is given by Goret (1993).

8.3.4 Active Galactic Nuclei

AGN are acknowledged as potential sources of cosmic rays of extremely high energy (>10^{20} eV) and contain matter and magnetic fields of sufficient energy density to provide an efficient target for gamma ray production. However, all of the AGN so far identified by the EGRET experiment are blazars. It is generally accepted that the gamma ray production within these

sources takes place in relativistic jets directed along our line of sight. Their differential spectral indices above 100 MeV range from -1.7 to -2.4 and their redshift ranges from 0.03 to 2.17. In March 1992 detections of gamma rays of energy > 1MeV were reported by the EGRET team for three BL Lac type AGN. One of these, Markarian 421, is the nearest such object with a red shift of 0.031. The Whipple collaboration observed this object and detected a D.C. flux of gamma rays above 0.5 TeV significant at the 6.3σ level (Punch et al., 1992). No evidence of emission was found from 8 other AGN including 3C279, an object which appeared to EGRET to be brighter than Markarian 421. 3C279 was also observed, at a more favourable zenith angle, from the southern hemisphere by the Durham group (Bowden et al., 1993a). This observation resulted in an upper limit for the flux from 3C279 which is close to the extrapolated EGRET spectrum. These non detections may be attributed to time variability of emission, which is evident in the data at a few GeV, or may be due to the predicted attenuation of VHE gamma rays by pair production with the IR and optical background photon flux. At z=1 Stecker et al., 1992 estimate the optical depth for gamma rays of energy E(TeV) to be $\tau(E) \sim \tau_o E^{1.55}$ with $\tau_o \sim 40$. Consequently gamma rays of energy > 100 GeV would be strongly attenuated, accentuating the requirement for sensitivity below this energy.

8.4 Conclusion

The broad spectrum of source types supporting different mechanisms for production of VHE gamma rays places numerous constraints on the observational strategies employed.

If the number of targets in the latest category of potential sources to emerge, the AGN, is to be increased, observations must be made in the

energy region below 100 GeV. The Mk.6 telescope will allow observations to be made of AGN at distances greater than z = 1, the typical distance to these sources. There is insufficient Cerenkov light in the images at these energies for the imaging technique to be of value. However, showers with primaries of energy greater than the gamma ray cut off imposed by the IR background can be rejected as hadronic. The signal is further enhanced by the dearth of Cerenkov light produced by the lower energy hadron initiated EAS, leaving the smaller numbers of higher energy hadrons which mimic low energy gamma ray events as the only background.

With regard to the galactic sources, the increase in count rate afforded by the reduction in energy threshold offers greatly improved statistics, and above a few hundred GeV the high resolution imaging capability of the Mk.6 telescope should prove a very powerful signal enhancement tool. It is hoped that this improvement in sensitivity will prove decisive in establishing variable sources such as the X-ray binaries as emitters of VHE gamma rays.

The efficacy of medium resolution and stereoscopic imaging of EAS has been demonstrated using the Mk.3 and Mk.5 telescopes, with significant enhancement of a periodic signal from AE Aquarii. The efficiency of the stereoscopic imaging technique can only be improved by the introduction of the Mk.6 telescope as a high resolution, low energy threshold component.

In conclusion, the Durham group is now poised to capitalize on a large amount of effort which has been directed towards the provision of a facility with sensitivity over a spectrum of energies. The low energy capability of the Mk.6 telescope opens the window on a region of the electromagnetic spectrum which is of enormous potential. The results are anticipated with interest.

Chadwick, P.M., et al. (1985) *Nature,* 318, 642

Chadwick, P.M. (1987) *PhD Thesis, University of Durham.*

Chadwick, P.M., McComb, T.J.L. and Turver, K.E. (1992) *Towards a Major Atmospheric Cerenkov Detector,* Fleury, P. and Vacanti, G. (Ed),

Chadwick, P.M. (1995) *To be published in Proc. 24th ICRC, Rome.*

Cheng, K.S., Ho, C. and Ruderman, M.A. (1986) *Ap. J.,* 300, 500

Chilingarian, A.A. and Cawley, M.F. (1991) *Proc. 22nd ICRC, Dublin,* 1, 460

Chincarni, G. and Walker, M.F. (1986) *Astron. Astrophys.,* 170, 187

Clay, R.W. et al. (1989) *Proc. Astro. Soc. Aust.,* 8, 41

Clear, J. et al. (1987) *Astron. Astrophys.,* 174, 85

Danaher, S. et al. (1993) *Astroparticle Physics,* 1, 357

De Jeger, O.C. and Meintjes, P.J. (1993) *Astron. Astrophys.,* 268, L1

Dowthwaite, J.C., et al. (1983) *Astron. Astrophys.,* 126, 1

Dowthwaite, J.C., et al. (1984) *The Astrophysical Journal,* 286, L35 - L38

Dowthwaite, J.C. (1987) *PhD Thesis, University of Durham.*

Eadie, W.T., et al. (1971) *"Statistical Methods in Experimental Physics",* North Holland, Amsterdam, 283

Erber, T. (1966) *Rev. Mod. Phys.,* 38, 626

Fazio, G.G. (1967) *Ann. Rev. Astron. Astrophys.* 5, 481

Fazio, G.G., et al. (1972) *Ap. J. (Lett.),* 175, L117

Fegan, D.J., et al. (1983) *Nuclear Instruments and Methods,* 211, 179

Fegan, D.J. (1992) *Towards a Major Atmospheric Cerenkov Detector, Palaiseau.* Fleury, P. and Vacanti, G. (Ed.) 3 - 41

Fegan, D.J., et al. (1994) *Towards a Major Atmospheric Cerenkov Detector III, Tokyo.,* Kifune, T. (Ed), Univeral Academy Press, 149

Fierro, J.M., et al. (1993) *Ap. J.*, 413, L27

Frank, I.M. and Tamm, Ig. (1937) *Dokl. Akad. Nauk.* 14, 109

Gibson, A.I., et al. (1982) *Nature,* 296, 883

Gibson, A.I., et al. (1982a) *Proc. of the International Workshop on VHE Gamma Ray Astronomy,* Ootacamund, India. Ramana Murthy, P.V., and Weekes, T.C. (Ed.), 97

Ginzberg, V. L. (1940) *Zh. fiz. SSSR,* 2, 441

Goeckel (1910) *Phys., Zeits.,* 11, 280

Goret, P. (1993) *Towards a Major Atmospheric Cerenkov Detector - II, Calgary,* Lamb, R.C. (Ed), 25

Gould, R.J. and Schreder, G.P. (1966) *Phys. Rev. Lett.*, 16, 252

Grindlay, J.E., et al. (1975) *Astrophys. J.*, 201, 82

Grindlay, J.E., et al. (1975) *Astrophys. J.*, (Lett.), 197, L9

Hara, T., et al. (1993) *Nucl. Inst. Methods. Phys. Res.*, A332, 300

Heaviside, O. (1890) *Electrical Papers*, 2, 494

Hess, V.F. (1911) *Phys. Zeits.*, 12, 998

Hillas, A.M. (1982) *J. Phys. G.*, 16, 1271

Hillas, A.M. (1985) *Proc. 19th ICRC, La Jolla*, 3, 445

Hillas, A.M. and Patterson, J.R. (1987) *Very High Energy Gamma Ray Astronomy,* Turver, K.E. (Ed.) Dordrecht : D. Reidel, 243

Hillier, R. (1984) *"Gamma Ray Astronomy"*, Clarendon Press, Oxford.

Jelley, J.V. (1966) *Phys. Rev. Lett.*, 16, 479

Jelley, J.V. (1967) *"Progress in Elementary Particle and Cosmic Ray Physics" Vol. 9,* Wilson, J. G. and Wouthuysen (Eds.), North Holland, 41

Kanbach, G., et al. (1988) *Space Science Reviews,* 49, 69-84

Kifune, K., et al. (1995) *Astrophys. J.*, 337, 467

Kornienko, A.P., et al. (1993) *Experimental Astronomy*, 4, 77

Lang, M.J. (1991) *PhD Thesis, University College, Dublin.*

Leahy, D.A., Elaner, R.F. and Weisskopf, M.C. (1983) *Ap. J.*, 272, 256

Longair, M.S. (1992) *"High Energy Astrophysics,"* Vol. 1. Cambridge: C.U.P.

Lorenz, E. (1993) *Towards a Major Atmospheric Cerenkov Detector II, Calgary*, Lamb, R.C. (Ed.) 182

Macrae, J.H. (1985) *PhD Thesis, University of Durham.*

Mallet, L. (1926) *C. R. Acad. Sci. (Paris)*, 183, 274

Mallet, L. (1928) *C. R. Acad. Sci. (Paris)*, 187, 222

Mallet, L. (1929) *C. R. Acad. Sci. (Paris)*, 188, 445

Mannings, V. (1990) *PhD Thesis, University of Durham.*

Mardia, K.V. (1972) *"Statistics of Directional Data"*, London: Acad. Press

Meintjies, P.J., et al. (1992) *Ap. J.*, 401, 325

Meintjies, P.J., et al. (1993) *Proc. 23rd Int. Cosmic Ray Conf.* 1, 338

Morrison, P. (1958) *Nuovo Cimento*, 7, 858

Ogio, S., et al. (1993) *Proc. 23rd ICRC, Calgary*, Vol 1, 409

Ogleman, H., et al. (1976) *Proc. Gamma Ray Symposium, Goddard.* 118

Pare, E. (1993) *Towards a Major Atmospheric Cerenkov Detector II*, Lamb, R.C. (Ed.), 250

Patterson, J., et al. (1979) *Ap. J.*, 235, 978

Patterson, J., et al. (1980) *Ap. J.*, 240, L133

Patterson, J.R. and Hillas, A.M. (1989) *Nucl. Instr. Meth. Phys. Res.*, A287, 553-564

Punch, M., et al. (1992) *Nature*, 358, 477.

Punch, M (1993) *PhD Thesis, University College, Dublin.*

Ramana-Murthy, P.V. and Wolfendale, A.W. (1986) *"Gamma Ray Astronomy"*, C.U.P.

Lord Rayleigh (1894) *Theory of Sound, Vol 1,* McMillan, 35

Reynolds, P.T. (1991) *Proc. 22nd ICRC, Dublin,* 1, 500

Reynolds, P.T., et al. (1993) *Astrophys. J.* 404, 206

Roberts, M.D. (1993) *PhD Thesis, University of Adelaide.*

Robinson, E.L., et al. (1991) *Astrophys. J.* 378, 286

Rutherford and Cooke (1903) *Phys. Rev.,* 16, 183

Schubnell, M., et al. (1992) *CGRO Science Symposium,* 1171

Simpson, J.A., Fonger, W. and Treiman, S.B. (1953) *Phys. Rev.*, 90, 934

Standish, E.M. (1982) *Astron. Astrophys.* 114, 297

Stecker, F.W., De Jeger, O.C. and Salamon, M.H. (1992) *Ap. J.*, 390, L49

Tumer, O.T., et al. (1985) *Proc. 19th ICRC., La Jolla,* 1, 139

Tumer, O.T., et al. (1990) *Proc. 21st ICRC, Adelaide,* 4, 238

Tumer, O.T., et al. (1993) *Towards a Major Atmospheric Cerenkov Detector - II,* Lamb, R.C. (Ed.), 259

Turver, K.E. and Weekes, T.C. (1977) *Nuovo Cimento,* 45b, 99

Vacanti, G., et al. (1991) *The Astrophysical Journal,* 337, 467-469

Vladimirsky, B.M., et al. (1989) *Proc. Int. Workshop Very High Energy Gamma Ray Astronomy, Crimean Astrophysical Observatory: Crimea,* 21

Weekes, T.C., et al. (1989) *Astrophys. J.,* 342, 379

Weiler, K.W. and Panagia, N. (1980) *Astron. Astrophys.,* 90, 269

Welsh, W.F., Horne, K. and Gomer, R. (1993) *Astrophys. J.,* 410, L39

Zatsepin, V.I. (1965) *Sov. Phys. JETP,* 20, 459

Zatsepin, V.I. and Chudakov, A.E. (1962) *Sov. Phys. JETP,* 15, 1126

Zinner, E. (1938) *Astron. Nach.,* 265, 345